Titre: Title:	Improvement of Barrier Properties of Poly(Ethylene Terephthalate)/Organoclay Nanocomposites
Auteur: Author:	Maryam Dini
Date:	2013
Type:	Mémoire ou thèse / Dissertation or Thesis
Référence: Citation:	Dini, M. (2013). Improvement of Barrier Properties of Poly(Ethylene Terephthalate)/Organoclay Nanocomposites [Ph.D. thesis, École Polytechnique de Montréal]. PolyPublie. https://publications.polymtl.ca/1286/

UNIVERSITÉ DE MONTRÉAL

IMPROVEMENT OF BARRIER PROPERTIES OF POLY(ETHYLENE TEREPHTHALATE)/ORGANOCLAY NANOCOMPOSITES

MARYAM DINI

DÉPARTEMENT DE GÉNIE CHIMIQUE

ÉCOLE POLYTECHNIQUE DE MONTRÉAL

THÈSE PRÉSENTÉE EN VUE DE L'OBTENTION

DU DIPLÔME DE PHILOSOPHIAE DOCTOR

(GÉNIE CHIMIQUE)

OCTOBRE 2013

UNIVERSITÉ DE MONTRÉAL

ÉCOLE POLYTECHNIQUE DE MONTRÉAL

Cette thèse intitulée:

IMPROVEMENT OF BARRIER PROPERTIES OF POLY(ETHYLENE TEREPHTHALATE)/ORGANOCLAY NANOCOMPOSITES

présentée par: DINI Maryam
en vue de l'obtention du diplôme de : Philosophiae Doctor

a été dûment acceptée par le jury d'examen constitué de :

M. FAVIS Basil, Ph.D., président

M. CARREAU Pierre, Ph.D., membre et directeur de recherche

M. KAMAL Musa R., Ph.D., membre et codirecteur de recherche

M. TON-THAT Minh-Tan, Ph.D., membre et codirecteur de recherche

M. AJJI Abdellah, Ph.D., membre

Mme KONTOPOULOU Marianna, Ph.D., membre

DEDICATION

To my lovely family

ACKNOWLEDGMENTS

I would like to express my deep and sincere gratitude to my research supervisors, Prof. Pierre J. Carreau, Prof. Musa R. Kamal and Prof. Minh-Tan Ton-That for their extensive support and providing me the great opportunity to study under their supervision. Their innovative and questioning approach, encouragement, patience and broad knowledge helped me throughout my study at the École Polytechnique de Montréal.

I would like to thank the organizers of rheology meetings (Prof. Pierre J. Carreau, Prof. Marie-Claude Heuzey and Prof. A. Ajji) and all the students of this group for their valuable comments and suggestions.

I wish also to thank all my professors at Amirkabir University (Polytechnic of Tehran) for encouraging me to continue my graduate studies.

A sincere appreciation goes to all the technical and administrative staffs of École Polytechnique de Montreal, chemical engineering department and also at the National Research Council Canada (NRCC), Mr. Guillaume Lessard, Ms. Claire Cerclé, Mr. Eric Cloutier, and Mrs. Florence Perrin-Sarazin. My special thanks go to Ms. Mélina Hamdine and Ms. Weawkamol Leelapornpisit for their sympathies, supports and great helps in rheological and morphological studies in this thesis.

I acknowledge helpful discussions with Dr. Hesam Ghasemi, Dr. Abbas Ghanbari, Dr. Feng. Xu, Dr.Tahereh Mousavand, Dr. Babak Esmaeili and Khalil Shahverdi, who worked in the same area.

Thanks to all my friends and my colleagues for their supports during my PhD.

I would like to appreciate very kind assistance of Marie Matet for the translation of the Abstract of this thesis to French.

I also acknowledge financial and infrastructure support received from National Science and Engineering Research Council (NSERC), NRCC and Business Development Bank of Canada (BDC).

Finally, all my special and deepest gratitude go to my family, especially my grandparents, parents, husband, sister and brother for their love, understanding and support.

RÉSUMÉ

Le poly(téréphtalate d'éthylène) (PET) est un polymère semi-cristallin, qui est largement utilisé dans l'industrie de l'emballage, en contact direct avec les denrées alimentaires, les boissons, les produits pharmaceutiques et les cosmétiques. Le développement vers de nouveaux marchés nécessite l'amélioration des propriétés barrières aux gaz du PET afin de l'utiliser dans l'emballage du vin, de la bière, et d'autres produits sensibles à l'oxygène, ainsi que d'améliorer la durée de vie des boissons gazeuses ; même une amélioration modérée des propriétés barrières aux gaz a un impact économique important. La présence de nano-argiles dans le PET comme phase imperméable et pour allonger le parcours tortueux peut résulter à une remarquable amélioration des propriétés consistant en la diminution de la perméabilité aux gaz. Les nanocomposites à base de PET peuvent être préparés in-situ ou par un mélange à l'état fondu. Cette dernière approche est plus économique, pratique et respectueuse de l'environnement dû à l'absence de monomères et/ou de solvants organiques. La microstructure des nanocomposites polymères joue un rôle important dans les propriétés macroscopiques des produits finaux. Afin d'optimiser de manière significative les performances, une bonne dispersion des nano-argiles dans la matrice et la compatibilité thermodynamique entre le polymère et les nano-argiles sont nécessaires.

Dans ce travail, les poly(téréphtalate d'éthylène) (PET) ont d'abord été préparés par un mélangeage à l'état fondu en utilisant une extrudeuse double-vis assistée par injection d'eau. Afin de faciliter la diffusion des molécules du PET à travers les nanofeuillets de l'argile, de la vapeur d'eau a été introduite dans l'extrudeuse. Par la suite, la réduction de la masse moléculaire (M_W) de la matrice PET due à l'hydrolyse causée par l'eau a été compensée par une polymérisation à l'état solide (SSP pour *solid-state polymerization*). Les effets du débit d'alimentation , de la compatibilité entre le PET et les nano-argiles (Cloisite Na^+, Cloisite 30B et Nanomer I.28E) et de la SSP ont été étudiés. Les résultats révèlent qu'il y a plus de délaminage des lamelles de l'argile organique dans les nanocomposites PET-C30B mis en forme à faible taux d'alimentation par rapport à ceux mis en forme à un fort taux d'alimentation. La présence d'eau permet d'obtenir un plus grand nombre de nanoparticules C30B à une ou deux couches ainsi que l'augmentation du facteur de forme dans les nanocomposites à base de PET. L'effet de l'eau sur la microstructure des nanocomposites de PET est fortement dépendant du choix du modificateur des nano-argiles.

La mise en forme avec de l'eau a des effets négatifs sur les nanocomposites PET-I28E, à cause de leur faible compatibilité. L'étude de la structure du PET après la SSP par spectroscopie RMN (résonance magnétique nucléaire) ^{1}H et RMN ^{13}C et par des mesures rhéologiques montre une structure moléculaire linéaire du PET.

L'effet de la concentration des nano-argiles sur les propriétés thermiques, mécaniques et barrières des nanocomposites à base de PET a été étudié dans la seconde partie de ce travail. Des analyses de DRX (diffractrométrie de rayons X), au MEB (microscope électronique à ballayage) et au MET (microscope électronique en transmission) montrent une morphologie intercalaire et exfoliée dans tous les nanocomposites PET-C30B, avec un degré d'intercalation et de délaminage plus grand pour le procédé assisté par injection d'eau. Des propriétés mécaniques et barrières améliorées sont obtenues pour les nanocomposites PET-C30B en comparaison avec le PET seul. Les nanocomposites présentent un module de Young plus haut et une perméabilité à l'oxygène plus faible après la SSP. L'élongation à la rupture est considérablement plus haute pour les nanocomposites préparés avec la SSP en comparaison avec les nanocomposites mis en forme par mélangeage à l'état fondu. L'allongement à la rupture pour les nanocomposites de PET conventionnels contenant 2 % en masse de C30B est de 6 %, par contre il est de 145 % pour les nanocomposites préparés avec la SSP. Une augmentation de 45 % du module de Young et de 42 % du comportement barrière est constatée pour les nanocomposites contenant 6 % en masse de C30B, comparé au PET pur. Le modèle de pseudo-inclusion a été utilisé pour prédire le module de Young des nanocomposites de PET et l'effet de l'intercalation de la microstructure sur le modèle de prédiction. De plus, les modèles de Nielsen et Bharadwaj ont été appliqués pour prédire la perméabilité en présence d'argiles organiques.

Dans la troisième partie de ce travail, la polymérisation à l'état solide du PET et des nanocomposites à base de PET et de Cloisite 30B à différentes concentrations a été étudiée pour différents temps de réaction dans le réacteur. De plus, l'effet de la taille des particules sur la vitesse de polymérisation à l'état solide a été examiné. Des mesures en viscosimétrie, en titrage, en rhéologie et en calorimétrie différentielle à balayage (DSC) ont été faites pour analyser les échantillons provenant de la SSP. La masse moléculaire moyenne en poids (M_W) augmente considérablement à la suite de la SSP. Le modèle de Maron-Pierce a été utilisé pour évaluer la masse moléculaire du PET dans les nanocomposites avant et après la SSP. A cause de l'effet

barrière des nanofeuillets d'argile, il est montré que l'étendue et la vitesse de réaction de la SSP dans les nanocomposites sont plus faibles par rapport à celles des PET. Les résultats du titrage montrent que de part la présence de C30B la concentration des groupes carboxyles dans les nanocomposites de PET augmente, alors que la SSP entraîne une réduction significative de ces groupes terminaux.

Dans la dernière partie de ce travail de recherche, des nanocomposites de PET contenant des nano-argiles non-modifiées (Cloisite Na^+) ont été préparés en suspension. Une suspension de Cloisite Na^+ et d'eau a été injectée dans l'extrudeuse double-vis et mélangée avec le PET à l'état fondu. Pour améliorer la dispersion des nano-argiles, de la carboxylmethylcellulose (CMC) et du polyéthylène glycol (PEG) ont été ajoutés à la suspension. Les nanocomposites contenant du PEG sont les échantillons qui présentent des propriétés mécaniques et barrières avec la plus grande amélioration. La couleur des échantillons préparés avec cette méthode est meilleure que celle obtenue pour les nanocomposites avec du Cloisite 30B.

ABSTRACT

Poly(ethylene terephthalate) (PET) is a semi-crystalline polymer, which has been widely used in the packaging industry and in direct contact with food, beverages, pharmaceutical products and cosmetics. Expansion to new markets requires an improvement of PET's gas barrier properties for use of PET packaging for wine, beer, and other oxygen-sensitive products, as well as for improving the shelf life of carbonated soft drinks; even a moderate improvement of barrier properties has a profound economic impact. The presence of nanoclays in PET as an impermeable phase and for increasing the tortuous path of permeates can result in outstanding property improvements in terms of decreasing gas permeability. PET nanocomposites can be prepared by in-situ or melt-mixing methods. The latter approach is more economical, practical and environmental friendly due to the absence of monomers and/or organic solvents. The microstructure of polymer nanocomposites substantially plays an important role in the determining macroscopic properties of final products. To achieve significant performance enhancements, good dispersion of the nanoclay in the matrix and thermodynamic compatibility between the nanoclay and the polymer are required.

In this work, poly(ethylene terephthalate) (PET) nanocomposites were prepared by water-assisted melt compounding in a twin-screw extruder. In order to facilitate the diffusion of PET molecules into clay galleries, steam was fed into the extruder. Subsequently, the molecular weight (M_W) reduction of the PET matrix, due to hydrolysis by water, was compensated by solid-state polymerization (SSP). Effects of feeding rate, compatibility between PET and nanoclay (Cloisite Na^+, Cloisite 30B and Nanomer I.28E) and SSP on the microstructure of the nanocomposites were studied. The results revealed more delamination of organoclay platelets in

PET-C30B nanocomposites processed at low feeding rate compared to those processed at high feeding rate. The presence of water resulted in a larger number of single and double layers of C30B nanoparticles as well as an increased aspect ratio of clay particles in PET nanocomposites. The effect of water on the microstructure of PET nanocomposites was strongly dependent on the nanoclay modifier. Processing with water had negative effects on the PET-I28E nanocomposites, because of its lower compatibility. Studies on the structure of PET after SSP by rheological measurements, Nuclear magnetic resonance (^{1}H NMR and ^{13}C NMR) spectra showed the linear molecular structure of PET.

The effect of organoclay concentration on the rheological, thermal, mechanical and barrier properties of the PET nanocomposites prepared by different methods was studied in the second part of this work. XRD, SEM and TEM analyses displayed intercalated/exfoliated morphology in all PET/C30B nanocomposites, with a higher degree of intercalation and delamination for the water-assisted process. Enhanced mechanical and barrier properties were obtained in PET-C30B nanocomposites compared to the neat PET. The nanocomposites exhibited higher tensile modulus and lower oxygen permeability after SSP. Elongation at break was significantly higher for SSP nanocomposites than for nanocomposites processed by conventional melt mixing. Elongation at break for conventional PET nanocomposites containing 2 wt% C30B was 6%, but for nanocomposites after SSP, the elongation at break was around 145%. Compared to the neat PET, improvements of 45% in tensile modulus and 42% in barrier behavior were found for nanocomposites containing 6 wt% C30B. The pseudo-inclusion model was used to predict the tensile modulus of PET nanocomposites and to determine the effect of intercalation

microstructure on the model predictions. Moreover, the Nielsen and Bharadwaj models were employed for the prediction of permeability in the presence of organoclay.

Studies of solid-state polymerization of PET and PET nanocomposites with different concentrations of Cloisite 30B and particle size were carried out at different reaction times in the third part of this work. Moreover, the effect of particle size on the rate of SSP was also investigated. Viscometry, titration, rheological and dynamic scanning calorimetry (DSC) measurements were used to analyze the samples from SSP. The weight-averaged molecular weight (M_W) of PET was shown to increase significantly following SSP. The Maron-Pierce model was utilized to evaluate the molecular weight of PET in the nanocomposites before and after SSP. It was also found that the extent and the rate of the SSP reaction in nanocomposites were lower than those for the neat PETs, due to the barrier effect of clay platelets. Titration results showed that by the presence of C30B the concentration of carboxyl groups was increased in PET nanocomposites while by SSP, these end groups were significantly reduced. Increases of half-time of crystallinity and reductions of both crystallization temperature and percentage of crystallinity with molecular weight of PET were found from DSC results.

In the last phase of this research work, PET nanocomposites containing an unmodifed nanoclay (Cloisite Na^+) were prepared by the slurry method. A slurry of Cloisite Na^+ and water was pumped into the twin-screw extruder to be melt-mixed with PET. To improve the nanoclay dispersion carboxymethyl cellulose (CMC) and poly(ethylyene glycol)(PEG) were added to the slurry. Mechanical and barrier properties showed more improvements for the nanocomposites containing PEG. The color of the nanocomposites prepared by this method was better than those obtained by conventional melt-mixing of PET and Cloisite 30B.

TABLE OF CONTENTS

LIST OF TABLES

LIST OF SCHEMES AND FIGURES

INTRODUCTION

Poly(ethylene terephthalate) (PET) is a semi-crystalline thermoplastic polymer with good thermal, mechanical and barrier properties, excellent transparency and recyclability. PET has different applications in synthetic fibers, medical and pharmaceutical, household and chemical, electronic and automotive, trays for frozen dinners, drink bottles including soft drinks and more, and flexible food packaging [1, 2]. More enhancement of O_2 and CO_2 barrier properties of PET will broaden the PET packaging for wine, beer, and the other oxygen-sensitive products, as well as improving the shelf life of carbonated soft drinks [3]. Some of the approaches to improve barrier properties of PET include surface coatings, polymer blending, multilayer structures, oxygen scavengers, anti-plasticization, crystallization, orientation and polymer nanocomposites [1, 4]. Among those mentioned methods, incorporation of nanoclays in polymer matrix is a new and promising way to enhance gas barrier properties due to the inducing longer tortuous path in the matrix. Exfoliating the nanoclays' platelets into the PET matrix leads to the most improvements of its properties [5]. Generally, PET nanocomposites are prepared by in-situ polymerization and melt-mixing [6-8]. While in-situ polymerization usually yields better dispersion of clay platelets than melt-mixing, the latter approach is more favourable due to the economical and environmental advantageous [9]. Several efforts have been done to reduce the rate of PET and organoclays degradation and enhance dispersion of organoclays in PET, by using a more stable clay modifier and increasing compatibility between PET and organoclays [10-12]. Other approaches considered the effects of processing conditions; screw speed, screw configuration and temperature profile in twin-screw melt extrusion of PET nanocomposites [13, 14]. All these efforts made only modest improvements in mechanical and barrier properties.

The main objective of this project was to prepare PET nanocomposites with enhanced barrier and mechanical properties. To achieve to this goal, water-assisted melt-mixing was used as a novel method to improve the organoclays dispersion in PET. The molecular weight reductions through melt-mixing were compensated by solid-state polymerization. The effect of feeding rate and thermodynamic compatibility between organoclays and PET on the microstructure of the final products were investigated. Effect of organoclay concentration on mechanical, barrier, thermal properties and rheological behavior of PET nanocomposites was also reported. Tensile

and barrier models were used to predict the properties of the final nanocomposites. In the third part of the work, the effect of organoclay concentration on the rate of SSP was studied using two different particle sizes of the samples. Systematic characterizations of nanocomposites before and after polymerization were performed by rheology, viscometry, titration and DSC. Furthermore, development of PET nanocomposite preparation with unmodified nanoclays was done by slurry method. Mechanical and barrier properties of these nanocomposites were also investigated.

This thesis is based on the following chapters;

- Chapter 1: A literature review related to the polymer nanocomposites, especially PET nanocomposite, water-assisted melt-mixing , solid state polymerization of PET and the objectives of this dissertation
- Chapter 2: Methodology; materials, processing conditions and characterizations
- Chapter 3: Organization of the articles
- Chapters 4, 5, and 6: Three papers containing the main results of this study
- Chapter 7: General discussion about the presented results
- Chapter 8: Conclusions and recommendations for future works
- Appendix: Slurry preparation method with the obtained results

CHAPTER 1 LITERATURE REVIEW

1.1 Permeation phenomena in polymers

Plastic films have been developed to prepare economic and efficient barrier materials to limit the passage of gases and organic liquids [15]. Generally, permeability rates of gases through any polymeric materials consist of three steps; a) absorption of the permeability species into the polymer, b) diffusion of the permeating species through the polymer, c) desorption of the permeating species from the polymer surface. Affecting parameters on the permeability are as: the solubility and diffusivity of the penetrate into the polymer, chain packing and side group complexity, polarity, crystallinity, orientation, filler and plasticization [15].

Figure 1-1 shows the oxygen and water vapor permeability of different polymers. Since PET is one of the desirable materials for food packaging and beverages, efforts have been done to improve the barrier properties of this polymer [15]. Different techniques have been used to enhance barrier properties of PET, including surface coating [1, 16], polymer blending [4, 17-20], using-oxygen scavengers' compounds [1, 21-23], anti-plasticization [3], crystallization and orientation [4, 17, 24, 25], and polymer nanocomposite preparation by adding nanolayer particles into the system [26, 27].

Silicon oxide (SiOx) films have good barrier properties, high transparency and microwave ability. Surface coating of PET films with plasma-enhanced chemical vapor deposition (PECVD) of SiOx films enhances PET barrier properties. On the other hand, these SiOx films are rigid thus causing cracking and adhesion problems in service [16]. Polymer blending of PET with high barrier polymers like ethylene vinyl alcohol copolymer (EVOH), poly(m-xylene adipamide) (MXD6), poly(ethylene 2,6-naphthalate) (PEN) as well as PET modification with isophthalic acid improves barrier properties of PET [4, 17-19]. Among those mentioned polymers, although EVOH has lower gas permeability than PET, it is more sensitive to humid atmospheres. While MXD6 does not have EVOH's limitation but its incompatibility with PET leads to haziness in the final product. Modification of PET with isophthalic acid reduces the linearity and crystallinity of PET chains but it decreases the permeability by suppression of phenyl ring flipping of isophthalic acid. Generally, the binary blends had poor mechanical properties due to lack of adhesion and

compatibility [4]. Presence of low molecular weight diluents in glassy polymers which is referred to as plasticization leads to an increase of elongation at break and a reduction of modulus. On the other hand, the low concentrations of those diluents result in anti-plasticization. It means a reduction of free volume and a suppression of polymer chains motions. Reduction of permeability in polymers is found by anti-plasticization effect. In the case of PET, Phenacetin and Aceranilide are loaded to PET samples at 35 °C. Consequently, oxygen barrier properties are improved 17% and 25% in PET containing 2.32 % phenacetin and 1.95% acetanilide, respectively. The enhancement of barrier properties is due to the reduction of free volume and the interaction energies of PET with those low molecular weight diluents [3]. Another approach is using active oxygen scavengers in PET films. PET compounds containing oxygen scavengers are obtained by melt-blending, reactive extrusion and/or direct polymerization of PET monomers. Oxygen scavengers can be unsaturated hydrocarbons like polybutadiene (PBD), materials with cycloalkene, or mono or di-unsaturated diols. The disadvantage of oxygen scavengers is the molecular weight loss or fragmentation due to the oxidative cleavage at the double bond [21-23]. By stretching the PET films, PET chains are aligned and strain-induced crystallization happens. Impermeable crystalline regions affect the oxygen permeability by increasing the tortuous path through polymer [4, 24] but crystallinity induces brittleness and reduces the transparency. Orientation of PET blends also enhances the barrier properties by transformation of spherical dispersed phase, MXD6, to high aspect ratio laminar morphology [4, 25]. Recently, improvements in barrier properties of polymer matrix by the presence of organoclay have been reported [28-36]. In polymer/layered silicates nanocomposites, both solubility and diffusivity of penetrate; gases and liquids, into the polymer matrix are decreased. Reduction in solubility is due to the decrement in polymer volume, while reduction in diffusivity is because of more tortuous path, which is illustrated in Figure 1-2. However, the portion of solubility is lower than diffusivity [37]. Finally, the increase in tortuous path is controlled by volume fraction of nanoparticles, their orientation to the diffusion direction, their shape and aspect ratio as well as their degree of dispersion [38]. Thus, more resistance to permeation of penetrates through the polymer matrix occurs in the exfoliated microstructures compared to the intercalated due to the higher tortuous path.

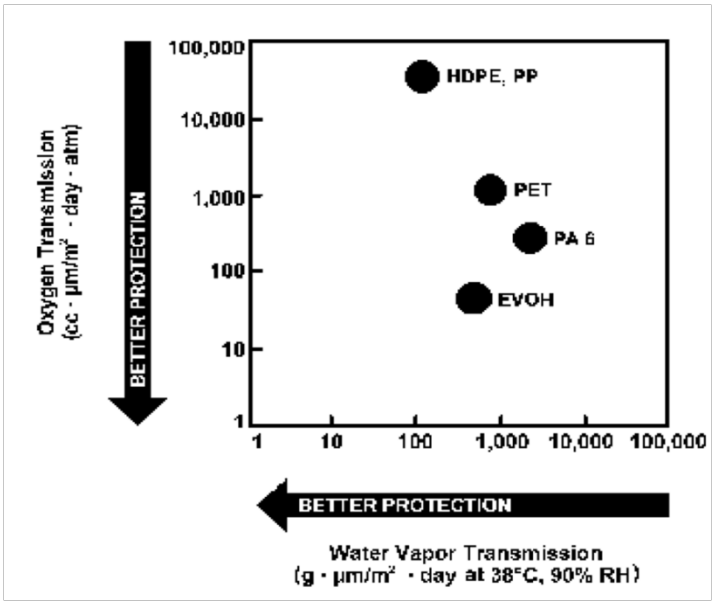

Figure 1-1 : The Oxygen and vapor permeability of different polymers [15].

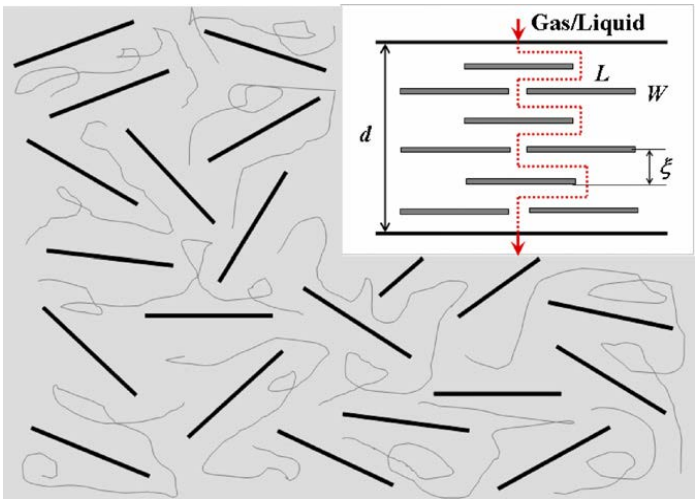

Figure 1-2 : Schematic of exfoliated polymer nanocomposites with randomly dispersed silicate platelets in a polymeric matrix. The inset illustrates the detour model proposed by Nielsen, a bricks-and-mortar idealization, in which molecules of gas/liquid pass through the matrix filled with parallel and staggered platelets along a tortuous path [38].

1.2 Structure of layered silicates

Clay known as montmorillonite (MMT) is often used for polymer nanocomposites and it belongs to phyllosilicates or 2:1 layered [5, 9, 39]. The layer thickness of MMT is 0.94 nm and its lateral dimensions are most probable between 100-200 nm. Montmorillonite contains one octahedral layer consisting of hydroxyl groups, oxygen, aluminum, iron, and magnesium atoms placed between two silicate tetrahedral layers with a central silicon atom and four oxygen atoms or hydroxyl groups (shown in Figure 1-3). Due to stacking of silicate layers, a regular van der Waals gap is formed which is called interlayer or gallery. Study of the crystal structure of the silicate shows the interlayer distance is 0.96 nm. Layers of silicate containing aluminum oxide with three valent aluminum atoms are replaced with divalent magnesium, create negative charges in the plane of the platelets that are counterbalanced with positive sodium cations. The excess negative charge of layered silicates leads to their capability to exchange ions can be quantified by the cation-exchange capacity (CEC) and expressed in mequiv/g. Montmorillonite expands and swells in water. Two specific characteristics of MMT in polymer nanocomposites are the ability to disperse into single layers and to exchange of sodium ions with their organic cations to form organomodified nanoclays. The organic cations increase the gallery spacing of nanoclays, lower the surface energy and increase the chance of the interaction with the polymer matrix [5, 9, 39].

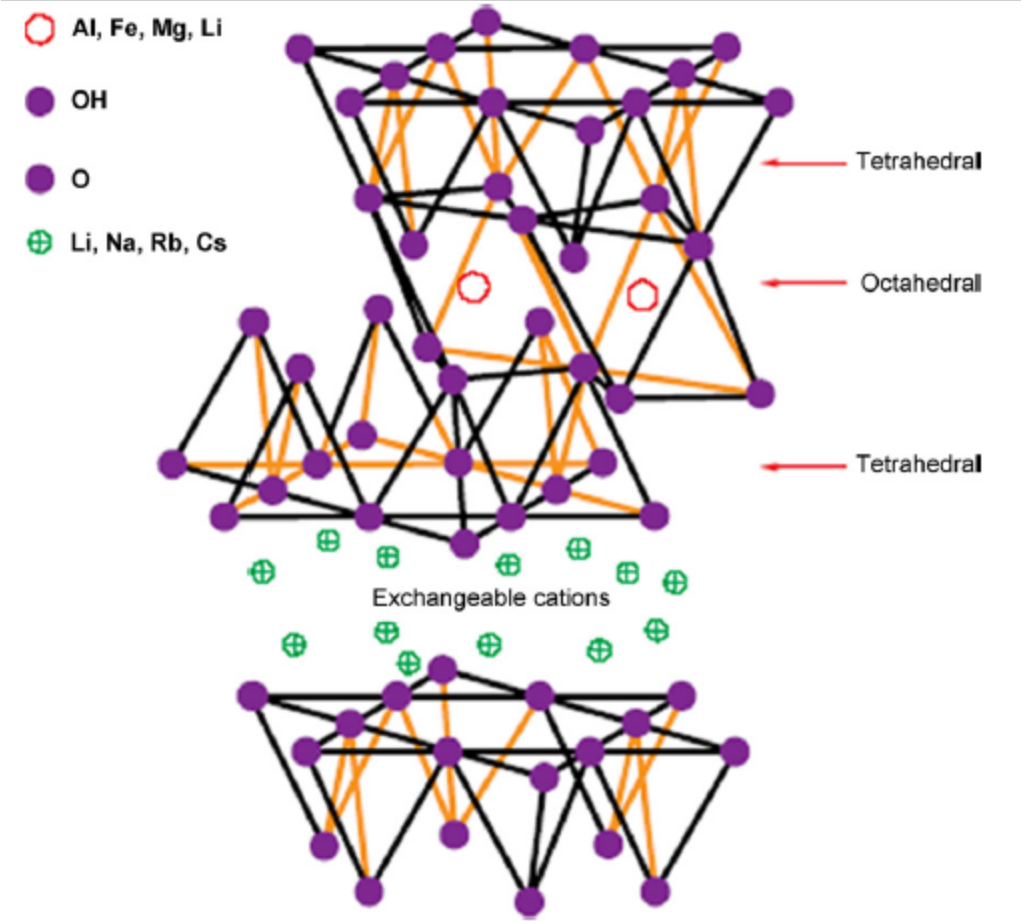

Figure 1-3 : The structure of a 2 :1 layered silicate [39].

1.3 Polymer nanocomposites

Preparation methods of nanocomposites are in-situ polymerization [6, 40-43], solution [44-46] and melt-mixing [8, 47, 48]. Melt-mixing is more favorable than the other preparation methods since, this is more environmental friendly due to the absence of organic solvent and monomers, more economical and more compatible with current industrial process. Therefore, depending on the processing conditions and importantly thermodynamic compatibility between nanoclays and polymer matrix, three kinds of microstructure are formed; immiscible, intercalated and exfoliated [49]. In the immiscible microstructures, nanoclays remain in the tactoids form and no opening of gallery spacing takes place, hence microcomposites are obtained. In exfoliated

nanocomposites, clay layers are dispersed into the polymer matrix in the form of single layers; in this morphology the *d*-spacing of nanoclays is larger than the wide angle X-ray detection (8-10 nm). Intercalated microstructure is formed due to the insertion of a polymer chains into the layered silicate structure but complete separation of clay platelets does not occur. In this case, the *d*-spacing of organoclays is larger than the pristine organoclays but less than exfoliated microstructures. Generally, diffusion of polymer chains into the gallery of nanoclays involves a significant entropy penalty that an energetic interaction between the polymer and the modifiers of nanoclays outweighs the entropic losses.

Achieving an exfoliated microstructure is a golden goal to maximize the interactions between polymer and nanoclays and consequently obtain significant improvements in the properties.

1.4 PET nanocomposites

In-situ polymerization of PET nanocomposites relies on first swelling of the organoclay by the monomer of PET, followed by an in-situ interlayer polymerization; therefore polymerization in the clay galleries facilitates the clay exfoliation. High polymerization temperature of PET, above 280 ºC, leads to decomposition of the modifier of organoclays and alteration of the interface between PET and clay [50]. On the other hand, unmodified nanoclays do not have an appropriate compatibility with PET [51]. High shear forces in the melt-mixing of PET with organoclays are also induced thermal degradation of both PET and organoclays [52]. Thus, many efforts have been made to the preparation of thermally stable organoclays and/or the compatibility improvements between PET and organoclays.

1.4.1 Effect of organoclay modifier and compatibilizers on PET nanocomposites

Chen et al. [51] used the monomer of PET (bis (hydroxyethyl) terephthalate (BHET)) to modify the Na-MMT. Nanodispersion and intercalated morphology were observed in nanocomposites containing BHET modifications. Transparency of the PET films with modified

nanoclays was the same as neat PET. In Zhang's research work [7], the montmorillonite was modified with hydroxypentyltrimethylammonium iodide (HPTA), then the modified MMT was copolymerized with bis(hydroxyethyl) terephthalate (BHET) to obtain PET nanocomposites with good optical and mechanical properties. XRD patterns indicated *d*-spacing increment of modified nanoclay and exfoliated microstructure of PET/HPTA-MMT nanocomposites. In addition, the transparency of the modified nanocomposites was like the neat PET, while the unmodified nanocomposites had less transparency. A 58 % improvement in tensile strength was also reported for modified PET nanocomposites containing 10 wt% of MMT compared to the neat PET.

The effect of hydroxyl groups and ammonium linkage of organoclay on the microstructure and molecular weight of PET nanocomposites obtained by melt-mixing was studied by Xu et al. [53]. Surface of sodium montmorillonite (Na-MMT) was modified with different chemicals such as acid, silane and alkyl ammonium groups as shown in Figure 1-4. Modified nanoclays with acid groups had large amount of hydroxyl groups which intensified the amount of polymer degradation during melt processing; intrinsic viscosity was reduced from 80 ml/g in neat PET to 30 ml/g in the presence of 5wt% of modified nanoclays with acid groups. On the other hand, molecular weight reduction in the nanocomposites containing modified organoclays with silane was the lowest due to the high thermal stability of silane groups and less amount of hydroxyl groups in nanoclay edges. PET nanocomposites containing organoclays modified with ammonium showed more degradation than modification with silane groups, indicating the decomposition of alkyl ammonium compounds at high temperature and the formation of acidic sites produced by Hofmann elimination reaction. Among the modified nanoclays, the largest *d*-spacing was 2.04 nm in PET nanocomposites containing nanoclays modified with ammonium. [53]. Xu et al. [53] also reported that, the presence of 0.35 wt% of chain extender (pyromellitic dianhydride(PMDA)) retarded the PET degradation in PET /organoclay nanocomposites (shown in Figure 1-5) while it did not have any effect on *d*- spacing of organoclays.

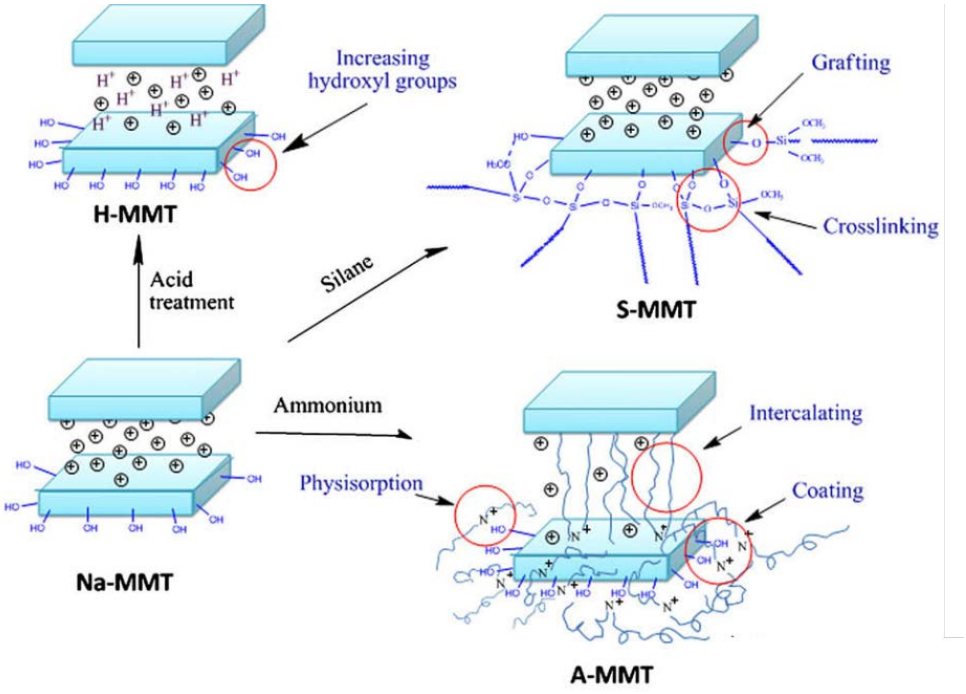

Figure 1-4 : Preparation of clays with different contents of hydroxyl groups on the edge of clay platelets and ammonium linkage on clay [53].

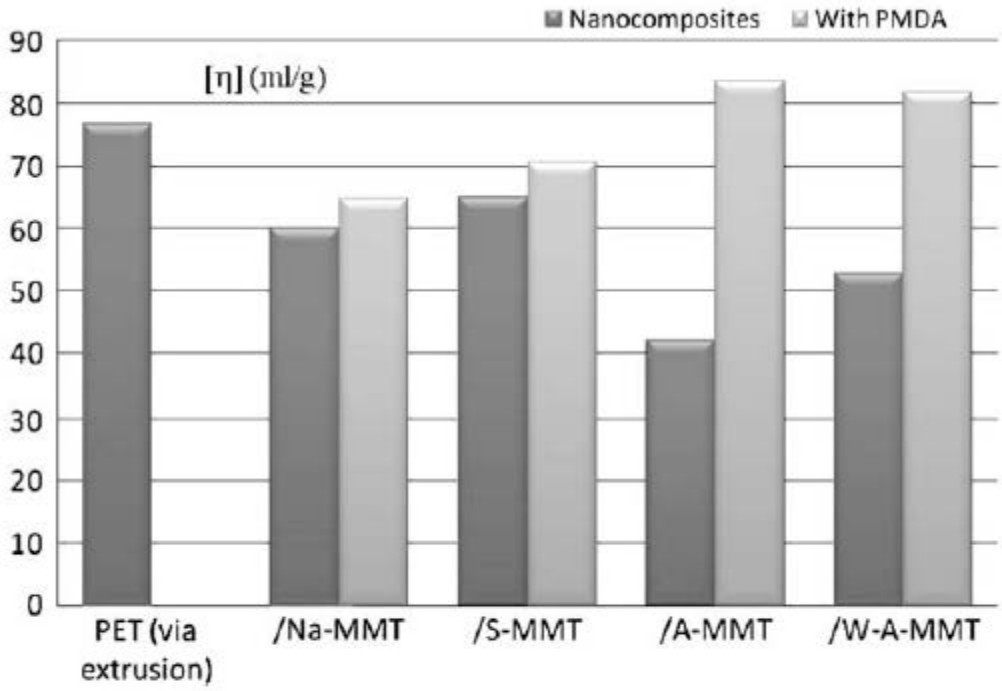

Figure 1-5 : Viscosity of PET and PET/clay nanocomposites by PMDA chain extender [53]. W-A-MMT represents washed nanoclays modified with ammonium groups.

Sanchez et al. [54] studied a series of melt blended PET/Na^+-MMT nanocomposites containing different additives. The additives were maleic anhydride (MAH), pentaerythritol (PENTA) and alkylammonium cholorides from amines of various chain lengths.

XRD results of organoclays showed that the gallery spacing of montmorillonite changed according to the type of modifier and amine chain length (Table 1-1). No peaks appeared in PET nanocomposites containing 1-3% wt of unmodified Na^+-MMT and Na^+-MMT modified by PENTA and MAH, whereas in Na^+-MMT modified by alkyl ammonium, *d*-spacing was dependent on the amine chain length. The largest distance was obtained using n-octadecylammonium.

Table 1-1 : Effect of the intercalant on clay interlayer distance [54]

Clay-intercalants	d_{001} (Å)
Montomorillonite	12.4
Montmorillonite-PENTA	14.5
Montmorillonite-MAH	12.4
Montmorillonite-n-Decacylammonium	17.1
Montmorillonite-n-Dodecylammonium	17.8
Montmorillonite-n-Tetradecylammonium	17.6
Montmorillonite-n-Octadecylammonium	23.0

Mechanical properties of PET nanocomposites containing Clay-MAH and Clay-PENTA showed that MAH and PENTA additives did not have any significant influences on improving the mechanical properties but by increasing the nanoclay concentrations, Young's modulus intensified and strain at break reduced. In this study [54], the effect of combination of Clay-MAH and Clay-PENTA (3:1 ratio) in PET nanocomposites was also investigated. By the presence of 1% wt of the mentioned modified nanoclays, both Young's modulus and strain at break increased 22% and 73%, respectively.

The mechanical results of PET nanocomposites containing modified nanoclays with different alkylammonium chain lengths are presented in Table 1-2. The exfoliated nanocomposites showed the considerable improvement in strain at break and tensile strength compared to the neat PET. Furthermore, the typical ductile fracture was found in the exfoliated samples, while the fragile fracture was observed in the intercalated samples.

Table 1-2 : Effect of intercalated Alkylammonium clays on tensile properties of PET and clay interlayer distance in the nanocomposite [54].

Samples	Tension Strength MPa	Strain at Break %	Young's Modulus MPa	d_{001} Å
PET extruded	47	150	1091	
PET + 1% clay-n-Decacylammonium	64	99	1336	Exfoliated
PET + 1% clay-n-Dodecylammonium	64	292	1319	Exfoliated
PET + 1% clay-n-Tetradecylammonium	46	6	1392	34.0
PET + 1% clay-n-Octadecylammonium	59	57	1376	33.8
PET + 2% clay-n-Decacylammonium	36	3	1466	23.1
PET + 2% clay-n-Dodecylammonium	7	7	1375	22.2
PET + 2% clay-n-Tetradecylammonium	57	10	1344	31.5
PET + 2% clay-n-Octadecylammonium	54	24	1423	32.5

To enhance compatibility between nanoclays and PET, Ammala et al. [10] used water dispersible PET ionomer. Two organomodified nanoclays (Cloisite 10A and Somasif MEE) and an unmodified nanoclay (Somasif ME100) were studied. In this work, an aqueous suspension of nanoclays and PET ionomer in water was prepared. The suspension was poured onto the PET and mechanical stirred with heat until water was evaporated. Finally, the PET nanocomposites were processed in a twin screw extruder.

An improved dispersion of nanoclays was found in the PET nanocomposites containing ionomer because of the ionic interactions between ionomer and nanoclays that assists to easier delamination of nanoclays. TGA results revealed the greatest degree of thermal decompositions in Cloisite 10A and the highest thermal stability in unmodified nanoclay than the organomodifed nanoclays. On the other hand, color of the PET nanocomposites obtained by unmodified nanoclay was the clearest than those with organomodified ones. However, chemical modification was necessary to achieve to the exfoliated microstructures that in this work was obtained by the presence of PET ionomer.

Xu et al.[55] also reported the improvement of Nanomer I28E dispersion in PET nanocomposites containing PET ionomer. However, lower tensile modulus in nanocomposites containing ionomer was found compared to the PET nanocomposites without ionomer, indicating the plasticization effect of ionomer. On the other hand, lower oxygen permeability was observed in nanocomposites with ionomer because of better dispersion and higher crystallinity. 19% and 20% improvements in barrier and tensile modulus of oriented PET nanocomposite films, respectively, were found with nominal 2wt% of organoclay.

The effect of 6 wt% PET ionomer (sulfopolyester) on the microstructure of PET nanocomposites containing 2wt% Cloisite 30B and Nanomer I.28E was also studied by Ghanbari et al. [56]. In nanocomposites with C30B and ionomer, clay dispersion and distribution became worse with the higher number of tactoids compared to the nanocomposites without ionomer since organoclays were located in the sulfopolyester phase. The degree of dispersion in nanocomposites with I.28E and ionomer was improved compared to the without ionomer. It could be due to the chemistry of the organomodifiers that C30B contains hydroxyl groups while the surface modifier of I.28E is octadecyl trimethyl ammonium.

The effect of organoclay modifier (Cloisite 15A, 30B and 10A) on the morphology of PET nanocomposites was reported by Calgano et al. [57]. Trend of surface hydrophobicity of organomodifers is C15A> C10A> C30B and the original *d*-spacing of organoclays before melt-mixing with PET is 1.85, 1.92 and 3.15 nm in C30B, C10A and C15A, respectively. After melt-mixing, *d*-spacing of all the nanocomposites was 3.39 nm due to the intercalation process that its extent was the highest in nanocomposites containing C30B. Intercalated/exfoliated microstructures were found in PET nanocomposites containing C30B and C10A but nanocomposites with C15A showed tactoids with a small amount of single layers. Exfoliation of clay platelets in polymer matrix during melt-mixing takes place by two mechanism; break-up and peeling. During melt-mixing, break-up occurs by imposing stress and shearing the big tactoids to smaller ones. Peeling is facilitated by polymer penetration into the galleries of organoclay, which is driven by affinity of the polymer to the organoclay surface [9]. Although the initial gallery spacing of C15A was larger than the other organoclays that could reduce the attraction forces between layers, unfavorable interactions between apolar groups of C15A with polar groups of PET restrict the intercalation process. On the other hand, the polar groups of C30B and C10A helped the diffusion of PET chains into the interlayers of organoclays[57].

Kim et al. [58] prepared PET nanocomposites with the same organoclays as Calgano's work [57]. Reduction of intrinsic viscosity in the nanocomposites containing Cloisite 30B was more than those with Cloisite 15A and Cloisite10A ; intrinsic viscosity was decreased from 0.68 dl/g in neat PET to 0.54, 0.58 and 0.61 in nanocomposites containing 3 wt% of C30B, C10A and C15A, respectively. Hydroxyl groups of Cloisite 30B could easily interact with polar groups of PET and accelerate the amount of degradation. On the other hand, more exposure of organoclays surfaces to PET matrix due to the better dispersion increases the thermal degradation [59].

1.4.2 Improvement of thermal degradation of PET nanocomposites

To improve the thermal stability of nanoclays to be useful for melt-mixing with PET, Stoeffler et al. [11] used alkyl phosphonium, alkyl pyridinium and dialkyl imidazolium surfactants. TGA results showed $T_{d\,5\%}$ of the modified nanocomposites increases from 291 ºC in

commercial Cloisite 20A to 364 ºC, 325 ºC and 349 ºC in phosphonium, pyridinium and immidazolium modified nanoclays, respectively. On the other hand, they reported that some dangerous volatile components were released before $T_{d\ 5\%}$ which limit the usage of these modifiers in some applications such as food packaging. Chloromethane was released in the range of 200–280 ºC in Cloisite 20A while Pyridine and tributyl phosphine were found above 250 ºC in modified clays with alkyl pyridinium and alkyl phosphonium, respectively. All of the mentioned modified nanoclays in this work caused PET discoloration (shown in Figure 1-6).

Formulation	Color	Aspect
PET		Transparent
PET/Cloisite Na^+		Opaque
PET/Cloisite 20A, original		Transparent
PET/Cloisite 20A, purified		Transparent
PET/$3C_4C_{16}$PBr–MMT		Transparent
PET/C_{16}PyBr–MMT		Transparent
PET/$2C_{18}$ImBr–MMT		Transparent

Figure 1-6 : Visual appearance of PET organoclay nanocomposites. $3C_4C_{16}$PBr, C_{16}PyBr and $2C_{18}$ImBr represent nanoclays modified by phosphonium, pyridinium and immidazolium, respectively.

Surface of nanoclay was modified with 1,2-dimethyle-3-N-hexadecyle imidazolium to increase its thermal stability and improve the compatibility between nanoclay and PET [14]. XRD of PET nanocomposites showed a great shift of major peak of hexadecyle-montmorillonite ($2\Theta \approx 5$) to lower 2Θ in the nanocomposites ($2\Theta \approx 3$). Moreover, TEM images displayed a good dispersion of organoclay platelets in the matrix. TGA thermograms of all samples also indicated that the presence of imidazolium did not have any effect on the inherent thermal stability of PET. This means that imidazolium was a good modifier for montmorillonite compared to quaternary alkylammonium compounds that intensified the level of PET degradation. Hayrapetian et al. [2] investigated the effect of polymeric imidazolium and sulfonated polyesters for the modification of nanoclays. Thermal stability increased to 330 ºC and 350 ºC in nanoclays modified with imidazolium and sulfonated polyesters, respectively, compared to 270 ºC in Cloisite 30B and Nanomer I.30T. Even though TEM images showed better dispersion of immidazolium than sulfonated polyesters but the improvements in the barrier properties of the nanocomposites containing sulfonated polyesters were more than those containing immidazolium. Water vapor transmission reduced by 22 and 30% in nanocomposites containing 5% of modified sulfonated polyester and immidazolium, respectively. Moreover, UV transmission was also decreased from 75% in neat PET to 25% in PET nanocomposites at 370 nm. Mechanical results showed that the presence of organoclays did not have any effect on tensile modulus due to the lack of good dispersion of organoclays into the matrix. The authors also reported that by these new modifications, transparency and clarity of PET nanocomposite films did not change compared to the commercial organoclays (Cloisite 30B and Nanomer I.30T). Ghasemi et al.[60] investigated the effect of three different modifications of nanoclays, phosphonium, immidazolium and C30B containing ammonium, in PET nanocomposites. The phosphonium based nanocomposites exhibited better thermal stability than ammonium and imidazolium-based nanocomposites; $T_{d\ 5\%}$ was 313-365 ºC in phosphonium, 271-288 ºC in imidazolium and 233 ºC in C30B. Phosphonium based nanocomposites showed a lower degree of intercalation than the ammonium (C30B) and imidazolium-based nanocomposites. Size of the agglomerates in the nanocomposites with phosphonium modified nanoclays was in the range of microns not nano. PET nanocomposites containing C30B showed better dispersion and distribution in PET matrix than the other modified nanoclays.

Costache et al. [61] reported the effect of hexadecyle-quinolinium bromide (Q16) and vinylbenzyl-ammonium chloride-lauryl-acrylate(L-surfactant) modifiers on the thermal stability of PET nanocomposites containing 3 wt% of montmorillonite(MMT). Structures of organo-modifiers are shown in Figure 1-7. XRD patterns and TEM images revealed an intercalated microstructure in PET/MMT-Q16 while an exfoliated microstructure was observed in PET/MMT-L due to the larger gallery spacing of MMT-L that PET chains could easily diffuse between the platelets and disperse the MMT layers. TGA analysis also demonstrated that thermal stability of the PET nanocomposites containing Q16 did not change compared to the neat PET, while the temperature of 10% mass loss in PET/MMT-L decreased 15°C in comparison to the neat PET.

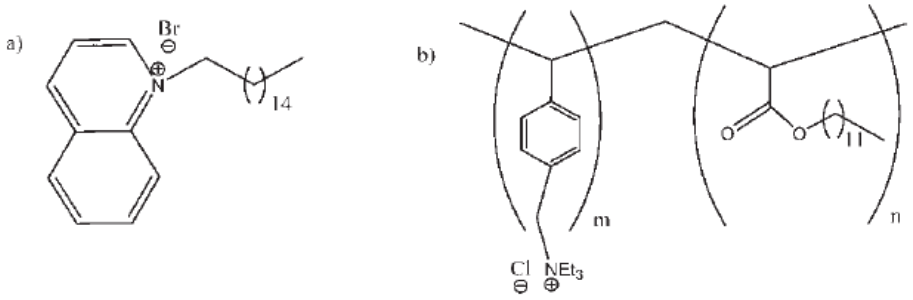

Figure 1-7 : Structures of hexadecyle-quinolinium bromide(Q16) (a) and lauryl acrylate-vinylbenzyl triethylammonium chloride (L-surfactant) (b) [61].

PET degradation in the presence of nanoparticles was also found by rheological measurements [52, 54, 55, 59, 62]. Ghanabri et al. [59] reported that by increasing C30B concentration, complex viscosity of PET nanocomposites at high frequencies became less than neat PET. Moreover, PET degradation was strongly dependent on the modifier of organoclays and the interactions between organoclay and PET. In low frequencies, solid-like behavior was found in PET/C30B nanocomposites containing more than 2wt% of C30B. An apparent yield stress was also observed in PET nanocomposites. Its value was strongly dependent on the level of dispersion and organoclay concentration. Reduction of complex viscosity in PET nanocomposites

was also investigated by Litchfield et al.[52] that the nanocomposites containing C30B showed more severe thermal degradation than those with C20A. Decomposition of modifiers of organoclays, at processing temperature of PET, to vinyl compounds, polyenes, ammonia, acetaldehyde with the formation of H protons and chain scission by alkyline hydrolysis of PET resulted in PET degradation in the presence of organoclays.

Ghanbari et al. [63] used multifunctional chain extender to control the thermal degradation of PET in the presence of organoclays. Delamination of organoclays was improved in the nanocomposites containing chain extenders due to the more shear forces induced by increasing the viscosity in the presence of chain extenders. A 46% reduction in oxygen permeability and a 60% enhancement in tensile modulus were found in the oriented PET nanocomposites containing 4 wt% of C30B and 1 wt% of chain extender. However, toughness was significantly decreased and the linear PET chains changed to the branched structure. Results of haze and clarity in this work showed that the presence of 1wt % of chain extender increased the haze from 10% in PET/C30B to 60% and reduced the clarity from 75% to 35%.

1.4.3 Processing of PET nanocomposites

The effect of organoclays on the mechanical properties of PET was studied by Frounchi et al. [31]. They applied two kinds of organoclays, Cloisite 15A (modified nanoclay with dimethyl, dihydrogenatedtallow, quaternary ammonium *d*-spacing: 3.1 nm, CEC:125 meq/100g) and NanolinDK2 (modified nanoclay with octadecylammonium, *d*-spacing: 2.4 nm, CEC:115-120 meq/100g). 1wt% of Cloisite 15A enhanced the tensile modulus 50% while NanolineDK2 did not have any significant effect on increasing the modulus. Effect of screw speed, 300 and 600 rpm, in nanocomposites containing 1wt% of Cloisite15A showed the same final properties in the nanocomposites obtained with two different screw speeds, indicating the higher thermal degradation of PET in high shear rates.

Ghasemi et al. [64] showed that the presence of 3 wt% C30B into the oriented PET films improved the barrier properties and tensile modulus 23% and 20% , respectively. The crystal

content of the PET nanocomposites was almost 2 times larger than the neat PET, partly accounting for the barrier and modulus improvements. On the other hand, tear resistance was significantly reduced in the nanocomposites compared to the neat PET. C30B delamination was also increased by using more intensive mixing elements, an increase of screw speed and a decrease of feeding rate [13], therefore, 27% reduction in oxygen permeability and 30 % enhancements in tensile modulus were observed. Enhancement of organoclay dispersion in PET nanocomposites by applying more mixing elements in twin screw extruder was also found by Ghanbari et al. [59].

Rajeev et al. [65] studied the effect of biaxial stretching on the orientation of organoclay and the properties of PET nanocomposites containing 2wt% of modified flouromica (Somasif MAE). Biaxial films were prepared by three different stretch ratios (2, 2.5 and 3). By imposing stretch on the nanocomposites, the number of nanoclay tactoids with smaller thickness and longer length was increased. TEM images showed a 10% increase in the number of tactoids with thickness around 1-2 nm in PET nanocomposites by biaxial stretching. In biaxially stretched PET nanocomposites, most of the tactoids had length more than 300 nm and nanoclays with length of 700 nm were appeared which were not observed in unstretched PET nanocomposites. This was due to the slippage of organoclay layers toward each other by the biaxial stretching. Moreover, the organoclays were chosen preferential tactoids orientation in stretched films whereas random orientation was pronounced in unstretched films. Decrement of oxygen permeability was found in the stretched PET nanocomposite films compared to the neat PET film, but the level of improvement in barrier properties was not significant. Dynamic mechanical thermal analysis (DMTA) showed the same value of storage modulus in neat PET and PET nanocomposites. The effect of biaxial stretching was also reported by Soon et al. [66] in PET/fluoromica nanocomposites. The biaxial stretching improved the orientation and exfoliation of nanoclays into the matrix (shown in Figure 1-8). By stretching ratio of 2 and 2.5 more improvement in modulus was found compared to the stretching ratio of 3. By increasing the stretching ratio, crystallinity and rigid oriented amorphous phase were also increased then the effect of tactoids alignment became less. Unstretched PET nanocomposites with 5wt% nanoclay showed 33% improvements in tensile modulus compared to the neat PET whereas in the stretched films with ratio of 2.5, the enhancements was 50%. Maximum 22% improvement in oxygen barrier

properties was also found in stretched PET nanocomposites with 5wt% organoclay. Based on DMTA results, storage modulus in temperatures higher than T_g and less than 120 ºC was more improved in nanocomposites than neat PET. Above T_g of PET, organoclays were rigid but PET chains were soft and they transformed from the glassy to rubbery state, thus, more reinforcing effect was observed. Soon et al. [67] in another work reported that the strain hardening started at lower stretch ratio in PET nanocomposites compared to the neat PET due to the higher degree of molecular entanglements in the presence of nanoclays. Shen et al. [68] reported 27% reduction in oxygen permeability coefficient and 44% increase in tensile modulus for biaxial oriented PET nanocomposites containing 6 wt% of modified fluoromica nanoclay, compared to neat PET. However, in unoriented films, the tensile modulus increased only 25% in nanocomposites.

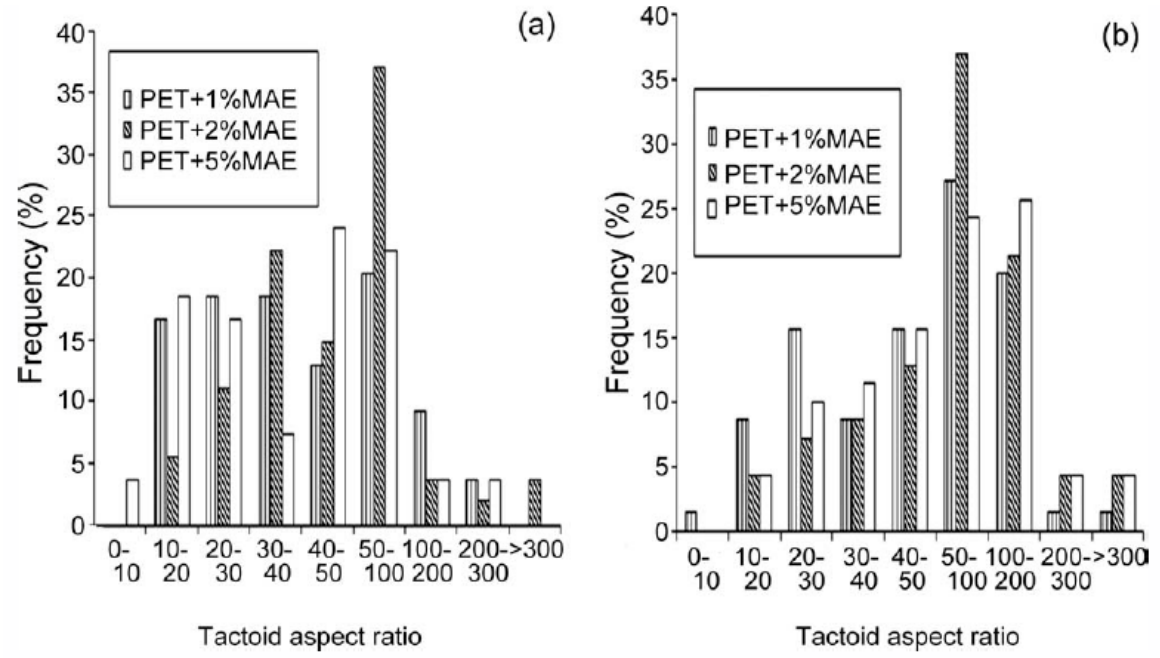

Figure 1-8 : Histogram of tactoids aspect ratio : a) unstretched nanocomposites, b) stretched nanocomposites (stretch ratio 3)[66].

The effect of super critical carbon dioxide ($scCO_2$) on mechanical and rheological properties of PET/organoclay nanocomposites was studied by Samaniuk et al. [69]. Nanocomposites containing Cloisite 20A and Cloisite 30B were processed in a single screw extruder. XRD results showed that the presence or absence of $scCO_2$ did not have any effect on the peak displacement of organoclays, while the intensity of peaks was reduced in the nanocomposites processed by $scCO_2$. Lower intensity was attributed to the more exfoliation. Young's modulus increased in all PET nanocomposites irrespective of the presence or absence of $scCo_2$. In PET/C30B nanocomposites with 5 wt% of organoclay, Young's modulus was improved 41% and 33 % in the PET nanocomposites processed with $scCo_2$ and without $scCo_2$, respectively. PET/C15A nanocomposites processed with $scCo_2$ showed 22% increase in Young's modulus with 5 wt% of C15A, compared to the neat PET. Tensile strength in nanocomposites containing C30B was higher than C20A because of the better compatibility between C30B and PET than C15A. Significant reduction of complex viscosity in whole frequencies was observed in the nanocomposites compared to the neat PET with the higher extent in PET nanocomposites containing C30B.

1.4.4 Effect of organoclays on the crystallinity of PET

Generally, heterogeneous nucleation, acceleration/retardation of crystallization, suppression of crystal growth and change in spherulite morphology were reported in polymer/organoclay systems [70]. Wan et al. [71] studied isothermal crystallinity of PET and its nanocomposites. Spherulitic structure with size 20 μm was found in neat PET but PET nanocomposites had irregular crystallites with size of 5 μm. In the nanocomposites, crystallites were formed rod shape and then they showed three-dimensional growth. On the other hand, crystal lattice parameters and crystallinity did not change (observed by XRD) while the crystal lamellar thickness was reduced with some imperfections due to the presence of nanoclays. Smaller crystallites with less perfection [72] and marginal effect of organoclays on the crystallinity were also found by DSC [2]. On the other hand, a reduction in cold crystallization temperature (T_{cc}) [73] and an increase in hot crystallization temperature (T_{hc}) [71] were found in PET nanocomposites without regarding to the interaction between organoclays and PET, indicating nucleating role of organoclays. It was reported that the rate of crystallization, reduction of $t_{1/2}$, in the presence of organoclay increased

[71-74], whereas the required work for chain folding and activation energy of crystal growth increased[72]. Stoeffler et al. [11] showed that the kinetics of nucleation and growth of crystallinity in PET nanocomposites were dependent on the dispersion state of organoclays in PET matrix and the interfacial properties of polymer/organoclays. The presence of double melting peaks was also observed in PET nanocomposites because of either two different lamella thicknesses, primary or secondary crystallization [75], or formation of smaller and imperfect crystallites in the presence of organoclays [2].

1.5 Water-assisted extrusion process

Water-assisted extrusion is an interesting method to prepare polymer nanocomposites using the benefits of both solution and conventional melt-mixing methods [76-83]. This method was successfully used to prepare polyamide (PA) - montmorillonite (MMT) nanocomposites with unmodified nanoclays with water content of 5 to 50 wt% and more preferably from 10 to 40 wt% [84, 85]. It is possible to prepare PA nanocomposites by simultaneous feeding PA and pristine clay into the twin-screw extruder then injecting water into the extruder [86]. Another possibility is to prepare clay slurry with water and feeding this suspension into the extruder to blend it with the molten PA [85]. Some researchers also reported significant effects of water injection into the TSE during the preparation of nanocomposites based on polypropylene (PP) and poly(styrene-co-acrylonitrile) [87, 88].

A research team from Toyota (Hasegawa et al.) [85] prepared PA/Cloisite Na^+ nanocomposites by slurry method. A suspension of 2 wt% of Cloisite Na^+ in water was injected into the twin-screw extruder to mix with molten PA. Configuration of screws allowed remaining water in liquid state and reducing the size of the slurry drops (shown in Figure 1-9). At the end of the extruder, water was evaporated by applying vacuum which also expanded the gallery spacing. PA nanocomposites obtained by this method showed mechanical properties close to PA/organoclay nanocomposites. However, the disadvantage of this work was a huge amount of water (49 wt %) pumped into the extruder to reduce the slurry viscosity. Yu et al. [84] reported a preparation of PA nanocomposites by injecting water into the extruder through the barrel while PA /nanoclay mixture fed simultaneously into the extruder. Tensile modulus of PA/Cloisite Na^+ nanocomposites containing 5 wt% of nanoclays processed with water increased 44% compared to

the neat PET while in PA/Cloisite Na^+ and PA/Cloisite 30B processed without water, tensile modulus increased 18% and 28%, respectively. An improvement of thermal stability was also observed in nanocomposites processed with water compared to the conventional melt-mixing.

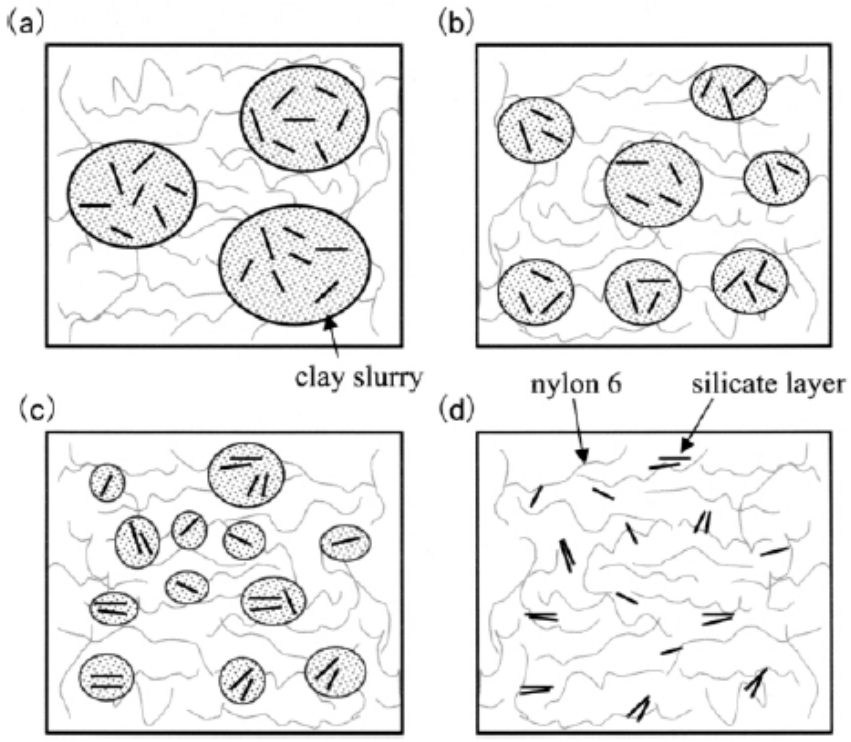

Figure 1-9 : Schematic figures depicting dispersion of the Na-montmorillonite silicate layers of the slurry into nylon 6 during compounding [85].

PA nanocomposites preparation under high pressure, temperature and shear-rate was studied by Touchaleaume et al. [80] and Fedullo et al. [79]. 66 ºC reduction of PA melting point without any degradation was found by water-assisted melt-mixing. Under high pressure, PA6 was miscible with water and the presence of water improved the dispersion of unmodified nanoclays. Polyamide chains can be water-solvated due to the hydrogen bonding. Under high temperature and high pressure both melting and crystallization temperature of PA6 were reduced in the presence of water which was called cryscopic effect [80]. DSC studies on PA, water systems showed two peaks at atmospheric pressure corresponding to water evaporation and melting point

of PA but by increasing the pressure (20 bar), one peak was found [79, 80]. In the extrusion process of PA with water in the final zone of extruder, there were both degassing and vacuum section to remove all the water and steam to avoid the presence of the voids in the final product. PA6/Cloisite Na^+ nanocomposites prepared by water-assisted showed similar microstructure to PA nanocomposites containing organomodified clay. The resulting mechanical performance of PA6/ Cloisite Na^+ was comparable to what was generally reported using modified nanoclays. [80]. Water played a plasticizer role for PA to diffuse between Cloisite Na^+ and consequently to expand the *d*-spacing of the clay layers. All of those promoted PA penetration into the nanoclay's interlayers. Figure 1-10 shows the efficient effect of water-assisted melt-mixing on limiting the degradation of PA under melt-mixing processing. Higher molecular weight of neat PA processed with water compared to the conventional melt-mixing showed that the thermal degradation of PA in the presence of water was less than conventional melt-mixing.

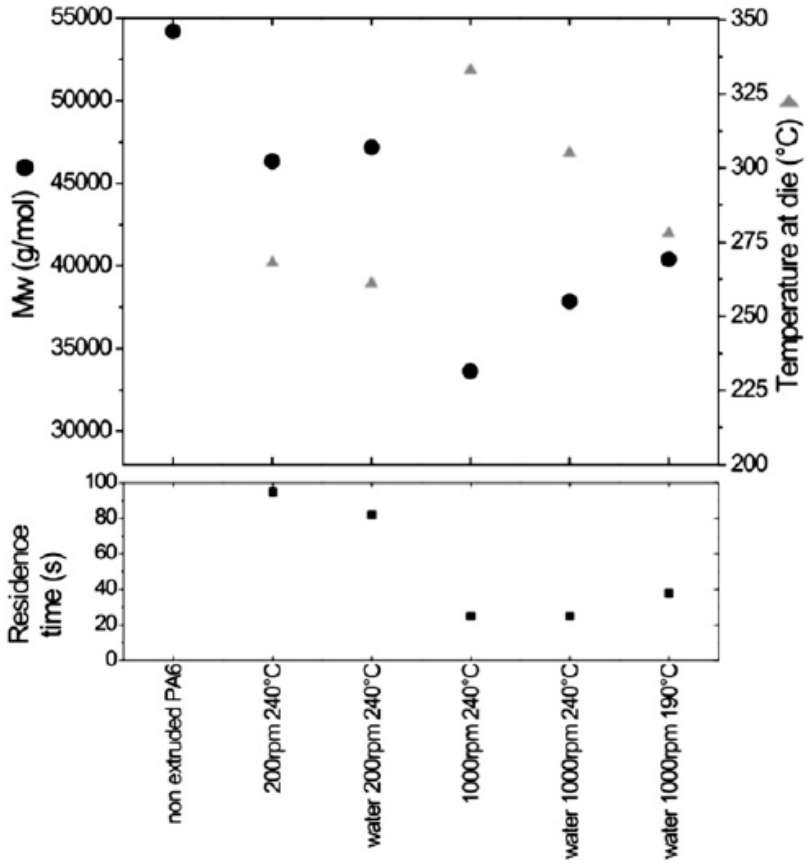

Figure 1-10 : Molecular weight, melt temperature at the die and residence time of PA6 extruded using various processing conditions[80].

The effect of water-assisted extrusion was investigated in polyether-block-amide (PEBA) nanocomposites. Touchaleaume et al. [89] showed that the amide part of the PEBA was miscible with water at high temperature and high pressure which improved the dispersion of unmodified and modified nanoclays in the matrix as well as reduced the amount of the matrix degradation during melt-mixing. Dynamic mechanical thermal analysis (DMTA) showed that the modulus of unmodified nanoclay processed by water-assisted was higher than modulus in conventional melt-mixing. Furthermore, microcomposites were found in PEBA containing unmodified nanoclay prepared by conventional melt-mixing while nanocomposites were obtained in water-assisted melt-mixing. In another work, Thouzeau et al. [90] reported an efficient effect of water to remove volatile moieties of the extrusion-degraded surfactant. As shown in Figure 1-11, odours

quantification is 8 times higher in PEBA/C30B nanocomposites prepared by conventional melt-mixing compared to the processing in the presence of water. Odour quantification was determined using Dynamic dilution olfactometry (DDO) at detection threshold with calibrated human assessors according to the EN 13725 European standard. It presented a common basis for evaluation of odour emissions with a universal odour scale based on a common unit of measurement: the European odour unit per cubic metre or OUE/m^3.

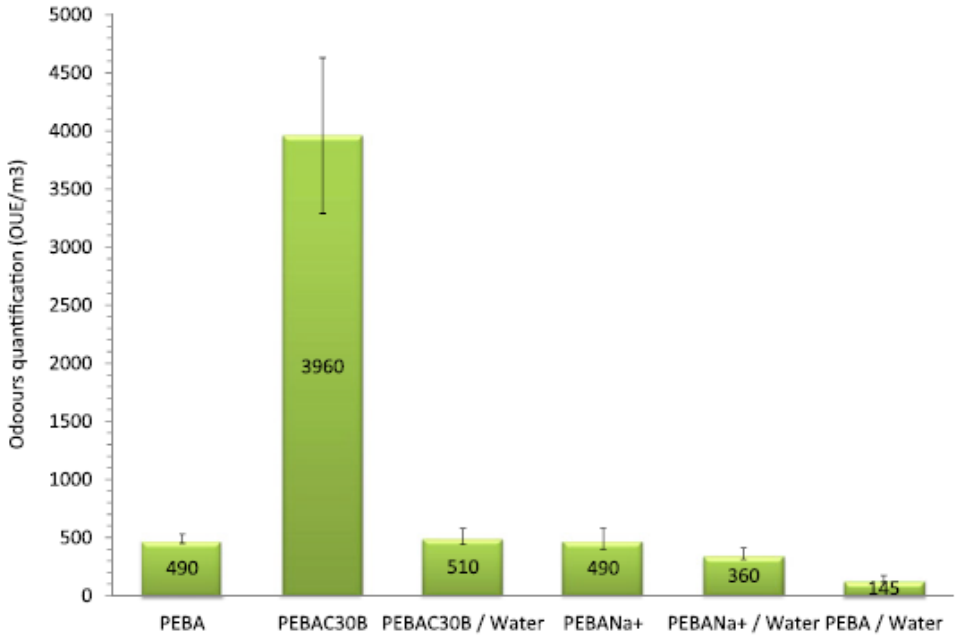

Figure 1-11 : Odours quantification in PEBA and its nanocomposites processed with and without water [90].

Water-assisted extrusion process was used to prepare PP/Cloisite 30B /PP-g-MA nanocomposites [87]. It was found by FTIR that the presence of water favors the reaction between C30B and MA of PP-g-MA. TEM images and mechanical properties showed significant improvements in dispersion and properties of nanocomposites processed with water compared to without water. In nanocomposites containing 5 wt% of C30B, maximum tensile modulus was 75% more than the

matrix in processing with water and 33% in processing without water. In the case of PP, rheological results of PP with and without water showed no degradation of PP or PP-g-MA in the presence of water. Rousseaux et al. [91] prepared PP nanocomposites containing unmodified halloysite nanotubes with water-assisted process. The presence of water caused an aqueous suspension of halloysite with improved nanodispersion. On the other hand, hydrolysis of anhydride group of PP-g-MA to carboxyl groups resulted in a reaction between this forming groups with SiO of nanotubes.

Poly(styrene-co-acrylonitrile) (SAN) nanocomposites was prepared through water-assisted melt-mixing by Mainil et al.[88]. Water was introduced at a rate of 23 wt%. For Cloisite Na^+ nanocomposites, the nanoclay dispersion was significantly promoted but because of lack of the chemical compatibility between Cloisite Na^+ and SAN, thermal and mechanical properties did not improve. Water enhanced C30B dispersion in SAN as well as improvements in mechanical and thermal properties compared to the nanocomposites without water.

1.6 Solid-state polymerization of poly (ethylene terephthalate)

PET production starts with an esterification reaction step where the terephthalic acid or its dimethyl ester, is dispersed in ethylene glycol and heated to produce a mixture with oligomers of a low degree of polymerization [92]. Polycondensation occurs at relatively high temperatures, generally in the range of 280-300 ºC, under vacuum so that byproducts (i.e., ethylene glycol and water) formed to be easily removed. The obtained PET at the end of polycondensation exhibits a relatively low intrinsic viscosity value, in the range of 0.4-0.65 dL/g, corresponding to a molecular weight too low for specific applications such as high performance plastic strapping and applications as carbonated soft drink bottles, etc. Since for plastic strapping high tensile strength is required to substitute steel strap, therefore PET should have high intrinsic viscosity more than 0.7 dl/g.

In order to achieve a higher molecular weight polymer, the previously described step is followed by the second step of polycondensation known as solid-state polymerization (SSP) [92, 93]. Generally, SSP is applied to increase the molecular weight of PET and to decrease its

degradation [94]. Solid state polymerization takes place at moderate temperatures between the melting point and the glass transition temperatures of PET. By this method, the amount of degradation and by-products are decreased and larger intrinsic viscosity than 0.8 dL/g are obtained [95-100]. In the solid-state process, PET polymerization is accomplished by two reversible reactions as follows (Figure 1-12):

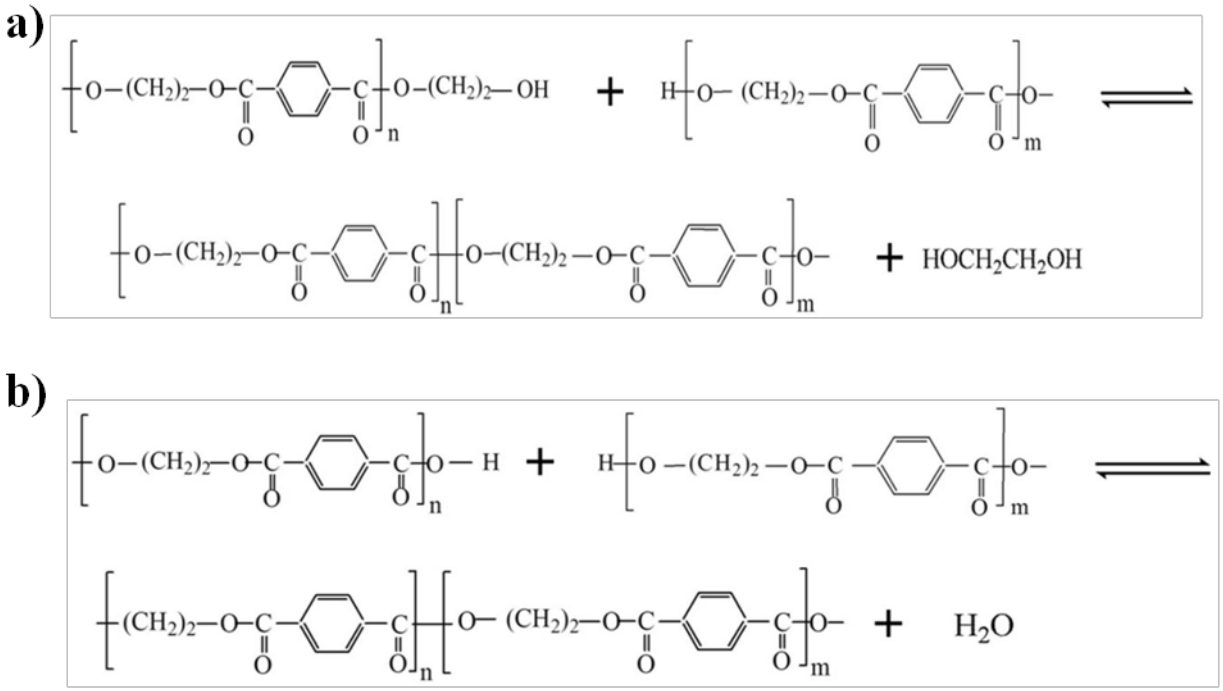

Figure 1-12 : SSP of PET; (a) Ester-interchange (transesterification), (b) esterification reactions.

The molecular weight of PET increases during solid state polymerization, this process is controlled by two types of diffusion. The diffusion of reaction by-products (physical diffusion) determines the rate of the forward reactions and the diffusion of end-groups (chemical diffusion) allows the reaction to proceed. These two types of diffusions are dependent on different parameters, such as: molecular weight of pre-polymer, particle size, temperature, polymer end

groups, catalyst, heat stabilizer and crystallinity of PET [96-103]. Both granule and powder forms of PET are used for SSP but as the particle size is decreased the rate of SSP is increased. The rate of SSP is also increased by increasing the temperature below the melting point of PET.

Achilias et al. [104] studied the effect of SiO_2 nanoparticles on SSP reaction rate. PET nanocomposites containing different concentration of SiO_2 were prepared by in-situ polymerization.

Figure 1-13 showed the rate of SSP process in the neat PET and the nanocomposites. The rate of SSP in the nanocomposites containing less than 1 wt% of SiO_2 was higher than neat PET due to the catalyst role of SiO_2 and the reaction of surface silanol groups with PET. Contrary to these results, when the concentration of SiO_2 increased to more than 1wt%, the rate of SSP decreased significantly compared to the neat PET (shown in Figure 1-14) due to the formation of branched macromolecules in the presence of multifunctional groups of SiO_2 and cross-linking structure instead of increasing molecular weight [105]. On the other hand, crystallinity increased in the presence of SiO_2, hence, the rate of diffusion and SSP process were reduced [104]. By increasing the SSP temperature, the rate of SSP was also increased in both neat PET and PET nanocomposites because of the increasing rates of transesterification and esterification reactions, and diffusion rates of by-products.

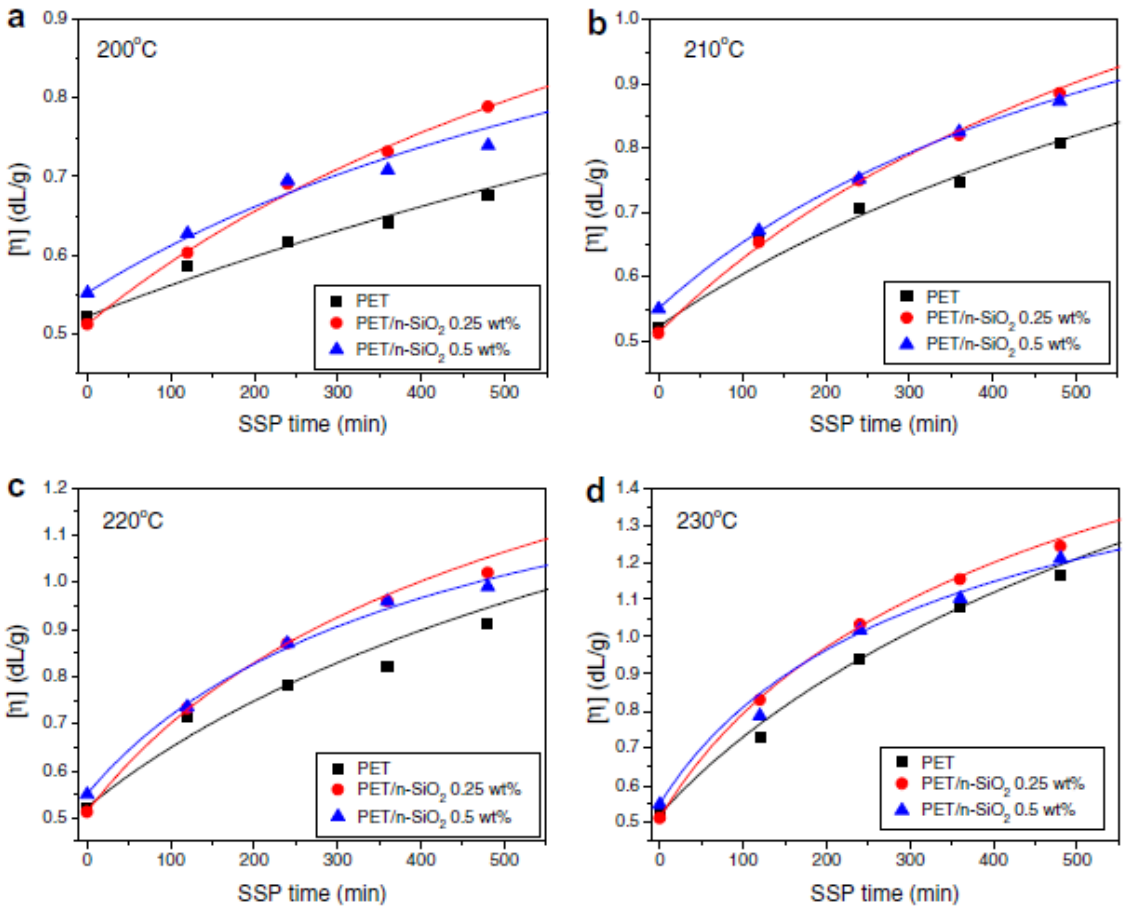

Figure 1-13 : Variation of intrinsic viscosity with time during the SSP of neat PET and PET containing nanosilica 0,25 and 0,5 wt %, at temperatures 200 (a), 210 (b), 220 (c) and 230 ºC (d) [104].

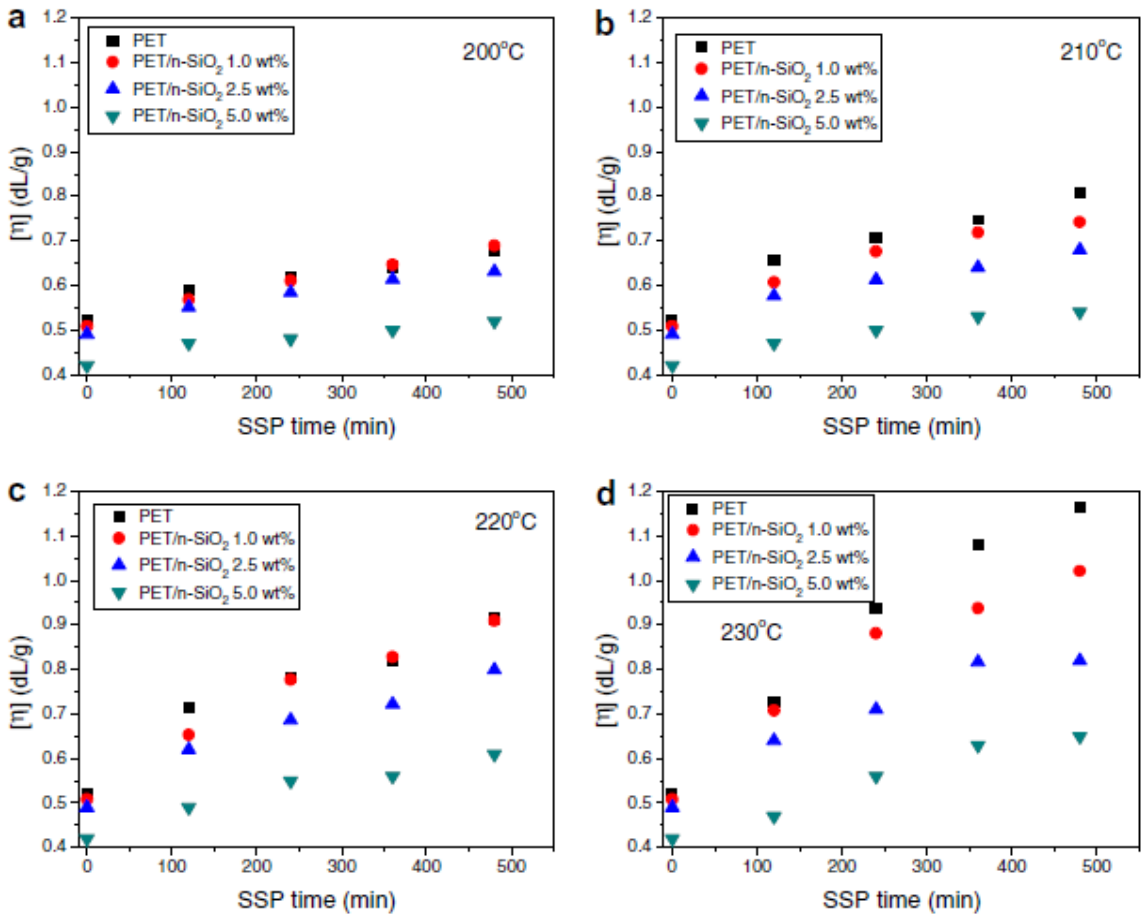

Figure 1-14 : Variation of intrinsic viscosity with time during the SSP of neat PET and PET containing nanosilica 1, 2.5 and 5 wt %, at temperatures 200 (a), 210 (b), 220 (c) and 230 ºC (d) [104].

The effect of PET molecular weight and chemistry of organomodifier on the SSP reaction after melt-mixing were investigated by Kim et al. [106]. They worked on PETs with three different intrinsic viscosities (0.48, 0.63, and 0.74 dL/g) containing 3 and 5 wt% of Cloisite 10A, 15A, and 30B. A significant reduction of PET molecular weight was observed after melt-mixing with organoclays while PET degradation was compensated after SSP. For example, intrinsic viscosity of neat PET was reduced from 0.74 dL/g to 0.55 dL/g in the presence of 3wt% of C30B but after 15h of SSP; intrinsic viscosity of that PET/C30B nanocomposite was 0.73 dL/g. The lowest

molecular weight PET nanocomposites containing C30B showed larger gallery spacing of organoclays after SSP due to the interaction between hydroxyl groups of C30B and the chain end groups of PET. Solid state polymerization (SSP) of PET nanocomposites obtained by in-situ polymerization was also studied by Kim et al. [107]. To prepare PET /organoclay nanocomposites by in-situ polymerization, organoclays could be added with monomers during the early stage of esterification (ES) or the early stage of transesterification of BHET (PC) (shown in Figure 1-15). Figure 1-16 shows that there is no difference in the rate of SSP by feeding order of organoclay whereas the SSP rate was strongly dependent on the interaction between the organoclays and PET. In other words, higher rate of SSP was also found in the nanocomposites containing Cloisite30B compared to the other nanocomposites. XRD patterns of PET nanocomposites before SSP showed one peak at $2\Theta=5.6°$ related to the degradation of organoclays. When organoclays are added in esterification reaction, the intensity of the XRD peak at $2\Theta=5.6°$ is higher than adding the organoclays in polycondensation step. This is due to the shorter residence time that organoclays faced with in polycondensation compared to early stage of esterification. The authors claimed that *d*-spacing of organoclays increased to some extent after SSP in the samples containing Cloisite10A and Cloisite30B whereas in samples with Cloisite15A no change was observed. The displacement of XRD peaks could be related to an increase of PET molecular weight and/ or diffusion of the PET chains into the organoclays' gallery [107].

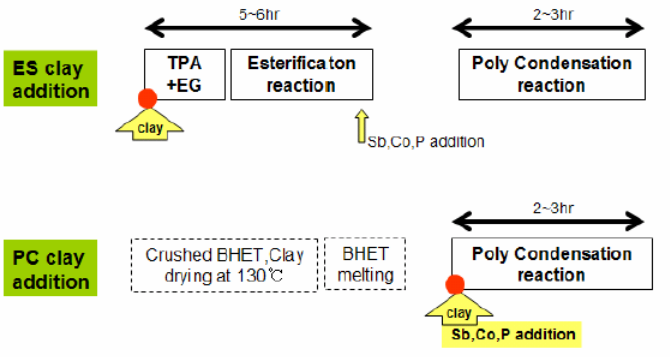

Figure 1-15 : Detailed process of clay addition before esterification or polycondensation [58].

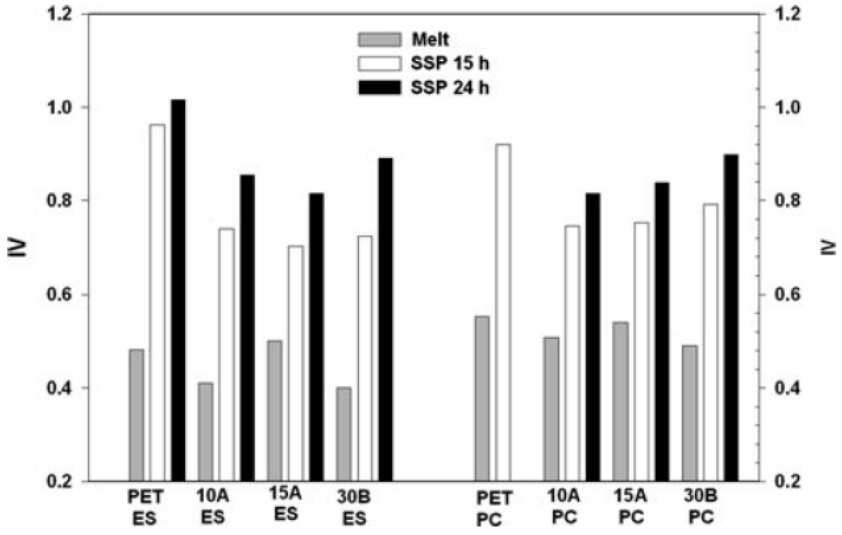

Figure 1-16 : Relative intrinsic viscosity (IV) values are shown for samples prepared through the esterification (ES) clay addition process and the polycondensation (PC) clay addition process. Values are given before SSP and after SSP at 230 ºC for 15 and 24h [107].

Wang et al. [108] worked on the preparation of PET and poly(m-xylylene adipamide)(MXD6) nanocomposites containing Cloisite Na^+ by water-assisted method. Slurry of nanoclays in water was prepared and pumped into the extruder. After extrusion process, SSP was done to increase the molecular weight of the nanocomposites. By this method, exfoliated microstructures were found in PET nanocomposites with 0.5 wt% to 2 wt% of nanoclays but intercalated/exfoliated microstructures were observed with 3wt% and 5 wt% of nanoclays. In MXD6 nanocomposites, exfoliated microstructures were detected even in high concentration. Oxygen barrier properties were increased by 50% in PET nanocomposites with 2wt% of nanoclay and 70% in MXD6 nanocomposites containing 3 wt% of nanoclay. Accelerated crystallization rate and nucleation effect of nanoclays were found in both PET and MXD6 nanocomposites while T_g and T_m were slightly increased.

The effect of SSP on the mechanical and rheological properties of PET nanocomposites after melt-mixing to rebuild the lost molecular weight was studied by Litchfield et al. [15]. SSP was

done in reaction times from 10 h to 50 h but no improvements in the intercalation process were found. Cloisite 20A was better intercalated in PET than C30B and the rate of C30B degradation was higher than C20A. After SSP lower molecular weight obtained in C30B nanocomposites than C20A due to the more degradation of C30B. The presence of organoclays affected on the drawability of PET, changed the crystallinity, and oriented the amorphous phase and/or connectivity of amorphous and crystalline chains. PET nanocomposites containing 1wt% of organoclays showed better mechanical results than 3wt% and 0.5 wt%. Molecular orientation of PET chains at small loadings of clay (0.5 wt %) was less than 1wt% and premature fibers were formed in nanocomposites with 3wt% of organoclays due to the large agglomerates of organoclays. Young's modulus and strength increased 28% and 63%, respectively in drawn PET fiber containing 1wt% of Cloisite 20A.

In summary, extensive research works have been devoted to enhance the barrier and mechanical properties of PET nanocomposites. It was found that the properties of PET nanocomposites were strongly dependent on the level of organoclay dispersion. However, degradation of the modifier of organoclays and inappropriate compatibility between organoclay and PET decreased their properties in both in-situ polymerization and melt-mixing. Thus, the effect of different compatibilizers, thermally stable organoclays and chain extenders were investigated. Nevertheless, the modest improvements in barrier and tensile modulus of PET nanocomposites were found while all of the obtained PET nanocomposites suffered from the brittle behavior. Therefore, there are still some demands to develop a new method for preparation of PET nanocomposites with exfoliated microstructure and good barrier and mechanical properties.

1.7 Objectives

The main objective of this work was ***"to improve the barrier properties of poly(ethylene terephthalate)/organoclay nanocomposite via melt-mixing"*** with intended applications for

single layer packaging to be used in food and beverage containers with high barrier and good mechanical properties.

To achieve to this goal, water assisted melt-mixing was used to prepare PET nanocomposites using the benefits of both solution and conventional melt-mixing methods to improve the organoclay dispersion into the PET. In the water-assisted melt-mixing, the effect of feeding rate and screw configuration were studied. Solid-state polymerization (SSP) was also done to compensate the molecular weight reduction during melt-mixing and to understand its effect on the microstructure of PET nanocomposites. On the other hand, the effect of surface modifier of organoclays and feeding rate on the microstructure of PET nanocomposites were studied. Then, the effect of organoclay concentration on mechanical, barrier, thermal and rheological properties of PET nanocomposites was investigated. Finally, the effects of organoclay concentration, reaction time and polymer particle size on the rate of SSP were also considered. Neat PET samples after water assisted melt-mixing and after SSP were studied by rheology, titration, intrinsic viscosity and NMR analysis. Titration measurements were also done to determine the effect of organoclay on the degradation of neat PET.

To our knowledge, no report has considered the combined effects of water-assisted melt-mixing and SSP on the improvement of the microstructure and properties of PET nanocomposites.

CHAPTER 2 METHODOLOGY

2.1 Materials

A general purpose PET (PET 9921, Eastman Co, Kingsport, TN) with molecular weight of 65 000 g/mol was used as a matrix. PET 9921 is a copolymer containing 1,4 cyclohexan dimethanol.

Poly(ethylene glycol) (PEG) with molecular weight of 35 000 g/mol supplied from Sigma Aldrich and carboxymethyl cellulose (CMC) (Finnix CMC, CP Kelco Co, Finland) were used as dispersing agents in slurry method.

Three types of nanoclay: Cloisite Na^+, Cloisite 30B (Southern Clay Products Inc., Gonzales, TX) and Nanomer I.28E (Nanocor Inc., Hoffman Estates, IL) were used as the nanoparticles without further modification. The surface modified clays are produced commercially by the substitution of interlayer sodium cations by methyl, tallow, bis-2-hydroxyethyl quaternary ammonium cations for Cloisite 30B and octadecyl trimethyl ammonium (trimethyl stearyl quaternary ammonium) for Nanomer I.28E. The chemical structures of the surfactant cations proposed by the suppliers are shown in Figure 2-1.

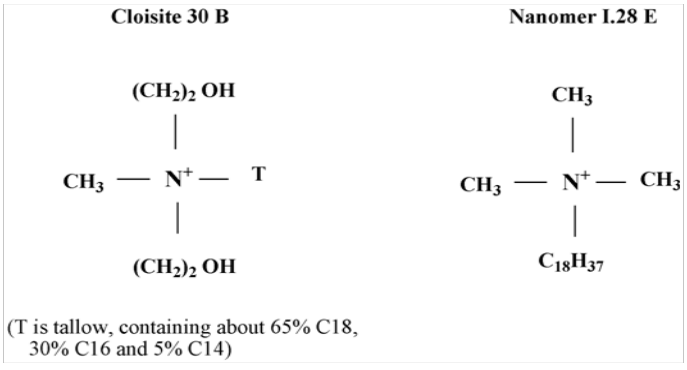

Figure 2-1 : The structures of alkylammonium cations used in the commercial nanoclays.

In the first part of the project, nominal 2 wt% of organoclays and nanoclays were used but in the second and the third part of this work, the nominal organoclay concentration was 2, 3.5 and 6 wt%.

In the slurry method, 3wt% of Cloisite Na^+ was dispersed in water. 1 wt% of PEO or CMC were also added in the suspension of water and Cloisite Na^+.

Phenol, 1, 1, 2, 2 - tetrachloroethane, chloroform-d ($CDCl_3$) and trifluoroacetic acid-d (TFA-d) supplied by Sigma Aldrich (Oakville, ON) were utilized for viscometry measurements and the nuclear magnetic resonance (NMR) analysis. O-cresol, dichloro methane, methanol and potassium hydroxide supplied by Fischer Scientific (ON, Canada) were used for the determination of the carboxyl groups.

All the materials were employed without additional purification.

2.2 Melt Compounding

PET and PET nanocomposites were prepared using a co-rotating twin screw extruder (TSE) (Berstorff ZE25, Hannover, Germany) with a 25 mm diameter (*D*) screw and length-to-screw diameter ratio of 28, at a screw speed of 200 rpm. The temperature profile was 245, 265, 260, 255, 255, and 255°C from the hopper to the die. Figure 2-2 a shows the first screw configuration. The melting section of the TSE (zones 1 and 2) contained three different types of kneading blocks (left hand 45°, 90° and right hand 45° staggering angles) followed by a mixing element, a blister ring and conveying elements (Zone 3). Zone 4 had one kneading block (90° staggering angles) and a blister ring. In zone 5, five short pitch conveying elements were used.

Ground PET pellets were dry-mixed with clay before melt compounding. The mixture was fed into the TSE at two different rates of 0.6, and 3.3 kg/h. They are identified in chapter 4 by suffix L and H, respectively. A 2-L pressure vessel (Parr Instrument Co., Moline, IL) was utilized to produce and feed steam in zone 2 of the TSE at a rate of 0.3 L/h.

In the second part of the project, the screw configuration was changed with the following screw configuration; the screw had three mixing zones (Figure 2-2 b). The first mixing zone

consisted of one kneading block (KB) (left hand 45 staggering angle), followed by one reverse element and two blister rings. The reverse elements and the 2 blister rings helped to raise the pressure before water injection. The second mixing zone contained one gear-type mixing elements (ZME) and one KB element with 90° staggering angles. In the third mixing zone, two kneading blocks (90° and right hand 45° staggering angles) and one ZME element were used. Dry-mixed ground PET pellets with clay were fed into the TSE at 3 kg/h and steam was feed at a rate of 0.3 L/h. The extruded samples were cooled by air, cut, pelletized and then ground.

In the slurry method, suspensions were pumped into the extruder at 1.75 Kg/h and compounded with the melted PET. PET was fed at 3 Kg/h. Plunger pump was used to pumping clay slurry into the extruder. This pump was worked with different speeds. At each speed, the flow rate of clay slurry into the extruder was collected for 10 min. After calibration of the pump, the required flow rate of clay slurry was pumped into the extruder. At the end of the extruder, water was removed from the vent by vacuum to obtain the PET nanocomposites. Nanocomposites prepared by slurry method were used as master-batch. Then, they were diluted by neat PET. Final nanocomposites had 1wt% of Cloisite Na^{+}.

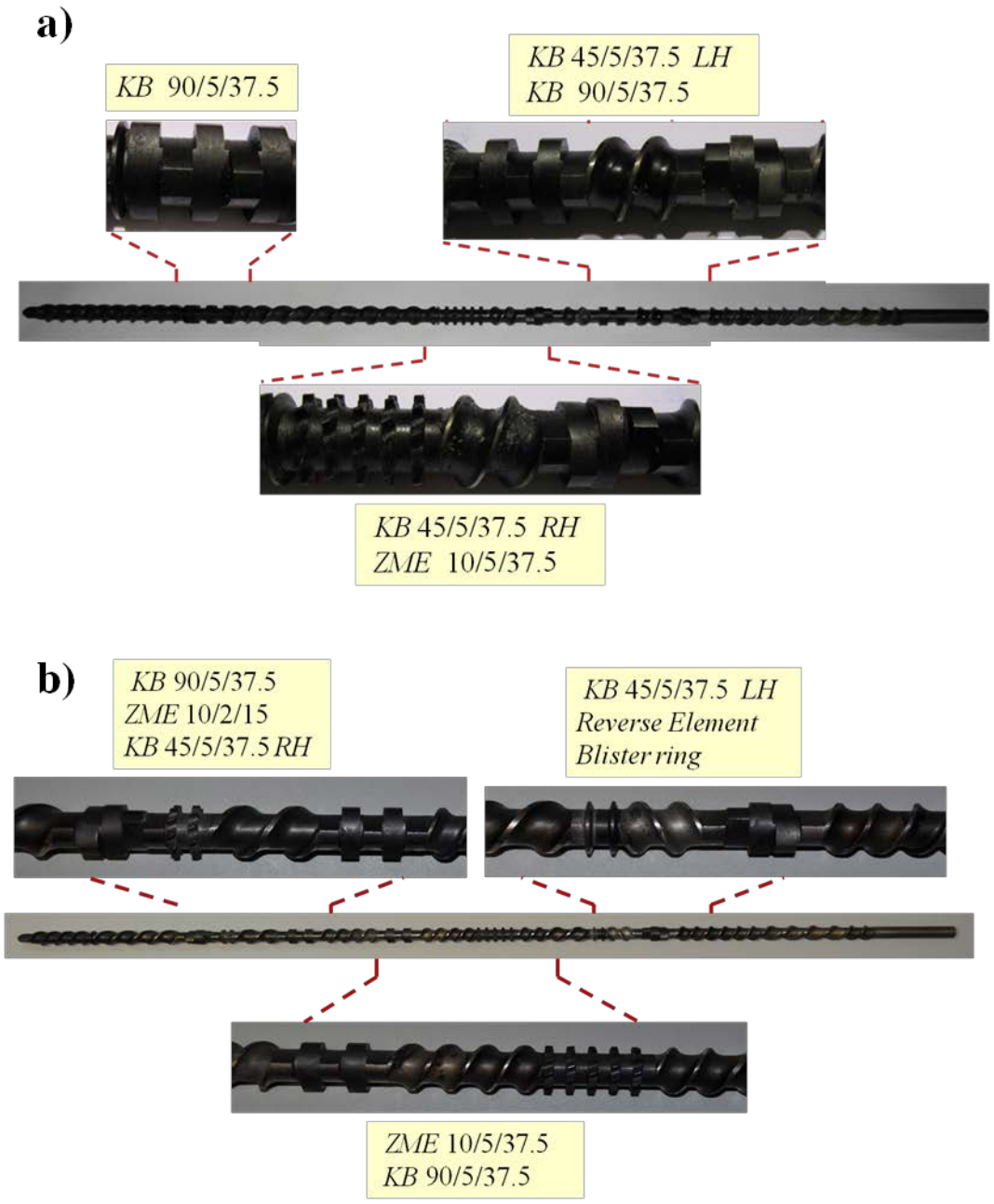

Figure 2-2 : Screw configuration, a) configuration # 1, b) configuration # 2

2.3 Solid-State Polymerization (SSP)

Solid-state polymerization (SSP) was carried out to rebuild the reduced M_W of hydrolyzed PET and PET nanocomposites. Before SSP, the PET and PET nanocomposites were ground and sieved to a powder of size less than 200 and 400 μm. SSP was performed in a 1 L stainless steel stirred reactor equipped with a heating jacket provided by Supercritical Fluid Technologies Inc. (Newark, USA). SSP reactions were done at 215°C under N_2 for 4, 8 and 12 h with powder size 400 μm. This temperature was the maximum value at which we could operate without encountering experimental difficulties. The effect of smaller powder size (200 μm) was also investigated for 8 h SSP. The flow rate of N_2 into the reactor was 2 L/min. After SSP, the heater was turned off, but the nitrogen purge was continued to decrease the temperature of the reactor to 100°C prior to collect the resulting polymer or nanocomposites.

Samples for rheometry, XRD and morphology analysis were molded in the form of disk-like plates with a diameter of 25 mm and a thickness of ~ 1.2 mm. Thin sheet samples with thickness of 250 μm and 450 μm for mechanical tests and thickness of 300 μm and 450 μm for barrier tests were prepared via compression molding. All samples were prepared using a hot press (Carver Laboratory Press, Model 3912) with a small chamber for nitrogen purge. The compression molding temperature and maximum pressure were 270 °C and 3 tons, respectively. All the samples were dried under vacuum for 24 h at 80 °C prior to melt processing and molding.

2.4 Characterization

Viscometry measurements: PET samples dissolved based on ASTM D 4603-3 in a mixture of phenol/1,1,2,2-tetrachloroethane (60/40, wt % /wt %) at 110 ºC for less than 30 min. The solution was then cooled to room temperature.

In the first part of this study, viscometry measurements of PET samples were performed at 30 ºC by measuring the flow time of the solution at a single concentration (0.5 g/dL). The relative viscosity of the samples was obtained from the ratio of average solution flow time (t) and average solvent flow time (t_0) in an Ubblehode capillary viscometer, namely:

$$\eta_r = \frac{t}{t_0} \qquad (2\text{-}1)$$

According to ASTM D 4603-3, the inherent viscosity, η_{inh}, was obtained from the following equation:

$$\eta_{inh}\left(\begin{smallmatrix}30°C\\0.5\%\end{smallmatrix}\right) = \frac{ln\,\eta_r}{c} \qquad (2\text{-}2)$$

where c is the concentration of PET.

The average viscometric molar weight ($M_V \approx M_W$) was calculated using the Mark–Houwink equation assuming that the inherent viscosity was equal to the intrinsic viscosity:

$$\eta_{inh} = KM_W^a \qquad (2\text{-}3)$$

with $K = 2.29\times10^{-4}$ dL / g and $a = 0.73$ [109].

In the third part of the project, the viscometry measurements were done at 25º C. The reason for changing the temperature of viscometry measurements from 30 º C to 25 º C was the limited information about the *k* and *a* constants of Mark-Houwink equation in the literature at 30 º C. The presented *k* and *a* in the literature were based on the correlation between inherent viscosity and M_v at 30 º C. On the other hand, at 25 º C, the Mark-Houwink constants of the correlations between intrinsic viscosity and M_w, M_n were reported [110-112]. Following equations were used to determine the intrinsic viscosity and the molecular weights.

Intrinsic viscosity was calculated by the Solomon–Ciuta equation [110]:

$$[\eta] = \frac{\left[2(\eta_r - 1 - \ln\eta_r)^{0.5}\right]}{c} \qquad (2\text{-}4)$$

The weight-average molar weight M_W was calculated using the Moore [111]:

$$[\eta] = 4.68\times10^{-4} M_W^{0.68} \qquad (2\text{-}5)$$

and the number-average molecular weight was determined by Ulgea equation [112]:

$$[\eta] = 2.52\times10^{-4} M_n^{0.8} \quad (2\text{-}6)$$

Nuclear magnetic resonance (NMR) analysis: The chemical structure of PET before and after SSP was analyzed by NMR. The spectra of ^{13}C and ^{1}H NMR were obtained using a Varian/Agilent VNMRS-500 spectrometer operating at 125 and 500 MHz, respectively. A mixed solvent of chloroform-d ($CDCl_3$) and trifluoroacetic acid-d6 (TFA-d) was used to observe the NMR peaks of PET at room temperature. Therefore, to prepare a sample for NMR analysis, 0.0062 g of PET was dissolved in a mixture of $CDCl_3$ / TFA-d (70/30) (wt % /wt %). Initially, all materials were loaded into the NMR tube. Then, the tube was shaken to dissolve the solid samples into the solvent.

Titration of carboxyl groups: carboxyl end group (CEG) content in the samples was obtained according to the ASTM D7409-07 method by titrating a solution of the PET and PET nanocomposites in o-cresol/dichloro methane. Approximately 1 g of PET was added in 60 ml of o-cresol solvent at 80°C. The mixture of solvent and PET maintained at this temperature and stirred until PET was completely dissolved. Then, the flask was removed from the hot source and 240 ml of dichloromethane was added and stirred for 5 min. Then, KOH (0.005 *M*) in methanol was used as a titrator solution and bromophenol blue as an indicator.

$$CEG = [(V_s - V_b)\times M \times 1000] / w \quad (2\text{-}7)$$

where V_s and V_b are volume of KOH to titrate the sample and the blank, respectively. *M* is molarities of the KOH/methanol solution and *w* is the weight of the PET sample.

X-ray diffraction: a wide angle X-ray diffractometer (WAXD) (D8 Discover, Bruker AXS Inc., Madison, WI) with CuKα radiation (λ=1.54056 Å) was used to estimate the basal spacing (d_{001}) between silicate layers. The generator was operated at 40 kV/ 40 mA and the nanocomposites were scanned from 0.8 to 10° at 0.015°/s.

Scanning Electron Microscopy (SEM): A field emission gun scanning electron microscope (FEG-SEM, S-4700, Hitachi, Tokyo, Japan) was used to investigate the distribution of clay in the PET matrix. The specimens were prepared using an Ultracut FC microtome (Leica, Wetzlar, Germany) with a diamond knife and then coated with platinum vapor.

Transmission Electron Microscopy (TEM): The quality of the clay dispersion was evaluated using transmission electron microscopy (TEM) (JEOL JEM-2100F, Tokyo, Japan, operating at 200 kV). The samples were microtomed into approximately 50-80 nm thick slices, using an Ultracut FC microtome system at -100 ºC.

Linear Viscoelastic Measurement: Rheological measurements were carried out at 265°C under nitrogen atmosphere using a Bohlin Gemini HR rheometer (Malvern Instrument, Worcestershire, UK) and an Advanced Rheometric Expansion System (ARES, TA Instruments), both with a 25 mm parallel plate geometry. The samples were dried under vacuum at 80°C for 24 h before the rheological tests. Time sweep tests were performed at frequency 0.1 Hz and frequency sweep tests were done in the linear viscoelastic region for each sample, as determined by strain sweep tests (done at 0.1 Hz and 10 Hz). Frequency sweep tests over a frequency range of 0.3- 100 rad/s were performed from low to high and high to low frequencies, to assure the repeatability of the data.

Rheology measurements of clay slurries were performed by Physica MCR501 (Anton Paar) rheometer over a shear rate range of 0.1-100 (s^{-1}) from low to high and high to low with a double couette geometry.

Differential Scanning Calorimetry (DSC): the thermal properties of the neat PET and PET nanocomposites were determined by differential scanning calorimetry (DSC Q1000, TA instruments, New Castle, DE) under N_2 atmosphere, The samples were heated from room temperature to 300 ºC and held at that temperature for 3 min, then cooled to 30 ºC and heated again to 300 ºC at a constant rate of 10 ºC/min.

Mechanical Measurement: Tensile measurements were conducted using an Instron 3365 universal tester with a 500 N load cell and according to the ASTM D882-10 standard. The tensile testing samples were cut to a rectangular shape (10 mm x 100 mm). The samples were tested at room temperature and a crosshead speed of 25 mm/min.

Barrier Measurements: Oxygen transmission rates (OTRs) were determined using Ox-Tran Model 2/21 oxygen permeability MD Module (MOCON Inc., USA) at 23 °C under a pressure of 0.96 atm. Dry oxygen (100%) was passed over one side of the sample and a mixture of 98% N_2 (nitrogen) with 2% H_2 (hydrogen) was used as the carrier gas. The test area of the samples was 5 cm^2. The oxygen permeation values reported in this work had been normalized by the film thickness. The permeability coefficient [*P*, in µL/(m.day.atm)] was obtained from the OTR values using the following formula:

$$P = \mathrm{OTR} \times L/p \qquad (2\text{-}8)$$

where *L* is the film thickness (m) and *p* is the testing pressure (atm).

CHAPTER 3 ORGANIZATION OF THE ARTICLES

The first paper of this work is presented in Chapter 4; *"Effect of Water-Assisted Extrusion and Solid-State Polymerization on the Microstructure of PET/Clay Nanocomposites"*. In this work PET/clay nanocomposites were prepared by water-assisted melt-mixing. Water/steam could diffuse between organoclay layers and act as a swelling agent, expanding the gallery spacing and reducing the inter-layer interactions. On the other hand, the reduction of M_W of PET by hydrolysis with water increased the PET chain mobility. Thus, both effects facilitated the diffusion of PET chains into the organoclay galleries. In raising the M_W by SSP, we recovered the critical properties of PET. The effect of the organoclay modification on the microstructure of PET nanocomposites was studied by using three different nanoclays. The dispersion of Cloisite 30B (C30B) in PET was found to be better than that of Nanomer I.28E (I28E) and Cloisite Na^+. The effect of feeding rate and consequently residence time on the properties of PET nanocomposites was also investigated. Morphological results showed more delamination of organoclay platelets in PET-C30B nanocomposites processed at low feeding rate compared to those processed at high feeding rate. Enhanced mechanical and barrier properties were observed in PET nanocomposites after SSP compared to the nanocomposites prepared by conventional melt-mixing. This paper has been accepted in *Polymer Engineering and Science*.

In chapter 5, the results of the second paper with the title of *"Microstructure and properties of PET/organoclay nanocomposites prepared by water-assisted extrusion: Effect of organoclay concentration"* is presented. In this work, the effect of organoclay concentration on the properties of PET nanocomposites obtained by conventional melt-mixing and water-assisted melt-mixing was studied. XRD, SEM and TEM analyses showed intercalated/exfoliated morphology in all PET/C30B nanocomposites, with a higher degree of intercalation and delamination in the water-assisted process. Rheological, thermal, mechanical and gas barrier properties of the PET nanocomposites were also investigated. The PET nanocomposites exhibited higher tensile modulus and lower oxygen permeability after SSP compared to those prepared by conventional melt-mixing. By increasing organoclay concentration, more reduction in oxygen permeability and more increase in tensile modulus were found. The elongation at break was significantly higher for SSP nanocomposites than for nanocomposites processed by conventional melt mixing. This paper has also been accepted in *Polymer Engineering and Science*.

Chapter 6 presents the results of the third paper entitling "*Effect of organoclay concentration on the solid-state polymerization of poly(ethylene terephthalate)*". In this work, the effect of organoclay concentration on SSP of PET nanocomposites was studied. Viscometry, titration, rheological and dynamic scanning calorimetry (DSC) measurements were used to analyze the samples after SSP. The weight-averaged molecular weight (M_W) of PET was increased significantly following SSP. PET nanocomposites exhibited a solid-like rheological behavior and the complex viscosity at high frequencies was scaled with the molecular weight of PET. The Maron-Pierce model was used to evaluate the molecular weight of PET in the nanocomposites before and after SSP. It was found that the rate of the SSP reaction in nanocomposites were lower than those for the neat PETs, due to the limited mobility of the reactive groups and the barrier effect of clay platelets. The effect of PET molecular weight on half-time crystallization, crystallization temperature and percentage of crystallinity was also investigated. This paper has been submitted to *Polymer Engineering and Science*.

CHAPTER 4 ARTICLE 1- EFFECT OF WATER-ASSISTED EXTRUSION AND SOLID-STATE POLYMERIZATION ON THE MICROSTRUCTURE OF PET/CLAY NANOCOMPOSITES[1]

Maryam Dini[1], Tahereh Mousavand[2], Pierre J. Carreau[1], Musa R. Kamal[2] and Minh-Tan Ton-That[3]

[1] *CREPEC, Chemical Engineering Department, Ecole Polytechnique, H3T 1J4, Montreal, Quebec, Canada*

[2] *CREPEC, Department of Chemical Engineering, McGill University, H3A 2B2, Montreal, Quebec, Canada*

[3] *Automotive and Surface Transport Portfolio, National Research Council of Canada, J4B 6Y4, Boucherville, Quebec, Canada*

Abstract

A new melt-mixing process has been used to prepare PET/clay nanocomposites with high degree of clay delamination. In this method, steam was fed into a twin-screw extruder (TSE) to reduce PET molecular weight and to facilitate their polymer chain diffusion into the gallery spacing of organoclays. Subsequently, the molecular weight (M_W) reduction of the PET matrix due to

---

[1] *Accepted in Polymer Engineering and Science; doi: 10.1002/pen.23685*

hydrolysis by water was compensated by solid-state polymerization (SSP). The effect of the thermodynamic compatibility of PET and organoclays on the exfoliated microstructure of the nanocomposites was also examined by using three different nanoclays. The dispersion of Cloisite 30B (C30B) in PET was found to be better than that of Nanomer I.28E (I28E) and Cloisite Na^+. The effect of feeding rate and consequently residence time on the properties of PET nanocomposites was also investigated. The results reveal more delamination of organoclay platelets in PET-C30B nanocomposites processed at low feeding rate compared to those processed at high feeding rate. Enhanced mechanical and barrier properties were observed in PET nanocomposites after SSP compared to the nanocomposites prepared by conventional melt-mixing.

4.1 Introduction

Poly(ethylene terephthalate) (PET) is a low-cost engineering polymer that is employed in a large variety of applications, due to its excellent transparency and good barrier properties [1]. One of the important applications of PET is in food and beverage packaging. Demands are increasing to improve the barrier properties of this semi-crystalline polymer for use in bottles for beer and other oxygen-sensitive liquids. Recent studies show that the presence of organoclay platelets in PET can lower permeability to oxygen and water vapor [2-5]. It also improves UV shielding [5].

The microstructure of polymer nanocomposites plays a substantial role in the macroscopic properties of final products. To achieve significant performance enhancements, good dispersion of the nanoclay in the matrix and thermodynamic compatibility between the organoclay and the polymer are required [6]. Polymer nanocomposites can be prepared by in-situ or melt-mixing methods. While in-situ polymerization usually yields better dispersion of clay platelets than melt-mixing, the latter approach is more economical and environmental friendly [6-9]. Preparation of PET nanocomposites by melt-mixing, however, faces challenges mainly related to the degradation of both PET and nanoclay modifiers at high processing temperatures.

Several efforts have been made to lower the rate of degradation and enhance dispersion of organoclays in PET, by using a more stable clay modifier [5, 10, 11]. Other approaches employ a clay supported catalyst [12, 13] or a chain extender [14]. The use of an ionomer [3, 15], swelling agent or plasticization of PET with carbon dioxide were also evaluated [16]. Other studies considered the effects on clay dispersion of screw speed, screw geometry and temperature profile in twin-screw melt extrusion of PET nanocomposites [2, 17]. All these efforts, however, led to only moderately enhanced mechanical and barrier properties.

Water assisted melt blending is a new method to prepare nanocomposites using the benefits of both solution and conventional melt-mixing methods [18, 19]. This method was successfully used to prepare polyamide (PA) - montmorillonite (MMT) nanocomposites with unmodified nanoclays with water content of 5 to 50 wt% and more preferably from 10 to 40 wt% [20, 21]. It is possible to prepare PA nanocomposites by simultaneous feeding PA and pristine clay into the TSE then injecting water into the extruder. Another possibility is to prepare clay slurry with water and feeding this suspension into the extruder to blend it with the molten PA [21]. Some researchers also reported significant effects of water injection into the TSE during the preparation of nanocomposites based on polypropylene (PP) and poly(styrene-co-acrylonitrile) [22, 23].

Solid-state polymerization (SSP) of PET nanocomposites is a practical route to overcome the polymer degradation caused by the melt-mixing processing. Different researchers demonstrated that SSP of PET in the presence of nanoclays and nano SiO_2 is feasible [24-26]. These studies have also shown a reduced rate of the solid-state polymerization compared to the neat PET. SSP is carried out under moderate temperature conditions. Thus, SSP can raise the molecular weight of PET with less thermal degradation than melt phase polymerization and also can reduce the contents of by-products such as acetaldehyde and oligomers to acceptable levels. The normal SSP reaction temperature range is 200 to 230°C and this temperature range can be varied depending on the melting point of the PET [27-30]. Understanding SSP and its utilization to achieve high molecular weight (M_W) polymer nanocomposites with tailored microstructure is still an open issue.

It is assumed in this work that water/steam can diffuse during extrusion between organoclay layers and act as a swelling agent, expanding the gallery spacing and reducing the inter-layer

interactions. On the other hand, the reduction of M_W of PET by hydrolysis with water can increase the PET chain mobility. Thus, both effects facilitate the diffusion of PET chains into the organoclay galleries. In raising the M_W by SSP we should recover the critical properties of PET. To the best of our knowledge, this is the first attempt to prepare PET nanocomposites using water-assisted extrusion. In this paper, morphology, rheological, mechanical, thermal and barrier properties of processed PET and PET nanocomposites are presented and discussed.

4.2 Experimental

4.2.1 Materials

A general purpose PET (PET 9921, Eastman Co, Kingsport, TN) with M_W of 65 000 g/mol was used in this study. Three types of nanoclay: Cloisite Na^+, Cloisite 30B (Southern Clay Products Inc., Gonzales, TX) and Nanomer I.28E (Nanocor Inc., Hoffman Estates, IL) were used as the nanoparticles without further modification.

The surface modified clays are produced commercially by the substitution of interlayer sodium cations by methyl, tallow, bis-2-hydroxyethyl quaternary ammonium cations for Cloisite 30B and octadecyl trimethyl ammonium (trimethyl stearyl quaternary ammonium) for Nanomer I.28E. The chemical structures of the surfactant cations proposed by the suppliers are shown in Figure 4-1.

Phenol, 1, 1, 2, 2 - tetrachloroethane, chloroform-d ($CDCl_3$) and trifluoroacetic acid-d (TFA-d) supplied by Sigma Aldrich (Oakville, ON) were used without additional purification for the determination of the inherent viscosity and the nuclear magnetic resonance (NMR) analysis.

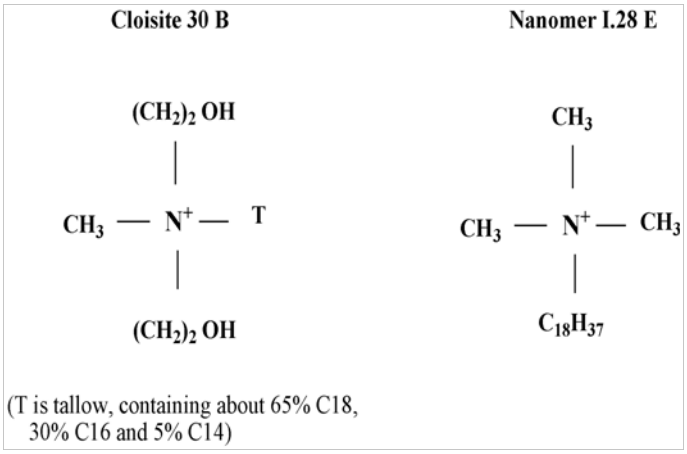

Figure 4-1 : The structures of alkylammonium cations used in the commercial nanoclays.

4.2.2 Melt Compounding

PET and PET nanocomposites were processed using a co-rotating TSE (Berstorff ZE25, Hannover, Germany) with a 25 mm diameter (*D*) screw and length-to-screw diameter ratio of 28, at a screw speed of 200 rpm. The temperature profile was 245, 265, 260, 255, 255, and 255°C from the hopper to the die. Figure 4-2 illustrates the screw configuration. The melting section of the TSE (zones 1 and 2) contains three different types of kneading blocks (left hand 45°, 90° and right hand 45° staggering angles) followed by a mixing element, a blister ring and conveying elements (Zone 3). Zone 4 has one kneading block (90° staggering angles) and a blister ring. In zone 5, five short pitch conveying elements are used.

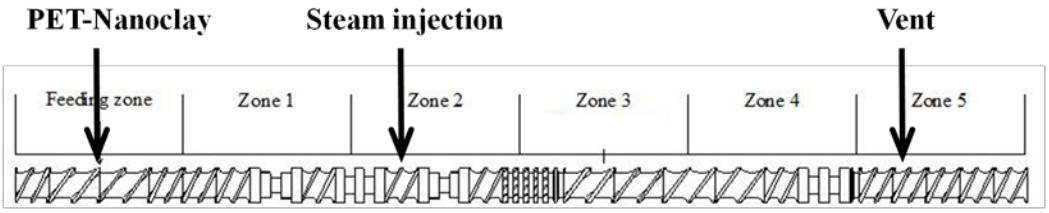

Figure 4-2 : Schematic of the screw configuration.

The nominal nanoclay content was 2 wt% in all the nanocomposites. Ground PET pellets were dry-mixed with clay before melt compounding. The mixture was fed into the TSE at two

different rates of 0.6, and 3.3 kg/h. They are identified here by suffix L and H, respectively. A 2-L pressure vessel (Parr Instrument Co., Moline, IL) was utilized to produce and feed steam in zone 2 of the TSE (see Figure 4-2) at a rate of 0.3 L/h, temperature of 160ºC. Finally, all the residual water was eliminated through the vent in zone 5 as shown in Figure 4-2. The extrudate was collected after reaching steady state. In the notation used for sample identification, the code of samples processed with water is ”W”, which is not included when no water was used during extrusion.

After extrusion, the extruded samples were granulated at room temperature and compression molded at 270 °C under a purge of nitrogen to obtain 25 mm disks. The disks were used for X-ray and morphological analysis, as well as rheometry. All the samples were dried under vacuum for 24 h at 80 °C prior to melt processing and molding.

4.2.3 Solid-State Polymerization (SSP)

Solid-state polymerization (SSP) was carried out to rebuild the reduced M_W of hydrolyzed PET and PET nanocomposites. Before SSP, the PET and PET nanocomposites were ground and sieved to a powder of size less than 400 (μm). SSP was performed in a cylindrical stainless steel reactor at 215°C under N_2 for 8 h. This temperature was the maximum value at which we could operate without encountering experimental difficulties. The flow rate of N_2 into the reactor was 2 L/min. After 8 h, the heater was turned off, but the nitrogen purge was continued to lower the temperature of the reactor to 100°C and collect the resulting polymer or nanocomposites.

4.2.4 Characterization

Viscometry tests and NMR analysis were used to characterize the PET samples before and after SSP. The inherent viscosity, η_{inh}, of PET samples was obtained based on the ASTM D 4603-3 method by measuring the flow time of the solution (Phenol/ 1, 1, 2, 2 – tetrachloroethane) at a single concentration of PET. The relative viscosity of the samples was obtained from the ratio of average solution flow time (t) and average solvent flow time (t_0) in a Ubblehode capillary viscometer, namely:

$$\eta_r = \frac{t}{t_0} \qquad (4\text{-}1)$$

According to ASTM D 4603-3, the inherent viscosity is obtained from the following equation:

$$\eta_{\text{inh}}\left(\begin{smallmatrix}30°C\\0.5\%\end{smallmatrix}\right) = \frac{ln\,\eta_r}{c} \qquad (4\text{-}2)$$

where c is the concentration of PET (g/dL).

The average viscometric molar weight ($M_V \approx M_W$) was calculated using the Mark–Houwink equation assuming that the inherent viscosity is equal to the intrinsic viscosity:

$$\eta_{\text{inh}} = KM_W^a \qquad (4\text{-}3)$$

with $K = 2.29\times10^{-4}$ dL / g and $a = 0.73$ [31].

The chemical structure of PET before and after SSP was analyzed by NMR. The spectra of ^{13}C and ^{1}H NMR were obtained using a Varian/Agilent VNMRS-500 spectrometer operating at 125 and 500 MHz, respectively. A mixed solvent of chloroform-d ($CDCl_3$) and trifluoroacetic acid-d6 (TFA-d) was used to observe the NMR peaks of PET at room temperature.

A wide angle X-ray diffractometer (WAXD) (D8 Discover, Bruker AXS Inc., Madison, WI) with CuKα radiation (λ=1.54056 Å) was used to estimate the basal spacing (d_{001}) between silicate layers. The generator was operated at 40 kV/ 40 mA and the nanocomposites were scanned from 0.8 to 10° at 0.015°/s.

A field emission gun scanning electron microscope (FEG-SEM, S-4700, Hitachi, Tokyo, Japan) was used to investigate the distribution of clay in the PET matrix. The specimens were prepared using an Ultracut FC microtome (Leica, Wetzlar, Germany) with a diamond knife and then coated with platinum vapor. The quality of the clay dispersion was evaluated using transmission electron microscopy (TEM) (JEOL JEM-2100F, Tokyo, Japan, operating at 200 kV). The samples were microtomed into approximately 50-80 nm thick slices, using an Ultracut FC microtome system at -100 ºC.

Rheological measurements were carried out at 265°C under nitrogen atmosphere using a Bohlin Gemini HR rheometer (Malvern Instrument, Worcestershire, UK) with a 25 mm parallel

plate geometry. The samples were dried under vacuum at 80°C for 24 h before the rheological tests. Time sweep tests were performed at frequency 0.1 Hz and frequency sweep tests were done in the linear viscoelastic region for each sample determined by strain sweep tests. Frequency sweep tests over a frequency range of 0.3- 100 rad/s were performed from low to high and high to low frequencies to make sure that the data were accurate.

The thermal properties of the neat PET and PET nanocomposites were determined by differential scanning calorimetry (DSC Q1000, TA instruments, New Castle, DE) under N_2 atmosphere using 10 °C/min scanning ramp from 30 °C to 300 °C. The crystallinity of the PET and PET nanocomposites used in the discussion of the mechanical and barrier properties was calculated using the following formula:

$$\Delta X(\%) = \frac{\Delta H_m - \Delta H_{cc}}{\Delta H_0(1-\phi)} \times 100 \qquad (4\text{-}4)$$

where ϕ is the weight fraction of clay, ΔH_m represents the enthalpy of melting, ΔH_{cc} is the enthalpy of cold crystallization and ΔH_0 refers to the heat of fusion of 100% crystalline PET, which is 140 J/g [1].

Tensile measurements were conducted via an Instron 3365 universal tester using a 500 N load cell and according to the ASTM D882-10 standard. 10 mm wide and 100 mm long samples were cut from sheets (thickness of 450 μm) prepared by compression molding. The samples were tested at room temperature and a crosshead speed of 25 mm/min.

Oxygen transmission rates (OTRs) were determined using an Ox-Tran Model 2/21 oxygen permeability MD Module from Mocon at 23 °C. 100% dry oxygen was used and all the tests were done under a pressure of 93.3 kPa (700 mmHg). The test area of the samples was 5 cm^2 and the samples had a thickness of 450 μm. The oxygen permeability values reported in this work have been normalized by the film thickness.

4.3 Results and discussion

4.3.1 Molecular weight determination and structural characterization of neat PET

According to previous research reports [32, 33], the M_W of PET decreases in the presence of water, especially under processing at temperatures higher than the melting point of PET. This is the result of the hydrolysis of PET according to the following equilibrium reaction in Scheme 4-1[34].

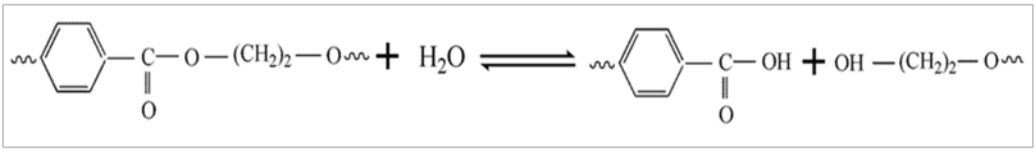

Scheme 4-1: Hydrolysis reaction of PET.

The η_{inh} and M_W values of different PET samples are reported in Table 4-1. We observe important decreases of η_{inh} and M_W of PET as a result of hydrolysis during the water-assisted extrusion for various processing conditions. The extrusion in the presence of water leads to a reduction of η_{inh} from 0.75 to 0.38 (dL/g) in the presence of water with a corresponding decrease of the molecular weight by a factor close to 3. Moreover, the feeding rate has a significant effect on the extent of hydrolysis of PET. η_{inh} of the PET extruded at high feeding rate (W-PET-H) is 0.52 dL/g while for W-PET-L it is 0.38 dL/g. As expected, the extent of the hydrolysis is larger for a longer residence time (lower feeding rate).

Table 4-1 : Values of the inherent viscosities and M_W

Sample	η_{inh} (dL/g)	M_W (g/mol)
As received PET	0.75± 0.020	65000 ± 2000
W-PET-L	0.38 ± 0.023	25000 ± 2100

SSP-W-PET-L	0.69± 0.033	58000 ± 4000
W-PET-H	0.52 ± 0.03	39000 ± 3200
SSP-W-PET-H	0.83 ± 0.04	75000 ± 5000

Suffix “W” means that the PETs were extruded in the presence of water (hydrolyzed samples) and “SSP” means the hydrolyzed samples were solid-state polymerized in a reactor. L and H stand for samples prepared at low and high feeding rates, respectively.

As shown in Table 4-1, SSP results in large increases of η_{inh} and M_W values of PET. η_{inh} of the samples after SSP is the average values of the results from two batches. Moreover, to confirm its value, the viscometry tests were carried out at different concentrations based on ASTM D 2857 as well as ASTM D 4603-3. The results of both methods were in agreement. After SSP at 215 °C for 8 h, η_{inh} increased from 0.38 to 0.69 dL/g for W-PET-L and from 0.52 to 0.83 dL/g for W-PET-H. These results confirm that the M_W of PET can be substantially rebuilt by SSP under these conditions. SSP of PET involves two reversible equilibrium reactions as presented in Scheme 4-2[35].

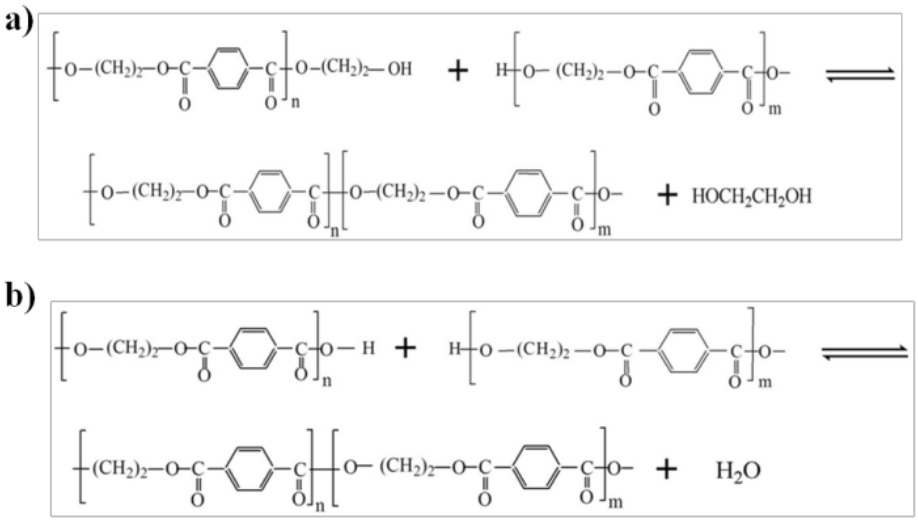

Scheme 4-2: SSP of PET; (a) Ester-interchange (transesterification), (b) esterification reactions.

^{1}H and ^{13}C NMR spectroscopy was used to confirm the presence of chemical entities in the "as received" PET, W-PET-H and SSP-W-PET-H samples. In the ^{1}H NMR spectra we observe the peaks at δ: 7.257 ppm and 11.3 ppm corresponding to protons of chloroform ($CDCL_3$) and those of trifluoroacetic acid-d6 (TFA-d), respectively (not shown here). The peak position of protons of "as received" PET is presented in Table 4-2 and Figure 4-3. PET contains four equivalent methylene protons of the terephthalic acid ring and protons of the ethylene glycol (EG) segments. The other resonances are assigned to the methylene protons of diethylene glycol (DEG) and the hydroxyl end groups. This analytical technique does not allow the detection of aromatic carboxyl end-groups because they show a peak at the same position as TFA-d. Since "as received" PET is a copolymer, there are additional signals, which are characteristics of cyclohexanedimethanol (shown in Table 4-2).

In ^{1}H NMR spectra, the area under each peak is related to the number of corresponding hydrogens in the molecules generating that peak [36]. The ratios of the integrals under the peaks assigned to CH_2 for EG, DEG and hydroxyl end groups show the differences in the molecular structure of the different PETs. The ratios of the CH_2 peak for EG to the CH_2 attached to the hydroxyl groups were 100, 190 and 300 in W-PET-H, "as received" PET and SSP-W-PET-H, respectively. Therefore, as expected, the amount of CH_2 attached to hydroxyl end-groups increases during the hydrolysis process, while a significant decrease is observed after SSP. The

ratios of the CH_2 peak for EG to the CH_2 attached to DEG are also determined. These ratios do not show significant changes for the different molecular weight samples and the ratio for the "as received PET" is 15.6. Thus, the significant differences for the three PETs are for the ratio of methylene groups adjacent to hydroxyl end groups and those of EG.

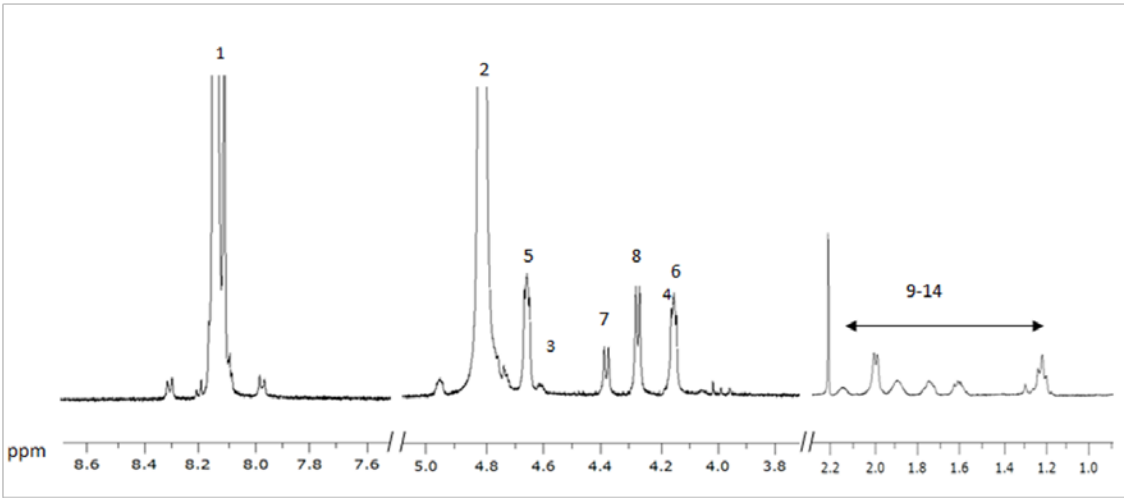

Figure 4-3 : ^{1}H NMR spectrum for the "as received" PET; the peak at δ: 2.2 ppm is due to impurities in the solvent. The spectra of the hydrolyzed samples before and after SSP are not shown here because they exhibit similar spectra as the "as received" PET.

Table 4-2 : Protons numbering in PET and their peak position in ^{1}H NMR spectra.

Units of PET copolymer	Peak position (ppm) of each numbered protons
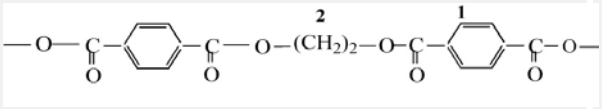	(1): 8.13, (2):4.8
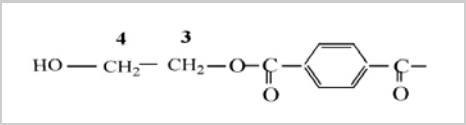	(3,4*): 4.61, 4.19
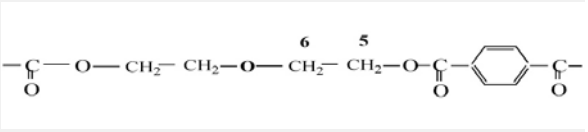	(5,6): 4.14, 4.65
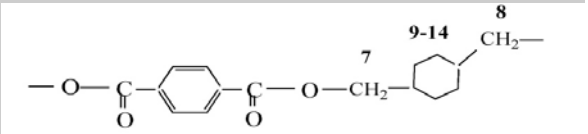	(7): 4.38, (8): 4.28 (9-14): 1.2,1.6,1.73,1.91,1.88,2.14

*small amount of TFA-d leads to esterification of hydroxyl end groups. Thus, signals of methylene end groups shift to the higher frequencies and overlap with the 4.6-4.8 ppm region.

Generally, the number of nonequivalent carbons and types of carbon atoms are determined by ^{13}C NMR [37]. An important parameter obtained from ^{13}C NMR in solution is the chemical shift. Figure 4-4 reports the ^{13}C NMR spectra of the samples. The carbons of chloroform ($CDCL_3$) exhibit four peaks from δ: 76.5 to 77 ppm and those of trifluoroacetic acid-d6 (TFA-d) show peaks from δ: 110.75-117.5 ppm and δ: 161-162.3 ppm. We observe peaks for carbons of ethylene glycol at δ: 63.86 ppm, of aromatic CH at δ: 129.98 ppm and of aromatic carbons at δ: 133.24 ppm; carboxyl end groups show a peak at δ: 167.89 ppm and carbonyl groups at δ: 162.3 ppm. The carbonyl peak is at the same position as TFA-d. Therefore, we cannot distinct from carbonyl groups in PET and carboxyl groups in TFA-d. These $^{13}CNMR$ spectra of the "as received" PET and hydrolyzed PET before and after SSP show the same peak positions. Therefore, these different PETs have all the same carbon atoms.

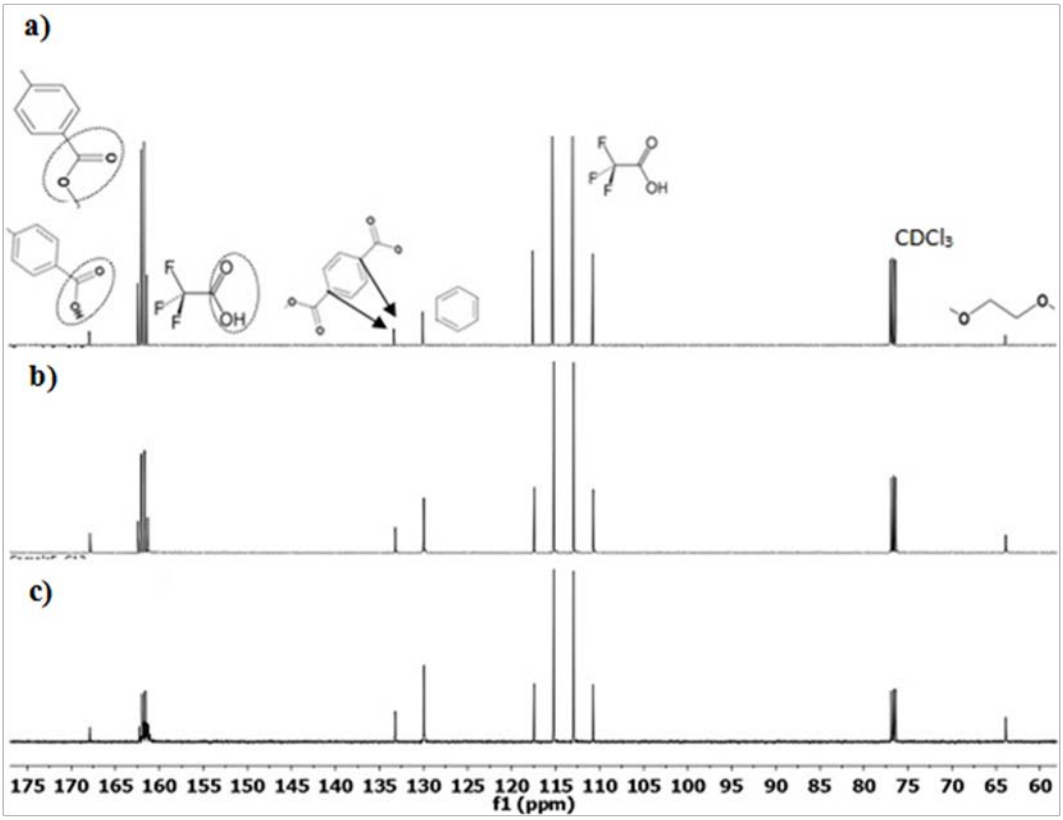

Figure 4-4 : ^{13}C NMR spectra for (a) the "as received" PET, (b) W-PET-H and, (c) SSP-W-PET-H.

4.3.2 XRD results of PET nanocomposites

The X-ray diffraction (XRD) patterns for the PET- Cloisite Na^+ nanocomposites processed with and without water show that the *d*-spacing of Cloisite Na^+ did not change after the melt-mixing process in either the dry extrusion process or with water (data not shown). This is due to the poor affinity between the pristine clay (Cloisite Na^+) and PET as well as the collapse of clay galleries under the strong platelet-platelet cohesive force of Cloisite Na^+ [23]. Hence, water did not contribute to intercalation during the extrusion process.

The XRD results of PET-C30B and PET-I28E nanocomposites prepared under different conditions are presented in Figure 4-5. For the nanocomposites obtained under dry extrusion (Figure 4-5a), two distinct peaks are observed for the C30B nanocomposites (*d*-spacing ~3.45 and 1.7 nm) and for the I28E nanocomposites (*d*-spacing ~3.35 nm and 1.6 nm). Since the *d*-spacing values for the pristine organoclays, C30B and I28E are 1.8 nm and 2.5 nm, respectively, the first peaks shown for the nanocomposites are indicative of some intercalation of organoclays by the PET chains. The second peaks suggest either possible degradation of the organo-modifiers during processing of PET or they could also be reflections of the first peaks according to Bragg's law. The WAXD results indicate that the dispersion of C30B in PET is better than that obtained with I28E, both *d*-spacing and increases in *d*-spacing are larger for C30B. This may be attributed to stronger interactions between PET and C30B, as suggested by the solubility parameters [59]. Finally, we note that the *d*-spacing is independent of the processing conditions. However, the first peak intensity for PET-C30B-L is smaller than for the others, indicative of better clay dispersion for the low feeding rate.

Figure 4-5b presents the diffraction peaks of the PET nanocomposites prepared in the presence of water. Although the peak position of C30B in nanocomposites processed with water slightly shifted to lower angles compared to processing without water, the shape and intensity of the C30B peaks are significantly changed in the water-assisted process. The first peak of this organoclay became broader and more asymmetric as well as of smaller intensity, compared to the case of the dry extrusion (Figure 4-5a). This indicates a higher degree of delamination in the presence of water. In W-PET-C30B-L, the first peak has almost disappeared, which suggests a high degree of exfoliation. On the other hand, the XRD peaks of nanocomposites containing I28E

prepared with or without water are similar. As also shown in Figure 4-5a, the reduction of intensity in the first XRD peak for the low feeding rate confirms that the degree of delamination is increased under the process with a longer residence time.

The XRD results for the PET nanocomposites after SSP are shown in Figure 4-5c. The nanocomposites exhibit peaks at the same 2θ values as before SSP (Figure 4-5b). This suggests that the net diffusion of polymer in and out of the galleries during SSP is negligible. Moreover, possible SSP of PET chains intercalated inside the galleries of the organoclays do not have any significant effects [26].

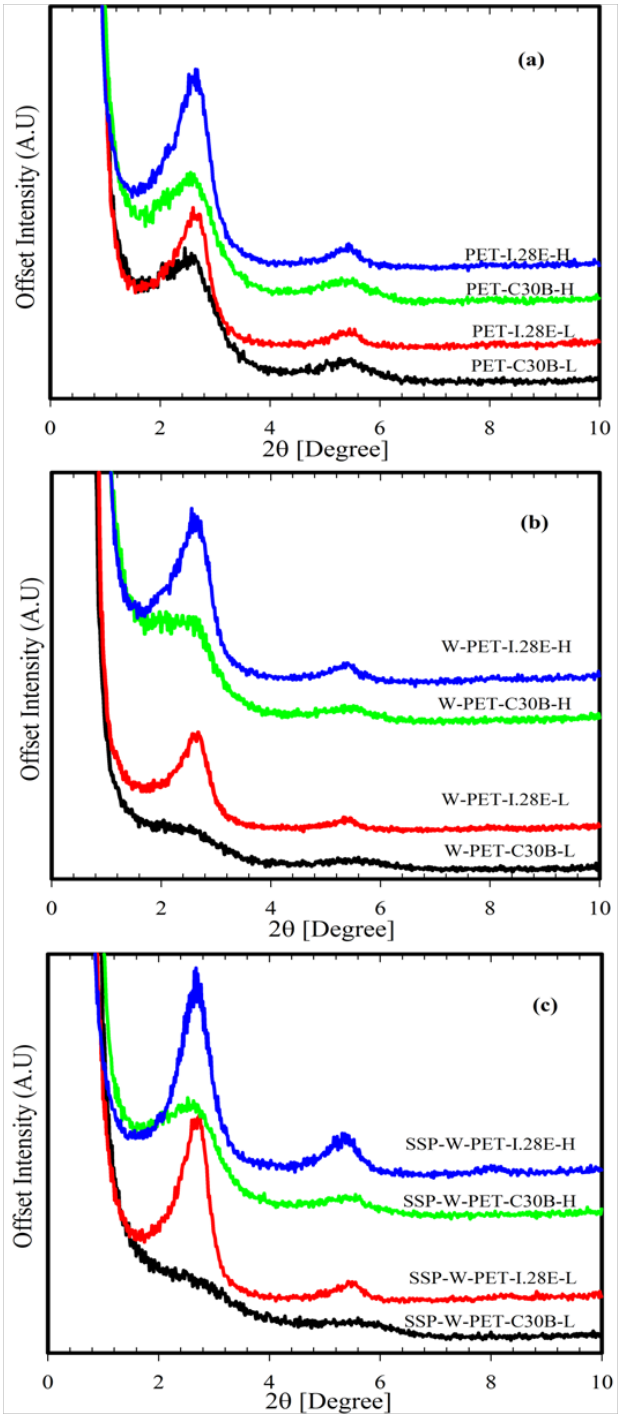

Figure 4-5 : XRD results of PET nanocomposites; (a) processed without water, (b) processed with water, (c) after SSP.

4.3.3 SEM and TEM images

SEM micrographs of PET nanocomposites containing Cloisite Na^+ prepared with and without water are presented in Figure 4-6. The white areas represent the clay particles and the dark regions correspond to the PET matrix. Although the aggregates of Cloisite Na^+ in the nanocomposites prepared via water-assisted extrusion are smaller than those of nanocomposites prepared in the absence of water, they are still quite large. These results are in good agreement with XRD results that showed no change in gallery spacing of Cloisite Na^+ in the presence of water. Water is a good swelling agent for Cloisite Na^+ [20] and a hydrolysis agent for PET [32,33]; but the poor affinity between Cloisite Na^+ and PET as well as strong electrostatic forces between adjacent platelets of Cloisite Na^+ limit the diffusion of PET chains into the galleries of the pristine clay.

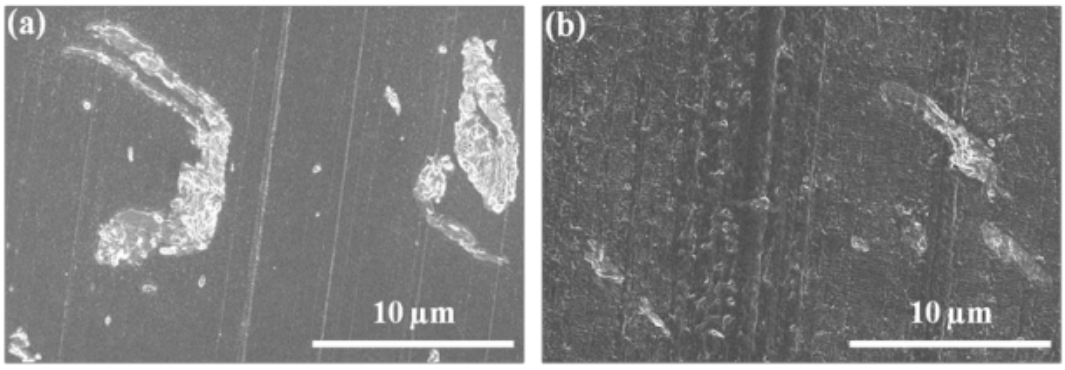

Figure 4-6 : SEM micrographs of PET nanocomposites containing Cloisite Na^+; (a) processed without water and (b) with water.

SEM micrographs of PET-C30B nanocomposites processed at different feeding rates are shown in Figure 4-7. Smaller dispersed aggregates with a more uniform distribution are observed for the nanocomposites processed at the lower feeding rate. This may be attributed to the longer residence time of around 300 s compared to 50 s for the high feeding rate. The size of C30B aggregates is also decreased in PET-C30B nanocomposites processed with water before and after SSP, compared to those processed without water. On the other hand, a comparison between the SEM micrographs of PET-C30B and PET-I28E shows that I28E is not distributed uniformly in

the matrix. The latter has larger aggregate size compared to C30B. The micrograph of Figure 4-7h shows that the presence of water in processing PET-I28E nanocomposites does not improve the particle distribution of I28E. In fact, it may have a negative effect.

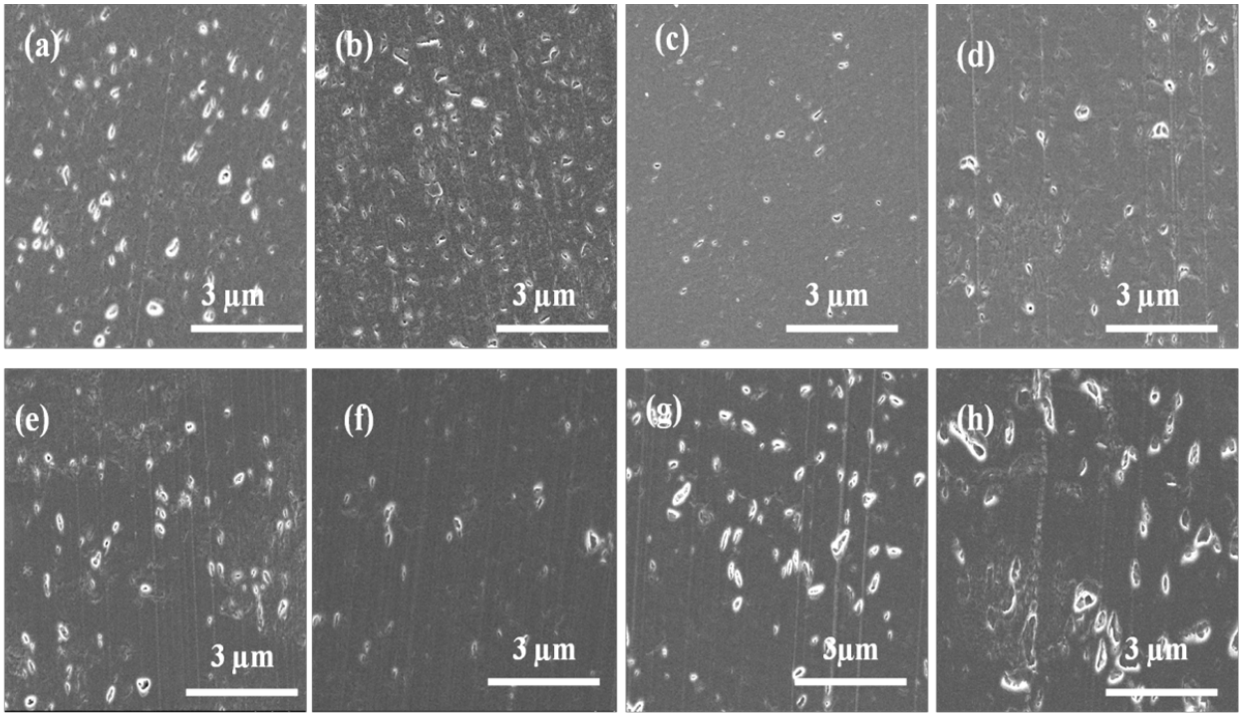

Figure 4-7 : SEM micrographs of PET nanocomposites processed under different conditions; (a) PET-C30B-L, (b) W-PET-C30B-L, (c) SSP-W-PET-C30B-L, (d) PET-C30B-H, (e) W-PET-C30B-H, (f) SSP-W-PET-C30B-H, (g) PET-I28E-L, (h)W-PET-I28E-L.

Figure 4-8 shows the TEM images of different PET nanocomposites. In the case of PET-C30B-L (Figure 4-8a), the organoclay appears to be dispersed very well. In most cases, single layers of organoclay are observed. On the other hand, PET-C30B-H (Figure 4-8b) exhibits slightly poorer dispersion of C30B as compared to the nanocomposites processed under the low feeding rate. Also, in nanocomposites processed with water (Figure 4-8 c and d), better dispersion and good distribution of C30B particles are observed in nanocomposites, especially

when processed at low feeding rate. Thus, lower feeding rate and accordingly longer residence time in the extruder lead to more breakup or delamination of stacks of clay platelets (tactoids). Figure 4-8a and f show a better dispersion of C30B in PET compared to I28E. Most of the particles of C30B are broken down to single layers, while I28E particles are in the form of tactoids (Figure 4-8e and f) and the apparent particle concentration of I28E is lower than that of C30B. The quality of dispersion of I28E is deteriorated by the presence of water (Figure 4-8g). This may be related to changes in the compatibility between PET and I28E by the hydrolysis reaction. By hydrolysis of PET, the number of carboxyl and hydroxyl groups is increased and, therefore, the incompatibility between PET and I28E is intensified.

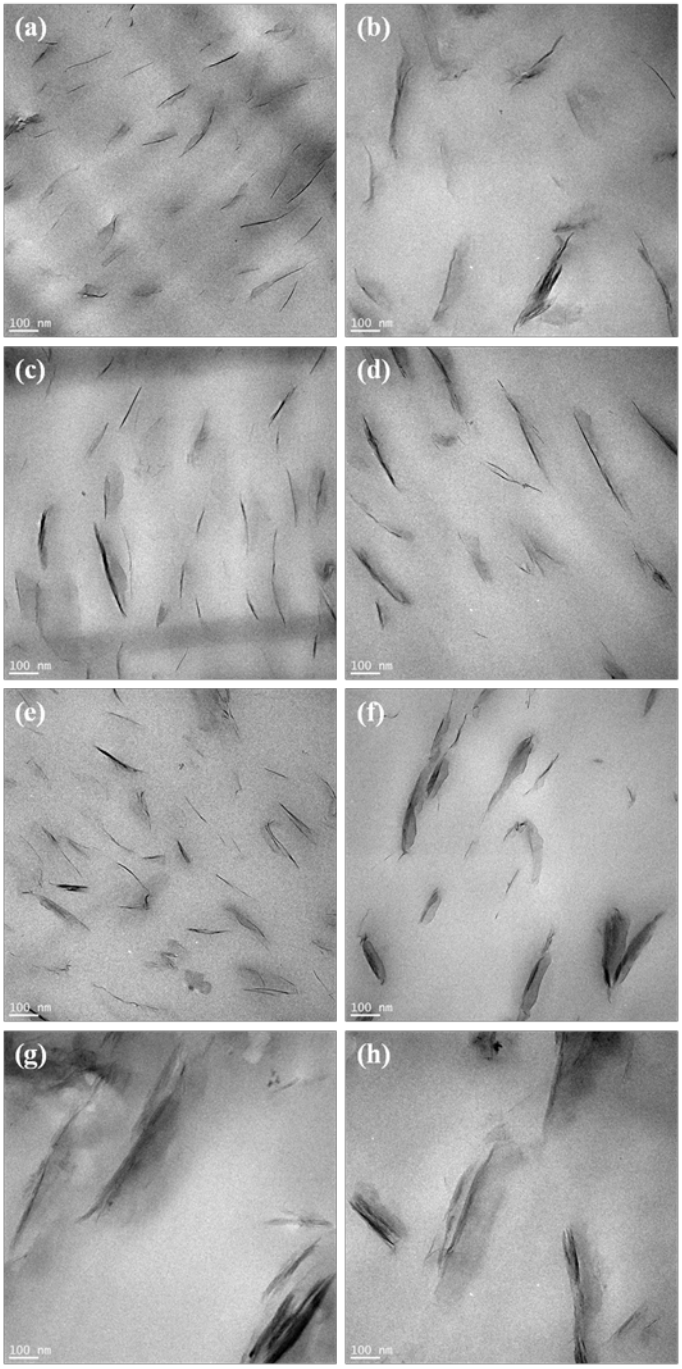

Figure 4-8 : TEM images of PET nanocomposites; (a) PET-C30B-L, (b) PET-C30B-H, (c) W-PET-C30B-L, (d) W-PET-C30B-H, (e) SSP-W-PET-C30B-L, (f) PET-I28E-L, (g) W-PET-I28E-L, (h) SSP-W-PET-I28E-L.

In order to obtain a quantitative estimate of the degree of dispersion of organoclay platelets in the PET matrix, the $D_{0.1}$ factor proposed by Luo and Koo [39] was calculated using between 600 and 700 measurements for each case. A value below 4% for $D_{0.1}$ suggests an immiscible system or microcomposite, and values over 8% indicate an exfoliated structure, while values between 4 and 8% indicate intercalation. The values of $D_{0.1}$ and of the aspect ratio, ($p = l/d$, length over diameter of particles) are reported in Table 4-3 (the method proposed by Ghasemi et al. [2] was applied to determine p, using TEM images and 200 measurements for each case).

Table 4-3 : Aspect ratio and $D_{0.1}$

Sample	**Aspect ratio (p)**	**$D_{0.1}$ (%)**
W-PET-C30B-L	42	6.5
PET-C30B-L	34	6.5
PET-I28E-L	34	4.3
W-PET-C30B-H	38	6.0
PET-C30B-H	30	4.9

$D_{0.1}$ and p for PET-C30B-L are larger than those for PET-C30B-H, which is a sign of more delamination at low feeding rate. The values of $D_{0.1}$ and p show an improvement in the degree of dispersion for W-PET-C30B-H compared to PET-C30B-H. Although the shear stresses in the dry extrusion process are larger than for processing with water, the presence of water leads to swelling of C30B and to hydrolysis of PET. Both these weaken the cohesive forces among clay platelets and facilitate the diffusion process. $D_{0.1}$ is the same for PET-C30B-L processed with and without water: however, the much larger aspect ratio (42 compared to 34) suggests more delamination for the water-processed nanocomposite. SSP does not affect the disordering of

C30B nanoparticles, since the value of $D_{0.1}$ of W-PET-C30B-L before and after SSP are the same (data not shown). $D_{0.1}$ is significantly larger for PET-C30B-L, compared to PET-I28E-L, as expected from the solubility parameters reported in ref [38]. Ghanbari et al [38] reported a $D_{0.1}$ value of 5.5% for a similar PET-C30B nanocomposite, while larger values (7.5% and 6.9 %) were obtained by Ghasemi et al [40], using a higher M_W PET and a larger TSE.

Larger aspect ratio in PET-C30B nanocomposites processed with water compared to the conventional melt-mixing is due to the more delamination of organoclays in PET matrix. Reduction of PET viscosity in water-assisted increases polymer chains diffusion into the interlayer of C30B. Screw configuration has also a significant effect on aspect ratio. However, in the case of I28E, because of increasing the incompatibility between PET and I28E in water-assisted, water has negative effect in dispersion and aspect ratio. It is noticeable that the initial aspect ratio of Cloisite Na+ based on the literature is 150 [2].

In order to further quantify the extent of delamination of C30B in different PET/clay nanocomposites, the number of platelets per clay particle was manually counted using the TEM images shown in Figure 4-9. In the case of PET-C30B-L, the single and double layers represent 69% while in PET-C30B-H is 56%. This confirms the effect of the residence time on the delamination or breakup of the clay particles. In the presence of water at low feeding rate (W-PET-C30B-L), the single and double layers represent 72%, compared to 65% for the high feeding rate case (WPET-C30B-H). Furthermore, the number of platelets per particle for W-PET-C30B-L is not affected by SSP.

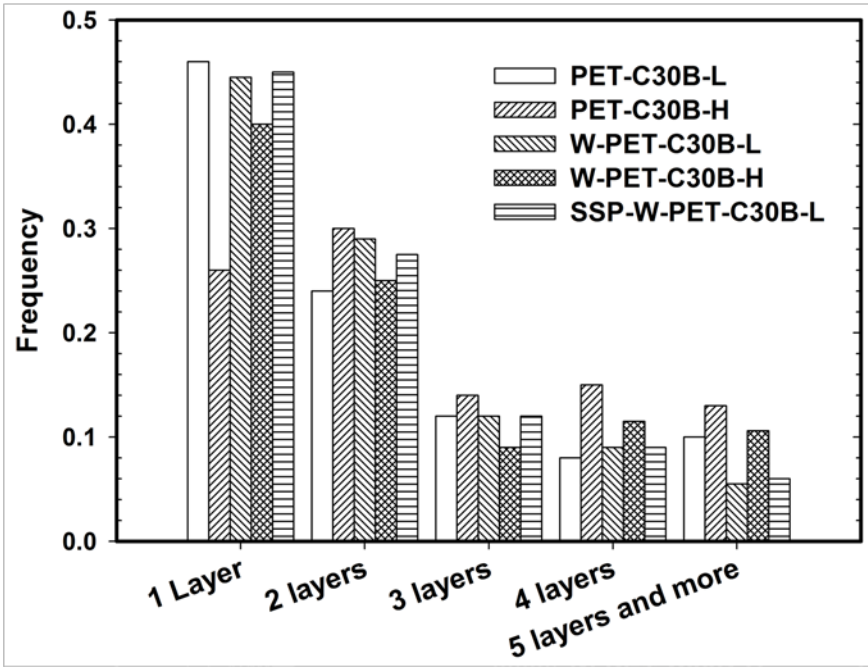

Figure 4-9 : Number of platelets per particle histogram. The total number of counted particles was around 600 for each nanocomposite.

4.3.4 Rheology

The total time for frequency sweep tests of the neat PET and PET nanocomposites was 230 s and during that period, the viscosity variation due to possible thermal degradation was less than 5%, hence, within the experimental errors.

The results of small-amplitude oscillatory frequency scans are reported in Figure 4-10. Figure 4-10a shows the effect of water, residence time and SSP on the complex viscosity of PET. The zero-shear viscosity (η_0) for PET-L, which was processed at dry conditions and low feeding rate, is 200 Pa.s, while when water was injected into the system, η_0 decreases to 100 and 20 Pa.s for W-PET-H and W-PET-L, respectively. Thus, the use of water and a longer residence cause significant reductions of the complex viscosity as a result of the hydrolysis reaction. On the other hand, solid-state polymerization helps to raise the M_W of hydrolyzed PET significantly. The η_0 values are 400 and 1250 Pa.s for SSP-W-PET-L and SSP-W-PET-H, respectively. It should be

noted that η_0 for the "as received" PET is 630 Pa.s. Therefore, SSP-W-PET-H has a higher M_W than the initial PET. Values of the M_W are reported in Table 4-1.

A Newtonian plateau is found in all PET samples irrespective of the processing method and M_W. As expected, the Newtonian plateau region is reduced for the higher M_W PETs obtained by SSP due to the increased number of chain entanglements. The value of 90^o for the loss angle at low frequencies and its behavior with frequency are typical of linear polymer chains [41]. As M_W increases, G' becomes more significant, and the value of the loss angle decreases with increasing frequency. The results show no indication that branching or cross-linking occurred during SSP. Thus, the linear structure of PET was maintained.

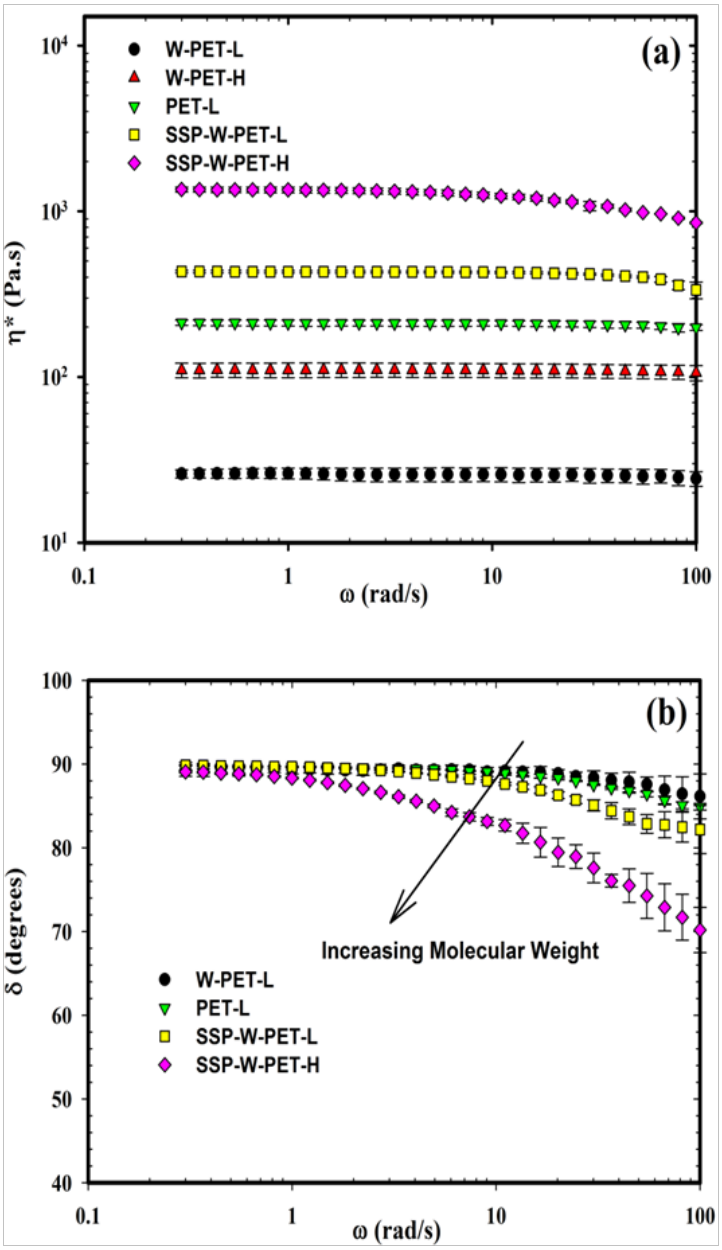

Figure 4-10 : Frequency sweep results of PET. (a) Complex viscosity vs. angular frequency, (b) loss angle vs. angular frequency.

The results of frequency sweep tests for nanocomposites processed at high feeding rate with and without water are presented in Figure 4-11. Figure 4-11a shows that both neat PETs (PET-H and W-PET-H) have a pseudo-Newtonian behavior, while the PET nanocomposites show shear-

thinning behavior. The presence of organoclays influences the rheology of the polymer nanocomposites, due to polymer-particle and particle-particle interactions and possible changes of the molecular structure of the polymer molecules. The complex viscosity of the nanocomposites at high frequencies, where the behavior of the matrix is dominant, is lower than that of the neat PET. This reflects PET degradation in the presence of organoclays. The complex viscosity of nanocomposites containing I28E is larger than those containing C30B in the whole frequency range. TEM and SEM images show a better dispersion and distribution of C30B within the PET matrix compared to I28E. Therefore, PET is more exposed to the surface of C30B than I28E, which leads to higher level of polymer degradation. Moreover, C30B has hydroxyl groups and unsaturated tallow groups that accelerate the PET degradation compared to the hydrogenated tallow of I28E.

Interestingly, W-PET-C30B-H processed with water exhibits a larger complex viscosity at low frequencies compared to the W-PET-H, while PET-C30B-H exhibits a lower complex viscosity compared to that for the neat PET. This suggests that, in the presence of water, the dispersion of organoclay improves. It also appears to compensate for the large reduction of the matrix viscosity due to hydrolysis.

The storage modulus versus angular frequency for the PET and PET nanocomposites is presented in Figure 4-11b. Both W-PET-H and PET-H have very low storage modulus. Significantly, the presence of 2wt% (nominal) organoclay increased the value of G' and reduced its slope at low frequencies and the solid-like behavior reflects the interconnected structure and geometric constraints as a result of the presence of organoclays. At high frequencies, the role of the matrix is more prominent. Smaller G' values are found for the nanocomposites processed under dry conditions due to the matrix degradation, compared to the neat polymer, whereas for the nanocomposites processed with water the opposite behavior is found. It shows the strong contribution of nanoparticles interactions that compensates the low G' of the hydrolyzed PET.

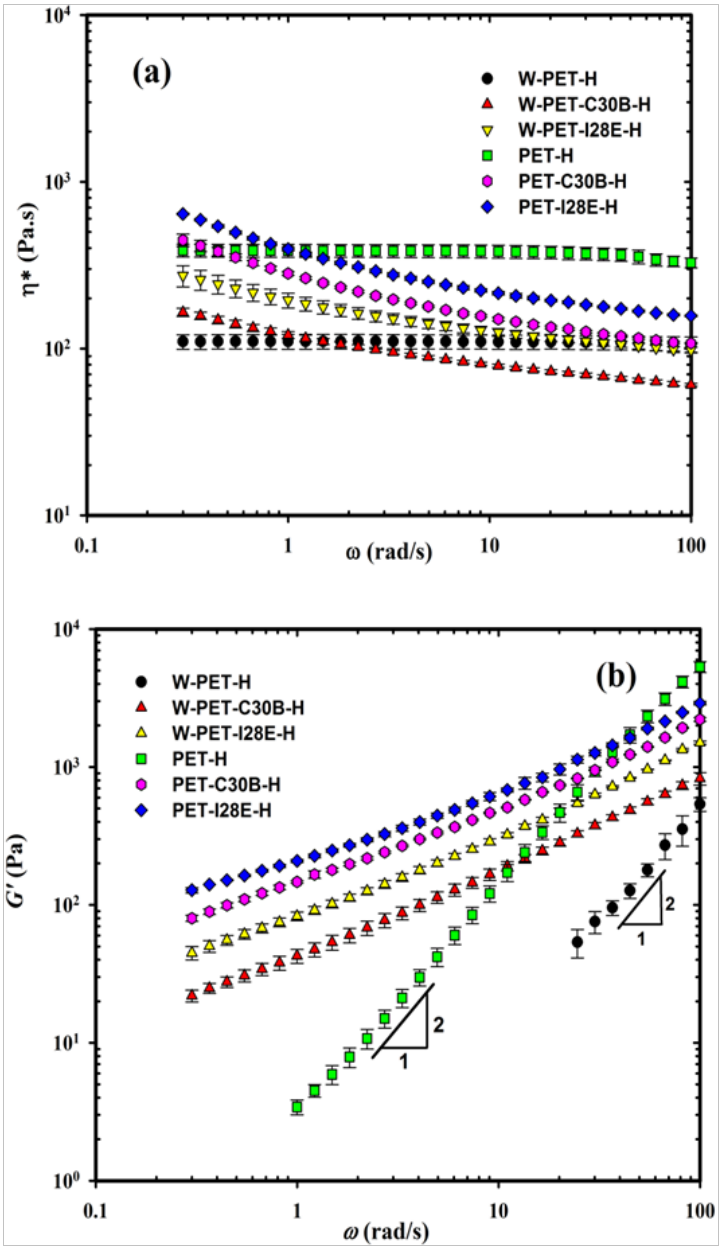

Figure 4-11 : Linear viscoelastic data for PET and PET nanocomposites processed at high feeding rate. (a) Complex viscosity vs. angular frequency; (b) storage modulus vs. angular frequency.

Rheological data for the PETs and PET nanocomposites after SSP are presented in Figure 4-12. The complex viscosity (Figure 4-12a) of the PET nanocomposites is much smaller than that

of the corresponding neat PETs after SSP. The situation is more complex for the storage modulus as reported in Figure 4-12b: at low frequencies, the modulus of the nanocomposite is larger than that of the corresponding neat PET, but the trend is reversed at high frequencies. The behavior is clearly indicative of strong degradation due to the presence of the nanoparticles.

The smaller complex viscosity in the nanocomposites compared to the neat PETs after SSP indicate that the presence of organoclay in the matrix slows down the diffusion of by-products due to the increased tortuosity.

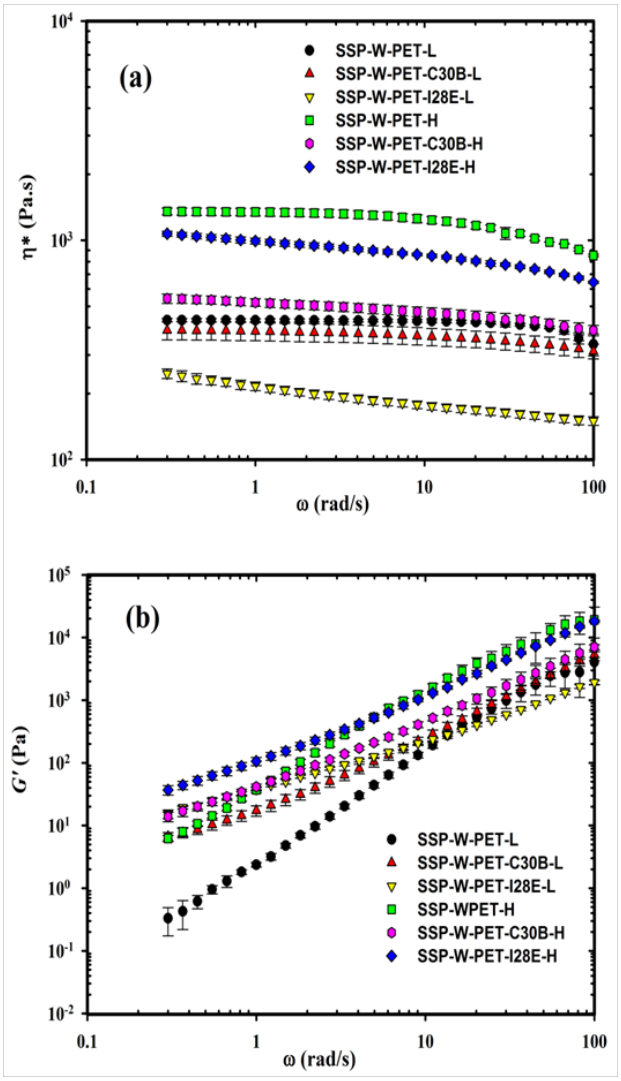

Figure 4-12 : Linear viscoelastic data for PET and PET nanocomposites after SSP. (a) Complex viscosity vs. angular frequency; (b) storage modulus vs. angular frequency.

4.3.5 Barrier Properties

The SEM and TEM analysis show that the best dispersion and distribution were obtained for C30B compared to I28E. Therefore, only the properties of PET-C30B nanocomposites are presented in Figure 4-13. The oxygen permeability values of the neat PET and PET-C30B nanocomposites, containing 2 wt% (nominal clay), processed with and without water are reported in the figure. The incorporation of C30B improves the barrier properties of PET nanocomposites, especially when processed with water. Although PET-C30B-L and SSP-W-PET-C30B-L show a better dispersion and distribution of C30B in the matrix compared to the nanocomposites processed at high feeding rate, the oxygen permeability of both nanocomposites is about the same. Ghasemi et al [40] also showed that the feeding rate did not have a significant effect on the barrier properties of PET nanocomposites. The permeability of PET-C30B-L and SSP-W-PET-C30B-L shows 19% and 26 % improvements, respectively compared to the neat PET. The improvement can be attributed to the increased tortuosity in the presence of C30B and the lower oxygen permeability of SSP-W-PET-C30B is due to the better dispersion and distribution of C30B in the presence of water. On the other hand, the presence of clay platelets changes the crystallinity of crystalline polymers that could affect the permeability. The percentage of crystallinity of PET-H, PET-C30B-H and SSP-W-PETC30B-H, PET-C30B-L, SSP-W-PET-C30B-L was determined using Eq.4 to be 5.9%, 7%, 4.8%, 8.4% and 6.1%, respectively. Hence, the changes in crystallinity cannot account for the enhanced barrier properties, at least for the SSP-W-PET-C30B nanocomposites. Ghasemi et al [2] showed that the presence of 3 wt% C30B into oriented PET films can improve by 23% the barrier properties compared to their neat PET, but the crystal content of their PET nanocomposites was almost 2 times larger than their neat PET, partly accounting for the barrier improvement. In another work, Shen et al [42] reported a 27% reduction in oxygen permeability for biaxial oriented PET nanocomposites containing 6 wt% of nanoclay compared to their neat PET.

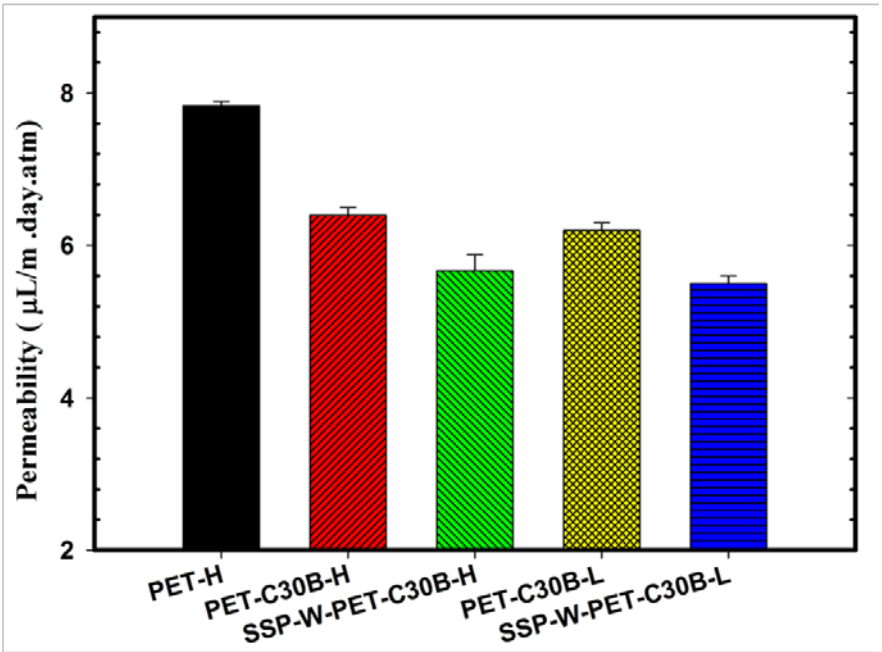

Figure 4-13 : Oxygen permeability of PET and PET nanocomposites.

4.3.6 Mechanical Properties

The tensile modulus and elongation at break of the neat PET and PET-C30B nanocomposites are reported in Figure 4-14. The presence of 2 wt% (nominal) of organoclay increases the tensile modulus of PET nanocomposites compared to the neat PET (Figure 4-14a). Two significant results are worth mentioning: on one hand, the PET-C30B nanocomposite processed at low feeding rate has slightly smaller tensile modulus although the morphology suggests a better dispersion and distribution of C30B. This is explained by the more severe degradation of the PET matrix at low feeding rates compared to the high feeding. The effect of feeding rate on the tensile modulus was also reported by Ghasemi et al [40], in good agreement with our results. On the other hand, PET-C30B, prepared by conventional melt-mixing, exhibits a smaller modulus compared to the nanocomposites prepared by water-assisted melt-mixing and subsequent SSP. For example, the tensile modulus is improved by 15% and 20% in PET-C30B-H and SSP-W-PET-C30B-H, respectively. Further improvement in the tensile modulus of nanocomposites is obtained by water-assisted melt-mixing and SSP compared to the conventional melt-mixed PET;

this is probably due to the better dispersion and distribution of C30B when processed with water compared to the conventional melt-mixing as well as the larger molecular weight obtained by SSP.

Ghasemi et al [2] reported a 20% larger tensile modulus for oriented PET nanocomposites containing 3 wt% of C30B compared to their neat PET, but, as mentioned before, the crystal content of their PET nanocomposites was almost 2 times larger than their neat PET. For samples prepared by compression molding other researchers [5] showed no improvement in the Young modulus in PET nanocomposites with 5 wt% of nanoclays compared to their PET matrix. Shen et al [42] reported a 25% increase in the tensile modulus of non oriented films of PET nanocomposites containing 6 wt% of nanoclays compared to their neat PET.

Figure 4-14b shows the effect of C30B and different processing conditions on the elongation at break of PET nanocomposites. As expected, the elongation at break significantly decreases in the presence of C30B in conventional PET nanocomposites. Moreover, the PET-C30B nanocomposites processed at low feeding rate have less elongation at break compared to those processed at high feeding rate. Surprisingly for nanocomposites obtained via the water-assisted extrusion and SSP, the elongation at break is reasonably high (the results were reproducible as shown by the error bars in Figure 4-14b): elongation at break is 130 and 180% for SSP-W-PET-C30B-L and SSP-W-PET-C30B-H, respectively, compared to 3 and 6% for PET-C30B-L and PET-C30B-H, respectively. It shows the strong potential of SSP for improving the ductility of PET nanocomposites.

The significant reduction of the elongation at break of nanocomposites compared to the neat PET can be attributed to aggregates of C30B, interfacial debonding of the clay particles at the PET matrix interface that could cause cavitations and micro-void formation. In the case of nanocomposites prepared by water-assisted melt-mixing and subsequent SSP (SSP-W-PET-C30B-L and H), a better dispersion and distribution of C30B into the matrix were obtained compared to the conventional PET-C30B nanocomposites, as shown in morphology images. Therefore, the better distribution of organoclay particles into the PET matrix results in an improvement of the stress distribution and smaller aggregates and, consequently, better mechanical properties. On the other hand, increasing the molecular weight of PET

nanocomposites through SSP and reconnecting the PET chains could lead to a significant enhancement of the elongation at break. It is generally accepted that the elongation at break increases with increasing molecular weight of linear polymers [43,44].

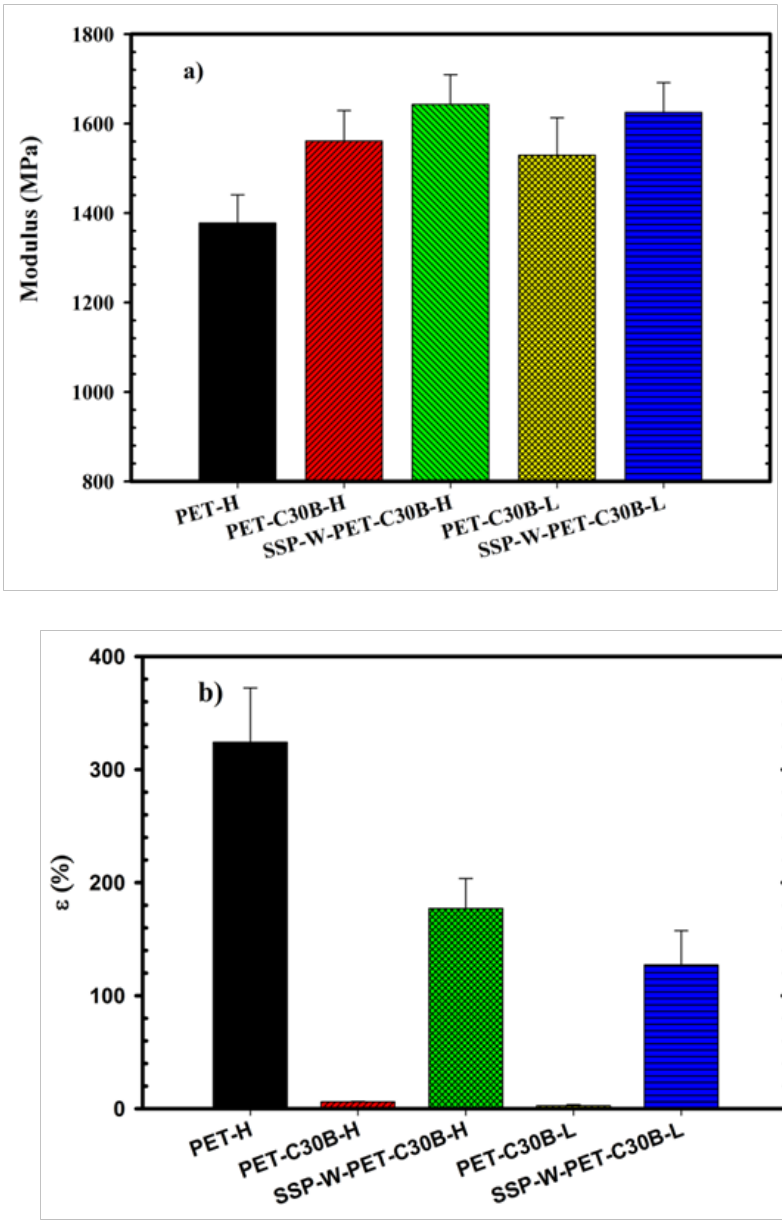

Figure 4-14 : Mechanical properties of PET and PET nanocomposites; (a) tensile modulus, (b) elongation at break.

4.4 Conclusions

There are significant advantages for the water-assisted melt-mixing process to produce partially exfoliated, well dispersed, and delaminated PET-C30B nanocomposites compared to the conventional melt-mixing. The presence of water results in a larger number of single and double layers of C30B nanoparticles as well as an increased aspect ratio in PET nanocomposites. The effect of water on the microstructure of PET nanocomposites is strongly dependent on the nanoclay modifier. Processing with water has negative effects on the PET-I28E nanocomposites, because of its lower compatibility.

Results of small amplitude oscillatory rheology and inherent viscosity showed that the M_W of PET increased significantly after SSP. The linear molecular structure of PET was maintained, as confirmed by ^{1}H NMR and ^{13}CNMR spectra as well as rheological measurements. It was also found that the extent of the SSP reaction in nanocomposites was lower than for the neat PETs, due to the barrier effect of clay platelets.

PET nanocomposites prepared by water-assisted extrusion followed by SSP (novel process) showed better mechanical and barrier properties compared to the nanocomposites prepared by the conventional melt-mixing process due to the only better dispersion and distribution of C30B in novel method since the percentage of crystallinity did not change significantly in different nanocomposites. In particular, the elongation at break for the SSPW-PET-C30B-H was appreciably improved to the order of 180% compared to 6% for the conventional nanocomposites (PET-C30B-H). Importantly, by using this novel method, enhanced barrier and mechanical properties were obtained without using any chemicals which would cause side reaction and changing the structure of PET. In addition, the extent of enhanced barrier properties in nanocomposites prepared by novel method compared to conventional melt-mixing was higher than using chain extender in the PET and PLA/C30B nanocomposites proposed by literature as well as observed brittle behavior in the nanocomposites with chain extenders. Importantly, by using this novel method, enhanced barrier and mechanical properties were obtained without using any chemicals which would cause side reaction and changing the structure of PET.

If we consider the typical shelf life of carbonated soft drinks as 90 days, it will increase to 107 and 113 days for the PET nanocomposites prepared by conventional melt-mixing and by the water-SSP novel method, respectively.

Acknowledgments

The authors acknowledge financial and infrastructure support received from The Natural Sciences and Engineering Research Council of Canada (NSERC), National Research Council of Canada (NRCC), Canada Development Bank (CDB). We would like to gratefully thank CREPEC members Mrs. W Leelapornpisit, Mrs. M Hamdine and Dr. B. Esmaeili for their technical help.

References

1. J.S. Lee, J. Leisen, R.P. Choudhury, R.M. Kriegel, H.W. Beckham, and W.J. Koros, *Polymer*, **53**, 213 (2012).
2. H. Ghasemi, P.J. Carreau, M.R. Kamal, and S.H. Tabatabaei, *Polym. Eng. Sci.*, **52**, 420 (2012).
3. X.F. Xu, A. Ghanbari, W. Leelapornpisit, M.C. Heuzey, and P.J. Carreau, *Int. Polym. Process.*, **26**, 444 (2011).
4. S. Li, K. Auddy, P. Barber, T.J. Hansen, J. Ma, H.-C. zur Loye, and H.J. Ploehn, *Polym. Eng. Sci.*, **52**, 1888 (2012).
5. S. Hayrapetyan, A. Kelarakis, L. Estevez, Q. Lin, K. Dana, Y.-L. Chung, and E.P. Giannelis, *Polymer*, **53**, 422 (2012).
6. D.R. Paul and L.M. Robeson, *Polymer*, **49**, 3187 (2008).
7. C. Chen, J. Samaniuk, D.G. Baird, G. Devoux, M. Zhang, R.B. Moore, and J.P. Quigley, *Polymer*, **53**, 1373 (2012).
8. S. Sinha Ray and M. Okamoto, *Prog. Polym. Sci.*, **28**, 1539 (2003).

9. E.P. Giannelis, *Adv. Mater.*, **8**, 29 (1996).

10. H. Ghasemi, P.J. Carreau, M.R. Kamal, and J. Uribe-Calderon, *Polym. Eng. Sci.*, **51**, 1178 (2011).

11. K. Stoeffler, P.G. Lafleur, and J. Denault, *Polym. Degrad. Stab.*, **93**, 1332 (2008).

12. T.-Y. Tsai, C.-H. Li, C.-H. Chang, W.-H. Cheng, C.-L. Hwang, and R.-J. Wu, *Adv. Mater.*, **17**, 1769 (2005).

13. W.J. Choi, H.L. Kim, K.H. Yoon, O.H. Kwon, and C.I. Hwang, *J. Appl. Polym. Sci.*, **100**, 4875 (2006).

14. X. Xu, Y. Ding, Z. Qian, F. Wang, B. Wen, H. Zhou, S. Zhang, and M. Yang, *Polym. Degrad. Stab.*, **94**, 113 (2009).

15. A. Ammala, C. Bell, and K. Dean, *Compos. Sci. Technol.*, **68**, 1328 (2008).

16. J.R. Samaniuk, *Improving the exfoliation of layered silicate in a poly (ethylene terephthalate) matrix using supercritical carbon dioxide*, M.S. Theisis , 2008, Virginia Tech, Blacksburg.

17. C. Davis, L. Mathias, J. Gilman, D. Schiraldi, J. Shields, P. Trulove, T. Sutto, and H. Delong, *J. Polym. Sci., Part B: Polym. Phys.*, **40**, 2661 (2002).

18. N. Fedullo, M. Sclavons, C. Bailly, J.-M. Lefebvre, and J. Devaux, *Macromol. Symp.*, **233**, 235 (2006).

19. F. Touchaleaume, J. Soulestin, M. Sclavons, J. Devaux, M.F. Lacrampe, and P. Krawczak, *Polym. Degrad. Stab.*, **96**, 1890 (2011).

20. Z.-Z. Yu, G.-H. Hu, J. Varlet, A. Dasari, and Y.-W. Mai, *J. Polym. Sci., Part B: Polym. Phys.*, **43**, 1100 (2005).

21. N. Hasegawa, H. Okamoto, M. Kato, A. Usuki, and N. Sato, *Polymer*, **44**, 2933 (2003).

22. D.D.J. Rousseaux, N. Sallem-Idrissi, A.-C. Baudouin, J. Devaux, P. Godard, J. Marchand-Brynaert, and M. Sclavons, *Polymer*, **52**, 443 (2011).

23. M. Mainil, L. Urbanczyk, C. Calberg, A. Germain, C. Jerome, S. Bourbigot, J. Devaux, and M. Sclavons, *Polym. Eng. Sci.*, **50**, 10 (2010).

24. D.S. Achilias, D.N. Bikiaris, V. Karavelidis, and G.P. Karayannidis, *Eur. Polym. J.*, **44**, 3096 (2008).

25. D. Bikiaris, V. Karavelidis, and G. Karayannidis, *Macromol. Rapid Commun.*, **27**, 1199 (2006).

26. D.W. Litchfield, D.G. Baird, P.B. Rim, and C. Chen, *Polym. Eng. Sci.*, **50**, 2205 (2010).

27. S.A. Jabarin and E.A. Lofgren, *J. Appl. Polym. Sci.*, **32**, 5315 (1986).

28. B. Duh, *Polymer*, **43**, 3147 (2002).

29. G. Barbara, S. Roger, and F.M. Timothy, *Macromol. Mater. Eng.*, **289**, 88 (2004).

30. B. Gantillon, R. Spitz, J.-L. Lepage, and T.F. McKenna, *Macromol. Mater. Eng.*, **289**, 119 (2004).

31. F. Samperi, C. Puglisi, R. Alicata, and G. Montaudo, *Polym. Degrad. Stab.*, **83**, 3 (2004).

32. T. Yalcinyuva, M.R. Kamal, R.A. Lai-Fook, and S. Ozgumus, *Int. Polym. Process.*, **15**, 137 (2000).

33. J.R. Campanelli, M.R. Kamal, and D.G. Cooper, *J. Appl. Polym. Sci.*, **48**, 443 (1993).

34. C.-Y. Kao, B.-Z. Wan, and W.-H. Cheng, *Ind. Eng. Chem. Res.*, **37**, 1228 (1998).

35. Y. Ma, U.S. Agarwal, D.J. Sikkema, and P.J. Lemstra, *Polymer*, **44**, 4085 (2003).

36. Q. Meng, M.-C. Heuzey, and P.J. Carreau, *Polym. Degrad. Stab.*, **97**, 2010 (2012).

37. D.L. Pavia, *Introduction to Spectroscopy*. 2009: Brooks/Cole, Cengage Learning.

38. A. Ghanbari, M.-C. Heuzey, P. Carreau, and M.-T. Ton-That, *Rheologica Acta*, **52**, 59 (2013).

39. Z.P. Luo and J.H. Koo, *Polymer*, **49**, 1841 (2008).

40. H. Ghasemi, P.J. Carreau, M.R. Kamal, and N. Chapleau, *Int. Polym. Process.*, **26**, 219 (2011).

41. N. Najafi, M.C. Heuzey, P.J. Carreau, and P.M. Wood-Adams, *Polym. Degrad. Stab.*, **97**, 554 (2012).

42. Y. Shen, E. Harkin-Jones, P. Hornsby, T. McNally, and R. Abu-Zurayk, *Compos. Sci. Technol.*, **71**, 758 (2011).

43. R.W. Nunes, J.R. Martin, and J.F. Johnson, *Polym. Eng. Sci.*, **22**, 205 (1982).

44. L. E. Nielsen, R.F. Landel, *Mechanical Properties of Polymers Composites 2e*, New York : Marcel Dekker (1994).

CHAPTER 5 ARTICLE 2- MICROSTRUCTURE AND PROPERTIES OF PET/ORGANOCLAY NANOCOMPOSITES PREPARED BY WATER-ASSISTED EXTRUSION: EFFECT OF ORGANOCLAY CONCENTRATION[1]

Maryam Dini[1], Tahereh Mousavand[2], Pierre J. Carreau[1], Musa R. Kamal[2] and Minh-Tan Ton-That[3]

[1] *CREPEC, Chemical Engineering Department, Ecole Polytechnique, H3T 1J4, Montreal, Quebec, Canada*

[2] *CREPEC, Department of Chemical Engineering, McGill University, H3A 2B2, Montreal, Quebec, Canada*

[3] *Automotive and Surface Transport Portfolio, National Research Council of Canada, J4B 6Y4, Boucherville, Quebec, Canada*

Abstract

PET/Cloisite 30B (C30B) nanocomposites containing different concentrations of the organoclay were prepared using two different twin-screw extrusion processes: conventional melt-mixing and water-assisted melt-mixing. The reduction of the molecular weight of the PET matrix, caused by hydrolysis during the water-assisted extrusion, was compensated by subsequent solid-state polymerization (SSP). XRD, SEM and TEM analyses showed intercalated/exfoliated morphology

---

[1] *Accepted in Polymer Engineering and Science; doi : 10.1002/pen.23736*

in all PET/C30B nanocomposites, with a higher degree of intercalation and delamination for the water-assisted process. Rheological, thermal, mechanical and gas barrier properties of the PET nanocomposites were also studied. Enhanced mechanical and barrier properties were obtained in PET-C30B nanocomposites compared to the neat PET. The nanocomposites exhibited higher tensile modulus and lower oxygen permeability after SSP. The elongation at break was significantly higher for SSP nanocomposites than for nanocomposites processed by conventional melt mixing.

5.1 Introduction

Polymer-layered silicate nanocomposites have attracted great interest because they have the potential to significantly enhance mechanical, barrier and thermal properties of some polymers at very low filler concentrations compared to conventional composites [1]. However, the achievement of significant performance enhancements requires good dispersion of the nanoclay in the matrix and thermodynamic compatibility between the organoclay and the polymer [1]. Melt-mixing and in-situ polymerization are the most common techniques to prepare polymer nanocomposites. Although, in-situ polymerization could yield better dispersion of clay platelets than melt-mixing, in-situ polymerization usually employs monomers and/or organic solvents that are toxic and environmentally hazardous [1, 2]. On the other hand, melt-mixing is more flexible, economical and practical. However, in the melt-mixing process, the polymer matrix and nanoclay modifiers could undergo thermal degradation at the high processing temperatures used. The microstructure of polymer nanocomposites plays an important role in determination the macroscopic properties of final products.

Poly(ethylene terephthalate) (PET) is a semi-crystalline engineering polymer with low cost and high performance. In view of its excellent transparency and good barrier properties, it is used in a large variety of applications such as containers, films, bottles and fibers [3]. One of the areas of growing interest for using PET is for food and beverage packaging. Substantial growth in this area requires improvement in the barrier to O_2 and CO_2, along with reduction of the weight of the final products. Recent studies show that the presence of organoclay platelets in PET can lower permeability to oxygen and water vapor [4, 5, 6]. Moreover, improvements of mechanical

properties of PET by incorporation of organoclays have been reported [5-8]. Thus, PET nanocomposites, that incorporate high aspect ratio nanoclay as an impermeable phase with high modulus (178 GPa), could provide products with both higher barrier and improved tensile modulus [1]. Several efforts have been made to achieve good dispersion of organoclay in PET by melt-mixing. However, a significant thermal degradation of PET and of the organo- modifier presents big challenges. Ghasemi et al [6] showed that the incorporation of 3 wt% Cloisite30B (C30B) in oriented PET/clay nanocomposite films raised the barrier and tensile modulus of PET by 27% and 30 %, respectively. Xu et al [5] reported 10% and 19% increases in barrier and tensile modulus, respectively, using 2wt% organoclay in oriented PET nanocomposite films. Shen et al [7] reported 27% reduction in oxygen permeability coefficient and 44% increase in tensile modulus for biaxial oriented PET nanocomposites containing 6 wt% of nanoclay, compared to neat PET. However, in unoriented films, the tensile modulus increased by only 25% in nanocomposites. An improvement of 46% in barrier properties was also obtained by Ghanbari et al [8] in oriented films of PET nanocomposites containing 4 wt% organoclay and 1 wt% chain extender.

Water assisted melt blending is a practical approach to preparing nanocomposites, combining the benefits of both solution and conventional melt-mixing methods [9,10]. Various reports referred the injection of water into the extruder to enhance the microstructure of nanocomposites based on PA6, PA11, and PP [11-14].

Solid-state polymerization (SSP) of PET nanocomposites is a practical route to compensate for polymer degradation that occurs during the melt-mixing process [15,16]. Kim et al [16] studied the effects of PET molecular weight and chemistry of organomodifiers on the SSP after melt-mixing. They claimed that SSP favored the opening of the basal spacing of organoclays, depending on the chemistry of organoclays and molecular weight of PET. Lower molecular weight PETs showed larger gallery spacing of organoclays after SSP. Litchfield et al [15] examined the effect of SSP on the mechanical and rheological properties of PET nanocomposites after melt-mixing. SSP was investigated for reaction times ranging from 10 to 50 h, but no improvement of the intercalation was found. On the other hand, melt-spun fibers of PET nanocomposites containing 1 wt% of Cloisite 20A showed a 28% improvement in the tensile modulus after SSP compared to the neat PET. Although one of the disadvantages of SSP is its

slower rate than those involving chain extenders, it does not lead to significant changes in the chemical structure of PET. Moreover, some chain extenders can cause side reactions with undesirable by-products.

The present work reports the results obtained using a novel approach for producing PET/clay nanocomposites by combining water-assisted melt-mixing and SSP. Emphasis is placed on the mechanical and barrier properties of the nanocomposites. Other properties include morphological, rheological and thermal properties obtained for different concentrations of nanoclay, Cloisite C30B clay from Southern Clay Products Inc. To our knowledge, no report has considered the combined effects of water-assisted melt-mixing and SSP on the improvement of the microstructure and properties of PET nanocomposites. Since SSP after conventional melt-mixing of PET nanocomposites has been addressed in the literature [15, 16], we did not repeat those investigations.

5.2 Experimental

5.2.1 Materials

A general purpose PET (PET 9921, Eastman Co, Kingsport, TN) with M_W equal to 65 000 g/mol was used. The organoclay used was Cloisite 30B (Southern Clay Products Inc., Gonzales, TX) at the following nominal concentrations: 2, 3.5, and 6 wt%. Cloisite 30B (C30B) is based on the modification of sodium montmorillonite by ion exchange with methyl, tallow, bis-2-hydroxyethyl quaternary ammonium cations.

5.2.2 Melt Compounding

The compounding of PET with Cloisite 30B to form the nanocomposites was carried out using a co-rotating twin screw extruder (TSE) (Berstorff ZE25, Hannover, Germany) with a 25 mm screw diameter (D) and length-to-screw diameter ratio of 28 at a screw speed of 200 rpm. The screw configuration is shown in Figure 5-1. The temperature profile was 245, 265, 260, 255, 255, and 255°C from the hopper to the die. The screw had three mixing zones. The first consisted

of one kneading block (KB) (left hand 45 staggering angle), followed by one reverse element and two blister rings. The reverse elements and the 2 blister rings help to raise the pressure before water injection. The second mixing zone contains one gear-type mixing elements (ZME) and one KB element with 90° staggering angles. In the third mixing zone, two kneading blocks (90° and right hand 45° staggering angles) and one ZME element were used.

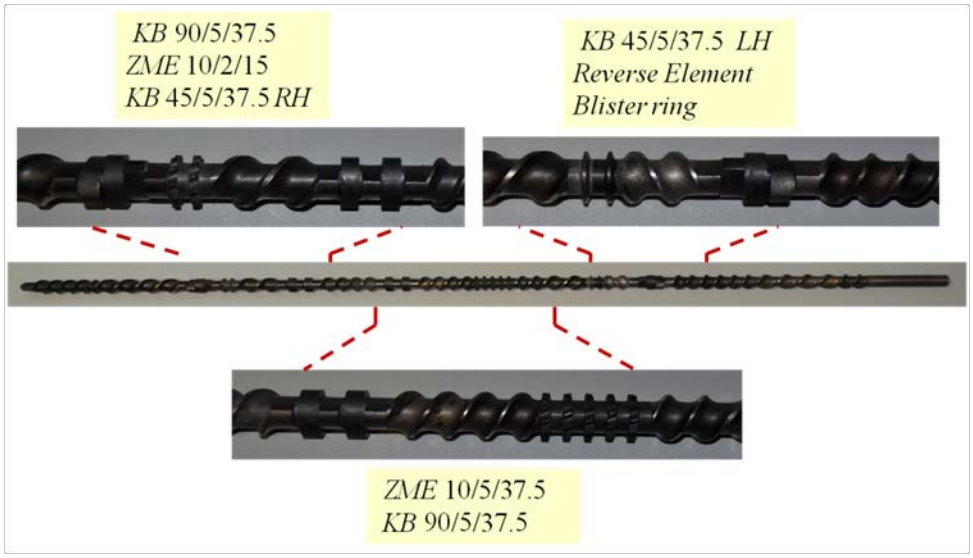

Figure 5-1 : Screw configuration (extrusion direction is right to left). In KB notation, the first number shows the staggering angle, the second is the number of kneading elements and the third number indicates the width of each kneading lobe in mm; left hand and right hand KB elements are shown by LH and RH, respectively. In gear type mixing elements (ZME), the first number indicates the number of teeth around the circumference, the second represents the number of gears in each ZME block and the third is the length of ZME block in mm.

Ground PET pellets were dry-mixed with clay before melt compounding. The mixture was fed into the TSE at 3 kg/h. A 2-L pressure vessel (Parr Instrument Co., Moline, IL) was utilized to produce and feed steam in the second zone of the TSE (see Figure 5-1) at 0.3 L/h, 160 ºC. The injection pressure was 550 kPa, hence saturated steam (quality ≈ 1) was injected into the extruder. Finally, the steam was removed from the TSE using a vacuum pump in the last zone of

the extruder. After reaching steady state, the extrudate was cooled by air, cut, pelletized and then ground.

5.2.3 Solid-State Polymerization (SSP)

Solid-state polymerization (SSP) was carried out to rebuild the reduced M_W of hydrolyzed PET and PET nanocomposites. Before SSP, the PET and PET nanocomposites were ground and sieved to a powder of size less than 400 µm. SSP was performed in a cylindrical stainless steel reactor at 215°C under N_2 for 8 h. This was the maximum practical operating temperature without encountering experimental difficulties. The flow rate of N_2 into the reactor was 2 L/min. After 8 h, the heater was turned off, but the nitrogen purge was continued to decrease the temperature of the reactor to 100°C prior to collecting the resulting polymer or nanocomposites.

Codes of the samples, which are processed in different conditions, are presented in Table 5-1.

Table 5-1 : Codes for the samples

Sample	Nominal C30B (wt %)	Inorganic content [1] (wt %)	Melt-Mixing Process
Neat PET	0	0	Conventional
PET-C30B-2	2	1.1 ± 0.2	Conventional
PET-C30B-3.5	3.5	2.1 ± 0.2	Conventional
PET-C30B-6	6	3.6 ± 0.4	Conventional
SSP-W-PET-C30B-2	2	1.2 ± 0.2	Water-assisted + SSP
SSP-W-PET-C30B-3.5	3.5	2 ± 0.3	Water-assisted + SSP
SSP-W-PET-C30B-6	6	3.7 ± 0.4	Water-assisted + SSP

The inorganic content in the nanoclays was determined by burning samples in a furnace at 750°C under air for 6 hrs.

Samples for rheometry, XRD and morphology analysis were molded in the form of disk-like plates with a diameter of 25 mm and a thickness of ~ 1.2 mm. Thin sheet samples 250 μm thick for mechanical tests and 300 μm thick for barrier tests were prepared via compression molding. All samples were prepared using a hot press (Carver Laboratory Press, Model 3912) with a small chamber for nitrogen purge. The compression molding temperature and maximum pressure were 270 °C and 3 tons, respectively. All the samples were dried under vacuum for 24 h at 80 °C prior to melt processing and molding.

5.2.4 Characterization

A wide angle X-ray diffractometer (WAXD) (D8 Discover, Bruker AXS Inc., Madison, WI) with CuKα radiation (λ=1.54056 Å) was used to estimate the basal spacing (d_{001}) for silicate layers. The generator was operated at 40 kV/ 40 mA and the nanocomposites were scanned from 0.8 to 10° at 0.015°/s.

A field emission gun scanning electron microscope (FEG-SEM, S-4700, Hitachi, Tokyo, Japan) was used to investigate the distribution of clay in the PET matrix. The specimens were prepared using an Ultracut FC microtome (Leica, Wetzlar, Germany) with a diamond knife and then coated with platinum vapor. The quality of the clay dispersion was evaluated using transmission electron microscopy (TEM) (JEOL JEM-2100F, Tokyo, Japan, operating at 200 kV). The samples were microtomed into approximately 50-80 nm thick slices, using an Ultracut FC cryomicrotome system at -100° C.

Rheological measurements were carried out at 265°C under nitrogen atmosphere using a Bohlin Gemini HR rheometer (Malvern Instrument, Worcestershire, UK) and an Advanced Rheometric Expansion System (ARES, TA Instruments), both with a 25mm parallel plate geometry. The samples were dried under vacuum at 80°C for 24 h before the rheological tests. Time sweep tests were performed at frequency 0.1 Hz and frequency sweep tests were done in the linear viscoelastic region for each sample, as determined by strain sweep tests. Frequency sweep tests over a frequency range of 0.3- 100 rad/s were performed from low to high and high to low frequencies, to assure the repeatability of the data.

The thermal properties of the neat PET and PET nanocomposites were studied by differential scanning calorimetry (DSC Q1000, TA instruments, New Castle, DE) under N_2 atmosphere using 10 °C/min scanning ramp from 30 °C to 300 °C.

Tensile measurements were conducted using an Instron 3365 universal tester with a 500 N load cell and according to the ASTM D882-10 standard. The tensile testing samples were cut from 250 µm thin sheets to a rectangular shape (10 mm x 100 mm). The samples were tested at room temperature and a crosshead speed of 25 mm/min.

Oxygen transmission rates (OTRs) were determined using Ox-Tran Model 2/21 oxygen permeability MD Module (MOCON Inc., USA) at 23 °C under a pressure of 0.96 atm. Dry oxygen (100%) was passed over one side of the sample and a mixture of 98% N_2 (nitrogen) with 2% H_2 (hydrogen) was used as the carrier gas. The test area of the samples was 5 cm^2. The oxygen permeation values reported in this work have been normalized by the film thickness. The permeability coefficient [*P*, in µL/(m.day.atm)] was obtained from the OTR values using the following formula:

$$P = \text{OTR} \times L/p \tag{5-1}$$

where *L* is the film thickness (m) and *p* is the testing pressure (atm).

5.3 Results and discussion

5.3.1 Morphology

XRD results for PET nanocomposites with two different clay concentrations prepared with and without water are presented in Figure 5-2. The PET/C30B nanocomposites show two peaks at $2\theta \approx 2.5^{o}$ and $2\theta \approx 5.2°$, which correspond to *d*-spacing ~3.45 and 1.7 nm, respectively. Since the *d*-spacing values for the pristine organoclay, C30B, is 1.8 nm, the first peak shown for the nanocomposites is indicative of diffusion of PET chains into the gallery spacing of C30B. The second peak suggests possible degradation of the organic modifier during processing or it could also be a reflection of the first peak. The same peak positions are observed for the PET nanocomposites containing different C30B concentrations, but the peak intensity increases with

concentration. This indicates more aggregates at larger C30B loadings. The intensity of the peaks is also lower for the water-assisted processed nanocomposites, compared to the dry extrusion nanocomposites. This indicates a higher degree of clay delamination in the presence of water.

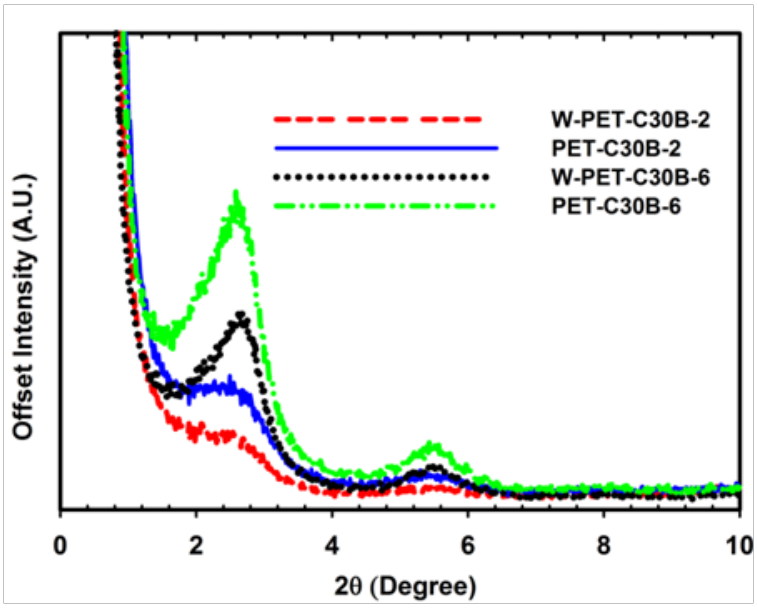

Figure 5-2 : XRD results of PET nanocomposites; the effect of organoclay concentration and water-assisted melt-mixing.

Furthermore, the color of the samples prepared by water-assisted and SSP was found to be is lighter compared to the color of the conventional melt-mixing sample. By increasing the C30B concentration, the number and size of the aggregates increase. For higher nanoparticles contents the inter-particle distance is reduced and this leads to a higher probability of C30B aggregation.

SEM micrographs for PET nanocomposites are presented in Figure 5-3. The brighter areas represent clay particles and the darker regions correspond to the PET matrix. For 2 wt% C30B, there is a significant difference in terms of particle size for the two nanocomposites. The number of particles per unit area appears to be significantly smaller for the sample prepared with water. The apparently low clay density can be related to the delamination of a number of C30B aggregates into much smaller aggregates, which cannot be captured by SEM. However, from a

close examination of the micrographs we observe a larger nanoclay density (more particles per unit area) for the 6 wt% nanocomposite processed by water-assisted extrusion, compared to the conventional melt-mixing sample, indicating a better dispersion and distribution of C30B. Moreover, for the 6wt% nanocomposite prepared by conventional melt-mixing large agglomerates are found, while such large agglomerates were not observed in the SEM micrographs for the water-assisted sample. Overall, there is good evidence of a better dispersion of the clay in nanocomposites prepared with water.

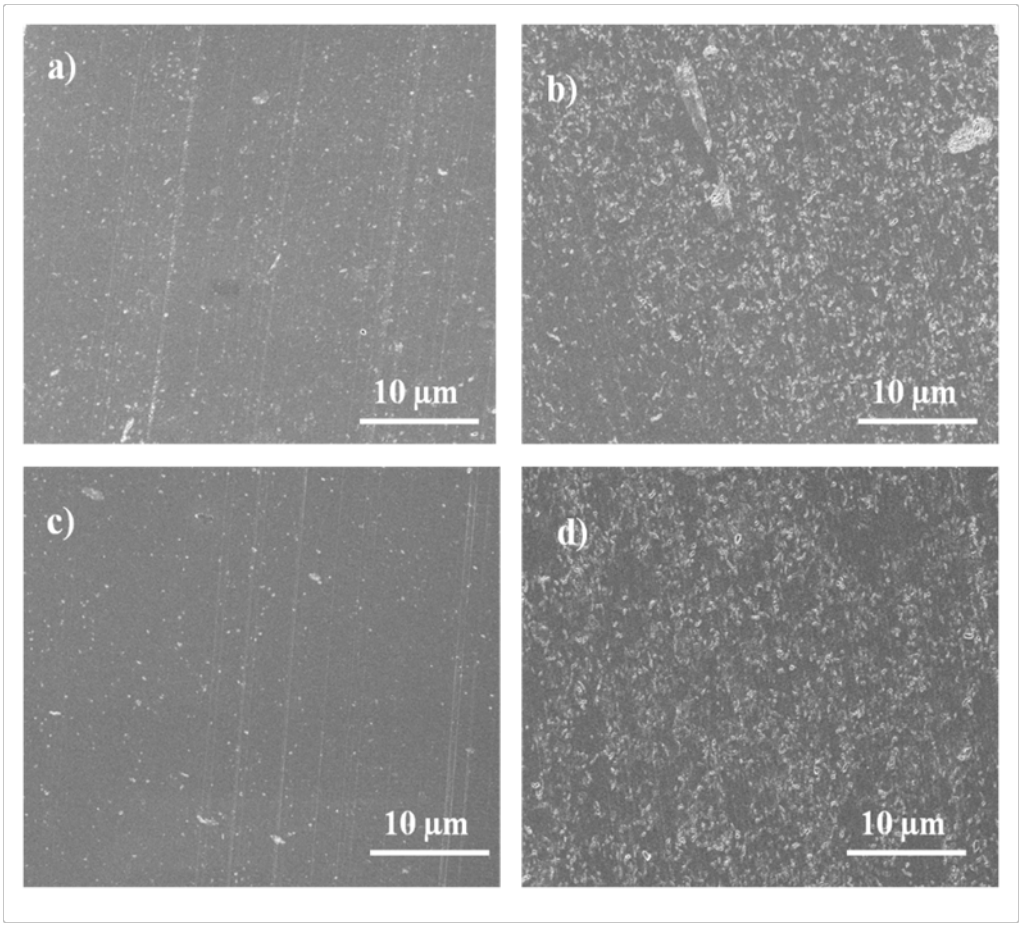

Figure 5-3 : SEM micrographs of PET nanocomposites processed under different conditions; a) PET- C30B-2, b) PET-C30B-6, c) W-PET-C30B-2, d) W-PET-C30B-6.

Figure 5-4 shows TEM images of PET/C30B nanocomposites processed with and without water. These images are typical of an intercalated/exfoliated morphology for all PET/C30B nanocomposites. There is evidence of clay with single, double and triple layers for the one prepared with water (Figure 5-4a). In order to obtain a quantitative estimate of the degree of dispersion of organoclay platelets in the PET matrix, the $D_{0.1}$ factor proposed by Luo and Koo [17] was calculated using 400 measurements based on TEM images. A value below 4% for $D_{0.1}$ suggests an immiscible system or microcomposite, and values over 8% indicate an exfoliated structure, while values between 4 and 8% indicate intercalation. Values of $D_{0.1}$ are 5.3, 6 and 4.9 for PET-C30B-2, W-PET-C30B-2, and PET-C30B-6, respectively. These values suggest more delamination of the aggregates in the nanocomposite processed with water, confirming the XRD results (Figure 5-2). Similar information is obtained by comparing the aspect ratios, α', of nanoparticles, using TEM images and 200 measurements for each case as done by Ghasemi et al. [4]. The aspect ratios, α', were found to be 37 and 40 for conventional melt-mixed nanocomposites and water-assisted nanocomposites, respectively, suggesting again more delamination for the water-processed nanocomposite. Histograms of calculated aspect ratio in PET nanocomposites containing 2wt% of C30B are presented in Figure 5-5. This figure clearly displays that, while the averaged aspect ratios for both cases are close to each other, the distribution of the aspect ratio is totally different for both samples. For the nanocomposite processed with water, the number of platelets of higher aspect ratio in the range of 60-80 is larger than for the conventional melt-mixing samples.

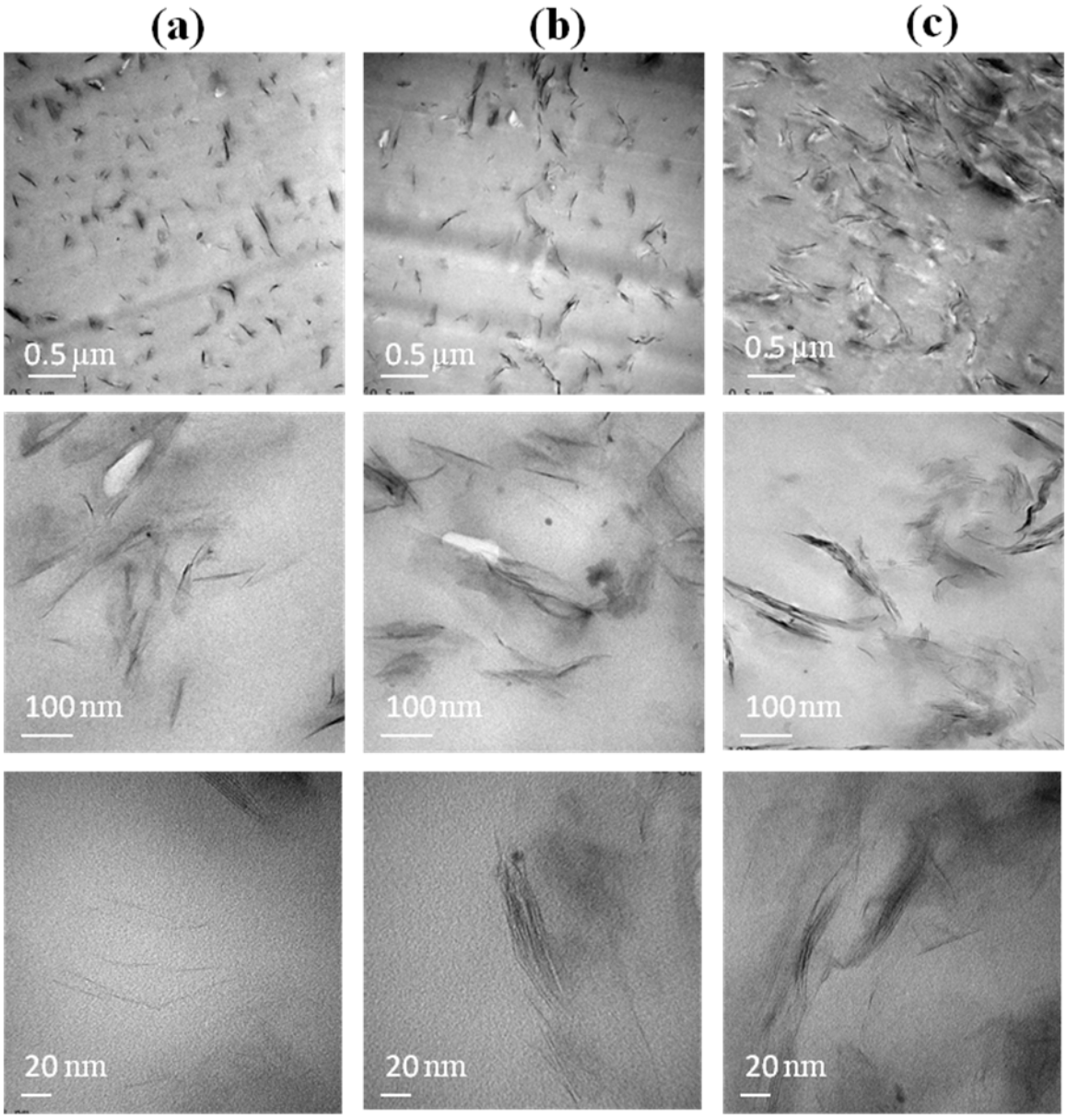

Figure 5-4 : TEM images; a) W-PET-C30B-2, b) PET-C30B-2, c) PET-C30B-6 at different magnifications.

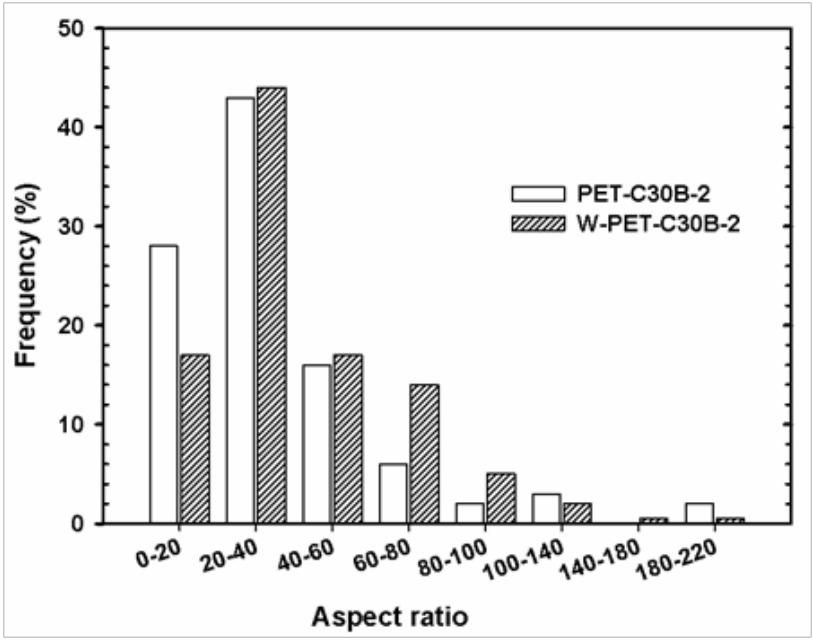

Figure 5-5 : Histogram of calculated aspect ratio for PET nanocomposites containing 2wt% of C30B.

5.3.2 Rheology

Figure 5-6 reports the linear viscoelastic data from frequency sweep tests for PET nanocomposites with different C30B concentrations processed without water. The total time for each frequency sweep test was 230 s. The viscosity variation during these tests, due to possible thermal degradation, was less than 5%. The complex viscosity of the neat PET (neat PET means extruded PET) is shown to be independent of frequency, whereas the PET nanocomposites exhibit a shear-thinning behavior that becomes more pronounced with increasing C30B concentration (Figure 5-6a). The nanocomposite containing 2wt% C30B has a lower complex viscosity than the neat PET, but the complex viscosity increases markedly with increasing C30B concentration, due to particle-particle interaction. However, the lower complex viscosity for the 2 wt% nanocomposite and the cross-over at high frequencies for the 3.5 and 6 wt% nanocomposites with respect to the neat PET suggest a severe PET degradation during processing in the presence of C30B.

Figure 5-6 presents the storage modulus versus angular frequency for the neat PET and nanocomposites containing different C30B loadings, processed by dry extrusion. The neat PET exhibits a terminal behavior with a slope of 2 on the log-log plot, as predicted by the Maxwell model [18]. At low frequencies, the storage modulus increases rapidly and the slope is reduced with increasing C30B concentration. The solid-like behavior (slope approaching zero) reflects the interconnected structure and geometric constraints as a result of the presence of nanoparticles.

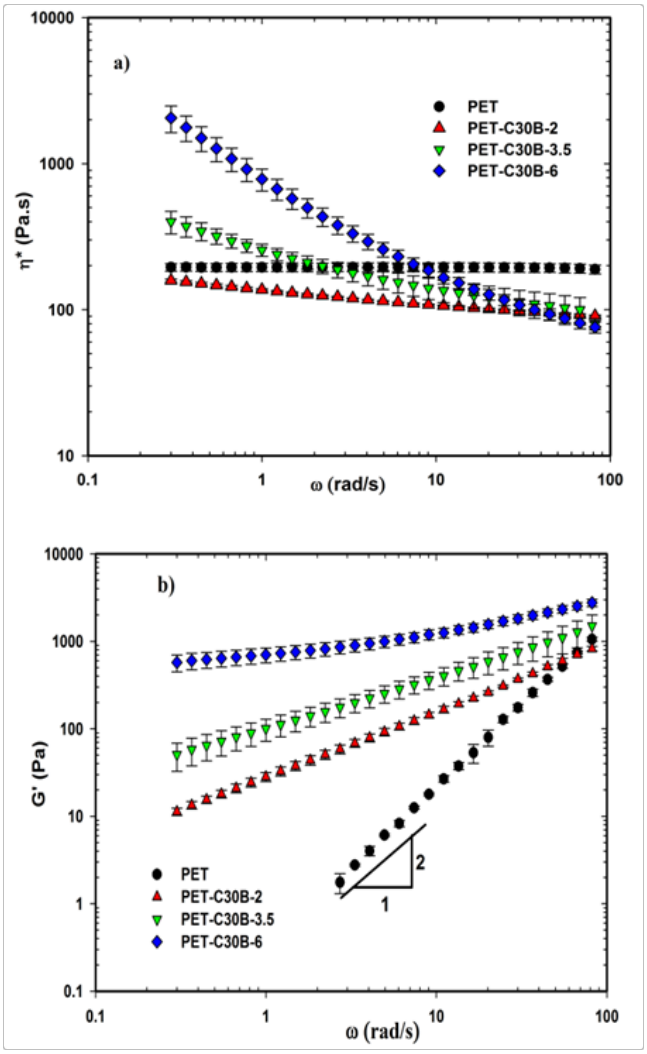

Figure 5-6 : Linear viscoelastic data for PET and PET nanocomposites processed via dry extrusion; a) complex viscosity vs. angular frequency; b) storage modulus vs. angular frequency.

Figure 5-7 reports the corresponding linear viscoelastic data for the PET and nanocomposites processed with water. As expected, the presence of water lowers the viscosity of the neat PET significantly. The complex viscosity of W-PET is 60 Pa.s, compared to 200 Pa.s for the PET processed under dry conditions. The rheological behavior of the nanocomposites processed with water is similar to that depicted in Figure 5-6a, for the nanocomposites processed via dry extrusion. However, the complex viscosity for the water-extruded nanocomposites is much larger than the matrix viscosity (W-PET). This suggests the presence of stronger particle-particle interactions in the water-extruded samples. These interactions may be attributed to a more complete delamination of the aggregates or tactoids, as seen in Figure 5-2 and Figure 5-3. We note finally that the complex viscosity of the 2wt% nanocomposite and that of the more concentrated nanocomposites at high frequencies are lower than that of W-PET, suggesting again degradation of the matrix in the presence of C30B. The complex viscosities of PET nanocomposites at high frequencies processed with water are lower than those of the corresponding nanocomposites obtained by conventional melt-mixing, due to the hydrolysis reaction.

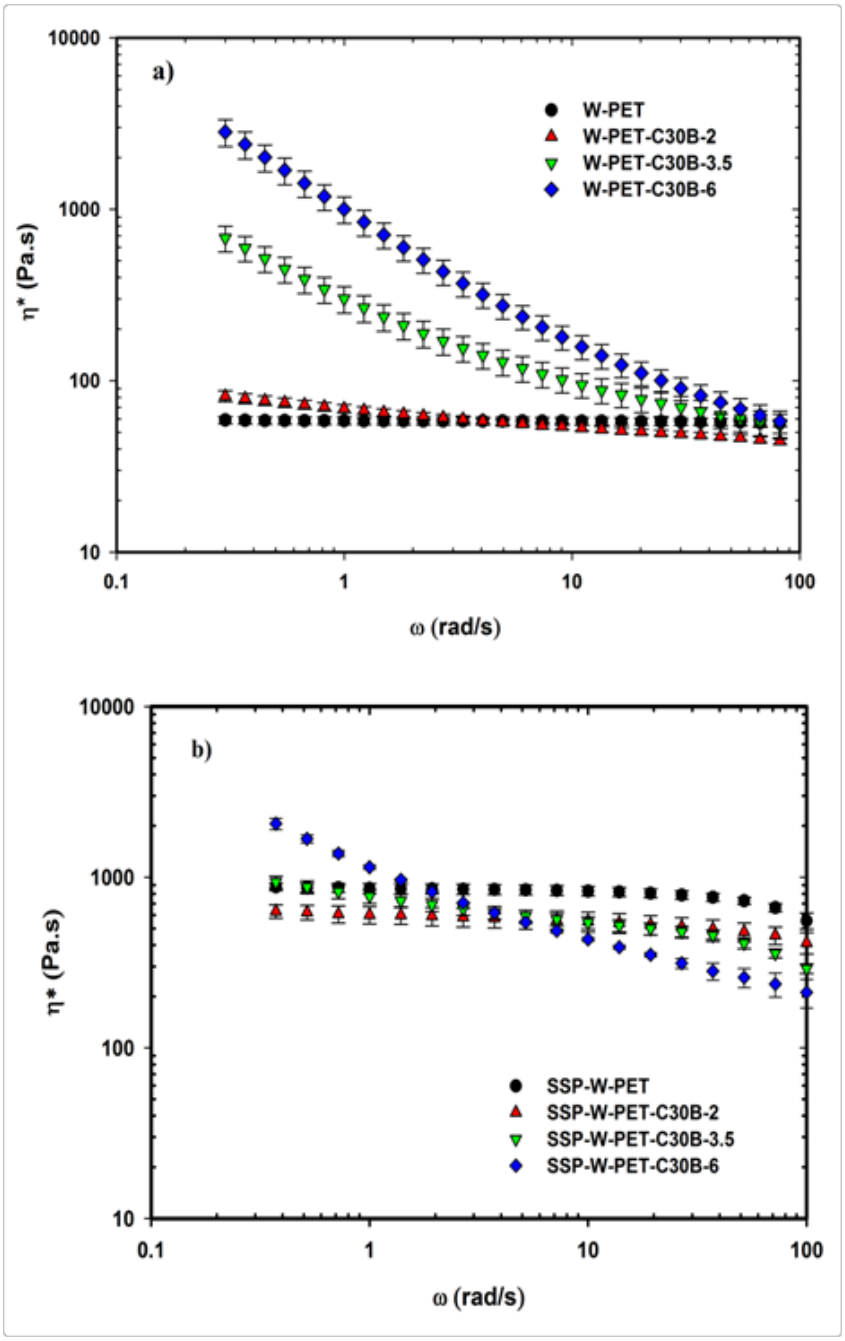

Figure 5-7 : Complex viscosity vs. angular frequency in PET and PET nanocomposites processed with water; a) before SSP, b) after SSP.

Figure 5-7b presents the rheological behavior of the nanocomposites after SSP: the zero-shear viscosity of SSP-W-PET is 800 Pa.s., which is larger than the zero-shear viscosity of PET

and W-PET. After SSP, the complex viscosity at high frequencies of the PET nanocomposites increases to values significantly larger than those of nanocomposites obtained by conventional melt-mixing. Figure 5-7b also illustrates the important shear-thinning behavior of the nanocomposites containing 3.5 wt% and 6 wt% after SSP. Moreover, the nanocomposites after SSP exhibit lower complex viscosities at high frequencies compared to the neat PET after SSP due to either degradation of the PET matrix or slower polymerization rate of PET in the presence of C30B.

The storage modulus vs. angular frequency curves for the neat PET and SSP-W-PET are presented in Figure 5-8a. The slope of the log-log plot for these two samples is 2, which is a sign of the linear chain structure of PET even after SSP. There are reports that the use of chain extender with PET forms a branched structure, causing a rise in the storage modulus and lowering of the slope of the log-log plot significantly [8, 19]. In our previous work, we verified by ^{1}H NMR and ^{13}C NMR that after SSP the structure of PET chains did not change and the linear structure was preserved [20]. The Han plots [19, 21] for the neat PET and SSP-W-PET are presented in Figure 5-8b. The rise of the molecular weight of PET due SSP does not cause a change in the slope of the plot. However, at the same G'', SSP-W-PET exhibits larger G' values compared to the neat PET, probably due to changes in the molecular weight distribution.

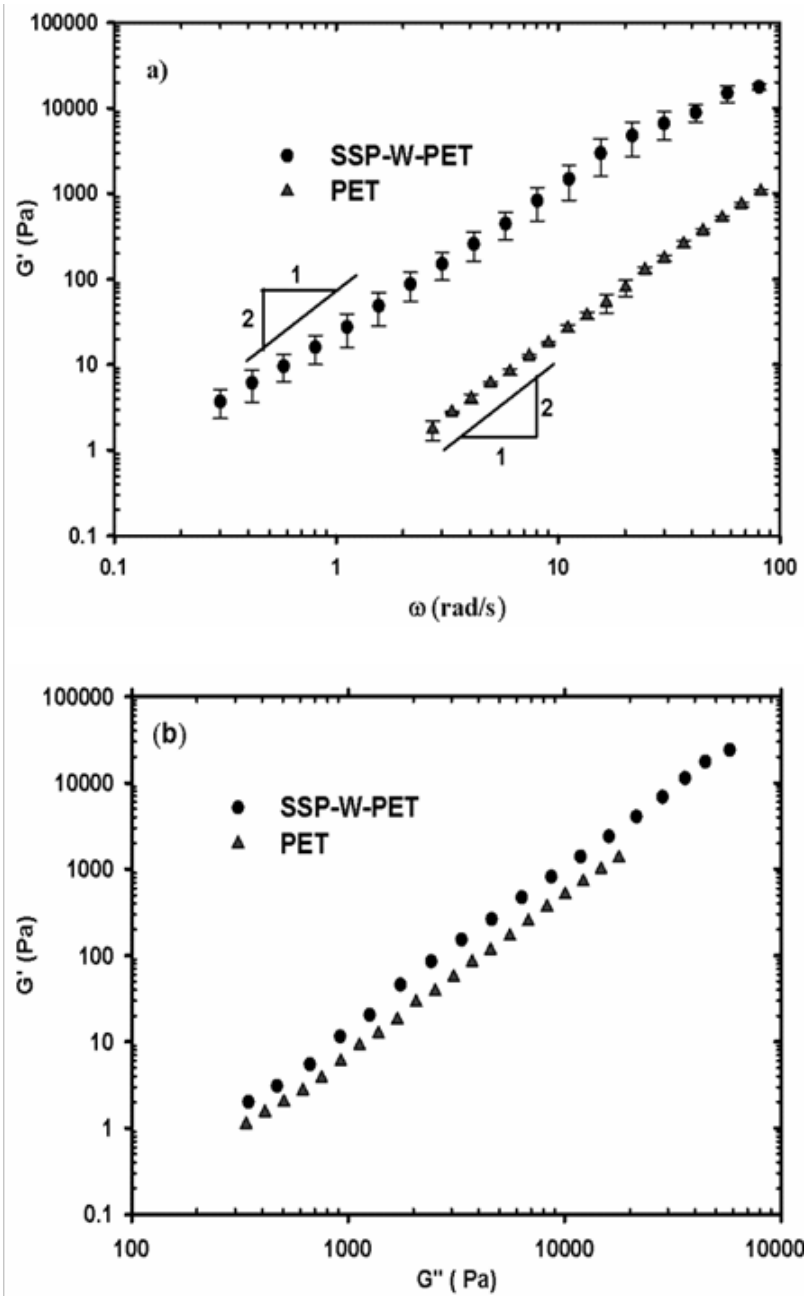

Figure 5-8 : a) Storage modulus vs angular frequency of PET and SSP-W-PET; b) Han plot.

Molecular weight of neat PET can be determined by viscometry measurements, but this method involves some problems when used in conjunction with PET nanocomposites. The complete separation of organoclays from PET is not possible. Thus, either filtering or not filtering of organoclays will affect the molecular weight determination using viscometry

measurements. Therefore, the molecular weights of PET for the nanocomposites, before and after SSP, are estimated using the Maron-Pierce model [22]. The apparent M_W of the matrix of polymer nanocomposites is determined based on the relation between the complex viscosity at 100 rad/s and M_W (Eq. 5-2).

$$\eta^*_{m(100rad/s)} = kM_W^a \tag{5-2}$$

The constants in Eq.5-2 are obtained by drawing $\log \eta^*_{m(100rad/s)}$ of different neat PETs versus log M_W of the neat PETs determined from the inherent viscosity measurement. The values of *a* and *k* are 3.14 and 3.94×10^{-13} Pa.s.mol$^{3.14}$/g $^{3.14}$, respectively. Table 5-2 shows the calculated values for the apparent matrix complex viscosity and M_W.

The M_W of the neat PETs obtained by intrinsic viscosity measurements show that hydrolysis significantly lowers the molecular weight of PET, but SSP causes the molecular weight of PET to rise appreciably. M_W is 68 000 g/mol for SSP-W-PET, compared to 47 000 g/mol and 33 000 g/mol for PET and W-PET, respectively.

As suggested earlier, Table 5-2 shows that the PET has lower molecular weights in melt processed PET nanocomposites compared to the neat PET, due to the matrix degradation in the presence of C30B. On the other hand, M_W increases significantly after SSP in the PET nanocomposites. The M_W of PET-C30B-2 is 34 000 g/mol compared to 54 000 g/mol for SSP-W-PET-C30B-2. This is an appreciable increase in the molecular weight by SSP that will have a significant effect on the final properties of PET nanocomposites.

Table 5-2 : Calculated values of the apparent complex viscosity and M_W of the matrix.

Sample	Apparent $\eta^*_{m(100rad/s)}$	$\boldsymbol{M_W}$[1] (g/mol)
PET	-	47 000 ± 2700
W-PET	-	33 000 ± 2000
PET-C30B-2	70	34 000 ± 2800
PET-C30B-3.5	51	31 000 ± 2300
PET-C30B-6	30	26 000 ± 1900
W-PET-C30B-2	35	28 000 ± 1500
W-PET-C30B-3.5	32	27 000 ± 2100
W-PET-C30B-6	24	24 000 ± 2000
SSP-W-PET	-	68 000 ± 4000
SSP-W-PET-C30B-2	282	54 000 ± 3200
SSP-W-PET-C30B-3.5	186	47 000 ± 2200
SSP-W-PET-C30B-6	91	37 000 ± 2500

[1] The M_W of the neat PETs (PET, W-PET and SSP-W-PET) was obtained from intrinsic viscosity measurements based on the ASTM D 4603-3.

5.3.3 Thermal Properties

The results of DSC scanning experiments are presented in Table 5-3, where the glass transition temperature (T_g), the melting temperature (T_m), the cold crystallization temperature (T_{cc}), the hot crystallization temperature (T_{hc}), and the crystallinity of PET in nanocomposite

films are reported. The crystallinity of the neat PET and PET in nanocomposites was calculated based on the following formula:

$$\Delta X(\%) = \frac{\Delta H_m - \Delta H_{cc}}{\Delta H_0 (1 - w_f)} \times 100 \qquad (5\text{-}3)$$

where w_f is the weight percentage of clay, ΔH_m represents the enthalpy of melting, ΔH_{cc} is the enthalpy of cold crystallization and ΔH_0 refers to the heat of fusion of 100% crystalline PET, which is 140 J/g [1].

Table 5-3 : Thermal properties of PET and PET nanocomposites

Sample	T_g (°C)	T_{cc} (°C)	T_m (°C)	ΔX (%)	T_{hc} (°C)
PET	74.4 ± 0.1	137 ± 0.2	246 ± 0.5	5.1 ± 0.5	188 ± 0.8
PET-C30B-2	72.6 ± 0.4	128 ± 0.1	246 ± 0.1	6.2 ± 0.2	197 ± 0.4
PET-C30B-3.5	70.5 ± 1	126 ± 0.2	246 ± 0.5	6.7 ± 0.1	199± 0.5
PET-C30B-6	70 ± 1	124 ± 1	246 ± 0.2	8.3 ± 0.1	201 ± 0.2
SSP-W-PET-C30B-2	74.6 ± 0.8	134 ± 0.7	245 ± 0.6	4 ± 0.1	191 ± 0.3
SSP-W-PET-C30B-3.5	73.2 ± 0.2	131 ± 0.2	244 ± 0.2	4.7 ± 0.2	194 ± 0.1
SSP-W-PET-C30B-6	72.6 ± 0.6	129 ± 0.2	244 ± 0.1	6.6 ± 0.5	197 ± 0.5

Table 5-3 shows that the cold crystallization temperature, T_{cc}, of PET in nanocomposites is lower than that of the neat PET and decreases with increasing C30B concentration. Similar decreases are observed for T_g and increases of T_{hc} are seen with increasing nanoclay content. The reductions of T_{cc} and T_g could be explained by the nucleating role of the organoclay [4, 5], the degradation of some of the organo modifier of C30B and PET degradation in the presence of

organo modifier. As reported by Thouzeau et al [23], the presence of nanoclay particles, especially C30B, causes a significant emission of volatile, which leads to a plasticization effect. It is also found that T_{hc} increases in the presence of C30B compared to the neat PET due to the nucleating role of the nanoclay. The values of T_g are slightly higher in the nanocomposites after SSP. Moreover, T_{cc} of PET in nanocomposites after SSP is higher than for the other nanocomposites, because of the higher molecular weight of the samples after SSP. The peak for the crystal formation is sharper in PET nanocomposites, compared to the neat PET (see Figure 5-9), indicative of faster crystallization. The crystallinity increases slightly in the presence of 2 wt% and 3.5 wt% of C30B, but the increase is substantial for the 6 wt% C30B conventional nanocomposites. Ghasemi et al [24] reported that the rate of crystallization increased in the presence of organoclay, whereas the required work for chain folding and activation energy for crystalline growth increased. Therefore, smaller crystals with fewer imperfections will be formed in the presence of organoclays [24]. After SSP, due to higher molecular weight of the samples, the degree of the crystallinity is lower than for the conventional nanocomposites. The degree of crystallinity presented here is for re-melted and compression molded nanocomposites. Therefore, the PET in the nanocomposites after SSP is of a higher molecular weight and exhibits a lower crystallinity. We note that the degree of crystallinity of SSP samples immediately after SSP should be much larger due to the long annealing time during SSP, as indicated by the reducing SSP rates at long times. The values of T_m show that the presence of organoclay does not have any significant effect on the melting point. The T_m values are reduced slightly by SSP.

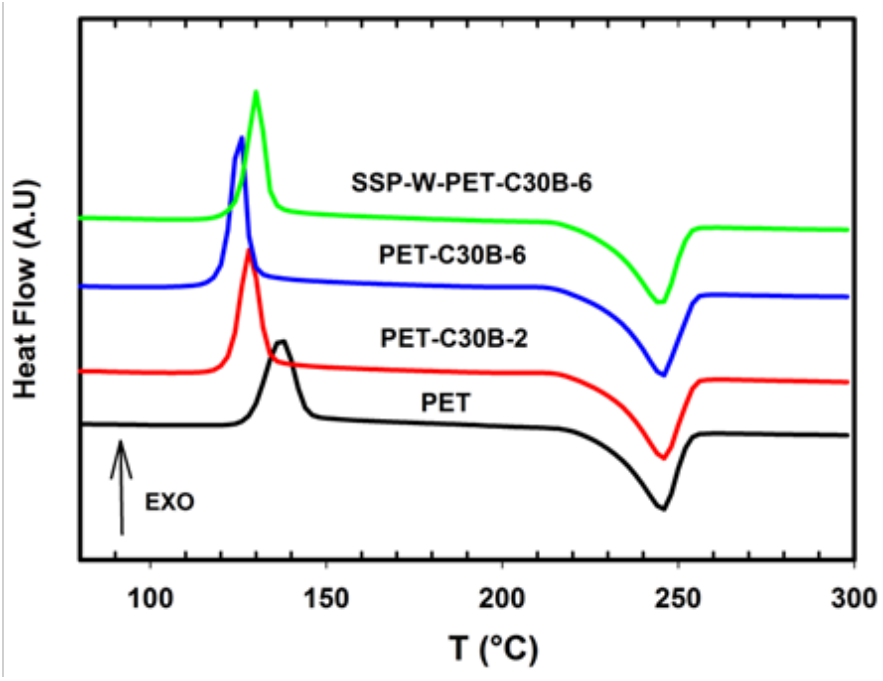

Figure 5-9 : DSC curves of PET and PET nanocomposites; first heating scans.

5.3.4 Mechanical Properties

Tensile modulus and elongation at break of PET and PET nanocomposites are shown in Figure 5-10. The presence of C30B increases the tensile modulus of the nanocomposites, compared to the neat PET, as observed elsewhere [4-8]. By adding 3.5 wt% (nominal) C30B in nanocomposites prepared by conventional melt-mixing, a 30% improvement in the tensile modulus is found, compared to the neat PET. On the other hand, after SSP, the nanocomposite containing 3.5wt% C30B displays an increase of 37% of its tensile modulus. The improvement is 45% with 6 wt% C30B. The improvement in the tensile modulus when the C30B content is increased from 3.5 to 6 wt% is not significant, probably due to the presence of large agglomerates and to the more extensive degradation of PET matrix at high concentration. Both effects could lower the reinforcing effect of C30B.

Figure 5-10b illustrates the effect of organoclay on the elongation at break of the nanocomposites. The presence of organoclay significantly reduces the elongation at break,

compared to the neat PET. The reduction of the elongation at break can be attributed to the PET degradation in the presence of C30B and the formation of C30B aggregates. Also, interfacial debonding of the clay-PET matrix interface causes cavitations and micro void formation [8]. For the nanocomposites containing 6 wt% C30B prepared by conventional melt-mixing, tensile tests could not be carried out due to the high brittleness of the samples. The presence of large aggregates, which could act as stress concentrators and ultimate mechanical failure points, causes a reduction of the elongation at break with increasing organoclay concentration.

For the nanocomposites after SSP, the elongation at break increases significantly, compared to the nanocomposites prepared by conventional melt-mixing, e.g., the elongation at break of PET-C30B-2 is 6%, while for SSP-W-PET-C30B-2 it is around 145%. This is attributed to the decreased crystallinity and smaller aggregates with less debonding for the SSP samples. Moreover, Table 5-2 shows that PET in SSP-W-PET-C30B nanocomposites has a higher molecular weight than the in conventional PET nanocomposites. For example, the molecular weight of PET in PET-C30B-2 is 34 000 g/mol, while for SSP-W-PET-C30B-2 the molecular weight is 54 000 g/mol. It is generally accepted that elongation at break increases with increasing molecular weight of linear polymers [25, 26]. At higher molecular weight, the number of entanglements that play a physical cross-linking role increases, resulting in increases in the modulus and elongation at break [27]. At 3.5 % C30B in SSP samples, the elongation at break is also larger than for the corresponding conventional melt-mixed nanocomposites, e.g., 20% for SSP-W-C30B-3.5 compared to 3% for PET-C30B-3.5. Nevertheless, this is much smaller than the elongations at break obtained for SSP-W-PET-C30B-2.

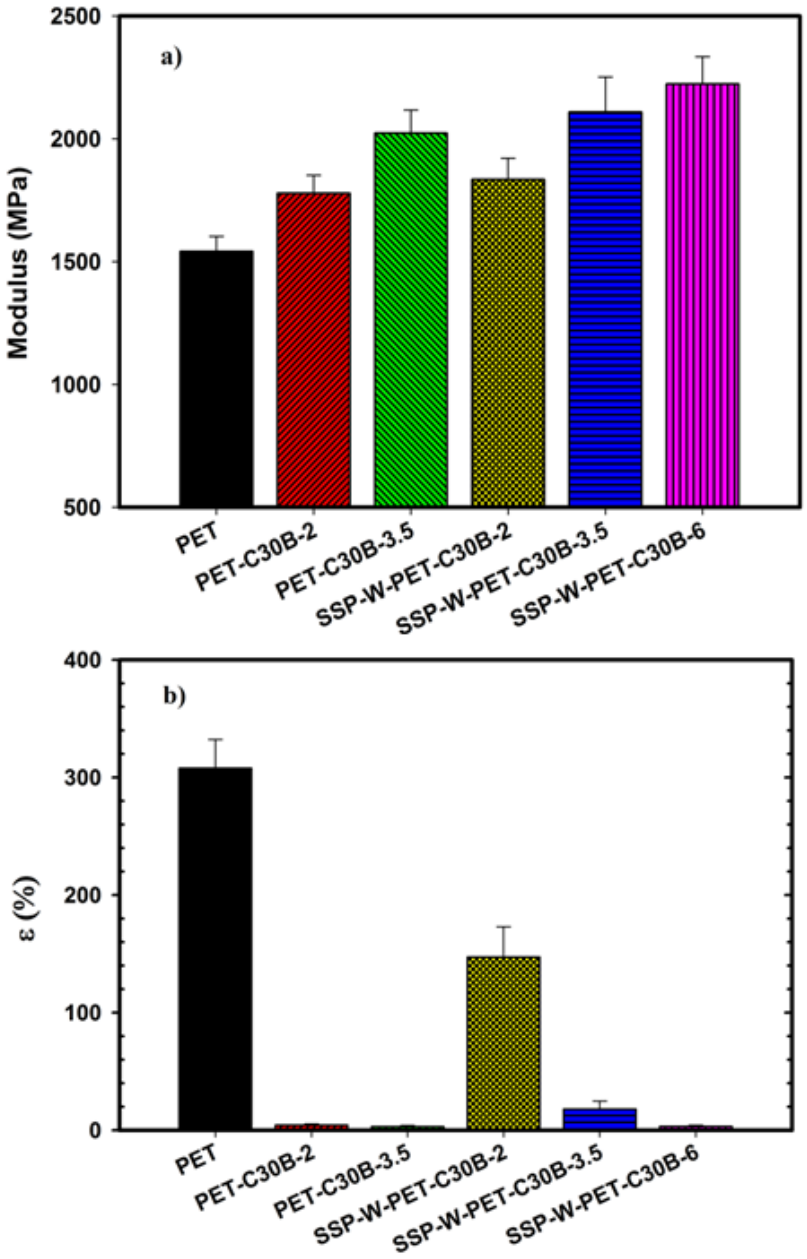

Figure 5-10 : a) Tensile modulus, b) elongation at break in PET and PET nanocomposites.

Figure 5-11 illustrates typical stress-strain curves for PET and PET nanocomposites containing 2 wt% C30B. This figure clearly shows the significant effect of SSP in improving the tensile performance of PET nanocomposites, mainly the elongation at break and toughness of the SSP nanocomposites.

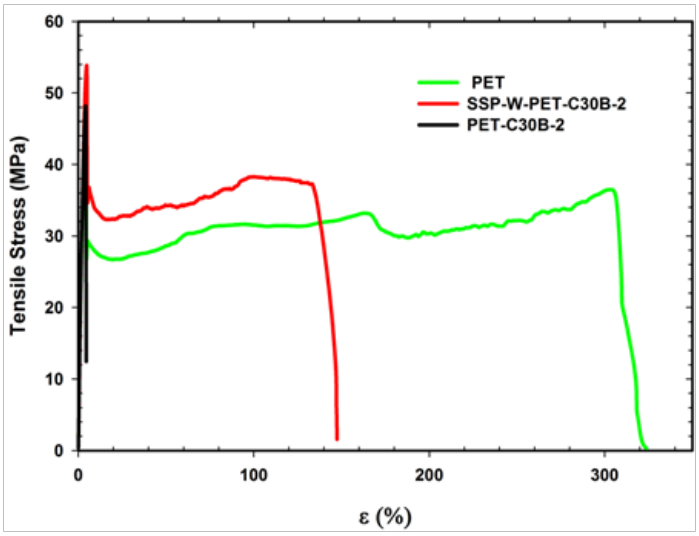

Figure 5-11 : Stress –strain behavior of PET and PET nanocomposites.

The tensile modulus of the PET nanocomposites may be estimated using the conventional pseudo-inclusion model of Brune and Bicerano [28]. In this model, the partly exfoliated polymer nanocomposite is treated as a composite composed of a matrix and pseudo-particles, which are stacks of individual platelets. This model also assumes perfectly aligned filler particles of uniform shape and *d*-spacing. The following equations are applied to obtain the modulus of nanocomposites:

$$\frac{E_c}{E_m} = \frac{1 + 2H'\phi_f' \alpha'}{1 - H'\phi_f'} \tag{5-4}$$

$$H' = \frac{E_r' - 1}{E_r' + 2\alpha'} \tag{5-5}$$

$$\phi_f = \frac{\rho_m w_f}{\rho_f - \rho_f w_f + \rho_m w_f} \tag{5-6}$$

$$\hat{N} = N + (1 - N)(\frac{d}{t})(\frac{\phi_f}{1 - \phi_f}) \tag{5-7}$$

$$b = 1 + (1 - \frac{1}{\hat{N}})(\frac{d}{t}) \quad (5\text{-}8)$$

$$\phi_f' = \phi_f \, b \quad (5\text{-}9)$$

$$\alpha' = \frac{\alpha}{\hat{N} b} \quad (5\text{-}10)$$

$$E_r' = \frac{E_r + 1 - b}{b} \quad (5\text{-}11)$$

where N is the number of platelets in each stack, and d/t is the ratio of the d-spacing between platelets in a stack to the thickness t of a platelet. For C30B, t is the 0.94 nm [29] and d is obtained from XRD measurements. E_c and E_m are the moduli of the nanocomposite and matrix, respectively; ϕ_f is the volume fraction of the nanoclay, and E_r is the relative modulus of a nanoclay platelet to the matrix (E_f/E_m). The modulus of nanoclay (E_f) is taken as 178 GPa [30], and α represents the nanoclay aspect ratio for fully exfoliated nanoclay, which is assumed to be 150 [4]. The densities of the matrix, ρ_m, and of the nanoclay, ρ_f, are equal to 1.33 and 2.86 g/cm^3, respectively.

Figure 5-12 compares the pseudo-inclusion model predictions to the data for the relative modulus. Based on this model, if the number of platelets per stack is 1 with an aspect ratio of 150, then the predicted relative modulus of the composite containing 2wt% (nominal) C30B is 1.47, compared to experimental values 1.15 and 1.2 for PET-C30B-2 and SSP-W-PET-C30B-2, respectively. Therefore incomplete exfoliation and partial alignment have significant effects on the predictions. The predicted relative modulus for the aspect ratio of 40 (obtained from TEM quantitative analysis) with one or two platelets per stack is also presented. A comparison of the predicted and experimental results suggests that the number of platelets per stack is in the range between one and two layers. However, TEM images suggest that the average numbers of platelets per stack for both the conventional and water-assisted samples are between 2 and 3 layers for 2wt% (nominal) C30B. Therefore, the pseudo-inclusion model underestimates the number of layers per stack. We note that the modulus is also function of the polymer crystallinity and the orientation of the crystals and nanoparticles.

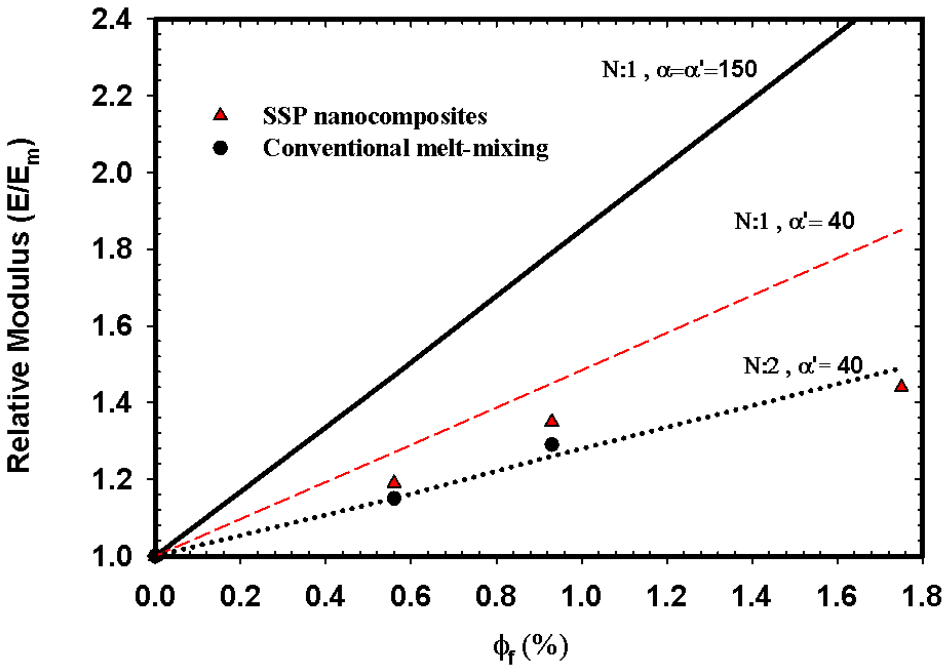

Figure 5-12 : Tensile modulus of PET nanocomposites relative to the neat PET and comparison with the pseudo-inclusion model predictions.

5.3.5 Barrier Properties

Permeability is influenced by the solubility and diffusivity of the diffusing material into the polymer, chain packing and side group complexity, polarity, crystallinity, orientation, filler, humidity and plasticization [31]. Improvements in barrier properties of polymers by the incorporation of organoclay have been reported by many investigators [32-36]. It is expected that solubility and diffusivity of gases decrease in polymer/layered silicate systems. The reduction in solubility is due to the lowering of the polymer free volume, while the reduction in diffusivity is related to the more tortuous path. However, the contribution of the solubility decrease is less than that of the diffusivity [37]. Finally, the increase in the tortuous path is controlled by the volume fraction of the nanoparticles, their orientation relative to the diffusion direction, their shape and aspect ratio as well as their degree of dispersion [38].

Figure 5-13 reports the permeability results of PET and PET nanocomposites. It is obvious that the presence of organoclay reduces the oxygen permeability and that the effect increases with increasing organoclay concentration. These results confirm that silicate layers act as an impermeable phase that can increase the tortuous path. On the other hand, based on DSC results, the crystallinity of the PET in the nanocomposites changes slightly compared to the neat PET. Therefore, it seems that the improvement in barrier properties in our samples is solely due to an increase of the tortuous path in the presence of organoclay particles. Furthermore, oxygen permeability in nanocomposites after SSP is lower than in the nanocomposite prepared by conventional melt-mixing. After SSP, the barrier behavior of the nanocomposites containing 3.5 wt% C30B is improved by 39 %, compared to the neat PET, while for 3.5 wt% C30B nanocomposites prepared by conventional melt-mixing, the oxygen permeability is reduced by 31%. This may be attributed to the better dispersion and distribution of C30B in the nanocomposites processed with water compared to those prepared by the dry processing. Ghasemi et al. [6] showed that the presence of 3 wt% C30B into oriented PET nanocomposite films could improve by 27% the barrier properties compared to their neat PET, but the crystal content of their PET nanocomposites was almost 2 times larger than their neat PET, partly accounting for the barrier improvement. If the crystal content does not change significantly in the presence of C30B, other reports [24] indicate that the size of PET crystallites changes in the presence of C30B, which can affect the oxygen permeability. On the other hand, it is well known that the free volume decreases as the molecular weight increases [31]. This can be the major reason for SSP nanocomposites to exhibit better barrier behavior compared to conventional nanocomposites. Finally, we note that the maximum improvement in barrier properties is obtained for nanocomposites containing 6 wt% C30B, but the gain is not significant compared to the 3.5 wt% case.

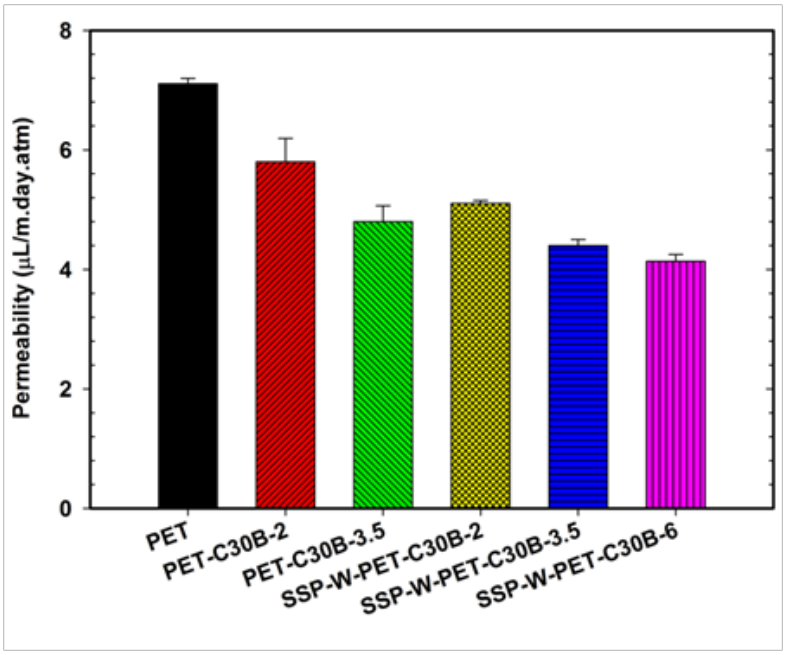

Figure 5-13 : Oxygen permeability of the neat PET and PET nanocomposites.

Figure 5-14a compares the Nielsen (Eq.5-12) and Bharadwaj (Eq.5-13) model [39] predictions and the oxygen permeability data of the PET nanocomposites.

$$K = \frac{P}{P_0} = \frac{1-\phi_f}{1+\frac{\alpha' \phi_f}{2}} \tag{5-12}$$

$$K = \frac{P}{P_0} = \frac{(1-\phi_f)}{1+\frac{\alpha' \phi_f}{2}\left(\frac{2}{3}\right)(s+\frac{1}{2})} \tag{5-13}$$

where K is the relative permeability, P and P_0 are the oxygen permeability rates of oxygen in the nanocomposite and the matrix, respectively; α' represents here the aspect ratio (fully exfoliated

nanoclay or not); *s* is an orientation factor, which changes from -0.5 to 1. *s* = 1 corresponds to the case of perfect alignment perpendicular to the diffusion path, and in the case of *s* = -0.5, silicate platelets are aligned in the same direction as the diffusion gas. Therefore, they are almost no barrier. *s* = 0 is for a random distribution of nanoclay platelets in a matrix.

The Nielsen model predicts for complete exfoliation of the nanoclay in the PET matrix (α'=150) slightly lower oxygen permeability values compared to the experimental data. For example, for 2wt% C30B (nominal), it predicts a *K* value of 0.69 compared to 0.72 and 0.82 for SSP-W-PET-C30B-2 and PET-C30B-2, respectively. However, with increasing organoclay concentration, the discrepancy between the experimental and predicted values increases due to the larger and more abundant agglomerates. We note that the Nielsen model assumes unidirectional orientation of the platelets normal to the gas permeation. On the other hand, if one uses the aspect ratio obtained from TEM images (α' =40), the predicted values of *K* are considerably larger than the experimental results.

Figure 5-14b illustrates the effect of the orientation factor (*s*) on the Bharadwaj model predictions for α' = 150. For *s* = 1, the predicted values are the same as the Nielsen model. In the case of random organoclay orientation (*s* = 0), the Bharadwaj model overpredicts considerably the data. However, using values of *s* = 0.5 and 0.8 the model predicts very well the data of conventional melt-mixing and SSP samples, respectively. A comparison between the predictions of the Nielsen and Bharadwaj models is shown in Figure 5-14a. Overall, the predicted *K* values in the Bharadwaj model with *s* = 0.5 are larger than the Nielsen model in both cases of α' = 150 and 40. It is worth noting that the above models consider only the aspect ratio of the nanoclay and the orientation in the Bharadwaj model as parameters influencing the tortuosity, and hence the permeability. However, the free volume, size and shape of crystallites and degree of crystallinity, interfacial region and particle agglomeration are important parameters that influence the diffusion rate of oxygen in polymer nanocomposites [37]. Orientation factors in this work are determined based on the Bharadwaj model. We chose the orientation factor between 0.5-0.8 because of the consistency of the experimental results to the model. Different values are reported in the literature in the range of 0.45 to 0.9 [40-43] and -0.4 to 0 [43].

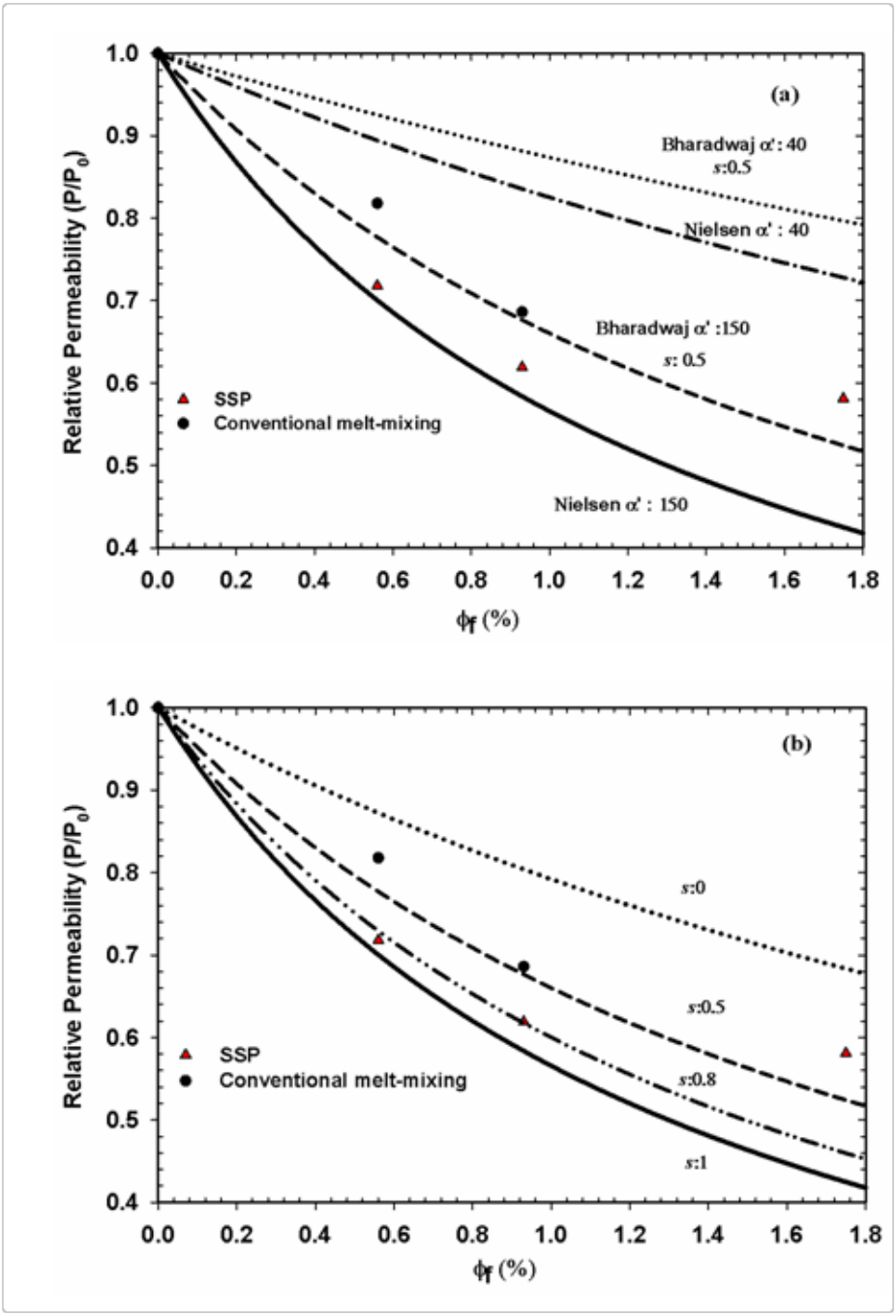

Figure 5-14 : a) Predictions of the relative oxygen permeability based on Nielsen and Bharadwaj's models, b) the effect of the orientation factor (*s*) on the Bharadwaj model predictions for α' = 150.

5.4 Conclusions

Intercalated/exfoliated morphology was found in all PET-C30B nanocomposites with a higher degree of intercalation and delamination of C30B for the water-assisted process compared to the conventional melt processing method. PET degradation in the presence of C30B was confirmed by rheological measurements. The molecular weight of the neat PET and the PET in nanocomposites was raised significantly by SSP. PET nanocomposites showed improvements in the tensile modulus and barrier properties compared to the neat PET, especially for water-assisted and SSP samples. SSP helped to recover the polymer molecular weight loss due to hydrolysis, resulting in less brittle nanocomposites. Elongation at break for conventional PET nanocomposites containing 2 wt% C30B was 6%, but for nanocomposites after SSP the elongation at break was around 145%. However, for larger C30B concentrations the elongation at break of PET nanocomposites after SSP was still low, compared to the neat PET and SSP-W-PET-C30B-2. Improvements of 45% in tensile modulus and 42% in barrier behavior were found for nanocomposites containing 6 wt% of C30B. Moreover, the color of the nanocomposites prepared according to the proposed water-assisted and SSP processing was significantly lighter than that of those prepared by the conventional melt mixing method.

The pseudo-inclusion model was shown to overpredict the tensile modulus in the case of fully exfoliated organoclays, but, upon using the experimentally determined aspect ratios and number of platelets per tactoid, the model was shown to underestimate the experimental results and the deviations increased with increasing organoclay concentration, On the other hand, the Nielsen model overpredicted the relative permeability in the case of fully exfoliated nanocomposites, and the Bharadwaj model showed that the predictions were highly sensitive to the orientation factor.

Obviously, the proposed process introduces some complexities and potential increases in costs for producing PET/clay nanocomposites. However, the results reported in this manuscript suggest advantages in relation to dispersion quality, color, molecular weight control; gas emissions, permeability and mechanical properties justified this method.

Acknowledgments

The authors acknowledge financial and infrastructure support received from The Natural Sciences and Engineering Research Council of Canada (NSERC), National Research Council of Canada (NRCC), and Canada Development Bank (CDB). We would like to gratefully thank CREPEC members Mrs. W Leelapornpisit, Mrs. M Hamdine and Dr. B. Esmaeili for their technical help.

References

1. D.R. Paul and L.M. Robeson, *Polymer*, **49**, 3187 (2008).
2. C. Chen, J. Samaniuk, D.G. Baird, G. Devoux, M. Zhang, R.B. Moore, and J.P. Quigley, *Polymer*, **53**, 1373 (2012).
3. J.S. Lee, J. Leisen, R.P. Choudhury, R.M. Kriegel, H.W. Beckham, and W.J. Koros, *Polymer*, **53**, 213 (2012).
4. H. Ghasemi, P.J. Carreau, M.R. Kamal, and S.H. Tabatabaei, *Polym. Eng. Sci.*, **52**, 420 (2012).
5. X.F. Xu, A. Ghanbari, W. Leelapornpisit, M.C. Heuzey, and P.J. Carreau, *Int. Polym. Process.*, **26**, 444 (2011).
6. H. Ghasemi, P.J. Carreau, M.R. Kamal, and N. Chapleau, *Int. Polym. Process.*, **26**, 219 (2011).
7. Y. Shen, E. Harkin-Jones, P. Hornsby, T. McNally, and R. Abu-Zurayk, *Compos. Sci. Technol.*, **71**, 758 (2011).
8. A. Ghanbari, M.C. Heuzey, P.J. Carreau, and M.T. Ton-That, *Polymer*, **54**, 1361 (2013).
9. N. Fedullo, M. Sclavons, C. Bailly, J.-M. Lefebvre, and J. Devaux, *Macromol. Symp.*, **233**, 235 (2006).

10. F. Touchaleaume, J. Soulestin, M. Sclavons, J. Devaux, M.F. Lacrampe, and P. Krawczak, *Polym. Degrad. Stab.*, **96**, 1890 (2011).

11. G. Stoclet, M. Sclavons, and J. Devaux, *J. Appl. Polym. Sci.*, **127**, 4809 (2013).

12. M. Kato, M. Matsushita, and K. Fukumori, *Polym. Eng. Sci.*, **44**, 1205 (2004).

13. Z. Liu, R. Yu, M. Yang, J. Feng, W. Yang, and B. Yin, *Front.Chem. Eng. Chin.*, **2**, 115 (2008).

14. M. Mainil, L. Urbanczyk, C. Calberg, A. Germain, C. Jerome, S. Bourbigot, J. Devaux, and M. Sclavons, *Polym. Eng. Sci.*, **50**, 10 (2010).

15. D.W. Litchfield, D.G. Baird, P.B. Rim, and C. Chen, *Polym. Eng. Sci.*, **50**, 2205 (2010).

16. S.G. Kim, E.A. Lofgren, and S.A. Jabarin, *J. Appl. Polym. Sci.*, **127**, 2201 (2013).

17. Z.P. Luo and J.H. Koo, *Polymer*, **49**, 1841 (2008).

18. P.J. Carreau, D.C.R. De Kee, and R.P. Chhabra, *Rheology of Polymeric Systems: Principles and Applications*. Munich: Hanser (1997).

19. L. Incarnato, P. Scarfato, L. Di Maio, and D. Acierno, *Polymer*, **41**, 6825 (2000).

20. M. Dini, T. Mousavand, P.J. Carreau, M.R. Kamal, and M.T. Ton-That, *Polym. Eng. Sci*, in press.

21. C.D. Han, *J. Appl. Polym. Sci.*, **35**, 167 (1988).

22. A. Ghanbari, M.-C. Heuzey, P. Carreau, and M.-T. Ton-That, *Rheol. Acta*, **52**, 59 (2013).

23. C. Thouzeau, C. Henneuse, M. Sclavons, J. Devaux, J. Soulestin J, and G. Stoclet, *Polym. Degrad. Stab.*, **98**, 557 (2013).

24. H. Ghasemi, P.J. Carreau, and M.R. Kamal, *Polym. Eng. Sci.*, **52**, 372 (2012).

25. R.W. Nunes, J.R. Martin, and J.F. Johnson, *Polym. Eng. Sci.*, **22**, 205 (1982).

26. R.F. Landel, L. E. Nielsen, *Mechanical Properties of Polymers Composites 2e*, New York : Marcel Dekker (1994).

27. G.H. Menary, C.W. Tan, E.M.A. Harkin-Jones, C.G. Armstrong, and P.J. Martin, *Polym. Eng. Sci.*, **52**, 671 (2012).

28. D.A. Brune and J. Bicerano, *Polymer*, **43**, 369 (2002).

29. K. Soon, E. Harkin-Jones, R.S. Rajeev, G. Menary, P.J. Martin, and C.G. Armstrong, *Polym. Eng. Sci.*, **52**, 532 (2012).

30. L. Cui, C. Troeltzsch, P.J. Yoon, and D.R. Paul, *Macromolecules* **42**, 2599 (2009).

31. L.H. Sperling, *Introduction to Physical Polymer Science*. 4th ed. New Jersey: Wiley Interscience (2006).

32. R.K. Bharadwaj, A.R. Mehrabi, C. Hamilton, C. Trujillo, M. Murga, R. Fan, A. Chavira, and A.K. Thompson, *Polymer*, **43**, 3699 (2002).

33. J. K. Kim, C. Hu, R.S.C. Woo, and M. L. Sham, *Compos. Sci. Technol.*, **65**, 805 (2005).

34. M. Frounchi, S. Dadbin, Z. Salehpour, and M. Noferesti, *J. Membr. Sci.*, **282**, 142 (2006).

35. M. Frounchi and A. Dourbash, *Macromol. Mater. Eng.*, **294**, 68 (2008).

36. H.M.C.D. Azeredo, *Food Res. Int.*, **42**, 1240 (2009).

37. G. Choudalakis and A.D. Gotsis, *Eur. Polym. J.*, **45**, 967 (2009).

38. C. Lu and Y. W. Mai, *Compos. Sci. Technol.*, **67**, 2895 (2007).

39. R.K. Bharadwaj, *Macromolecules*, **34**, 9189 (2001).

40. L.J. van Rooyen, J. Karger-Kocsis, O.C Vorster, and L.D Kock. *J. Membr. Sci.*, **430**, 203 (2013).

41. R.M. Cadambi RM and E. Ghassemieh. *Adv. Polym. Technol.*, **32**, E103 (2013).

42. N. Tenn, N. Follain, J. Soulestin, R. Crétois, S. Bourbigot, and S. Marais. *J. Phys. Chem. C*, **117**, 12117 (2013).

43. S. Cheng, R.A. Cairncross, Y.G. Hsuan, and C.Y. Li. *Polyme*r, **54**, 5016 (2013).

CHAPTER 6 ARTICLE 3- EFFECT OF ORGANOCLAY CONCENTRATION ON THE SOLID-STATE POLYMERIZATION OF POLY(ETHYLENE TEREPHTHALATE)1

Maryam Dini[1], Pierre J. Carreau[1], Musa R. Kamal[2], Minh-Tan Ton-That[3], and Babak Esmaeili[1]

[1] *CREPEC, Chemical Engineering Department, Ecole Polytechnique, H3T 1J4, Montreal, Quebec, Canada*

[2] *CREPEC, Department of Chemical Engineering, McGill University, H3A 2B2, Montreal, Quebec, Canada*

[3]*Automotive and Surface Transport Portfolio, National Research Council of Canada,J4B 6Y4, Boucherville, Quebec, Canada*

Abstract

Poly(ethylene terephthalate) (PET) /Cloisite 30B (C30B) nanocomposites of different organoclay concentrations were prepared using a water-assisted extrusion process. The reduction of the molecular weight (M_W) of the PET matrix, caused by hydrolysis during water-assisted extrusion, was compensated by subsequent solid-state polymerization (SSP). Viscometry, titration, rheological and dynamic scanning calorimetry (DSC) measurements were used to

[1] Submitted to *Polymer Engineering and Science.*

analyze the samples from SSP. The weight-average molecular weight (M_W) of PET increased significantly through SSP. PET nanocomposites exhibited solid-like rheological behavior, and the complex viscosity at high frequencies was scaled with the M_W of PET. The Maron-Pierce model was used to evaluate the M_W of PET in the nanocomposites before and after SSP. It was found that the extent and the rate of the SSP reaction in nanocomposites were lower than those for the neat PETs, due to the barrier effect of clay platelets. On the other hand, the SSP rate of PET increased with decreasing particle size for the neat PET and PET nanocomposites. The effect of the M_W of PET on the crystallization temperature, crystallinity and the half-time, $t_{½}$, of non-isothermal crystallization was also investigated. With increasing M_W of PET, $t_{½}$ increased whereas T_c and X_c decreased.

6.1 Introduction

Poly(ethylene terephthalate) (PET) is a semi-crystalline engineering polymer with high performance. In view of its excellent transparency and good barrier properties, it is used in a large variety of applications such as containers, films, bottles and fibers [1]. One of the areas of growing interest for using PET is for food and beverage packaging. Substantial growth in this area requires improvements in the barrier to O_2 and CO_2, along with a reduction of the weight of the final products. Recent studies show that the presence of organoclay platelets in PET can lower permeability to oxygen [2-5] and water vapor [6,7]. Moreover, improvements of mechanical properties of PET by incorporation of organoclays have been reported [3, 5, 8, 9]. The preparation of polymer nanocomposites by melt-mixing at high temperature, however, faces challenges mainly related to the degradation of both polymer and nanoclay modifiers at high processing temperatures. In the case of PET nanocomposites, several efforts have been made to lower the rate of degradation and enhance dispersion of organoclays in PET, by using a more stable clay modifier [6, 10, 11]. Other approaches employ a clay supported catalyst [12, 13] or a chain extender [9, 14].

Solid-state polymerization (SSP) of PET nanocomposites is a common process in the production of PET. It is also a practical route to compensate for polymer M_W reduction that

occurs during the melt-mixing process [15]. While SSP reactions are slower than those involving chain extenders, the former do not lead to significant changes in the chemical structure of PET. Moreover, some chain extenders can cause side reactions with undesirable by-products. Different researchers have demonstrated that SSP of PET in the presence of nanoclays and nano SiO_2 was feasible [15-17]. These studies have also shown a reduced rate of the SSP, compared to the neat PET. SSP is usually carried out under moderate temperature conditions in the reaction temperature range of 200 to 230°C. Thus, SSP could raise the molecular weight of PET with less thermal degradation than melt phase polymerization, while reducing the contents of by-products, such as acetaldehyde and oligomers, to acceptable levels [18-21]. SSP of PET involves two reversible equilibrium reactions, esterification and transesterification [22] and it is controlled by two types of diffusion. The diffusion of reaction by-products (physical diffusion) that determines the rate of the forward reactions and the diffusion of end-groups (chemical diffusion) that allows the reaction to proceed. These two types of diffusion are controlled by different parameters, such as M_W of the pre-polymer, particle size, temperature, polymer end groups, catalyst, heat stabilizer and crystallinity of PET [23]. At temperatures below 200 °C, as the mobility of the chain ends is quite low, the reaction rate is determined by diffusion of chain ends. However, at higher temperatures where PET particles can be fused together, the diffusion of by-products (water and ethylene glycol) out of the reactor becomes more difficult; thus by-product diffusion controls SSP. Inert gas plays a significant role in SSP by removing the by-products, excluding oxygen and preventing polymer oxidation [20, 23-25].

Rheological methods are useful to characterize and analyze the microstructure of polymer nanocomposites as well as their processability [26]. Several researchers studied the state of organoclay dispersion in polymer matrices using small amplitude oscillatory shear rheometry [27, 28]. A transition from liquid-like to solid-like behavior at low frequencies was observed from the storage modulus and complex viscosity in nanocomposites and filled composites [29-31]. On the other hand, polymer degradation and M_W reduction were also detected from changes in the storage modulus and complex viscosity data at high frequencies, where these parameters were found to be lower than those of the neat polymer [32-35]. However, the rheological behavior of polymer nanocomposites is quite complex and dependent on so many parameters including the organoclay dispersion, the aspect ratio, nanoclay orientation, interactions between nanoclay and

polymer chains, and nanoclay-nanoclay interactions, as well as M_W of the polymer matrix [26, 36].

This work considers SSP of PET and PET nanocomposites incorporating different concentrations of Cloisite 30B in a batch reactor for different reaction times. Moreover, the effect of polymer particle size on the rate of SSP is analyzed. Rheological measurements, intrinsic viscosity and titration measurements are used to characterize the samples after SSP. More specifically, the changes in the rheological behavior of PET nanocomposites with increasing M_W of the matrix are also presented. SSP was carried on PET and PET nanocomposites of different C30B concentration prepared first by water-assisted melt-mixing. The novelty of this work compared to our previous investigations is to report SSP data for different particle sizes and different reaction times as well as to establish the relationships between rheological and thermal properties and molecular weight and end groups of neat PET and PET nanocomposites. It should be pointed out that, in our previous work [4, 38], we obtained better dispersion and distribution of C30B in the PET nanocomposites prepared using water-assisted melt-mixing compared to the preparation without water.

6.2 Experimental

6.2.1 Materials

A general purpose PET (PET 9921, Eastman Co, Kingsport, TN) was utilized as the matrix; it has a molecular weight of 65 000 g/mol, a melting point of 243 °C and a glass transition of 77°C. The organoclay Cloisite 30B (C30B) (Southern Clay Products Inc., Gonzales, TX) was used at nominal concentrations: 2, 3.5, and 6 wt%. Cloisite 30B (C30B) is based on the modification of sodium montmorillonite by ion exchange with methyl, tallow, bis-2-hydroxyethyl quaternary ammonium cations [37]. This organoclay has platelet shape. The modifier concentration of this organoclay is 90 meq/100g clay. Based on the information presented by the

supplier, the typical dry particle size of this organoclay is 2 μm (less than 10%), 6 μm (less than 50%) and 13 μm (less than 90%).

Phenol, 1, 1, 2, 2 - tetrachloroethane, o-cresol, dichloro methane, methanol and potassium hydroxide (KOH) supplied by Fischer Scientific (ON, Canada) were used without additional purification for the determination of the intrinsic viscosity and carboxyl groups.

6.2.2 Melt Compounding

PET and the nanocomposites were processed using a co-rotating twin screw extruder (TSE) (Berstorff ZE25, Hannover, Germany) with a 25 mm diameter (*D*) screw and length-to-screw diameter ratio of 28 at a screw speed of 200 rpm. The screw configuration is presented in ref [38]. The temperature profile was 245, 265, 260, 255, 255, and 255°C from the hopper to the die. We used liquid nitrogen to cool the PET granules and then by using a grinder supplied by Waring Commercial (Heavy duty blender model) the PET powder and the organoclay were put in a box and dry mixed .The mixture was fed into the TSE at 3 kg/h. A 2-L pressure vessel (Parr Instrument Co., Moline, IL) was utilized to produce and feed steam in the second zone of the TSE at a rate of 0.3 L/h, temperature of 160ºC and pressure of 550 kPa. The temperature of the second zone of the extruder was 265 ºC. Finally, water was removed from the TSE by using a vacuum pump in the last zone of the extruder. The extrudate was collected after reaching steady state, dried and ground using the Waring blender.

6.2.3 Solid-State Polymerization (SSP)

SSP was carried out to rebuild the reduced M_W of hydrolyzed PET and PET nanocomposites. Before SSP, the ground PET and PET nanocomposites were sieved to a powder of size less than 200 and 400 μm. SSP was performed in a 1 L stainless steel stirred reactor equipped with a heating jacket provided by Supercritical Fluid Technologies Inc., Newark, USA. The reactor was operated at 215°C under N_2 for 4, 8 and 12 h with the powder size of 400 μm. This temperature

was the maximum value at which we could operate without encountering experimental difficulties. The effect of smaller powder size (200 μm) was also investigated for 8 h SSP. The flow rate of N_2 into the reactor was 2 L/min. After SSP, the heater was turned off, but the nitrogen purge was continued to lower the reactor temperature to 100°C, prior to collecting the resulting polymer or nanocomposites. Some of the sample codes are presented in Table 6-1.

After SSP, the samples were compression molded at 270 °C under nitrogen to obtain 25 mm disks, used for rheometry. All the samples were dried under vacuum for 24 h at 80 °C prior to melt processing and molding.

Table 6-1 : Sample description

Sample code	**Nominal C30B (wt %)**	**Duration of SSP (h)**	**Particle size (μm)**
S-0	0	0	-
S -4, 400	0	4	< 400
S -8, 400	0	8	< 400
S -8, 200	0	8	< 200
S -C2-4, 400	2	4	< 400
S -C3.5-4, 400	3.5	4	< 400
S -C6-4, 400	6	4	< 400
S -C6-8, 200	6	8	< 200

In the codes, 4, 8 and 12 represent duration of SSP and 0 indicates before SSP. The size of the particles is shown as 400 or 200. The letter “S’ indicates SSP, while “C” refers to a nanocomposite incorporating Cloisite 30B.

6.2.4 Characterization

Intrinsic viscosity, [η], measurements were performed using an Ubblehode capillary viscometer at 25 ºC in a mixture of phenol/1,1,2,2-tetrachloroethane (60/40, w/w). The samples were maintained in the mixture of the above solvent at 110 ºC for less than 30 min to be completely dissolved. The solution was then cooled to room temperature. Intrinsic viscosity was calculated using the Solomon–Ciuta equation [22]:

$$[\eta] = \frac{\left[2(\eta_r - 1 - \ln \eta_r)^{0.5}\right]}{c} \qquad (6\text{-}1)$$

where η_r is relative viscosity obtained from the ratio of average the solution flow time (t) to the average solvent flow time (t_0) in an Ubblehode capillary viscometer, c is the polymer solution concentration, g/dL. The weight-average molecular weight M_W was calculated using the equation proposed by Moore [39]:

$$[\eta] = 4.68 \times 10^{-4} M_W^{0.68} \qquad (6\text{-}2)$$

and the number-average molecular weight was estimated based on the Ulgea equation [40]:

$$[\eta] = 2.52 \times 10^{-4} M_n^{0.8} \qquad (6\text{-}3)$$

Carboxyl end group (CEG) content in the samples was determined by titrating a solution of the PET and PET nanocomposites in o-cresol/dichloro methane according to the ASTM D7409-07. KOH (0.005 M) solution in methanol was used as a titrator solution and bromophenol blue as indicator. The CEG content is then from the following equation:

$$CEG = [(V_s - V_b) \times M \times 1000] / w \qquad (6\text{-}4)$$

where V_s and V_b are the volumes of KOH to titrate the sample and the blank, respectively. M is molarity of the KOH/methanol solution and w is the weight of the PET sample or the weight of the PET in the nanocomposites by subtraction of the weight of the nanoclay.

Rheological measurements were carried out at 265°C under nitrogen using a Bohlin Gemini HR rheometer (Malvern Instruments, Worcestershire, UK) and an Advanced Rheometric Expansion System (ARES, TA Instruments, New Castle, DE, USA), both with a 25mm parallel plate geometry. The samples were dried under vacuum at 80°C for 24 h before the rheological tests. Time sweep tests were performed at 0.1 Hz and frequency sweep tests were done in the linear viscoelastic region for each sample determined by strain sweep tests. Frequency sweep tests over an angular frequency range of 0.3 - 100 rad/s were performed from low to high and high to low frequencies to assure the repeatability of the data.

The thermal properties of the neat PET and its nanocomposites were determined by differential scanning calorimetry (DSC Q1000, TA instruments, New Castle, DE, USA) under N_2 atmosphere, The samples were heated from room temperature to 300 ºC at 10 ºC/min and held at that temperature for 3 min, then cooled to 30 ºC at a constant rate of 10 ºC/min.

6.3 Results and Discussion

6.3.1 Molecular weight changes during SSP

The intrinsic viscosity ([η]) and molecular weight (M_W) of PETs obtained after different SSP times are presented in Table 6-2. It shows that hydrolysis during melt-mixing in the presence of steam, causes a reduction of the M_W of PET from 65 000 to 32 000 g/mol, while the polydispersity becomes slightly smaller. This can be related to the more favorable hydrolysis of the long chains compared to shorter ones. During SSP, M_W of PET increases significantly, thus, after 4 h of SSP, M_W increases from 32 000 to 57 000 g/mol. The effects of time and particle size are also observed in Table 6-2. The particle size has a significant effect on M_W. During 8 h of SSP, the PET with particle size of 400 µm reaches a M_W of 68 000 g/mol, while in the case of 200 µm particles the M_W attains 84 000 g/mol, which is close to the M_W of the PET exposed to SSP for 12 h for the 400 µm particles. The SSP rate of PET increases with decreasing particle size, suggesting that SSP is controlled by diffusion of the by-products; as the particle decreases, the larger interfacial area and the shorter diffusion path to the particle surface facilitate by-products diffusion.

During the initial stage of SSP, the polymerization reaction is believed to occur primarily near the pellet surface because the by-products can be removed easier. As SSP progresses, however, end-group concentrations at the pellet surface are depleted and the SSP reactions proceed at greater depths within the pellets; then, by-products diffusion becomes increasingly important, limiting the SSP rate.

Table 6-2: Intrinsic viscosity ([η]), weight average molecular weight (M_W) and polydispersity (PD) of the neat PETs.

Sample	**[η] (dL/g)**	M_W **(g/mol)**	PD (M_W/M_n)
As received PET	0.87 ± 0.02	64 500 ± 2200	2.42
S-0	0.54 ± 0.01	31 800 ± 900	2.18
S -4, 400	0.8 ± 0.02	56 700 ± 2100	2.38
S -8, 400	0.9 ± 0.04	67 500 ± 4400	2.44
S -12, 400	1.03± 0.01	82 300 ± 1200	2.52
S -8, 200	1.04± 0.04	83 500 ± 4700	2.52

Table 6-2 shows that the polydispersity increases significantly during SSP, from 2.18 for hydrolyzed PET before SSP to 2.52 after 12 h of SSP. As the forward reactions (esterification and transesterification, shown in Figure 6-1) continue, diffusion limitations of by-products (water and ethylene glycol) become noticeable, leading to a radial concentration gradient of by-products inside the particles with a lower concentration in outer regions of the particles [23]. Therefore, the effective polymerization rate in outer regions is greater resulting in a gradient in the local M_W,

which in turns leads to an increase of the overall polydispersity [23]. Moreover, a distribution of polymer crystallite sizes could cause a microscopic non-uniformity of the solid reactant, which consequently will lead to a larger polydispersity as observed in SSP for PA-6 [23].

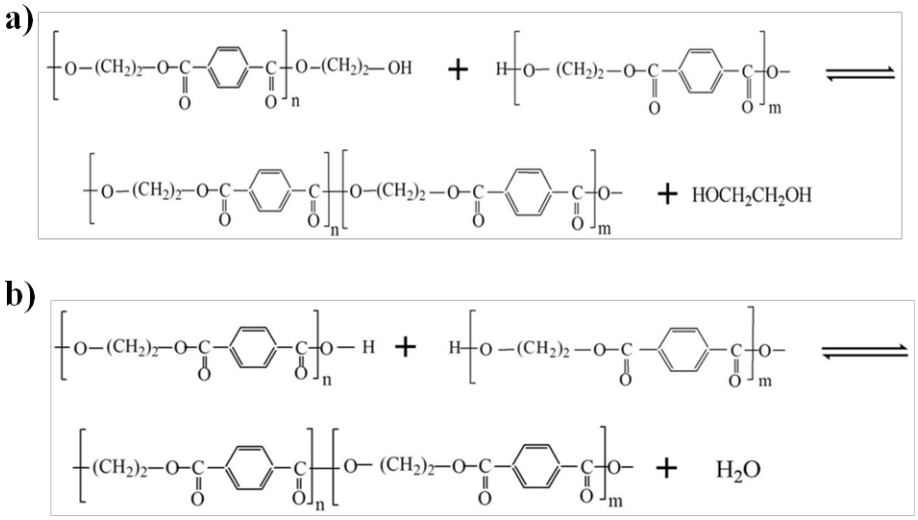

Figure 6-1: SSP of PET; (a) ester-interchange (transesterification), (b) esterification reactions.

6.3.2 Rheology – molecular weight-nanostructure relations

The rheological results of small-amplitude oscillatory frequency scans are reported in Figure 6-2. Figure 6-2a illustrates the effects of SSP and particle size on the complex viscosity (η*) vs. angular frequency for the neat PETs. Higher complex viscosity values are observed with increasing SSP time and decreasing particle size. The zero-shear viscosity (η_{m_0}) changes from 60 Pa.s in hydrolyzed PET before SSP to 2100 after 12 h SSP. On the other hand, by reducing the particle size of the neat PET, the zero-shear viscosity becomes larger: η_{m_0} is 800 Pa.s for the 400 μm particle size samples, while it is 2200 Pa.s for the 200 μm particle size sample. The increases of the complex viscosity for the PET samples after SSP are in accordance with the increasing [η] and related M_W. It is also observed that as M_W increases, the behavior of neat PET changes from pseudo-Newtonian to non-Newtonian, which is due to the increased number of chain entanglements with increasing chain length. The zero-shear viscosity, η_{m_0}, can be used as a

scaling factor to obtain a master curve for the complex viscosity data of all the PETs, independent of M_W, as shown in Figure 6-2b. All the curves are superimposed to one line, indicating that the structure of all of the PET chains before and after SSP is the same.

Figure 6-2c reports the storage modulus vs. the loss modulus for the different PET samples. All PET data are superimposed on each other, except those of the PET before SSP (S-0), which exhibits very low *G'* values. Generally at the same M_W, polymers with larger polydispersity show higher *G'* since the high molecular chains contribute significantly to the elastic modulus [41, 42]. Hence, PET with the smaller polydispersity exhibits a lower *G'*. However, the slopes of all the curves are the same, which is another signature of the linear chain structure of PET even after SSP. In our previous work, we verified by ^{1}H NMR and ^{13}C NMR that after SSP, the structure of PET chains did not change and the linear structure was preserved after SSP [4].

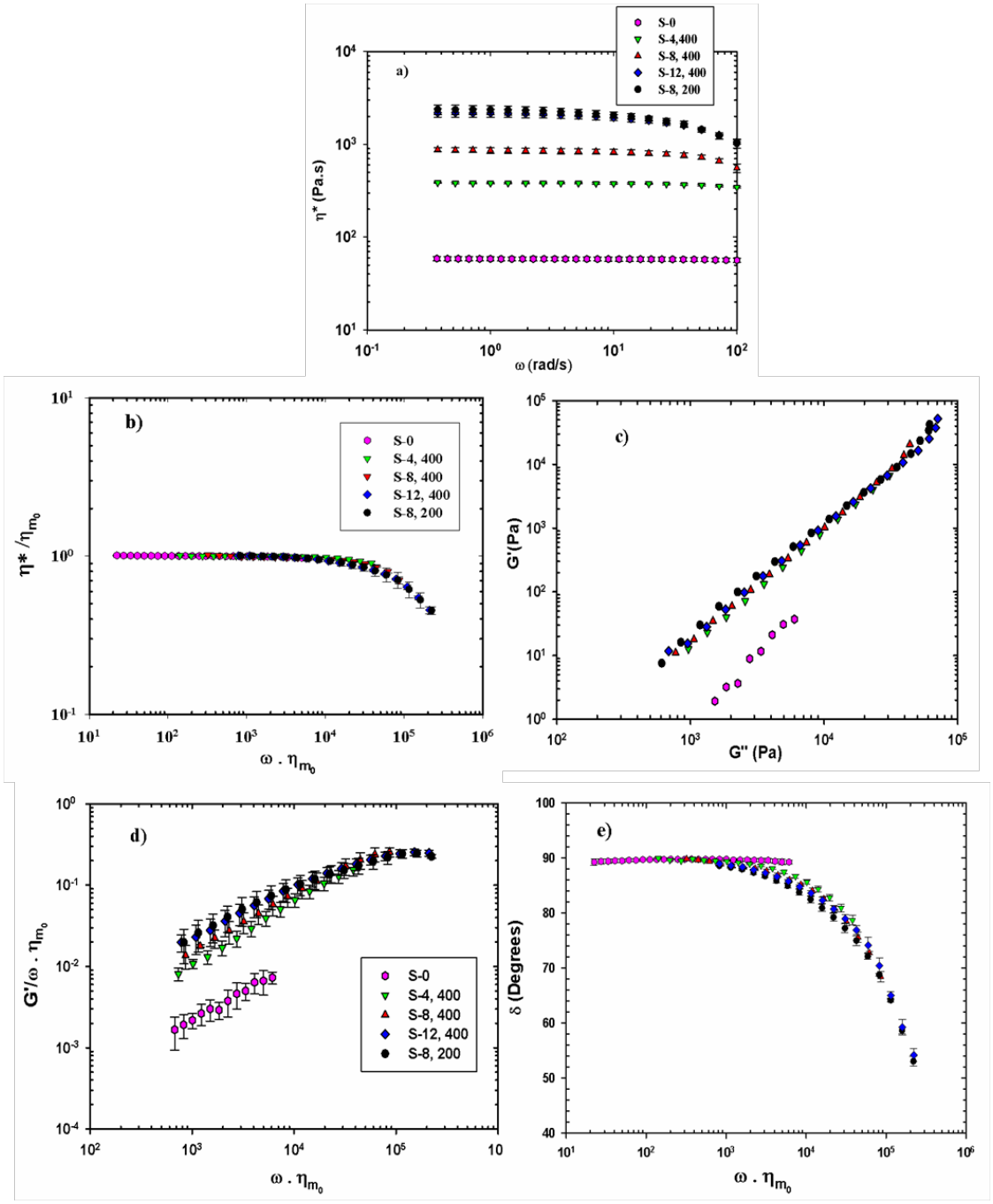

Figure 6-2 : Frequency sweep results for the neat PETs; (a) complex viscosity vs. angular frequency, (b) reduced complex viscosity curves, (c) storage modulus vs. loss modulus, (d) reduced storage modulus curves, (e) shifted phase angle plots.

The reduced storage modulus ($G'/\omega\cdot\eta_{m_0}$) as a function of $\omega\cdot\eta_{m_0}$ for the different PETs is also presented in Figure 6-2d. We observe that η_{m_0} is not an as good scaling factor for the storage modulus compared to the complex viscosity as illustrated in Figure 6-2b. As explained for Figure 6-2c, *G'* is highly sensitive to polydispersity due to the more important contribution of the tail of the high M_w polymer chains to the elasticity of the polymer [41]. As depicted in Figure 6-2e. the value of the phase angle (δ) at low frequencies is 90^o and it decreases with shifted frequency; this is the typical behavior of linear polymer chains [34]. As M_W increases, *G'* becomes more significant compared to the loss modulus (*G''*), and δ decreases with increasing frequency. These results show no indication that branching or cross-linking occurred during SSP and that the linear structure of PET was maintained. Finally, the effect of polydispersity can be noted as the reduction of the phase angle with frequency is more rapid for the larger polydispersity (more elastic) PET.

Figure 6-3 presents the relationship between the zero-shear viscosity and the weight-average molecular weight of PET in the range of 25 000 to 84 000 g/mol at a reference temperature of 265 °C, using the formula;

$$\eta_{m_0} = kM_w^a \qquad (6\text{-}5)$$

The values of *a* and *k* are found to be 3.6 and 2.95×10^{-15} Pa. s. mol $^{3.6}$/g $^{3.6}$, respectively. The value of *a* demonstrates that the molecular weight of the PETs studied here are above the critical molecular weight for entanglements (M_c) and η_{m_0} of PET scales with M_W within the range as expected for linear flexible polymer chains. The value of 3.6 compared to the usual 3.4 could be attributed to the polydispersity larger than 2, and also the presence of co-monomer in the structure of the as-received PET [4].

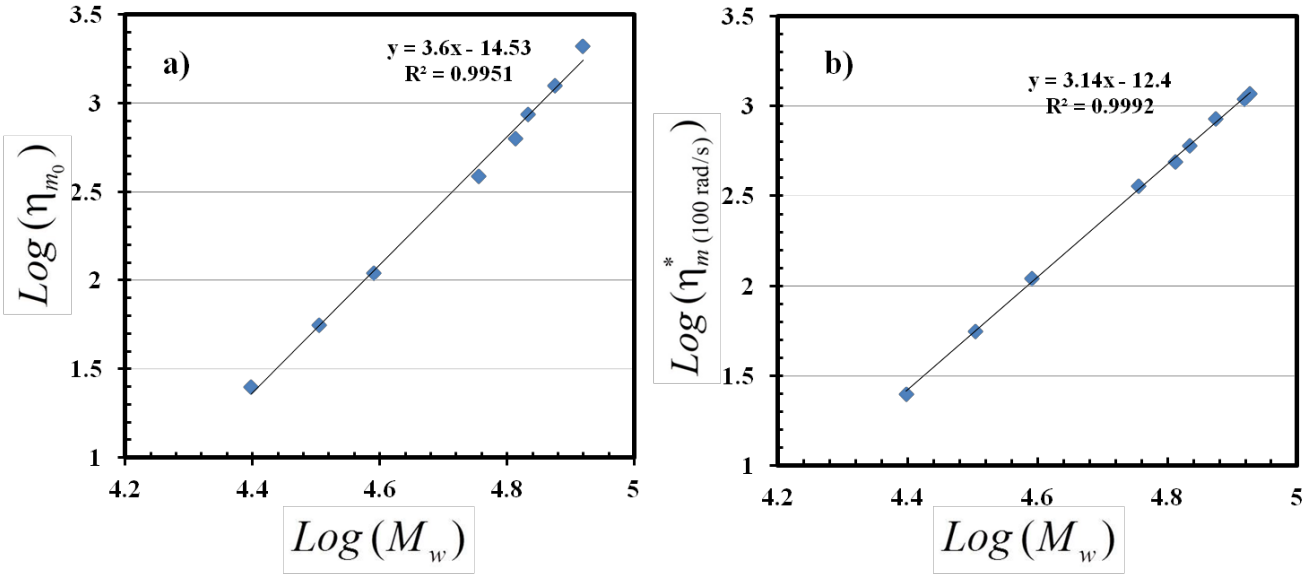

Figure 6-3 : Scaling of the zero-shear viscosity (a) and complex viscosity (b) at 100 rad/s against M_W for the PET samples. The units for the zero-shear viscosity and complex viscosity are Pa.s and g/mol for M_W.

The complex viscosity at 100 rad/s can also be scaled with M_W using:

$$\eta^*_{m(100\,\mathrm{rad/s})} = kM_w^a \qquad (6\text{-}6)$$

The values of a and k are found to be 3.14 and 3.94×10^{-13} Pa. s. mol $^{3.14}$/g $^{3.14}$.

The linear viscoelastic data of the neat PET and PET nanocomposites before SSP have been presented elsewhere [38]. However, we present in Figure 6-4a plots of the complex viscosity vs. complex modulus that illustrate better the effect of clay concentration on the rheological behavior of the PET nanocomposites. Above 2 wt% C30B, the complex viscosity is seen to rapidly increase with decreasing complex modulus (or frequency), indicative of an apparent yield stress for the concentrated nanocomposites, due to the stronger particle–particle and/or polymer–particle interactions. On the other hand, these results show that the percolation threshold is somewhere between 2 and 3.5 wt%. Plots of the storage modulus vs. loss modulus (Figure 6-4b),

analogous to Cole-Cole plots, are used to investigate changes in the microstructure of the PET nanocomposites. We observe that for a given loss modulus, the storage modulus increases significantly with increasing nanoclay content. The slope of the storage modulus vs. loss modulus (log-log plot) is reduced significantly with increasing nanoclay content, illustrating changes in the microstructure with a transition from liquid to solid-like behavior.

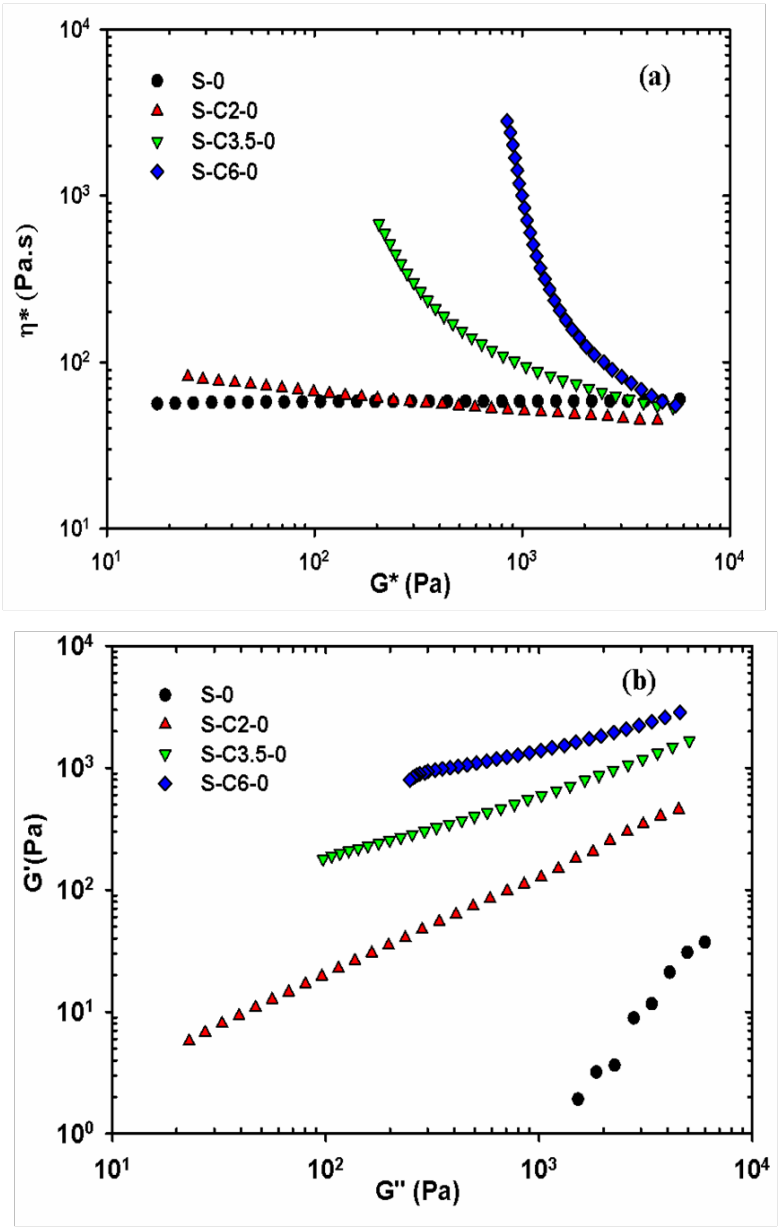

Figure 6-4 : Linear viscoelastic data for the neat PET and PET nanocomposites before SSP; (a) complex viscosity vs. complex modulus; (b) storage modulus vs. loss modulus.

Figure 6-5 reports the complex viscosity and storage modulus data for the PET nanocomposites after SSP for different reaction times and two particle sizes. Figure 6-5 a-c present the data for the 2, 3.5 and 6 wt % organoclays, respectively. As expected, the complex viscosity in the whole range of angular frequency increases with SSP time and decreased particle size in nanocomposites with 2 wt% C30B (Figure 6-5a). In the linear viscoelastic regime, the behavior of the matrix is prominent at high frequencies, whereas the low frequency data are quite sensitive to the organoclay interactions and structure formation in the nanocomposites. The increased complex viscosity values at high frequencies are due to the significant M_W increases of the PET after SSP. It is worth noting that for the larger nanoclay contents (3.5 and 6 wt %) the complex viscosity at low frequencies does not change much with SSP time (see Figure 6-5b and c), but the complex viscosity at high frequencies increases with SSP time. The corresponding storage modulus data are reported in Figure 6-5 d-e, which shows that *G'* increases in the whole frequency range with increasing SSP time and decreasing particle size. At low frequencies the non-terminal behavior (tendency towards a plateau) observed for the storage modulus data is another indication of solid-like behavior due to the nanoclay-nanoclay and/or polymer-nanoclay interactions. The increases at high frequencies are more important than those at low frequencies, due to the sensitivity of high frequency data to M_W of the matrix.

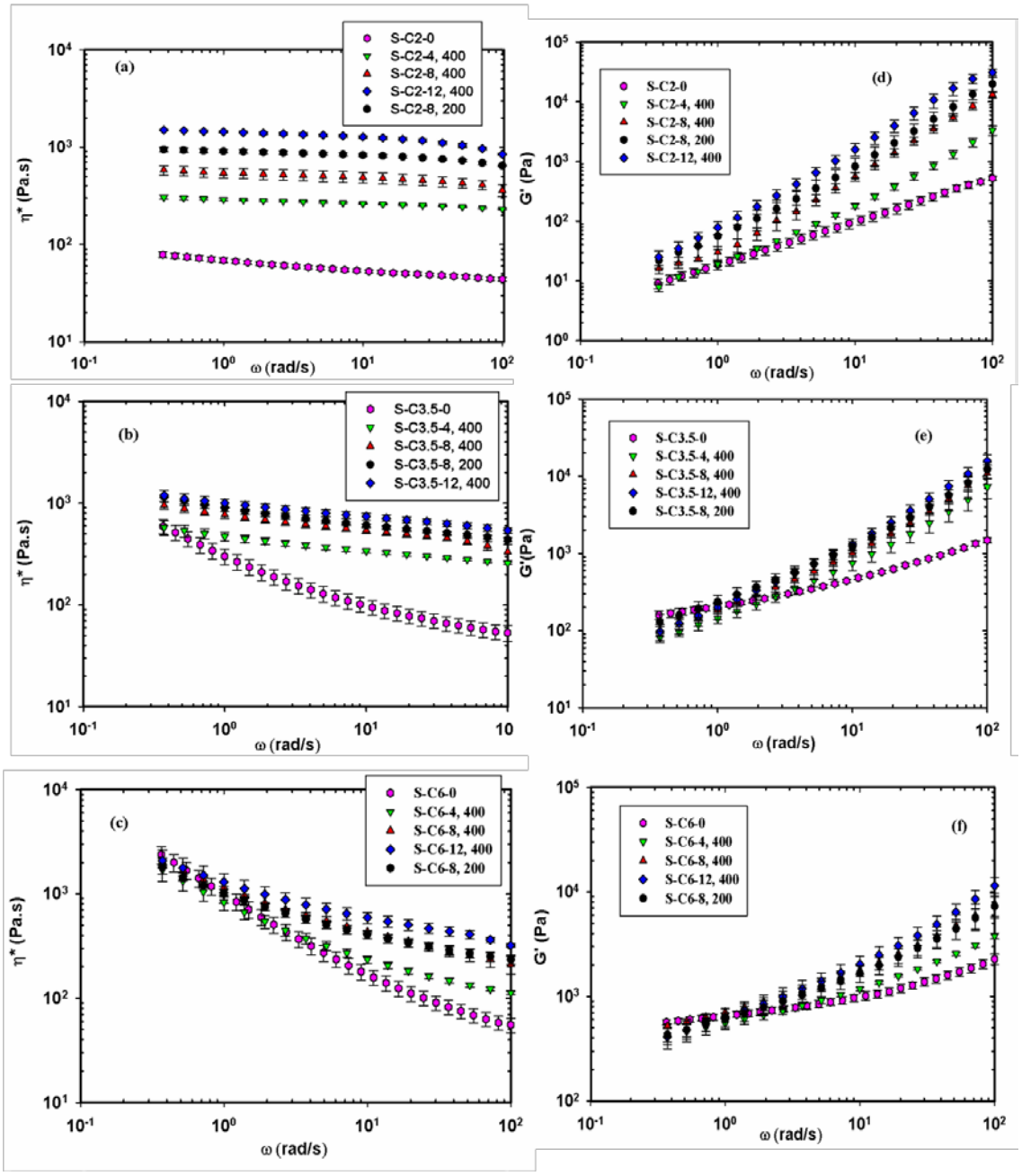

Figure 6-5 : Complex viscosity vs. angular frequency of PET nanocomposites for different C30B concentrations after SSP compared to the data of the corresponding samples before SSP: a) 2 wt%, b) 3.5 wt%, c) 6 wt%. Storage modulus vs. angular frequency: d) 2 wt%, e) 3.5 wt%, f) 6 wt%.

Figure 6-6 compares the linear viscoelastic data of the samples before and after SSP as plots of the complex viscosity (overall flow resistance), η*, against the overall deformation resistance *G**. For the nanocomposites, the behavior becomes more shear-thinning as the nanoclay content is increased, in the case of the nanocomposites containing 3.5 and 6 wt% C30B a significant yield stress is observed, however at lower extent than for the samples prior to SSP. This is due to the stronger interactions between C30B and hydrolyzed PET in the melt state compared to the SSP samples, as discussed below.

The following modified Herschel-Bulkley model (Eq. 6-7) was used to determine the apparent yield stress of the PET nanocomposites containing 3.5 and 6 wt% C30B before and after SSP.

$$\eta^* = \frac{G_0^*}{\omega} + k\,(\gamma^0\,\omega)^{n-1} \qquad (6\text{-}7)$$

where G_0^* is the magnitude of the complex modulus at the lowest frequency, γ^0 is the strain amplitude, *k* is a constant, and *n* is the flow index. Then, the apparent yield stress is $\sigma_0 = G_0^* \gamma^0$. σ_0 and *n* are related to the microstructure of the nanocomposites and their values, determined from the best fits of the data of Figure 6-6b and c are presented in Table 6-3. With increasing M_W of the PET during SSP, *n* increases whereas σ_0 decreases. This suggests that the hydrodynamic interactions become more dominant compared to the particle-particle interactions.

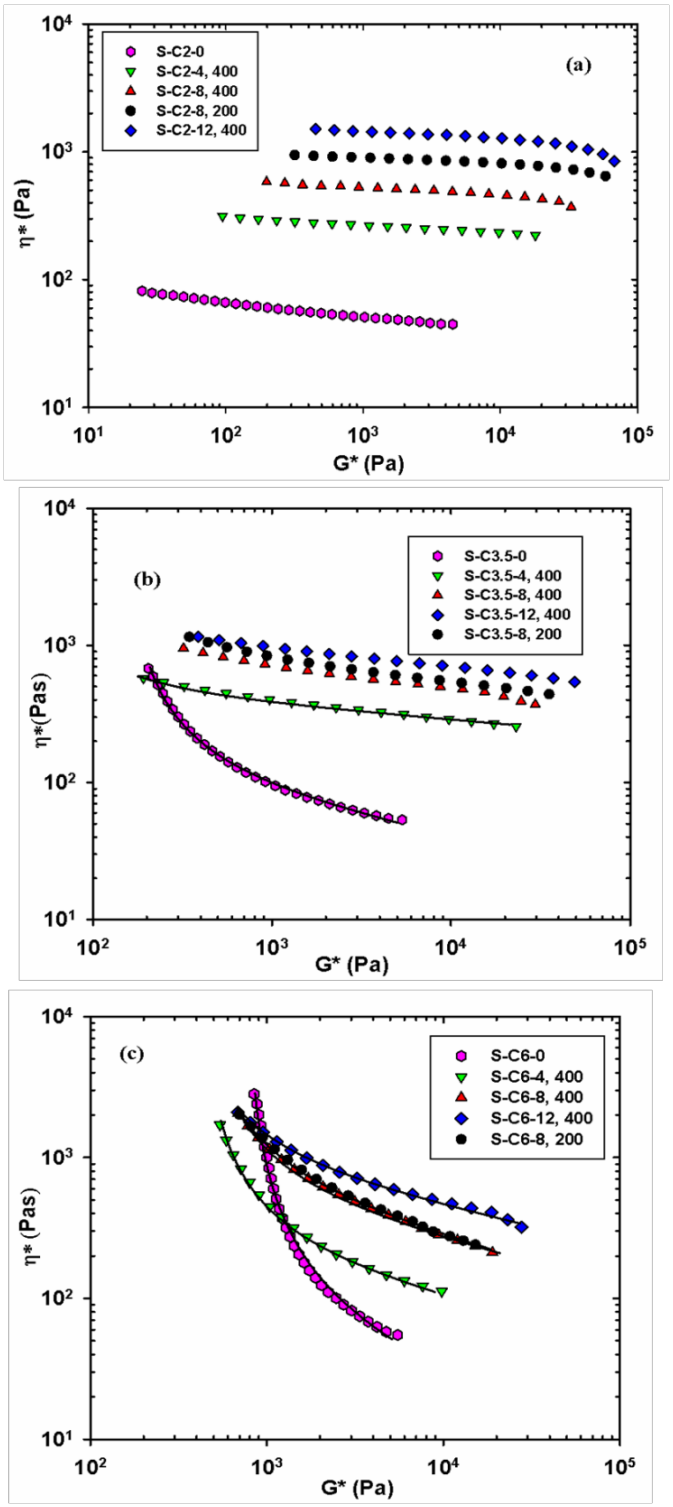

Figure 6-6 : η^* vs. G^* of PET nanocomposites before and after SSP. Solid lines represent the fits of the Herschel-Bulkely model to the experimental data with the parameters given in Table 6-3.

Table 6-3 : Herschel-Bulkley parameters of PET nanocomposites containing 3.5 and 6 wt% C30B.

Sample	$\sigma_0 = G_0^* \gamma^0$ **(Pa)**	***k* (Pa.s^n)**	***n***
S- C6-0	39	78.0	0.68
S -C6-4,400	21.5	150	0.75
S -C6-8,400	16	219	0.75
S -C6-12,400	4.5	355	0.77
S -C6-8,200	11	275	0.77
S- C3.5-0	7.5	72	0.76
S –C3.5-4,400	2	303	0.9

In all our work [4, 38] so far on PET/clay nanocomposites, there was an evidence of matrix degradation in the presence of organoclays during processing. The PET degradation in nanocomposites was quantified by Ghanbari et al. [33]. We follow the same approach here to calculate the apparent molecular weight of the PET in the nanocomposites after SSP, using the empirical model of Maron-Pierce, written for the complex viscosity as:

$$\frac{\eta^*}{\eta_m^*} = \left(1 - \frac{\phi}{\phi_m}\right)^{-2} \qquad (6\text{-}8)$$

where η^* and η_m^* are the complex viscosities of the nanocomposite and the matrix, respectively. ϕ is the volume fraction of the clay and ϕ_m is the maximum packing volume fraction. ϕ_m is estimated based on the following formula [43, 44]:

$$\phi_m = \frac{3.55}{p} \qquad (6\text{-}9)$$

where p is the clay aspect ratio determined from TEM analysis, taken as 40, as reported in our previous work [38]. Since, at high angular frequencies, the hydrodynamic interactions are dominant, the complex viscosity at 100 rad/s is used in Eq. 6-8 to determine the apparent molecular weight of the PET matrix for each nanocomposite. The apparent M_W of the PET nanocomposites was estimated using Eq. 6-6 whereas M_W of the neat PETs were determined from the intrinsic viscosity measurements using Eq. 6-2 and reported in Table 6-2. The variations of M_W with SSP time for the neat PET and the different nanocomposites are presented in Figure 6-7. We observe strong non-linear increases of M_W with SSP time, but markedly less for the nanocomposites. The reduction of the reaction rate for the neat PET with time, as observed by the decreasing slope in the figures, is attributed to the increasing crystallinity of PET as SSP proceeds at 215 ^{o}C. The M_W changes with SSP time are reported in

Sample	In first 4 h of SSP (g/mol)	From 4 to 12h (g/mol)	In first 8 h (g/mol)
S, 400	6250	3250	4500
S-C2 , 400	4750	2500	3250
S-C3.5 , 400	3800	1750	2750
S-C6 , 400	1750	1500	1750
S , 200	-	-	6500
S-C2 , 200	-	-	4875
S-C3.5 , 200	-	-	3250

S-C6 , 200	-	-	1800

Table 6-4. For the neat PET with particle size of 400 µm, the increase of M_W during the first 4 h of SSP is 6250 g/mol, while it is only 1750 g/mol for the nanocomposite containing 6 wt% C30B. On the other hand, for the neat PET, the M_W increase during the first 8 h of 4500 g/mol jumps to 6500 g/mol by reducing the particle size from 400 to 200 µm. However, for the nanocomposite containing 6 wt% C30B, the corresponding rise is only from 1750 to 1800 g/mol. Hence, the lower increases of the apparent M_W of PET in the case of the nanocomposites suggest that the organoclay platelets restrict the mobility of the reactive groups as well as increase the diffusion path length of the by-products, thus reducing the rate of the SSP reactions. Another contributing factor could be related to the changes of the crystallinity in the presence of C30B [45].

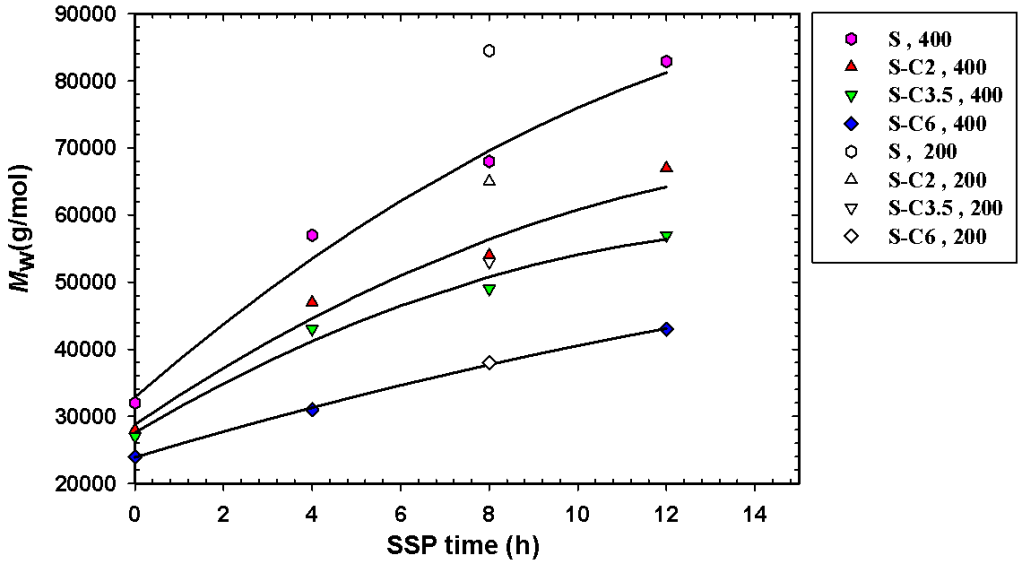

Figure 6-7 : Apparent molecular weight of the PET in the nanocomposites. “S” represents neat PET, “S-C2, S-C3.5, S-C6” indicate nanocomposites containing 2, 3.5 and 6 wt% of C30B, respectively.

Sample	In first 4 h of SSP (g/mol)	From 4 to 12h (g/mol)	In first 8 h (g/mol)
S, 400	6250	3250	4500
S-C2 , 400	4750	2500	3250
S-C3.5 , 400	3800	1750	2750
S-C6 , 400	1750	1500	1750
S , 200	-	-	6500
S-C2 , 200	-	-	4875
S-C3.5 , 200	-	-	3250
S-C6 , 200	-	-	1800

Table 6-4 : Changes of M_W with time during SSP

6.3.3 Carboxyl group concentration during SSP

The reduction of the carboxyl groups of PET chains during SSP is an indicator of the rise of M_W of PET. On the other hand, an increase of these groups before SSP is an indication of more polymer degradation. Figure 6-8 shows the variations of the carboxyl end group concentration with the reaction time for the different samples. The carboxyl end group concentration decreases sharply during the first stage of SSP. For example, the carboxyl content of PET before SSP is 75 µmol/g, while after 4 h and 12 h of SSP it is reduced to 44 and 9 µmol/g, respectively. These results indicate that SSP of PET is a useful method to obtain PET products with a considerably low concentration of carboxyl end groups. This decrease is in accordance with the corresponding

increase of the intrinsic viscosity and molecular weight (Table 6-2). It is also found that before SSP the concentrations of the carboxyl groups of the nanocomposites are larger than for the neat PET, for example: 90 µmol/g for the nanocomposite containing 2 wt% C30B compared to 75 µmol/g for the neat PET. The carboxyl content increases when the concentration of C30B is raised to 6 wt%. The higher carboxyl group concentrations in the nanocomposites before SSP are attributed to the accelerated degradation of PET in the presence of C30B during melt-mixing, which is intensified with increasing C30B concentration. On the other hand, it is observed that the rate of the carboxyl group reduction (slope in Figure 6-8) for the nanocomposites during SSP is less than for the neat PET, indicating a restricted mobility of the reactive groups and a lower diffusion rate of the by-products since it is well-known that polymers that contain nanoparticles exhibit a lower permeability to gases. Figure 6-8 also shows that the carboxyl group content for the 200 µm particle sample is less than for the 400 µm particle sample. It is another indication of the significant effect of reducing the particle size on the rate of SSP. Overall, the reduction of carboxyl group content is in agreement with the rise of M_W reported in Figure 6-7.

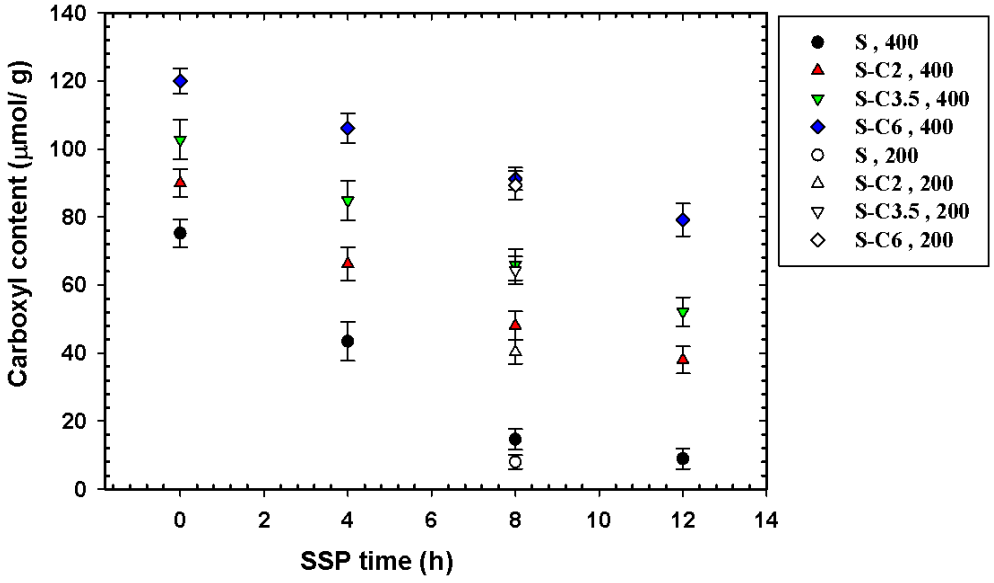

Figure 6-8 : Variations of the carboxyl content with SSP time of the neat PET (symbol: S) and PET containing 2, 3.5 and 6.0 wt% C30B (symbols: S-C2, S-C3.5, S-C6).

The reduced viscosity (η^*/η_{m_0}) and storage modulus ($G'/(\eta_{m_0}\times 100\,\text{rad/s})$) of PET nanocomposites as functions of $\omega\cdot\eta_{m_0}$ are reported in Figure 6-9. The angular frequency of 100 rad/s was arbitrary chosen and η_{m_0} is the zero-shear viscosity of the matrix (PET) calculated from Eq. 6-5, using the determined apparent M_W values reported in Figure 6-7. Figure 6-9a-c show that reasonable master curves for the complex viscosity of the PET nanocomposites for the three different C30B contents. The deviations observed could be attributed to the mild influence of the carboxyl groups on the complex viscosity. However, the effect of the carboxyl group contents on the reduced storage modulus as illustrated in Figure 6-9d-f. We observe that $G'/(\eta_{m_0}\times 100\,\text{rad/s})$ increases markedly with increasing carboxyl group content (values indicated in the figure).

In our previous paper [4], we reported based on XRD and TEM analysis that SSP did not have any effect on the *d*-spacing of the clay galleries and on the organoclay dispersion. On the other hand, the rheological results show a more solid-like behavior and larger apparent yield stress values (Figure 6-6b and c) for the nanocomposites before SSP (see also Dini et al. [4, 38]) compared to the samples after SSP. Therefore, based on the results of Figs.9 d-f, it can be concluded that the presence of more carboxyl groups (before SSP) causes more polymer chain interactions with the hydroxyl groups of C30B leading to a stronger structure.

6.3.4 SSP effects on crystallization of PET and nanocomposites

Since PET is a semi-crystalline polymer, its microscopic properties are strongly dependent on its degree of crystallinity and crystal structure. On the other hand, crystallization studies are very useful to understand the thermal properties of PET with different molecular weights and PET nanocomposites. Therefore, DSC studies will provide important information about macroscopic characteristics of the samples. DSC experiments were carried out on the samples after SSP, and the results of the second ramp (cooling) are presented. The cold crystallization temperature (T_c) and degree of crystallinity (X_c) of PET and PET nanocomposites are reported as functions of M_W in Figure 6-10. The crystallinity of the neat PET and PET nanocomposites was calculated using the following formula:

$$X_c(\%) = \frac{\Delta H_c}{\Delta H_0 (1 - w)} \times 100 \qquad (6\text{-}10)$$

where w is the weight fraction of clay, ΔH_c represents the enthalpy of crystallization and ΔH_0 refers to the heat of fusion of 100% crystalline PET, which is 140 J/g [1].

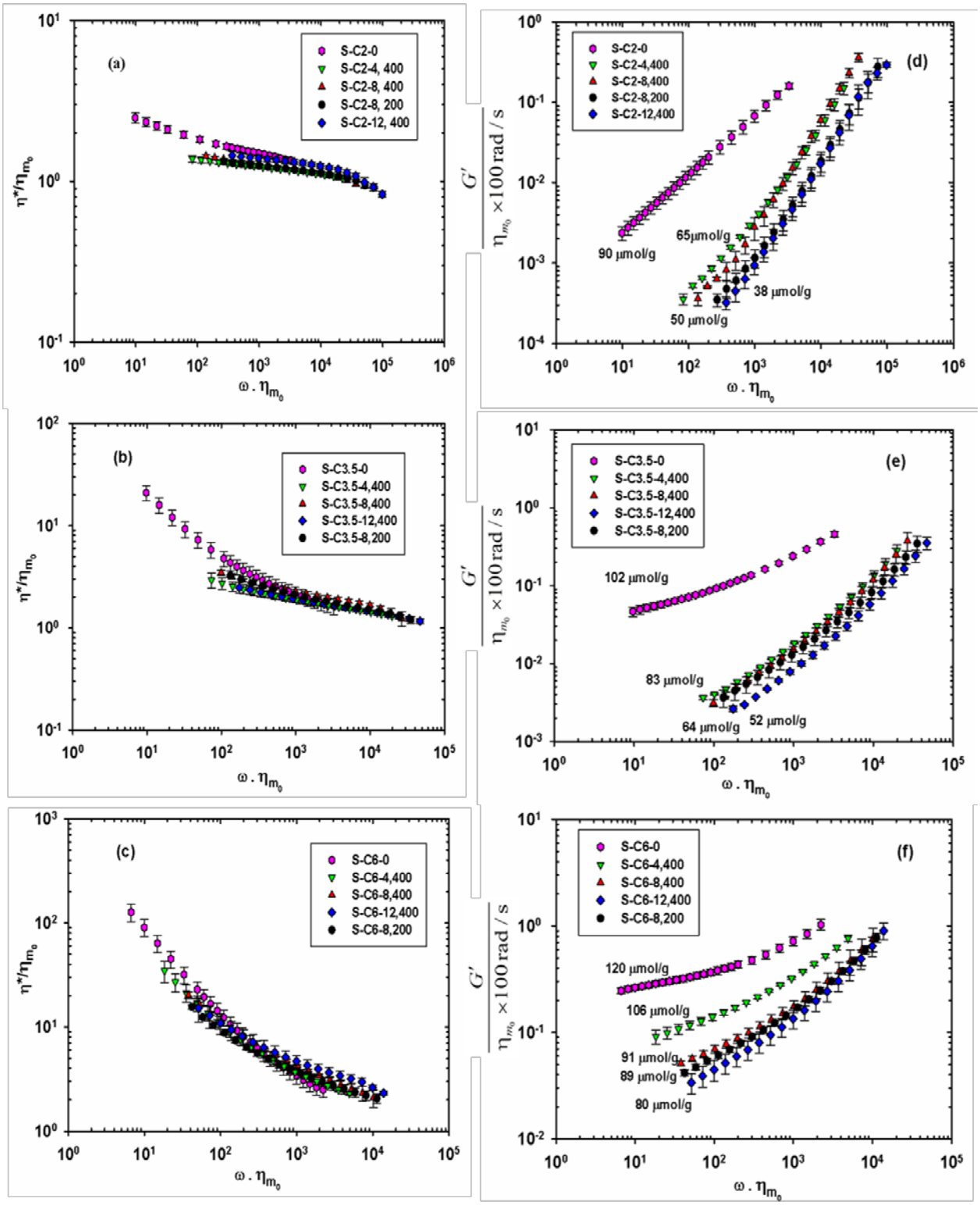

Figure 6-9 : Reduced complex viscosity (a-c) and reduced storage modulus (d-f) for the PET nanocomposites.

Both T_c and X_c of PET (Figure 6-10) decrease with increasing M_W. For the neat PET, as M_W increases from 32 000 to 83 000 g/mol, X_c decreases from 33% to 22.5% and T_c decreases from 187 to 156 ºC. High M_W PETs start to crystallize at a lower temperature and the reduction of X_c with M_W is an indication of thinner and/or less perfect crystals [46]. We note X_c is a unique function of M_W of the PET, and T_c is slightly higher for the nanocomposites. As Figure 6-10 a shows at a same M_W, e.g. 67 000 g/mol, T_c of the 2 wt% nanocomposite is 174 °C but for the PET without organoclay it is 166 °C. Increases of T_c in the presence of C30B can be attributed to the reduction of the chain mobility and decrease of the chain entropy to nucleate crystals. Various researchers [6, 47] have reported increases of T_c in nanocomposites after melt-mixing compared to neat PETs, which they explained by the nucleating role of the nanoclay, but they did not account for the PET degradation in the presence of organoclays. Therefore, our results show that M_W is a much more important parameter than the presence of C30B as a nucleating agent.

At the same M_W of PET, the presence of C30B restricts the motion of polymer chains and results in the imperfect crystallites with different shape and size compared to the neat PET; therefore, the changes of the final crystallinity compared to the neat PET is negligible. Marginal effects of nanoclays on the crystallinity of PET have been also reported [6, 48]. Figure 6-11presents the DSC curves of the neat PET and PET nanocomposites containing 2wt% of C30B for different PET molecular weights. The differences observed in the DSC exothermic peaks are mostly attributed to the differences in the M_W of the various samples.

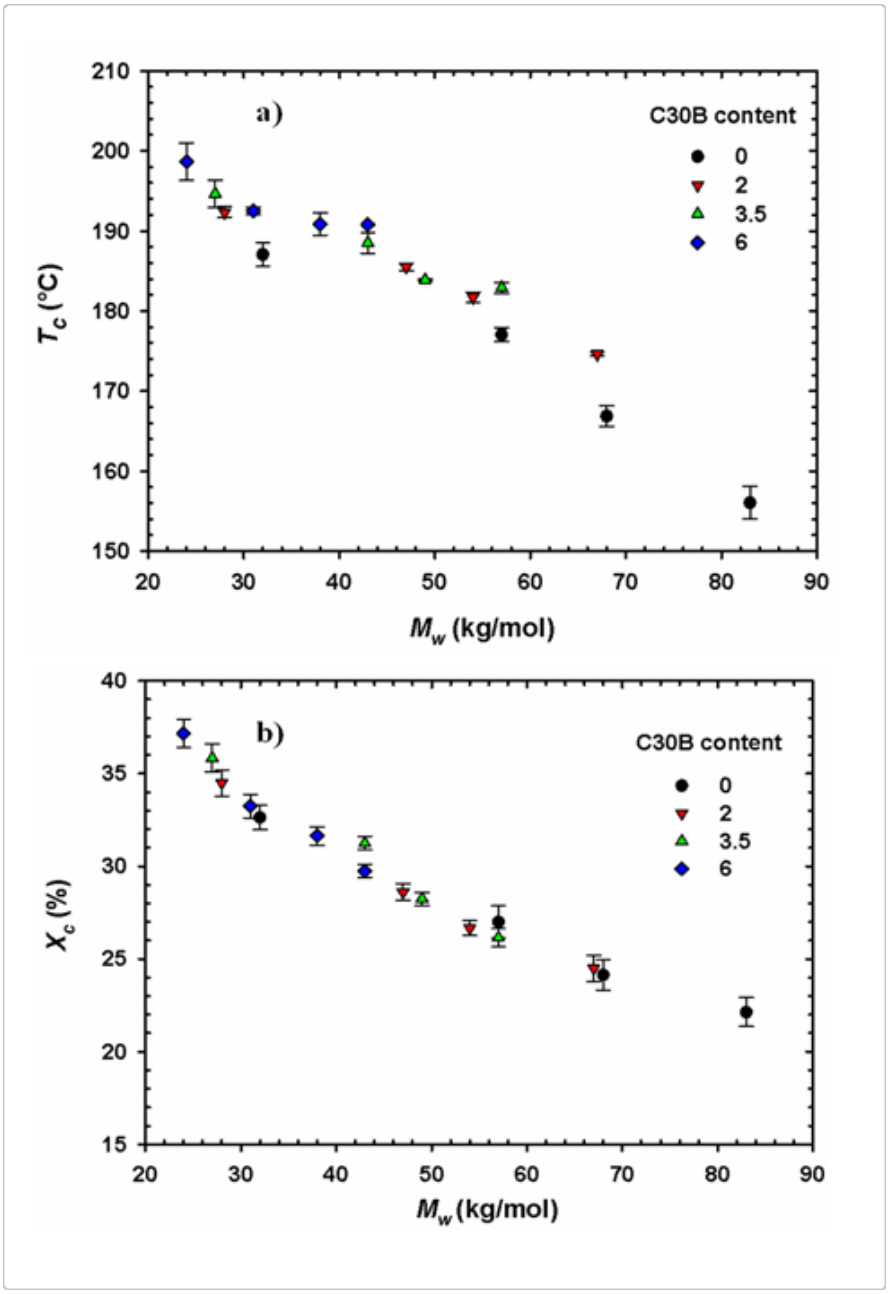

Figure 6-10 : Crystallization temperature (T_c) vs. M_W (a) and degree of crystallinity (X_c) vs. M_W (b) of the neat PET and PET nanocomposites.

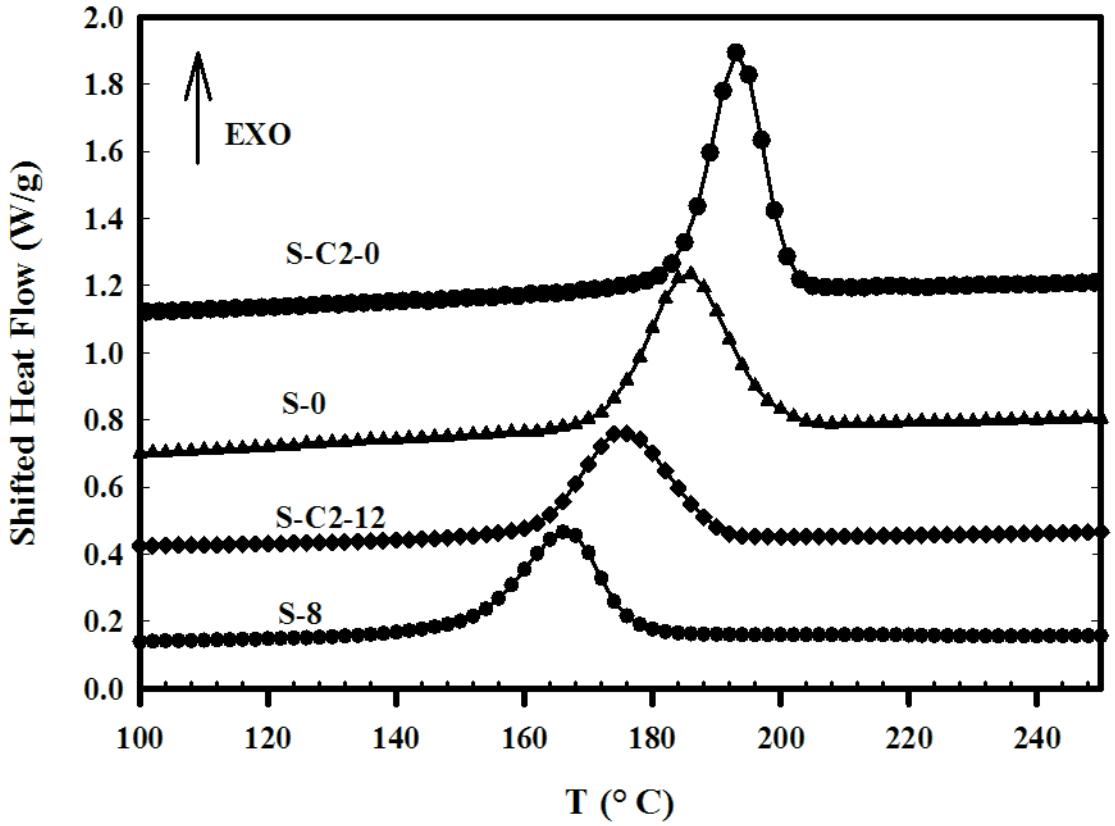

Figure 6-11 : DSC curves of PET and PET/C30B nanocomposites; S-0 and S-C2-0 represent neat PET and PET with 2wt% of C30B after melt-mixing and before SSP. S-8 and S-C2-12 are the code of PET and PET-C30B containing 2wt% of organoclay with approximately the same molecular weight of 67 000 g/mol.

Figure 6-12 reports the variations of the degree of crystallinity as functions of time for the cooling crystallization cycle of different samples. The half-time for crystallization ($t_{½}$), defined as the time required to reach half of the final crystallinity, can be easily obtained from the figure. For the data prior to SSP (Figure 6-12a), $t_{½}$ is shown to decrease from 101 to 60 s when 6 wt% clay is added to the PET. Therefore, the presence of organoclay increases the rate of the crystallization. However, as shown in Figure 6-10 b the degree of crystallinity raises only due to

the decreased M_W, hence, degradation of the PET in the presence of the organoclay. Moreover, Ghasemi et al. [47] reported that the rate of crystallization in the presence of organoclay increases, whereas the required work for chain folding and activation energy of crystal growth increases. However, their measured enhanced crystallization rate could have been due to the PET degradation (lower M_W) in the presence of organoclays as well as nucleating role of organoclays.

Figure 6-12b and c depict the effect of SSP and, consequently, increasing M_W on $t_{½}$ for the neat PET and PET nanocomposites containing 6 wt% C30B. For the neat PET, as M_W is increased from 32 000 to 84 000 g/mol, $t_{½}$ rises from 101 to 168 s, while in PET nanocomposites containing 6wt% C30B, $t_{½}$ increases from 60 s before SSP to 89 s after 12 h of SSP. The increase in polymer chain mobility, either by a M_W reduction during compounding or by a plasticization effect coming from low molecular weight degradation products may considerably speed up the crystal growth rate. Therefore, with decreasing M_W, $t_{½}$ decreases whereas T_c and X_c increase.

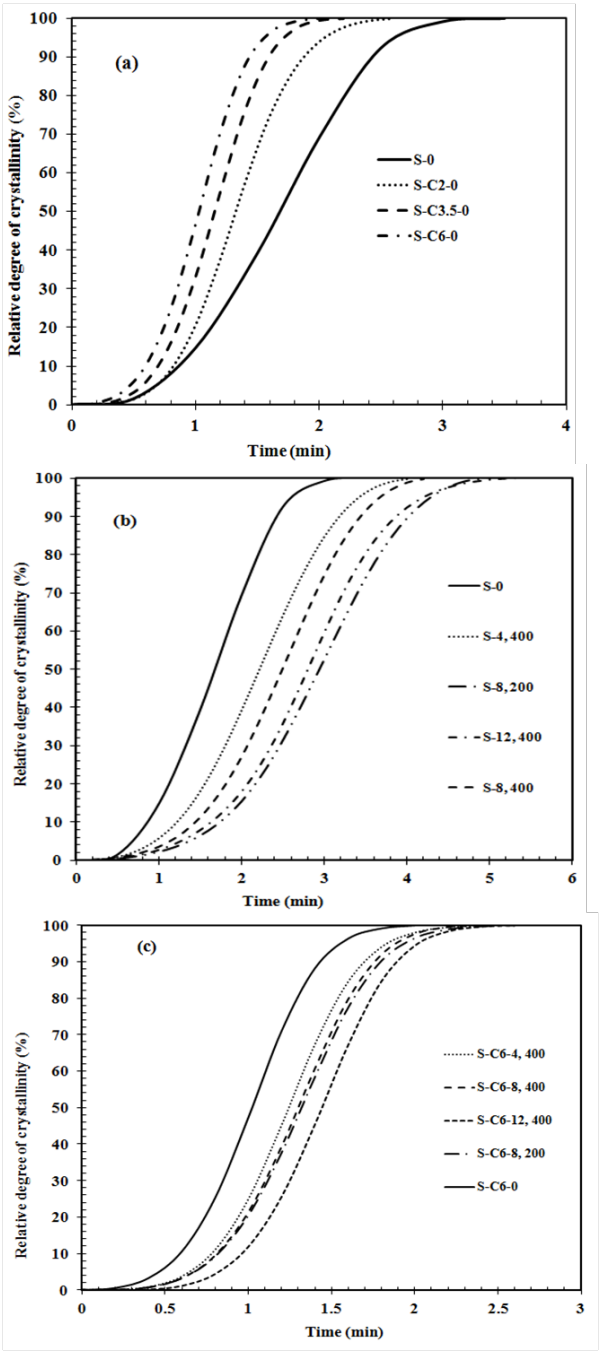

Figure 6-12 : Relative degree of crystallinity from the cooling cycle as a function of crystallization time; a) PET and PET nanocomposites before SSP, b) neat PETs before and after SSP, c) PET-C30B-6 nanocomposites before and after SSP.

6.4 Conclusions

PET/Cloisite 30B (C30B) nanocomposites of different organoclay contents were prepared using water-assisted melt-mixing. The reduction of the molecular weight of the PET matrix, caused by hydrolysis during the water-assisted extrusion, was compensated by subsequent solid-state polymerization (SSP). SSP of PET was carried out at a temperature below the melting point but above the glass transition of PET using two particle sizes for different reaction times. The zero-shear viscosity was found to vary with the weight-average molecular weight to the 3.6 power for the linear PETs. The Maron-Pierce model was used in this work to determine the molecular weight of the PET in the nanocomposites. Significant increases in molecular weight (M_W) were found for the neat PETs and PET nanocomposites using SSP, which were accompanied by substantial reductions of the carboxyl end groups. Lower M_W was observed for the nanocomposites compared to the neat PETs. This could be attributed to a restricted mobility of reactive groups and diffusion of by-products formed during SSP (i.e. water and ethylene glycol) due to the presence of nanoparticles. The linear viscoelastic data for the neat PETs and PET nanocomposites could be correlated using the zero-shear viscosity of the matrix. However, our results showed enhanced rheological properties (mostly for the storage modulus) for samples containing more carboxyl groups, suggesting that the interactions between PET chains and C30B for hydrolyzed samples in the melt state was stronger than for SSP samples due to the larger content of carboxyl groups. DSC results showed reductions in the crystallization temperature and the degree of crystallinity as well as increases in the half-time of crystallization with increasing M_W of PET.

Acknowledgements

The authors acknowledge financial and infrastructure support received from The Natural Sciences and Engineering Research Council of Canada (NSERC), National Research Council of Canada (NRCC), Canada Development Bank (CDB). We would like to gratefully thank CREPEC members, Dr. T. Mousavand and Mrs. M. Hamdine for their technical help.

References

1. J.S. Lee, J. Leisen, R.P. Choudhury, R.M. Kriegel, H.W. Beckham, and W.J. Koros, *Polymer*, **53**, 213 (2012).
2. H. Ghasemi, P.J. Carreau, M.R. Kamal, and S.H. Tabatabaei, *Polym. Eng. Sci.*, **52**, 420 (2012).
3. X.F. Xu, A. Ghanbari, W. Leelapornpisit, M.C. Heuzey, and P.J. Carreau, *Int. Polym. Process.*, **26**, 444 (2011).
4. M. Dini, T. Mousavand, P.J. Carreau, M.R. Kamal, and M.T. Ton-That, *Polym. Eng. Sci*, 2013, doi: 10.1002/pen.23685.
5. H. Ghasemi, P.J. Carreau, M.R. Kamal, and N. Chapleau, *Int. Polym. Process.*, **26**, 219 (2011).
6. S. Hayrapetyan, A. Kelarakis, L. Estevez L, Q. Lin, K. Dana K, Y.L Chung, and E.P. Giannelis. Polymer 2012;53(2):422-426.
7. S. Li, K. Auddy, P. Barber, T.J. Hansen, J. Ma, H.-C. zur Loye, and H.J. Ploehn, *Polym. Eng. Sci.*, **52**, 1888 (2012).
8. Y. Shen, E. Harkin-Jones, P. Hornsby, T. McNally, and R. Abu-Zurayk, *Compos. Sci. Technol.*, **71**, 758 (2011).
9. A. Ghanbari, M.C. Heuzey, P.J. Carreau, and M.T. Ton-That, *Polymer*, **54**, 1361 (2013).
10. H. Ghasemi, P.J. Carreau, M.R. Kamal, and J. Uribe-Calderon, *Polym. Eng. Sci.*, **51**, 1178 (2011).
11. K. Stoeffler, P.G. Lafleur, and J. Denault, *Polym. Degrad. Stab.*, **93**, 1332 (2008).
12. T.Y. Tsai, C.H. Li, C.H. Chang, W.H. Cheng, C.L. Hwang, and R.J. Wu, *Adv. Mater.*, **17**, 1769 (2005).

13. W.J. Choi, H.L. Kim, K.H. Yoon, O.H. Kwon, and C.I. Hwang, *J. Appl. Polym. Sci.*, **100**, 4875 (2006).

14. X. Xu, Y. Ding, Z. Qian, F. Wang, B. Wen, H. Zhou, S. Zhang, and M. Yang, *Polym. Degrad. Stab.*, **94**, 113 (2009).

15. D.W. Litchfield, D.G. Baird, P.B. Rim, and C. Chen, *Polym. Eng. Sci.*, **50**, 2205 (2010).

16. D.S. Achilias, D.N. Bikiaris, V. Karavelidis, and G.P. Karayannidis, *Eur. Polym. J.*, **44**, 3096 (2008).

17. D. Bikiaris, V. Karavelidis, and G. Karayannidis, *Macromol. Rapid Commun.*, **27**, 1199 (2006).

18. S.A. Jabarin and E.A. Lofgren, *J. Appl. Polym. Sci.*, **32**, 5315 (1986).

19. B. Duh. *Polymer*,**43**, 3147 (2002)

20. B. Gantillon, R. Spitz, J.L. Lepage, and T.F. McKenna, *Macromol. Mater. Eng.*, **289** ,88(2004).

21. B. Gantillon, R. Spitz, J.L. Lepage, and T.F. McKenna, *Macromol. Mater. Eng.*, **289**, 119 (2004).

22. Y. Ma, U.S. Agarwal, D.J. Sikkema, and P.J. Lemstra, *Polymer*, **44**, 4085 (2003).

23. S.N. Vouyiouka, E.K. Karakatsani, and C.D. Papaspyrides, *Prog. Polym. Sci.*, **30**, 10 (2005).

24. T.Y. Kim, E.A. Lofgren, and S.A. Jabarin, *J. Appl. Polym. Sci.*, **89**, 197 (2003).

25. C. Shuya, S. Ming-Fa, and C. Shu-May. *J. Appl. Polym. Sci*, **28**, 3289 (1983).

26. S. Sinha Ray and M. Okamoto, *Prog. Polym. Sci.*, **28**, 1539 (2003).

27. P. Cassagnau. *Polymer* , **49**, 2183 (2008)

28. E.P Giannelis, R. Krishnamoorti, and E. Manias. *Polymer-Silicate Nanocomposites: Model Systems for Confined Polymers and Polymer Brushes*. In: S. Granick, K. Binder, P.G. Gennes, E.P. Giannelis, G.S. Grest, H. Hervet, R. Krishnamoorti, L. Léger, E.

Manias, E. Raphaël, and S.Q. Wang, editors. *Polymers in Confined Environments*, vol. 138: Springer Berlin Heidelberg, pp. 107-147 (1999).

29. M.Y. Gelfer, C. Burger, B. Chu, B.S. Hsiao, A.D. Drozdov, M. Si, M. Rafailovich, B.B. Sauer, and J.W. Gilman. *Macromolecules*, **38**, 3765 (2005).
30. S. Abbasi, P. Carreau, A. Derdouri, M Moan. *Rheol. Acta*, **4**8, 943 (2009).
31. G. Hu, C. Zhao, S. Zhang, M. Yang, and Z. Wang. *Polymer* , **47**, 480 (2006).
32. H**.** Zhao, Z. Cui, X. Wang, L.S Turng, and X. Peng**.** *Compos B Eng.*,**51**,79 (2013).
33. A. Ghanbari, M. C. Heuzey, P.J. Carreau, and M. T. Ton-That, *Rheol. Acta*, **52**, 59 (2013).
34. N. Najafi, M.C. Heuzey, P.J. Carreau, and P.M. Wood-Adams, *Polym. Degrad. Stab.*, **97**, 554 (2012).
35. D.H.S. Souza, C.T. Andrade, and M.L. Dias. *Mater. Sci. Eng.: C,* **33**,1795 (2013).
36. R. Krishnamoorti and T. Chatterjee. *Rheology and Processing of Polymer Nanocomposites*. *Applied Polymer Rheology*: John Wiley & Sons, Inc., pp. 153-177 (2011).
37. H.R. Dennis, D.L. Hunter, D. Chang, S. Kim, J.L. White, J.W. Cho, and D.R.Paul. *Polymer*,**42**, 9513 (2001).
38. M. Dini, T. Mousavand, P.J. Carreau, M.R. Kamal, and M.T. Ton-That, *Polym. Eng. Sci*, 2013, doi 10.1002/pen.23736.
39. B. Fox, G. Moad, G. van Diepen, I. Willing, and W.D. Cook. *Polymer*,**38**,3035 (1997) .
40. G.P. Karayannidis, D.E. Kokkalas, and D.N. Bikiaris. *J. Appl. Polym. Sci.*,**50**, 2135 (1993).
41. J. Vlachopoulos and N. Polychronopoulos. *Basic Concepts in Polymer Melt Rheology and Their Importance in Processing*. *Applied Polymer Rheology*: John Wiley & Sons, Inc., pp. 1-27 (2011)
42. J. Dealy and J. Wang. Linear Viscoelasticity. *Melt Rheology and its Applications in the Plastics Industry*: Springer Netherlands, pp. 49-89 (2013)

43. L. Sun, W.J. Boo, J. Liu, A. Clearfield, H.J. Sue, N.E. Verghese, H.Q. Pham, and J. Bicerano, *Macromol. Mater. Eng.*, **294**, 103 (2009).

44. T. Wan, B. Wang, S. Liao, and M. Clifford, *J. Appl. Polym. Sci.*, **125**, E27 (2012)

45. S.G. Kim, E.A. Lofgren, and S.A. Jabarin, *J. Appl. Polym. Sci.*, **127**, 2201 (2013).

46. F.J. Medellin-Rodriguez, R. Lopez-Guillen, and M.A. Waldo-Mendoza. *J. Appl. Polym. Sci.*, **75**, 78 (2000).

47. H. Ghasemi, P.J. Carreau, and M.R. Kamal, *Polym. Eng. Sci.*, **52**, 372 (2012).

48. T. Wan, L. Chen, Y.C. Chua, and X. Lu. *J. Appl. Polym. Sci.*,**94**, 1381(2004).

CHAPTER 7 GENERAL DISCUSSION

Generally, the related investigations about PET nanocomposites without mentioning the preparation methods (melt-mixing and/or in-situ polymerization) have focused on the reduction of the degradation rate of the modifiers of organoclays and of PET [2, 11, 52-54, 61]. PET nanocomposites containing modified nanoclays with thermally stable surfactants showed the intercalated microstructures with more tactoids compared to the commercially available organoclays [11, 60]. Other approaches to control thermal degradation of PET made use of a chain extender [53, 63]. Depending on the functionality of chain extenders, different microstructures and noticeably different changes in the PET chains were formed. Importantly, chain extenders could also yield side-reactions, which could be harmful in the final products for food packaging. On the other hand, other studies were devoted to the enhancement of compatibility of PET and organoclays by the use of compatibilizers, swelling agents or plasticization of PET with carbon dioxide for example [10, 54, 56, 69]. The presence of compatibilizers sometimes led to localization of nanoclays in the compatibilizer phase, not in the matrix and plasticization with carbon dioxide ($scCO_2$) did not show significant improvements in the case of PET nanocomposites. $scCO_2$ as a plasticizer resulted in a viscosity reduction of the melted polymer and swelling of organoclays. Any plasticizer that improves the intercalation and exfoliation process can be used in PET nanocomposites but the key point is the thermodynamic compatibility between PET and plasticizer, thermal stability and the structure of plasticizer. Better compatibility between plasticizer and organoclays than PET and organoclays could cause the organoclays localizations on the plasticizer phase not in the PET matrix. In melt-mixing, other studies considered the effects of the screw speed, screw geometry and temperature profile on the dispersion of organoclays in PET. All these efforts, however, led to only moderately enhanced mechanical and barrier properties.

In this work we investigated a novel method to prepare PET/organoclay nanocomposites by injecting water into the twin screw extruder. Water/steam had two effects in PET nanocomposites; the reduction of M_W of PET by hydrolysis, expansion of the gallery spacing of organoclays and reducing the inter-layer interactions. Thus, both effects assisted the diffusion of PET chains into the organoclay galleries. Since microstructure of polymer nanocomposites is

strongly dependent on the thermodynamic compatibility between organoclays and PET, one commercially available unmodified nanoclay (Cloisite Na^+) and two modified nanoclays (C30B and I28E) were studied. Both C30B and I28E are quaternary ammonium modified, but the modifier of C30B has two hydroxyl groups and modifier of I28E contains long alkyl chains. The presence of two hydroxyl groups in C30B led to good compatibility between PET chains and the organoclay and consequently more delamination compared to I28E and Cloisite Na^+, as observed by XRD, SEM and TEM. On the other hand, the poor affinity between Cloisite Na^+ and PET as well as strong electrostatic forces between adjacent platelets of Cloisite Na^+ hindered the diffusion of PET chains into the galleries of the pristine clay.

Exfoliation of clay platelets in polymer matrix during melt-mixing takes place by two mechanisms; break-up and peeling. During melt-mixing, break-up occurs by imposing stress and shearing the big tactoids to smaller ones. Peeling is facilitated by polymer penetration into the galleries of organoclay, which is driven by affinity of the polymer to the organoclay surface. Morphological analyses of PET/C30B nanocomposites exhibited that longer residence time and lower PET molecular weight had significant effects to facilitate the diffusion process and to improve the delamination of C30B.

Presence of water in the nanocomposites containing I28E had a negative effect on the dispersion. Larger agglomerates of I28E were formed in processing with water compared to without water. By hydrolysis of PET, the number of carboxyl and hydroxyl groups was increased and, therefore, the incompatibility between PET and I28E was intensified.

SSP was used to compensate the molecular weight reduction of PET and PET nanocomposites after extrusion process. SSP is a general and commercial process to manufacture PET with high molecular weight and less thermal degradation. Increasing the molecular weight of neat PETs by SSP and their chemical entities were confirmed by viscometry, rheological measurements and NMR analysis. Investigations on the microstructure of PET nanocomposites displayed that the *d*-spacing and microstructure of the PET nanocomposites did not alter after SSP, indicating that the net diffusion of polymer in and out of the galleries during SSP was negligible. Moreover, possible SSP of PET chains intercalated inside the galleries of the organoclays did not have any significant effects.

In the second phase of this thesis, PET nanocomposites containing different concentration of C30B were prepared since C30B showed the best morphological results among I28E and Cloisite Na^+. Moreover, the screw configuration of extruder was changed to have more shear elements into the extruder as well as increasing the residence time by using reverse elements. The aspect ratio of organoclay for the second screw configuration was higher than the first one, 37 vs. 30 in nanocomposites prepared by conventional melt-mixing.

The presence of organoclays influences the rheology of the polymer nanocomposites, due to polymer-particle, particle-particle interactions and possible changes of the molecular structure of the polymer molecules. PET degradation in the presence of organoclays was found by lower complex viscosity of PET nanocomposites at high frequencies, where the behavior of the matrix is dominant, compared to the neat PET. PET degradation was also increased by increasing the organoclay concentrations. The complex viscosity of nanocomposites containing I28E was larger than those containing C30B in the whole frequency range. Better dispersion and distribution of organoclays in PET made more exposure of the matrix to the surface of organoclays which led to a higher level of polymer degradation. On the other hand, hydroxyl groups and unsaturated tallow groups of C30B accelerated the PET degradation more than the hydrogenated tallow groups of I28E.

The PET nanocomposites prepared by the novel method (water-assisted and SSP) showed a larger enhancement of barrier and mechanical properties than those for the conventional melt-mixing whose extent increased with organoclay concentration.

Approximately, neat PET and PET nanocomposites have the same crystallinity in our work, therefore, the effect of the percentage of crystallinity does not consider in increasing the modulus and barrier properties. However, the crystal content does not change significantly in the presence of C30B, other reports [72] indicate that the size of PET crystallites changes in the presence of C30B, which can affect the oxygen permeability. On the other hand, it is well known that the free volume decreases as the molecular weight increases [113] that all of these parameters affect on modulus and barrier properties.

Fundamental study in this area is required to understand the effect of the size of the crystals and free volume in the presence of organoclay and by changing the molecular weight, consequently, the effect of these parameters on the properties of final products.

Elongation at break in the nanocomposites prepared by the novel method was also significantly higher than those prepared by the conventional method due to the better dispersion and distribution of C30B in the wet processed nanocomposites as well as the larger molecular weight obtained after SSP. Compared to the neat PET, improvements of 45% in tensile modulus and 42% in barrier behavior were found for nanocomposites containing 6 wt% of C30B. In fact, the presence of a mix of intercalated structure and dispersed tactoids in PET nanocomposites significantly reduced the aspect ratio of organoclays and the reinforcement efficiency.

Generally, increasing the organoclay concentration leads to a reduction of elongation at break compared to the neat polymer [114-116] due to the PET degradation in the presence of C30B and the formation of C30B aggregates. Also, interfacial debonding of the clay-PET matrix interface causes cavitation and micro void formation. The presence of large aggregates, which could act as stress concentrators and ultimate mechanical failure points, causes a reduction of the elongation at break with increasing organoclay concentration.

If in the exfoliated systems, individual platelets prevent microcrack propagation then elongation at break will increase [52] and it is usually seen in the organoclay concentration less than 1wt%. Even in the case of PA nanocomposites with exfoliated microstructures containing organoclay concentration 1wt% and 3.5 wt%, the lower elongation at break in nanocomposites was observed compared to the neat PA [114, 116, 117]. Usually exfoliated microstructures have higher elongation at break than intercalated microstructure.

In the case of PET nanocomposites even after SSP, lower elongation at break was found compared to the neat PET due to the large agglomerates of C30B at high concentration. On the other hand, molecular weight of PET nanocomposites with higher organoclay concentration is less than the neat PET and low C30B concentration because of the reduction of SSP rate by increasing the organoclay concentration.

An increase in crystallinity resulted in an increase in modulus but a reduction in elongation at break at temperature below T_g. Unoriented crystallites leads to polymer brittleness due to the

imposed strain on amorphous phase by crystallites, voids formation during crystallization and/or stress concentration imposed by crystallites. On the other hand, chain ends and molecular imperfection which are in the amorphous portions between crystallite lamellae causes a brittle material [118].

The presence of organoclays causes PET degradation, reduction of molecular weights and increasing of the chain ends as an imperfection in the polymer network, therefore, increasing the molecular weight and subsequently increasing the number of entanglements leads to higher elongation at break after SSP. It is generally accepted that the elongation at break increases with increasing molecular weight of linear polymers [118, 119]. In our work, by increasing the molecular weight and subsequently chain entanglements, the molecular chains are long enough to be stretched and straightened but short enough that entanglements cannot inhibit the straightening. It was also seen that for a given molecular weight, the branched polymers had fewer entanglements than the linear polymers, thus, the strength and the elongation to break were lower for the branched polymers [120]. On the other hand, the broad molecular-weight distribution polymers gave somewhat higher elongation at break than the narrower molecular-weight distribution. As reported in the third paper, SSP leads to broadening of molecular-weight distribution. It could be another reason for increasing the elongation at break after SSP.

The color of the samples containing 2wt% of C30B prepared via the novel method and conventional melt-mixing is illustrated in Figure 7-1. The nanocomposites prepared using the novel method was lighter compared to the conventional melt-mixed samples. The percentage of crystallinity was 4% and 6% in SSP-WPET-C30B-2 and PET-C30B-2, respectively.

If the shelf life of carbonated soft drinks is considered to be 90 days, for our PET nanocomposites obtained by conventional melt-mixing containing 2wt% C30B it will be 107 days and in the novel preparation method it will increase to 113 days.

Obviously, the proposed process introduces some complexities and potential increases in costs for producing PET/clay nanocomposites. However, the results reported in this thesis suggest advantages in relation to dispersion quality, color, molecular weight control, gas emissions, permeability and mechanical properties.

Finally, although the rate of increasing the molecular weight of PET by using chain extenders was higher than SSP, the chain extenders like joncryl resulted in branching structure and also increasing the haze and clarity while SSP did not change the linear structure and visibility of the PET and PET nanocomposites. Moreover, the branching structure of PET in some cases like melt-spinning led to several problems because of the reduction of PET crystallinity and substantial increase in melt viscosity. In addition, the extent of enhanced barrier properties in nanocomposites prepared by novel method compared to conventional melt-mixing was higher than using chain extender in the PET [63] and PLA/C30B [121] nanocomposites proposed by literature as well as observed brittle behavior in the nanocomposites with chain extenders. However, the effect of chain extenders like joncryl in improving the mechanical properties of PET nanocomposites is higher than SSP. Importantly, by using this novel method (water-assisted and SSP), enhanced barrier and mechanical properties were obtained without using any chemicals which would cause side reaction and changing the structure of PET.

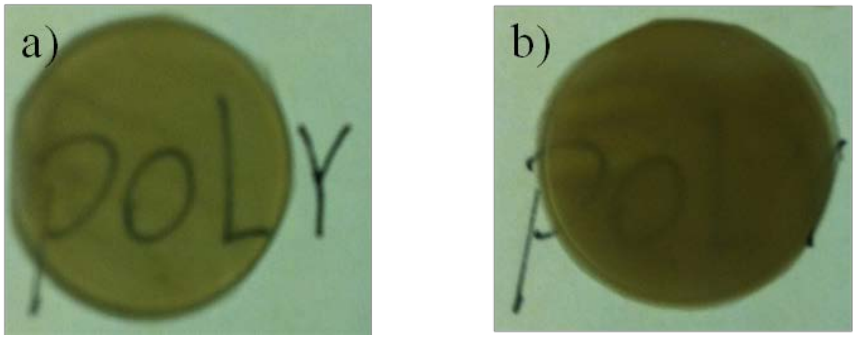

Figure 7-1 : Color of the nanoocmposites containing 2wt% C30B; a) SSP-W-PET-C30B-2. b) PET-C30B-2

In the third part of this study, we found an increased rate of SSP with decreasing particle size, suggesting that SSP was controlled by diffusion of the by-products; as the particle size decreased, the larger interfacial area facilitated by-products diffusion. We also observed strong non-linear increases of M_W with SSP time, but markedly less for the nanocomposites. The lower increases of the apparent M_W of PET in the nanocomposites indicated the restricted mobility of the reactive groups and increased diffusion path length of the by-products in the presence of

organoclay platelets. Molecular weight of PET in the nanocomposites was estimated using the Maron-Pierce model. Viscometry measurements of PET nanocomposites involved some problems since complete separation of organoclays from PET was not possible and either filtering or not filtering of organoclays influenced the molecular weight determination. We also verified the PET degradation in the presence of organoclays by end group (carboxyl group) titration. Titration experiments showed that the carboxyl groups increased in the presence of the organoclay after melt-mixing while by SSP the carboxyl groups were reduced. End groups also had the significant effects on the rheological behavior of PET nanocomposites; stronger structure was observed at low frequencies with higher carboxyl contents.

Our DSC results showed that the effect of the reduction of PET molecular weight in increasing the cold crystallization temperature and crystallinity was a much more than the presence of C30B. The increase in polymer chain mobility, either by a M_W reduction during compounding or by a plasticization effect coming from low molecular weight degradation products may considerably speed up the crystal growth rate. Moreover, the presence of organoclays restricts the motion of polymer chains and results in the imperfect crystallites.

The slurry method (suspension of Cloisite Na^+ in water) was also investigated to examine the feasibility of the water-assisted extrusion method for PET nanocomposite based on unmodified nanoclay. The presence of water expanded the nanoclay, but when this suspension pumped into the extruder, the rate of evaporation of water and the collapsing of the nanoclay was more important than the possible gain of the diffusion of PET chains into the galleries of the nanoclay. However, polymers like PEG and CMC added to the suspension could migrate to the interlayer of the nanoclay and help to improve the dispersion and distribution of nanoparticles in the final product. In the final product there is approximately 0.2 wt% of PEG and CMC which their effect on PET degradation is negligible. The color of PET nanocomposites obtained by this method was better than for nanocomposites containing C30B. On the other hand, Cloisite Na^+, PEG and CMC are FDA approved and safe for food packaging.

CHAPTER 8 CONCLUSIONS AND RECOMMENDATIONS

8.1 Conclusions

In this dissertation, a new melt-mixing process has been used to prepare PET/clay nanocomposites called water-assisted melt-mixing. In this method, steam was fed into a twin-screw extruder (TSE) to hydrolyze the PET chains and to facilitate their diffusion into the gallery spacing of organoclays. Cloisite Na^+, Cloisite 30B and Nanomer I.28E were used to evaluate the effect of organoclay modifiers on the microstructure of PET nanocomposites. I28E has a higher *d*-spacing (2.5 nm) than C30B (1.8 nm) and Cloisite Na^+ (0.9 nm). The hydroxyl groups of C30B enhanced compatibility between the PET and the organoclay. XRD, SEM and TEM analysis showed a better dispersion of Cloisite 30B (C30B) in PET compared to Nanomer I.28E (I28E) and Cloisite Na^+, indicating the importance of thermodynamic compatibility between organo-modifier and PET.

By water-assisted melt-mixing, partially exfoliated, well-dispersed and delaminated PET-C30B nanocomposites were obtained. TEM images displayed a larger number of single and double layers of C30B nanoparticles as well as an increased aspect ratio in the PET nanocomposites. Interestingly, it was found that the effect of water on the microstructure of PET nanocomposites was strongly dependent on the nanoclay modifier; water-assisted melt-mixing had negative effects on the nanocomposites containing I28E. Results of the linear viscoelastic data showed lower complex viscosity at high frequencies in nanocomposites containing C30B than I28E due to the more degradation of PET in the presence of C30B.

Solid-state polymerization (SSP) was used to increase the molecular weight (M_W) of the PET matrix following a reduction due to hydrolysis by water. The linear structure of PET chains after SSP was revealed by ^{1}H NMR and ^{13}C NMR spectra. Morphological analysis of PET nanocomposites showed that the microstructure of PET nanocomposites did not change after SSP due to the limited PET chains mobility at temperatures less than the melting point.

The effect of feeding rate and consequently residence time on the properties of PET nanocomposites was also investigated. Morphological results revealed more delamination of organoclay platelets in PET-C30B nanocomposites processed at the low feeding rate compared to

those processed at the high feeding rate. The PET nanocomposites prepared by water-assisted extrusion followed by SSP showed enhanced mechanical and barrier properties compared to the nanocomposites prepared by the conventional melt-mixing process.

In the second part of this work, the effect of C30B concentrations on the mechanical, barrier, thermal and rheological behaviour of PET nanocomposites prepared using two different twin-screw extrusion processes (conventional melt-mixing and water-assisted melt-mixing) was studied. Microstructure analyses showed intercalated/exfoliated morphology in all PET/C30B nanocomposites, with a higher degree of intercalation and delamination for the water-assisted process. PET degradation in the presence of C30B was confirmed by rheological measurements: M_W of extruded PET reduced from 47 000 to 34 000 and 26 000 g/mol in nanocomposites containing 2 wt% and 6 wt% C30B, respectively.

PET nanocomposites showed improvements in the tensile modulus and barrier properties compared to the neat PET, especially for the water-assisted and SSP samples. SSP helped to recover the polymer molecular weight loss due to hydrolysis, resulting in less brittle nanocomposites. Elongation at break for conventional PET nanocomposites containing 2 wt% C30B was 6%, but for the wet processed nanocomposites after SSP the elongation at break was around 145%. However, in nanocomposites with 3.5 and 6 wt% C30B, the elongation at break after SSP was still low, compared to the neat PET and nanocomposites with 2 wt% of C30B due to the presence of more agglomerates of C30B at high concentrations. PET nanocomposites containing 6wt% C30B showed significant improvements in the tensile modulus and barrier properties compared to the neat PET.

A comparison of the predicted tensile modulus using the pseudo-inclusion model with the experimental value showed a noticeable difference, which was intensified with increasing C30B concentration. This was due to the some limitations of the model, which considers unidirectional orientation, homogenous dispersion of single layers or tactoids and good compatibility between the polymer and the nanoclay. On the other hand, the model does not consider polymer crystallinity and orientation of the crystals. The Nielsen model overpredicted the relative permeability in the case of fully exfoliated nanocomposites, and the Bharadwaj model showed that the predictions were highly sensitive to the orientation factor. In fact, free volume, size and

shape of crystallites and degree of crystallinity, interfacial region and particle agglomeration as well as aspect ratio and orientation are important parameters that influence the diffusion rate of oxygen in polymer nanocomposites.

In the third part, SSP of nanocomposites containing different concentration of C30B was extensively studied using viscometry, titration, rheological and dynamic scanning calorimetry (DSC) measurements. SSP of PET was carried out at a temperature below the melting point but above the glass transition of PET using two different particle sizes for different reaction times. The weight-averaged molecular weight (M_W) of PET was shown to increase following SSP significantly with reduction of particle size, increasing M_W from 32 000 to 68 000 g/mol after 8 hours with particle size of 400 μm and 84 000 g/mol with particle size of 200 μm. The zero-shear viscosity was found to vary with the weight-average molecular weight to the 3.6 power for the linear PETs.

PET nanocomposites exhibited a solid-like rheological behavior and the complex viscosity at high frequencies was scaled with the molecular weight of PET. The Maron-Pierce model was used to evaluate the molecular weight of PET in the nanocomposites before and after SSP. It was also found that the extent and the rate of the SSP reaction in nanocomposites were lower than those for the neat PET, due to the reduction of mobility of chain ends and barrier effect of clay platelets. Results of titration revealed increases of the carboxyl group content in nanocomposites compared to the neat PET before SSP, indicative of PET degradation in the presence of C30B. On the other hand, by SSP, the carboxyl groups were reduced for the neat PET and its nanocomposites. However, enhanced rheological properties for samples containing more carboxyl groups were found, suggesting that the interaction between PET and C30B for hydrolyzed samples in the melt state was stronger than for samples after SSP. DSC results demonstrated reductions in the crystallization temperature and degree of crystallinity as well as increases in half-time crystallization with increasing M_W of PET.

Slurry of water and Cloisite Na^+ was used to investigate the effect of pre-exfoliation of Cloisite Na^+ in water on the properties and microstructure of PET nanocomposites. PEG and CMC were also added in the slurry of water and nanoclays to diffuse between the interlayer of the nanoclay. XRD and SEM results showed increases of the *d*-spacing of the nanoclay in the

presence of PEG and CMC as well as a better dispersion and distribution of nanoparticles in the PET matrix. Enhanced Young modulus and reduced oxygen permeability for the nanocomposites compared to the neat PET were obtained.

8.2 Original contributions

As mentioned in the introduction section, most of these investigations in the literature on PET nanocomposites are related to the processing conditions, using different modifications of nanoclays and compatibilizers. In this work, we proposed for the first time to prepare PET nanocomposites by the water-assisted extrusion process and solid-state polymerization. We also intensely studied the microstructure, thermal, mechanical and barrier properties of the obtained nanocomposites. Our results revealed the efficient effect of this novel method to improve dispersion and distribution of Cloisite 30B into the PET compared to the conventional melt-mixing with enhanced mechanical and barrier properties. This is promising way to prepare polymer nanocomposites. We also studied the effect of organoclay compatibility with PET and feeding rate on the final microstructure of PET nanocomposites. In this work, the effect of organoclay concentration on the PET degradation was comprehensively investigated by titration and rheological measurements. Solid-state polymerization (SSP) was introduced to compensate the PET degradation during melt-mixing. It is also a capable method to increase the molecular weight of polyesters without using any chemicals that leads to side reactions. Therefore, SSP of PET and PET nanocomposites containing different concentrations of Cloisite 30B were conducted in a batch reactor at different reaction times and two different polymer particle sizes. Rheological measurements, intrinsic viscosity and titration measurements were used to characterize the samples following SSP. More specifically, the changes in the rheological behavior of PET nanocomposites with increasing molecular weight of the matrix were presented. The effect of the molecular weight of PET and PET nanocomposites on the thermal properties was also reported.

8.3 Recommendations

The following subjects are recommended for future research:

- Study on the extrusion process of PET under high temperature and high pressure extruder to investigate if water plays a plasticizer role to reduce the melting point of PET without hydrolysis or with minimal hydrolysis reaction. This could be carried out with high pressure DSC instruments.
- Since melt-mixing conditions are important in the dispersion and distribution of nanoparticles in the polymer matrix, the effect of the screw configuration with more mixing elements should be studied.
- Mechanical results showed that the elongation at break of nanocomposites following SSP was significantly increased. Elongation at break may have a close relationship with molecular weight of the matrix. Hence, the effect of PET molecular weight of nanocomposites on the mechanical and barrier properties should be fundamentally investigated.
- It would also be interesting to characterize the free volume, shape and size of the crystals with increasing molecular weight of PET and their effects on the properties of the final products.
- Film casting and blow molding of PET nanocomposites after SSP should be carried out with the characterization of their barrier and mechanical properties.
- On the other hand, scale-up and modeling of SSP of PET nanocomposites are important issues that need to be investigated.
- In order to improve the slurry method for more opening of the gallery spacing of Cloisite Na^+ and to obtain a better morphology, the effect of PEO or of other compatibilizers with high thermal stability should be studied.
- The slurry method can be applied for any polymer and nanofiller systems, especially the new kind of the nanofillers such as cellulosic nanofillers.

REFERENCES

[1] S. A. Jabarin, "Advances in barrier concepts for improvedrigid packaging," presented at ANTEC, annual technical conference: May 4-8, Nashville, Tennessee: conference proceedings2003.

[2] S. Hayrapetyan, *et al.*, "Non-toxic poly(ethylene terephthalate)/clay nanocomposites with enhanced barrier properties," *Polymer*, vol. 53, pp. 422-426, 2012.

[3] J. S. Lee, *et al.*, "Antiplasticization-based enhancement of poly(ethylene terephthalate) barrier properties," *Polymer*, vol. 53, pp. 213-222, 2012.

[4] İ. Özen, *et al.*, "Improvement in gas permeability of biaxially stretched PET films blended with high barrier polymers: The role of chemistry and processing conditions," *European Polymer Journal*, vol. 46, pp. 226-237, 2010.

[5] S. Sinha Ray and M. Okamoto, "Polymer/layered silicate nanocomposites: a review from preparation to processing," *Progress in Polymer Science*, vol. 28, pp. 1539-1641, 2003.

[6] Y. Imai, *et al.*, "Properties of poly(ethylene terephthalate)/layered silicate nanocomposites prepared by two-step polymerization procedure," *Polymer Journal*, vol. 35, pp. 230-235, 2003.

[7] G. Zhang, *et al.*, "PET-clay hybrids with improved tensile strength," *Materials Letters*, vol. 57, pp. 1858-1862, 2003.

[8] L. V. Todorov and J. C. Viana, "Characterization of PET nanocomposites produced by different melt-based production methods," *Journal of Applied Polymer Science*, vol. 106, pp. 1659-1669, 2007.

[9] D. R. Paul and L. M. Robeson, "Polymer nanotechnology: nanocomposites," *Polymer*, vol. 49, pp. 3187-3204, 2008.

[10] A. Ammala, *et al.*, "Poly(ethylene terephthalate) clay nanocomposites: Improved dispersion based on an aqueous ionomer," *Composites Science and Technology*, vol. 68, pp. 1328-1337, 2008.

[11] K. Stoeffler, *et al.*, "Thermal decomposition of various alkyl onium organoclays: Effect on polyethylene terephthalate nanocomposites' properties," *Polymer Degradation and Stability*, vol. 93, pp. 1332-1350, 2008.

[12] J. W. Chung, *et al.*, "Thermally stable exfoliated poly(ethylene terephthalate) (PET) nanocomposites as prepared by selective removal of organic modifiers of layered silicate," *Polymer Degradation and Stability*, vol. 93, pp. 252-259, 2008.

[13] H. Ghasemi, *et al.*, "Effect of Processing Conditions on Properties of PET/Clay Nanocomposite Films," *International Polymer Processing*, vol. 26, pp. 219-228, May 2011.

[14] C. Davis, *et al.*, "Effects of melt-processing conditions on the quality of poly (ethylene terephthalate) montmorillonite clay nanocomposites," *Journal of Polymer Science Part B: Polymer Physics*, vol. 40, pp. 2661-2666, 2002.

[15] L. K. Massey, "Introduction," in *Permeability Properties of Plastics and Elastomers (Second Edition)*, ed Norwich, NY: William Andrew Publishing, 2003, pp. 1-56.

[16] J. Jiang, *et al.*, "Oxygen barrier coating deposited by novel plasma-enhanced chemical vapor deposition," *Journal of Applied Polymer Science*, vol. 115, pp. 2767-2772, 2010.

[17] Y. S. Hu, *et al.*, "Improving oxygen barrier properties of poly(ethylene terephthalate) by incorporating isophthalate. II. Effect of crystallization," *Journal of Applied Polymer Science*, vol. 98, pp. 1629-1642, 2005.

[18] Y. S. Hu, *et al.*, "Improving gas barrier of PET by blending with aromatic polyamides," *Polymer*, vol. 46, pp. 2685-2698, 2005.

[19] A. Polyakova, *et al.*, "Oxygen-barrier properties of copolymers based on ethylene terephthalate," *Journal of Polymer Science Part B: Polymer Physics*, vol. 39, pp. 1889-1899, 2001.

[20] R. Y. F. Liu, *et al.*, "Improving oxygen barrier properties of poly(ethylene terephthalate) by incorporating isophthalate. I. Effect of orientation," *Journal of Applied Polymer Science*, vol. 98, pp. 1615-1628, 2005.

[21] K. Mahajan, "Synthesis and characterization of new active barrier polymers," Ph.D Dissertation, Chemical Engineering, The University of Toledo, United States, Ohio, 2010.

[22] K. Mahajan, *et al.*, "Development of active barrier systems for poly(ethylene terephthalate)," *Journal of Applied Polymer Science*, vol. 129, pp. 2196-2207, Aug 2013.

[23] H. Li, "Kinetics and mechanisms of the oxidation processes for unsaturated-hydrocarbon-modified scavengers," Ph.D Dissertation, College of Engineering, The University of Toledo, United States, Ohio, 2010.

[24] A. A. Natu, *et al.*, "Effect of morphology on barrier properties of poly(ethylene terephthalate)," *Polymer Engineering and Science*, vol. 45, pp. 400-409, Mar 2005.

[25] Y. S. Hu, *et al.*, "Improving transparency of stretched PET/MXD6 blends by modifying PET with isophthalate," *Polymer*, vol. 46, pp. 5202-5210, 2005.

[26] S. H. Kim and S. C. Kim, "Synthesis and properties of poly(ethylene terephthalate)/clay nanocomposites by in situ polymerization," *Journal of Applied Polymer Science*, vol. 103, pp. 1262-1271, 2007.

[27] W. J. Choi, *et al.*, "Preparation and barrier property of poly (ethylene terephthalate)/clay nanocomposite using clay-supported catalyst," *Journal of Applied Polymer Science*, vol. 100, pp. 4875-4879, 2006.

[28] R. K. Bharadwaj, *et al.*, "Structure-property relationships in cross-linked polyester-clay nanocomposites," *Polymer*, vol. 43, pp. 3699-3705, 2002.

[29] J.-K. Kim, *et al.*, "Moisture barrier characteristics of organoclay-epoxy nanocomposites," *Composites Science and Technology*, vol. 65, pp. 805-813, 2005.

[30] M. Frounchi, *et al.*, "Gas barrier properties of PP/EPDM blend nanocomposites," *Journal of Membrane Science*, vol. 282, pp. 142-148, 2006.

[31] M. Frounchi and A. Dourbash, "Oxygen barrier properties of poly (ethylene terephthalate) nanocomposite films," *Macromolecular Materials and Engineering,* vol. 294, pp. 68-74, 2008.

[32] H. M. C. d. Azeredo, "Nanocomposites for food packaging applications," *Food Research International,* vol. 42, pp. 1240-1253, 2009.

[33] S. Takahashi, *et al.*, "Gas barrier properties of butyl rubber/vermiculite nanocomposite coatings," *Polymer,* vol. 47, pp. 3083-3093, 2006.

[34] V. Sridhar and D. K. Tripathy, "Barrier properties of chlorobutyl nanoclay composites," *Journal of Applied Polymer Science,* vol. 101, pp. 3630-3637, 2006.

[35] B. Brulé and J. J. Flat, "High Barrier Polyamide/Polyolefin/Organoclay Nanocomposites," *Macromolecular Symposia,* vol. 233, pp. 210-216, 2006.

[36] E. Picard, *et al.*, "Barrier properties of nylon 6-montmorillonite nanocomposite membranes prepared by melt blending: Influence of the clay content and dispersion state: Consequences on modelling," *Journal of Membrane Science,* vol. 292, pp. 133-144, 2007.

[37] G. Choudalakis and A. D. Gotsis, "Permeability of polymer/clay nanocomposites: A review," *European Polymer Journal,* vol. 45, pp. 967-984, 2009.

[38] C. Lu and Y. W. Mai, "Permeability modelling of polymer-layered silicate nanocomposites," *Composites Science and Technology,* vol. 67, pp. 2895-2902, 2007.

[39] S. Pavlidou and C. D. Papaspyrides, "A review on polymer-layered silicate nanocomposites," *Progress in Polymer Science,* vol. 33, pp. 1119-1198, 2008.

[40] X. Yuan, *et al.*, "Thermal degradation investigation of poly(ethylene terephthalate)/fibrous silicate nanocomposites," *Polymer Degradation and Stability,* vol. 93, pp. 466-475, 2008.

[41] M. Yin, *et al.*, "In-situ synthesis of poly (ethylene terephthalate)/clay nanocomposites using TiO 2/SiO 2 sol-intercalated montmorillonite as polycondensation catalyst," *Polymer Engineering & Science,* vol. 49, 2009.

[42] T.-Y. Tsai, *et al.*, "Preparation of exfoliated polyester/clay nanocomposites," *Advanced Materials,* vol. 17, pp. 1769-1773, 2005.

[43] M. Mun, *et al.*, "Preparation of poly (ethylene terephthalate) nanocomposite fibers incorporating a thermally stable organoclay," *Polymer Bulletin,* vol. 57, pp. 797-804, 2006.

[44] N. Ogata, *et al.*, "Structure and thermal/mechanical properties of poly(l-lactide)-clay blend," *Journal of Polymer Science Part B: Polymer Physics,* vol. 35, pp. 389-396, 1997.

[45] Y. Furuhashi, *et al.*, "Preparation and some properties of stereocomplex-type poly(lactic acid)/layered silicate nanocomposites," *Journal of Applied Polymer Science,* vol. 127, pp. 1615-1622, 2013.

[46] Y. Li, *et al.*, "Properties of Poly(Lactic Acid)/ Organo-Montmorillonite Nanocomposites Prepared by Solution Intercalation," *Journal of Macromolecular Science, Part B*, vol. 52, pp. 1041-1055, 2013/07/01 2013.

[47] R. Scaffaro, *et al.*, "Effect of kind and content of organo-modified clay on properties of PET nanocomposites," *Journal of Applied Polymer Science*, vol. 122, pp. 384-392, 2011.

[48] S. S. Ray and M. Bousmina, "Poly(butylene sucinate-co-adipate)/montmorillonite nanocomposites: effect of organic modifier miscibility on structure, properties, and viscoelasticity," *Polymer*, vol. 46, pp. 12430-12439, 2005.

[49] E. P. Giannelis, *et al.*, "Polymer-Silicate Nanocomposites: Model Systems for Confined Polymers and Polymer Brushes," in *Polymers in Confined Environments*. vol. 138, S. Granick, *et al.*, Eds., ed: Springer Berlin Heidelberg, 1999, pp. 107-147.

[50] B. Esmaeili, *et al.*, "In situ polymerization of PET in the presence of pristine and organo-modified clays," *Intern. Polymer Processing* vol. XXVIII, 2013.

[51] Z. Chen, *et al.*, "Preparation and properties of organo-modifier free PET/MMT nanocomposites via monomer intercalation and in situ polymerization," *Polymers for Advanced Technologies*, 2009.

[52] D. W. Litchfield, *et al.*, "Improved mechanical properties of poly(ethylene terephthalate) nanocomposite fibers," *Polymer Engineering & Science*, vol. 50, pp. 2205-2215, 2010.

[53] X. Xu, *et al.*, "Degradation of poly(ethylene terephthalate)/clay nanocomposites during melt extrusion: Effect of clay catalysis and chain extension," *Polymer Degradation and Stability*, vol. 94, pp. 113-123, 2009.

[54] A. Sanchez-Solis, *et al.*, "Mechanical and rheological studies on polyethylene terephthalate-montmorillonite nanocomposites," *Polymer Engineering and Science*, vol. 44, pp. 1094-1102, 2004.

[55] X. F. Xu, *et al.*, "Effect of Ionomer on Barrier and Mechanical Properties of PET/Organoclay Nanocomposites Prepared by Melt Compounding," *International Polymer Processing*, vol. 26, pp. 444-455, 2011.

[56] A. Ghanbari, *et al.*, "Morphology and properties of polymer/organoclay nanocomposites based on poly (ethylene terephthalate) and sulfopolyester blends," *Polymer International*, 2012.

[57] C. I. W. Calcagno, *et al.*, "The effect of organic modifier of the clay on morphology and crystallization properties of PET nanocomposites," *Polymer*, vol. 48, pp. 966-974, 2007.

[58] S. g. KIM, "PET nanocomposites Development with Nanoscale Materials," Doctor of Philosophy, Colledge of Engineering, The university of Toledo, 2007.

[59] A. Ghanbari, *et al.*, "Morphological and rheological properties of PET/clay nanocomposites," *Rheologica Acta*, vol. 52, pp. 59-74, 2013/01/01 2013.

[60] H. Ghasemi, *et al.*, "Preparation and characterization of PET/clay nanocomposites by melt compounding," *Polymer Engineering & Science*, vol. 51, pp. 1178-1187, 2011.

[61] M. Costache, *et al.*, "Preparation and characterization of poly (ethylene terephthalate)/clay nanocomposites by melt blending using thermally stable surfactants," *Polymers for Advanced Technologies,* vol. 17, pp. 764-771, 2006.

[62] J. K. Kim, *et al.*, "Morphology and rheological behaviors of polyethylene terephthalate nanocomposites containing polyhedral oligomeric silsesquioxanes," *Journal of Applied Polymer Science,* vol. 107, pp. 272-279, 2008.

[63] A. Ghanbari, *et al.*, "A novel approach to control thermal degradation of PET/organoclay nanocomposites and improve clay exfoliation," *Polymer,* vol. 54, pp. 1361-1369, 2013.

[64] H. Ghasemi, *et al.*, "Properties of PET/clay nanocomposite films," *Polymer Engineering & Science,* vol. 52, pp. 420-430, 2012.

[65] R. S. Rajeev, *et al.*, "Studies on the effect of equi-biaxial stretching on the exfoliation of nanoclays in polyethylene terephthalate," *European Polymer Journal,* vol. 45, pp. 332-340, 2009.

[66] K. Soon, *et al.*, "Morphology, barrier, and mechanical properties of biaxially deformed poly(ethylene terephthalate)-mica nanocomposites," *Polymer Engineering & Science,* vol. 52, pp. 532-548, 2012.

[67] K. H. Soon, *et al.*, "Characterisation of melt-processed poly(ethylene terephthalate)/syntheticmica nanocomposite sheet and its biaxial deformation behaviour," *Polymer International,* vol. 58, pp. 1134-1141, 2009.

[68] Y. Shen, *et al.*, "The effect of temperature and strain rate on the deformation behaviour, structure development and properties of biaxially stretched PET–clay nanocomposites," *Composites Science and Technology,* vol. 71, pp. 758-764, 2011.

[69] J. R. Samaniuk, "Improving the exfoliation of layered silicate in a poly (ethylene terephthalate) matrix using supercritical carbon dioxide," Master of Science Chemical engineering, Virginia Tech, Blacksburg, 2008.

[70] J. P. Jog, "Crystallisation in polymer nanocomposites," *Materials Science and Technology,* vol. 22, pp. 797-806, 2006.

[71] T. Wan, *et al.*, "Crystalline morphology and isothermal crystallization kinetics of poly(ethylene terephthalate)/clay nanocomposites," *Journal of Applied Polymer Science,* vol. 94, pp. 1381-1388, 2004.

[72] H. Ghasemi, *et al.*, "Isothermal and non-isothermal crystallization behavior of PET nanocomposites," *Polymer Engineering & Science,* vol. 52, pp. 372-384, 2012.

[73] J. Bandyopadhyay, *et al.*, "Thermal and Thermo-mechanical Properties of Poly (ethylene terephthalate) Nanocomposites," *Journal of Industerial and Engineering Chemistry,* vol. 13, p. 614, 2007.

[74] C. I. W. Calcagno, *et al.*, "The role of the MMT on the morphology and mechanical properties of the PP/PET blends," *Composites Science and Technology,* vol. 68, pp. 2193-2200, 2008.

[75] Y. Kong and J. N. Hay, "Multiple melting behaviour of poly(ethylene terephthalate)," *Polymer,* vol. 44, pp. 623-633, 2003.

[76] A. Dasari, *et al.*, "Clay exfoliation and organic modification on wear of nylon 6 nanocomposites processed by different routes," *Composites Science and Technology,* vol. 65, pp. 2314-2328, 2005.

[77] N. Fedullo, *et al.*, "Polymer-based nanocomposites: Overview, applications and perspectives," *Progress in Organic Coatings,* vol. 58, pp. 87-95, 2007.

[78] K. Stoeffler, *et al.*, "Polyamide 12 (PA12)/clay nanocomposites fabricated by conventional extrusion and water-assisted extrusion processes," *Journal of Applied Polymer Science,* vol. 130, pp. 1959-1974, 2013.

[79] N. Fedullo, *et al.*, "Nanocomposites from Untreated Clay : A Myth ?," *Macromolecular Symposia,* vol. 233, pp. 235-245, 2006.

[80] F. Touchaleaume, *et al.*, "One-step water-assisted melt-compounding of polyamide 6/pristine clay nanocomposites: An efficient way to prevent matrix degradation," *Polymer Degradation and Stability,* vol. 96, pp. 1890-1900, 2011.

[81] M. Kato, *et al.*, "Development of a new production method for a polypropylene-clay nanocomposite," *Polymer Engineering and Science,* vol. 44, pp. 1205-1211, 2004.

[82] Z. Liu, *et al.*, "A novel approach in preparing polymer/nano-$CaCO_3$ composites," *Frontiers of Chemical Engineering in China,* vol. 2, pp. 115-122, 2008.

[83] G. Stoclet, *et al.*, "Relations between structure and property of polyamide 11 nanocomposites based on raw clays elaborated by water-assisted extrusion," *Journal of Applied Polymer Science,* vol. 127, pp. 4809-4824, 2013.

[84] Z.-Z. Yu, *et al.*, "Water-assisted melt compounding of nylon-6/pristine montmorillonite nanocomposites," *Journal of Polymer Science Part B: Polymer Physics,* vol. 43, pp. 1100-1112, 2005.

[85] N. Hasegawa, *et al.*, "Nylon 6/Na-montmorillonite nanocomposites prepared by compounding Nylon 6 with Na-montmorillonite slurry," *Polymer,* vol. 44, pp. 2933-2937, 2003.

[86] V. Molajavadi and H. Garmabi, "Water assisted exfoliation of PA6/clay nanocomposites using a twin screw extruder: Effect of water contact time," *Journal of Applied Polymer Science,* vol. 119, pp. 736-743, 2011.

[87] D. D. J. Rousseaux, *et al.*, "Water-assisted extrusion of polypropylene/clay nanocomposites: A comprehensive study," *Polymer,* vol. 52, pp. 443-451, 2011.

[88] M. Mainil, *et al.*, "Morphology and properties of SAN-clay nanocomposites prepared principally by water-assisted extrusion," *Polymer Engineering & Science,* vol. 50, pp. 10-21, 2010.

[89] F.Touchaleaume, *et al.*, "Efficient one-step melt-compounding of copolyetheramide/pristine clay nanocomposites using water-injection as intercalating/exfoliating aid," *Exp Polym Lett,* vol. 5, pp. 1085-1101, 2011.

[90] C. Thouzeau, *et al.*, "Emission of volatile organic compounds during processing and use of organoclay-based nanocomposites," *Polymer Degradation and Stability,* vol. 98, pp. 557-565, 2013.

[91] B. Lecouvet, *et al.*, "Water-assisted extrusion as a novel processing route to prepare polypropylene/halloysite nanotube nanocomposites: Structure and properties," *Polymer,* vol. 52, pp. 4284-4295, 2011.

[92] K. Pang, *et al.*, "Review of conventional and novel polymerization processes for polyesters," *Progress in Polymer Science,* vol. 31, pp. 1009-1037, 2006.

[93] S. R. Turner and Y. Liu, "5.14 - Chemistry and Technology of Step-Growth Polyesters," in *Polymer Science: A Comprehensive Reference*, M. Editors-in-Chief: Krzysztof and M. Martin, Eds., ed Amsterdam: Elsevier, 2012, pp. 311-331.

[94] C. D. Papaspyrides and S. N. Vouyiouka, *Solid State Polymerization*. Hoboken, NJ, USA.: John Wiley & Sons, 2009.

[95] D. Wu, *et al.*, "Reaction Kinetics and Simulations for Solid-State Polymerization of Poly(ethylene terephthalate)," *Macromolecules,* vol. 30, pp. 6737-6742, 1997.

[96] B. Gantillon, *et al.*, "The Solid State Postcondensation of PET, 1," *Macromolecular Materials and Engineering,* vol. 289, pp. 88-105, 2004.

[97] T. Y. Kim, *et al.*, "Solid-state polymerization of poly(ethylene terephthalate). I. Experimental study of the reaction kinetics and properties," *Journal of Applied Polymer Science,* vol. 89, pp. 197-212, Jul 2003.

[98] C. Shuya, *et al.*, "Solid-state polymerization of poly(ethylene terephthalate)," *Journal of Applied Polymer Science,* vol. 28, pp. 3289-3300, 1983.

[99] S. N. Vouyiouka, *et al.*, "Solid state polymerization," *Progress in Polymer Science,* vol. 30, pp. 10-37, 2005.

[100] S. A. Wadekar, *et al.*, "Recent developments in solid state polymerization of poly(ethylene terephthalate)," *Solid state polymerization,* p. 233, 2009.

[101] B. Duh, "Effects of crystallinity on solid-state polymerization of poly(ethylene terephthalate)," *Journal of Applied Polymer Science,* vol. 102, pp. 623-632, 2006.

[102] B. Duh, "Reaction kinetics for solid-state polymerization of poly(ethylene terephthalate)," *Journal of Applied Polymer Science,* vol. 81, pp. 1748-1761, 2001.

[103] B. Duh, "Effect of antimony catalyst on solid-state polycondensation of poly(ethylene terephthalate)," *Polymer,* vol. 43, pp. 3147-3154, 2002.

[104] D. S. Achilias, *et al.*, "Effect of silica nanoparticles on solid state polymerization of poly(ethylene terephthalate)," *European Polymer Journal,* vol. 44, pp. 3096-3107, 2008.

[105] D. Bikiaris, *et al.*, "A new approach to prepare poly(ethylene terephthalate)/silica nanocomposites with increased molecular weight and fully adjustable branching or crosslinking by SSP," *Macromolecular Rapid Communications,* vol. 27, pp. 1199-1205, 2006.

[106] S. G. Kim, *et al.*, "Dispersion of nanoclays with poly(ethylene terephthalate) by melt blending and solid state polymerization," *Journal of Applied Polymer Science,* vol. 127, pp. 2201-2212, 2013.

[107] S. G. Kim, *et al.*, "Nanocomposite Development with Organically Modified Clay through In Situ Polymerization of Poly(ethylene terephthalate)," *Advances in Polymer Technology,* pp. n/a-n/a, 2013.

[108] Y. Wang and S. A. Jabarin, "Novel preparation method for enhancing nanoparticle dispersion and barrier properties of poly(ethylene terephthalate) and poly(m-xylylene adipamide)," *Journal of Applied Polymer Science,* vol. 129, pp. 1455-1465, 2013.

[109] F. Samperi, *et al.*, "Thermal degradation of poly(ethylene terephthalate) at the processing temperature," *Polymer Degradation and Stability,* vol. 83, pp. 3-10, 2004.

[110] B. Gantillon, *et al.*, "The Solid State Postcondensation of PET, 4," *Macromolecular Materials and Engineering,* vol. 289, pp. 119-130, 2004.

[111] B. Fox, *et al.*, "Characterization of poly(ethylene terephthalate) and poly(ethylene terephthalate) blends," *Polymer,* vol. 38, pp. 3035-3043, 1997.

[112] G. P. Karayannidis, *et al.*, "Solid-state polycondensation of poly(ethylene terephthalate) recycled from postconsumer soft-drink bottles. I," *Journal of Applied Polymer Science,* vol. 50, pp. 2135-2142, 1993.

[113] L. H. Sperling, *Introduction to Physical Polymer Science*. 4th ed. New Jersey: Wiley Interscience (2006).

[114] T. Fornes, *et al.*, "Nylon 6 nanocomposites: the effect of matrix molecular weight," *Polymer,* vol. 42, pp. 9929-9940, 2001.

[115] L. Cui, *et al.*, "Morphology and Properties of Nanocomposites Formed from Poly(ethylene-co-methacrylic acid) Ionomers and Organoclays: Effect of Acid Neutralization," *Macromolecules* vol. 42, pp. 2599-2608, 2009.

[116] T. D. Fornes, *et al.*, "Effect of sodium montmorillonite source on nylon 6/clay nanocomposites," *Polymer,* vol. 45, pp. 2321-2331, 2004.

[117] T. D. Fornes, *et al.*, "Effect of organoclay structure on nylon 6 nanocomposite morphology and properties," *Polymer,* vol. 43, pp. 5915-5933, 2002.

[118] L. E. Nielsen and R. F. Landel, *Mechanical Properties of Polymers Composites 2e*: New York : Marcel Dekker, 1994.

[119] R. W. Nunes, et al., "Influence of molecular weight and molecular weight distribution on mechanical properties of polymers," *Polymer Engineering & Science,* vol. 22, pp. 205-228, 1982.

[120] R. Landel and L. Nielsen, "Mechanical properties of polymers and composites," *Marcel Dekker, Inc,* 1994.

[121] N. Najafi, *et al.*, "Control of thermal degradation of polylactide (PLA)-clay nanocomposites using chain extenders," *Polymer Degradation and Stability*, vol. 97, pp. 554-565, 2012.

[122] M. Dini, *et al.*, "Microstructure and properties of PET/organoclay nanocomposites prepared by water-assisted extrusion: Effect of organoclay concentration," *Polymer Engineering & Science*, 2013, doi: 10.1002/pen.23736.

APPENDIX A PET/CLOISITE NA NANOCOMPOSITE PREPARATION BASED ON THE SLURRY METHOD

Abstract

A modified melt-mixing method was developed to prepare PET nanocomposites using a water slurry containing Cloisite Na^+. In this method, the slurry of Cloisite Na^+ (CNa) was injected into PET during the extrusion process. Morphology, thermal, mechanical and barrier properties of the PET nanocomposites were studied.

A.1 Experimental

A.1.1 Materials

A general purpose PET (PET 9921, Eastman Co, Kingsport, TN) with molecular weight of 65 000 g/mol was used. The nanoclay used was Cloisite Na^+ (CNa) (Southern Clay Products Inc., Gonzales, TX) with a cation exchange capacity of 92.6 meq/100 g clay. Poly (ethylene glycol) (PEG) with molecular weight of 35 000 g/mol supplied from Aldrich and carboxymethyl cellulose (CMC) (Finnix CMC, CP Kelco Co, Finland) were used as dispersing agents. All the materials were used without additional treatment, except drying.

A.1.2 Melt Compounding

PET and the nanocomposites were processed using a co-rotating twin screw extruder (TSE) (Berstorff ZE25, Hannover, Germany) with a 25 mm diameter (D) screw and length-to-screw diameter ratio of 28 at a screw speed of 200 rpm. The screw configuration was presented in ref [122]. The temperature profile was 245, 265, 260, 255, 255, and 255°C from the hopper to the die. The feeding rate of PET into the extruder was 3 Kg/h.

To obtain CNa suspensions, 3wt% of CNa was added to water at 60 ºC. Stirring time was considered as the time required to ensure the clay particles were completely dispersed in the water during 6 h of stirring. The color of the suspension (slurry) was bright yellow.

1wt% of PEG and CMC were also added in the suspension of water and CNa. The clay slurries were pumped into the extruder at 1.75 Kg/h and compounded with the melted PET. A plunger pump was used to inject the clay slurries into the extruder. Water was removed from extruder by vacuum via a vent located at the end of the extruder (before it exits die). The nanocomposites prepared by the slurry method were used as masterbatches. They were diluted by neat PET to obtain the final nanocomposites had 1wt% of CNa. In the final product there were approximately 0.2 wt% of PEG and CMC. The extruded samples were cooled by air and pelletized.

Samples for XRD and morphology analysis were molded in the form of disk-like plates with a diameter of 25 mm and a thickness of ~ 1.2 mm. Thin sheet samples 250 μm thick for mechanical tests and 300 μm thick for barrier tests were prepared via compression molding. All samples were prepared using a hot press (Carver Laboratory Press, Model 3912) with a small chamber for nitrogen purge. The compression molding temperature and maximum pressure were 270 °C and 3 tons, respectively. All the samples were dried under vacuum for 24 h at 80 °C prior to melt processing and molding.

A.1.3 Characterization

A wide angle X-ray diffractometer (WAXD) (D8 Discover, Bruker AXS Inc., Madison, WI) with CuKα radiation (λ=1.54056 Å) was used to estimate the basal spacing (d_{001}) for silicate layers. The generator was operated at 40 kV/ 40 mA and the nanocomposites were scanned from 1.5 to 10° at 0.015°/s.

A field emission gun scanning electron microscope (FEG-SEM, S-4700, Hitachi, Tokyo, Japan) was used to investigate the distribution of clay in the PET matrix. The specimens were prepared using an Ultracut FC microtome (Leica, Wetzlar, Germany) with a diamond knife and

then coated with platinum vapor. The quality of the clay dispersion was evaluated using transmission electron microscopy (TEM) (JEOL JEM-2100F, Tokyo, Japan, operating at 200 kV). The samples were microtomed into approximately 50-80 nm thick slices, using an Ultracut FC cryomicrotome system at -100° C.

Rheology measurements of suspensions were performed by Physica MCR501 (Anton Paar) rheometer with double couette geometry at 25 ºC over a shear rate range of 0.1-100 (s^{-1}). Measurements were done from high to low and low to high shear rates.

The thermal properties of the neat PET and PET nanocomposites were studied by differential scanning calorimetry (DSC Q1000, TA instruments, New Castle, DE) under N_2 atmosphere using 10 °C/min scanning ramp from 30 °C to 300 °C.

Tensile measurements were conducted using an Instron 3365 universal tester with a 500 N load cell and according to the ASTM D882-10 standard. The tensile testing samples were cut from 250 µm thin sheets to a rectangular shape (10 mm x 100 mm). The samples were tested at room temperature and a crosshead speed of 25 mm/min.

Oxygen transmission rates (OTRs) were determined using an Ox-Tran Model 2/21 oxygen permeability MD Module from Mocon (Minneapolis, MN) at 23 °C. 100% dry oxygen was used and all the tests were done under a pressure of 93.3 kPa (700 mmHg). The test area of the samples was 5 cm^2 and the samples had a thickness of 300 µm. The oxygen permeability values reported in this work have been normalized by the film thickness.

A.2 Results and discussion

A.2.1 Rheology of suspensions

Figure A-1 shows the steady shear viscosity of suspensions. In the present study, all the suspensions exhibit non-Newtonian flow behaviour. Adding 3 wt% of CNa in water significantly increases the viscosity from 0.001 Pa.s in water to 0.1 Pa.s in W-CNa (water-Cloisite Na+) sample which is a sign of a good dispersion of CNa in water. It is observed that a smaller quantity of CMC in W-CNa suspensions leads to a significant viscosity increase and a shear thinning

behavior, while PEG slightly changes the viscosity compared to water-CNa suspensions. Therefore, CNa is better dispersed in water in the presence of CMC compared to the suspensions containing PEG.

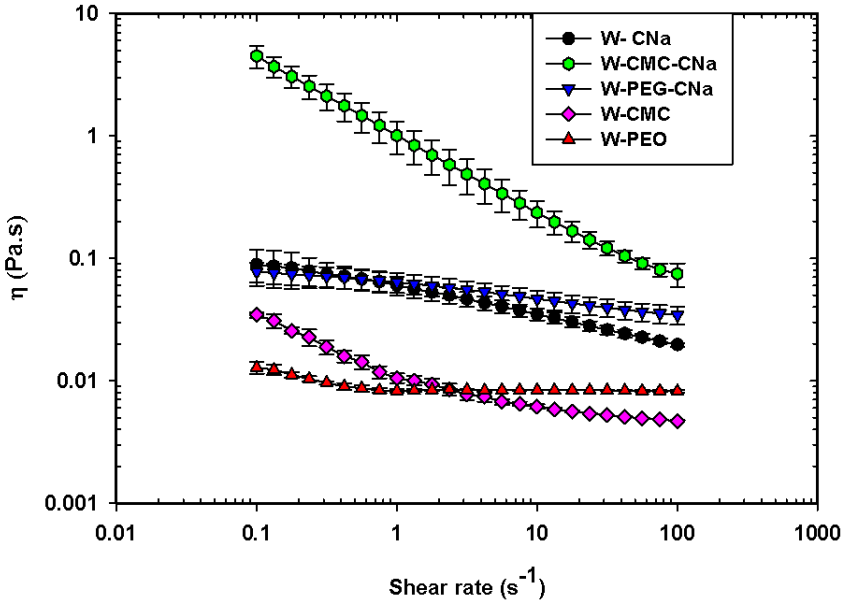

Figure A- 1: Steady shear viscosity of water-CNa suspensions

A.2.2 Microstructure of PET nanocomposites

XRD results of PET nanocomposites are presented in Figure A-2. PET/CNa nanocomposites containing PEG or CMC show one peak at 2θ ≈5 °, which correspond to *d*-spacing ~ 1.9 nm. Since the *d*-spacing value for the pristine nanoclay, CNa, is 0.9 nm, the observed peak at 2θ ≈5 ° is an indication of polymer chains diffusion into the gallery spacing of CNa. The CNa nanocomposites without PEG or CMC show no diffracted peak, possibly because of clay dilution due to the agglomerate formation. In fact, the disappearence of a diffraction peak cannot always be directly attributed to an exfoliated morphology. Although in a suspension of CNa in water, water expands the gallery spacing of nanoclays, it seems that the rate of water evaporation in the twin screw extruder is faster than the diffusion of PET chains into the interlayers of nanoclays.Therefore the clays collapse during the melt-mixing. On the other hand, PEG and CMC can diffuse and remain into the gallery of nanoclays.

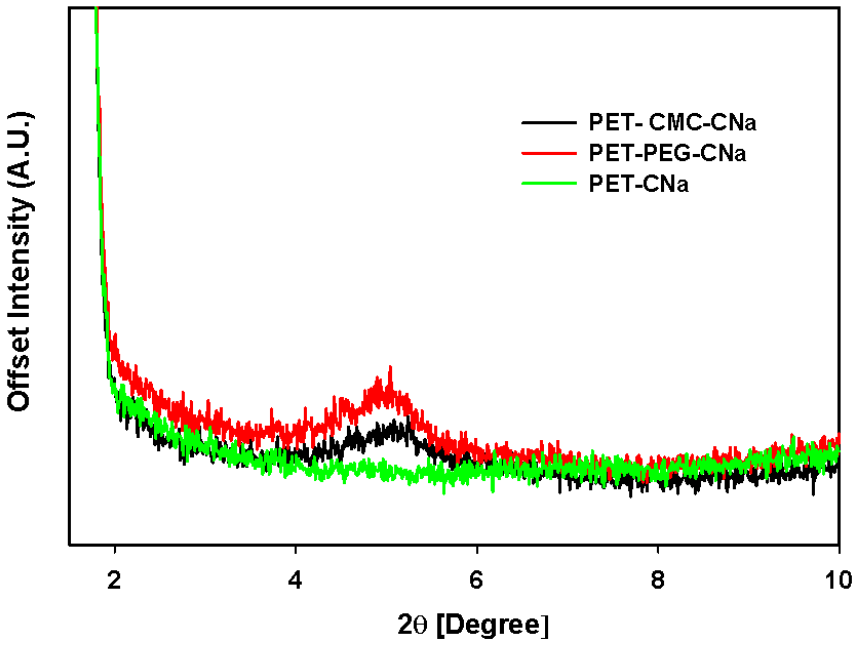

Figure A- 2: XRD patterns of PET nanocomposites

SEM micrographs of PET nanocomposites are shown in Figure A-3. Figure A-3a shows the SEM micrographs of the nanocomposites prepared by conventional melt-mixing method. It displays the presence of big agglomerates of Cloisite Na^+ with size of 10 µm. The PET-CNa nanocomposites processed with slurry method (Figure A-3b) have much more smaller agglomerates compared to the conventional melt-mixing but there is not a good dispersion or distribution of CNa into the matrix. Moreover, Figure A-3c and d exhibit the effect of CMC and PEG on improvements of CNa dispersion and distribution in PET matrix.

TEM images of PET-CNa nanocomposites are presented in Figure A-4. Although big agglomerates are observed in some places, nanoclays are also dispersed in the form of single layers. They are the promising results indicating that the clay slurry method can assist to open the gallery spacing of CNa. It is noticeable that in this sample the concentration of CNa is 0.5 wt%.

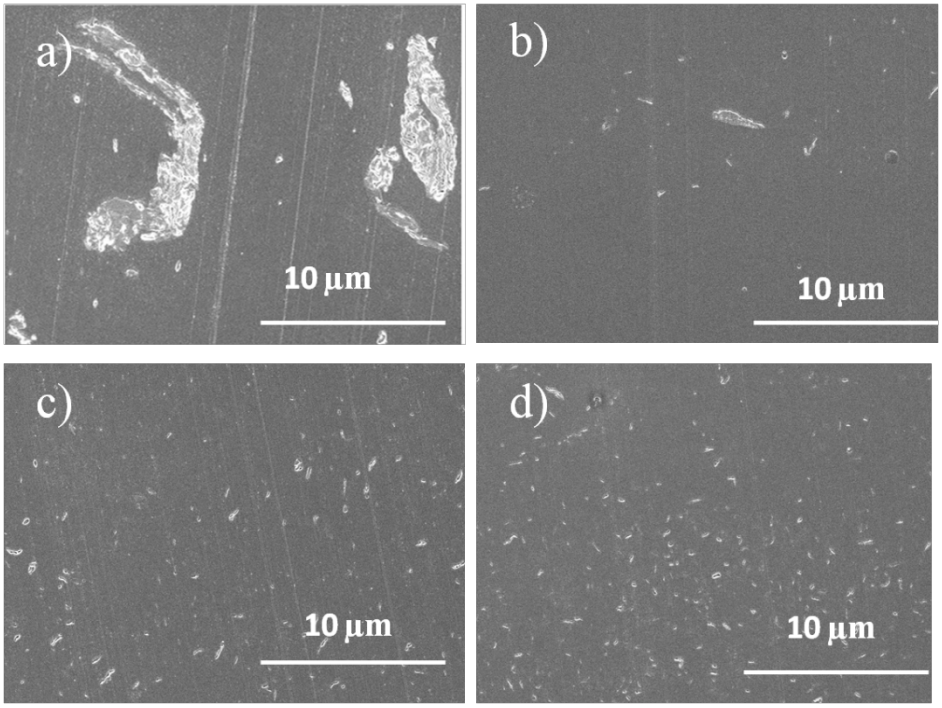

Figure A- 3: SEM micrographs of PET nanocomposites; a) PET-CNa prepared by conventional melt-mixing, b) PET-CNa prepared by slurry method, c), PET-CMC-CNa , d) PET-PEG-CNa

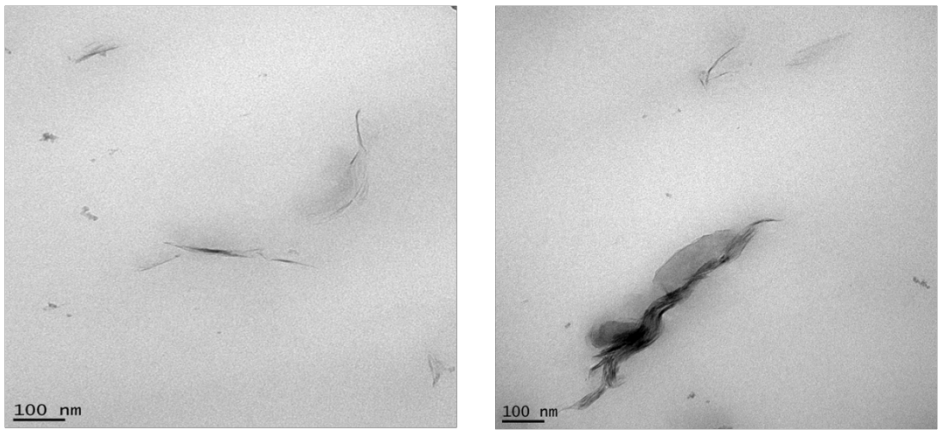

Figure A- 4: TEM images of PET-CNa nanocomposites prepared by slurry method.

A.2.3 Thermal, mechanical and barrier properties of PET nanocomposites

Results of DSC experiments are presented in Table A-1 where glass transition temperature (T_g), melting temperature (T_m), cold crystallization temperature (T_{cc}), and crystallinity of PET in the nanocomposite films are reported. Table A-1 shows that the T_{cc} of PET nanocomposites is lower than that of the neat PET but no significant changes are observed for T_g and T_m. The reduction of T_{cc} in the presence of CNa is due to the nucleating role of the nanoclay. Moreover, crystallinity of PET nanocomposite films is significantly higher than neat PET.

Table A-1 **:** Thermal properties of PET and PET nanocomposites

Sample	T_g (°C)	T_{cc} (°C)	T_m (°C)	ΔX (%)
PET	75± 0.6	133 ± 0.5	246 ± 0.2	6.4 ± 0.2
PET- CNa	75 ± 0.5	123 ± 0.4	245 ± 0.4	11.5 ± 1.5
PET- PEG-CNa	74 ± 0.3	122 ± 1	245 ± 0.5	10.7 ± 0.9
PET- CMC-CNa	74 ± 1	121± 0.1	245 ± 0.1	10.3 ± 0.7

Figure A-5 reports tensile modulus of the samples. Adding 1wt% CNa leads to 13% increase in tensile modulus of the nanocomposites compared to the neat PET. On the other hand, 25 % improvement was found in tensile modulus of PET-PEG-CNa. However, the extent of tensile modulus enhancement in the nanocomposites containing CMC is approximately the same as PET-CNa. Higher tensile modulus of the nanocomposites compared to the neat PET is attributed to the presence of high modulus nanoclay platelets and higher crystallinity in the nanocomposites.

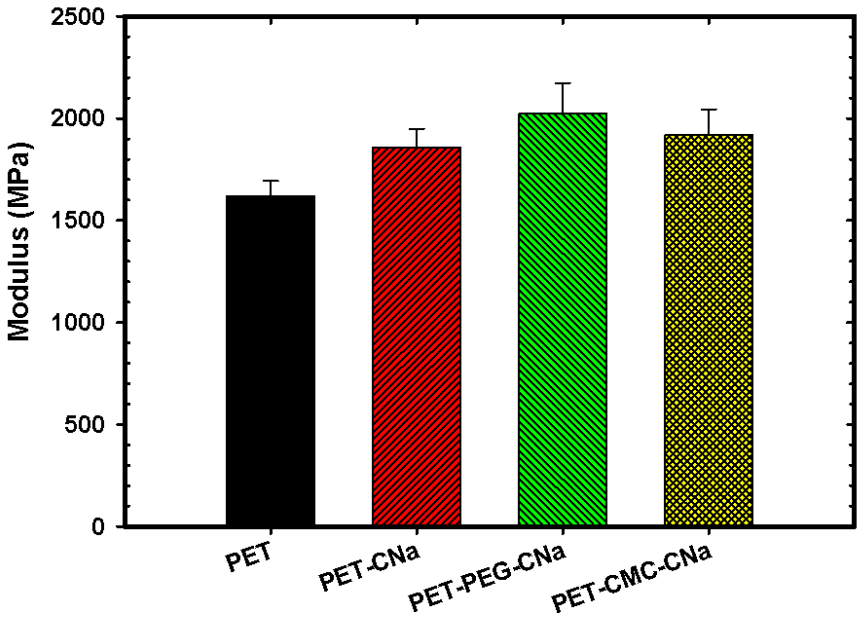

Figure A- 5: Tensile modulus in PET and PET nanocomposites

Oxygen permeability of PET nanocomposites (shown in Figure A-6) is less than the neat PET. PET-CNa shows 18 % improvement in barrier properties while reduction of oxygen permeability in nanocomposites with PEG and CMC is around 27%. The presence of organoclay reduces the oxygen permeability due to increasing the tortuous path. More barrier improvement in nanocomposites with PEG and CMC is due to the better dispersion and distribution of nanoclays. Moreover, impermeable crystalline phase of polymer reduces the gas permeability. Therefore, higher crystallinity in nanocomposites compared to the neat PET is another parameter to improve the barrier properties.

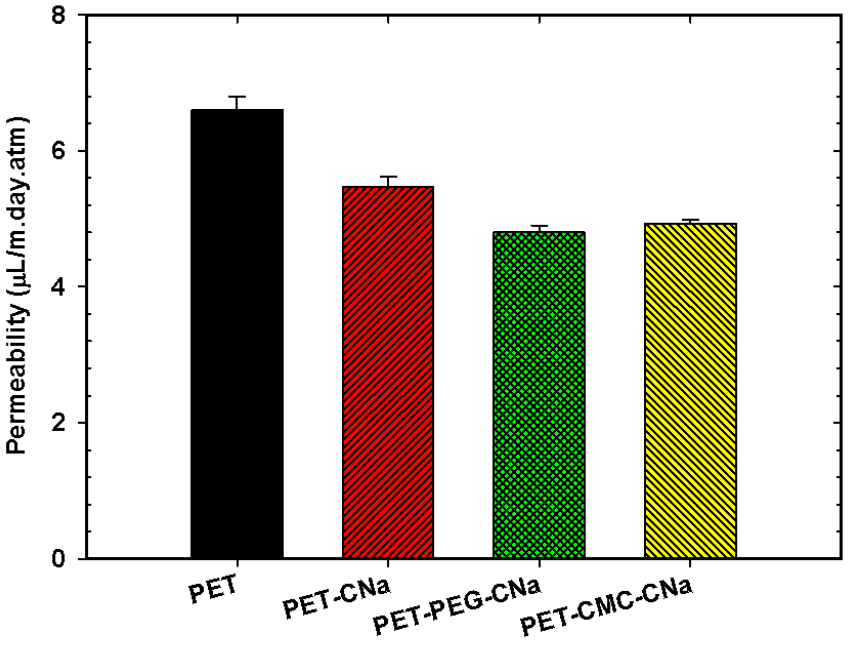

Figure A- 6: Oxygen permeability in PET and PET nanocomposites

The nanocomposite samples are presented in Figure A-7. The color of the sample containing C30B is dark brown compared to the nanocomposites containing CNa. In the presence of CMC and PEG, the color of the nanocomposites changes but they still have brighter color than the nanocomposites with C30B.

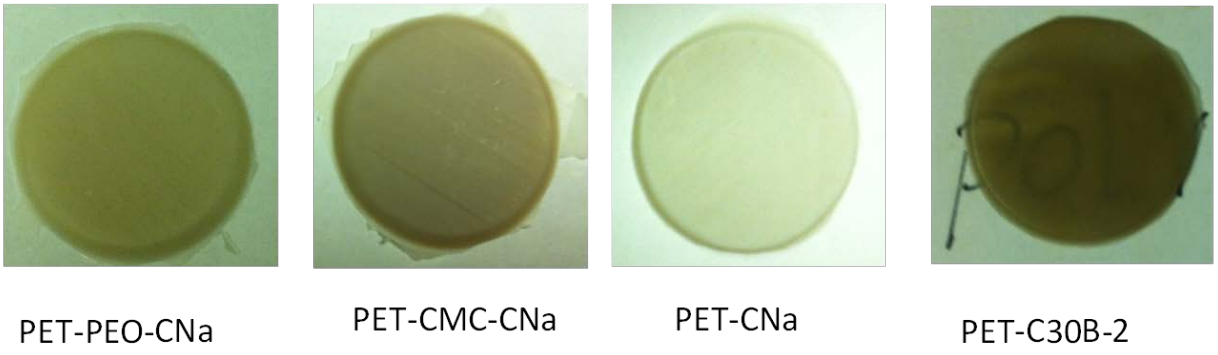

Figure A- 7: Color of PET nanocomposites

A.3 Conclusion

Preparation of PET nanocomposites through melt-mixing of PET and water-based suspensions of Cloisite Na^+ resulted in smaller nanoparticles compared to conventional melt-mixing. The importance of this method is to prepare nanocomposites based on the unmodified nanoclays. The presence of PEG and CMC in the nanocomposites led to better dispersion and distribution of nanoclays in PET matrix. 25% and 27% improvements in mechanical and barrier properties of PET nanocomposites prepared by this slurry method were found.